FABRICATION OF TISSUE ENGINEERED OSTEOCHONDRAL GRAFTS AND EFFICACY ASSESSMENT IN LAPINE & CAPRINE MODELS

FRANCIS BONIFACE FERNANDEZ

PhD THESIS
2014

SREE CHITRA TIRUNAL INSTITUTE FOR MEDICAL SCIENCES AND TECHNOLOGY
THIRUVANANTHAPURAM
INDIA

2014

DECLARATION

I, **Francis Boniface Fernandez**, hereby certify that I had personally carried out the work depicted in the thesis entitled, ***"Fabrication of Tissue Engineered Osteochondral Grafts and Efficacy Assessment in Lapine & Caprine Models"*****,** except where due acknowledgment has been made in the text. No part of the thesis has been submitted for the award of any other degree or diploma prior to this date.

Thiruvananthapuram
01-07-2014

Francis Boniface Fernandez
Reg.No: PhD/2009/09

SREE CHITRA TIRUNAL INSTITUTE FOR MEDICAL SCIENCES & TECHNOLOGY, TRIVANDRUM

Thiruvananthapuram – 695011, INDIA
(An Institute of National Importance under Govt. of India)
Phone-(91)0471-2520215 Fax-(91)0471-2341814
Email-ajkari@sctimst.ac.in Web site – www.sctimst.ac.in

Dr. Annie John

Scientist F & Head

Transmission Electron Microscope,

BMT Wing, SCTIMST, Thiruvananthapuram

This is to certify that **Mr. Francis Boniface Fernandez**, in the lab of Transmission Electron Microscope of this Institute has fulfilled the requirements prescribed for the Ph. D. degree of the Sree Chitra Tirunal Institute for Medical Sciences and Technology, Thiruvananthapuram. The thesis entitled, **"*Fabrication of Tissue Engineered Osteochondral Grafts and Efficacy Assessment in Lapine & Caprine Models*"** was carried out under my direct supervision. No part of the thesis was submitted for the award of any degree or diploma prior to this date.

* Clearance was obtained from the Institutional Ethics Committee/ Institutional Animal Ethics Committee for carrying out the study.

Thiruvananthapuram
01.07.2014

Dr. Annie John
(Research Supervisor)

The thesis entitled

"Fabrication of Tissue Engineered Osteochondral Grafts and Efficacy Assessment in Lapine & Caprine Models".

Submitted by

Francis Boniface Fernandez.

for the degree of

Doctor of Philosophy

Of

SREE CHITRA TIRUNAL INSTITUTE
FOR MEDICAL SCIENCES AND TECHNOLOGY,
THIRUVANANTHAPURAM - 695011

is evaluated and approved by

……. ……..

Dr. Annie John
(Research Supervisor)

Examiner

DEDICATED TO
MY FAMILY & TEACHERS

ACKNOWLEDGEMENT

It is with gratitude, satisfaction and the divine blessings of the Almighty that I submit this dissertation. I take this opportunity to humbly thank all who contributed in many ways for the success of this study.

My gratitude and respect to my supervisor Dr. Annie John Scientist – F, TEM, SCTIMST is beyond description. Dr. Annie has offered constant support, strong encouragement & motivation throughout the course of this study. I thank her for the systematic guidance, and for lighting the path of my budding research career via the preparation of this thesis.

I thank the members of my doctoral advisory committee, Dr. T. V. Kumary Scientist G, TIC, SCTIMST, Dr. H. K. Varma, BCL, SCTIMST, Dr. Prabha D Nair, DTERT, SCTIMST for their timely suggestions, ideas and comments, which helped in the improvement of the quality of this work.

I thank Council of Scientific and Industrial Research, Govt. of India for the fellowship provided during the doctoral programme and Department of Biotechnology Advanced National Center for Tissue Engineering for funding the project and I also thank Department of Biotechnology & Department of Science and Technology, Government of India for funding for the international conferences which I attended in China and USA.

I am grateful to the Director of SCTIMST and the Head, BMT Wing for all support provided during the course of my work. I am thankful to Dr. Jayasingh the Deputy Registrar, Prof. Tharakan & Prof Nair the Deans, Dr. Sharma & Dr. Prabha D. Nair the Associate Deans of Ph. D., all members of academic division and Director's office for their assistance.

The valuable help and guidance from Dr. H. K. Varma & Dr. Suresh Babu for scaffold preparation has significantly contributed to this thesis. I gratefully acknowledge him for the personal support and encouragement at difficult times. All members past and present of Bioceramics Laboratory are sincerely acknowledged.

I thank Dr. Umashankar for providing the facilities for large animal experiments. My sincere thanks to Dr. Sachin J Shenoy for his help with surgical procedures and management of the large animal experiments. I'm indebted to Dr. Annie John, Dr. A.C. Fernandez for small animal experimental facilities. Sincere thanks to Dr. Scahin J Shenoy & Dr.Harikrishnan V.S, for helping with the surgical procedures during the lapine animal study and timely advice for giving appropriate care for experimental animals. I thank all members of

DIMT & DLAS, for their assistance during the animal experiments. I acknowledge Dr. Mira Mohanthy, Dr. Sabareeswaran, Mr Joseph and all members of histopathology who helped with technical advice and histology evaluation.

I also thank Mr Ramesh Babu and Staff of Precision fabrication facility for fabricating templates for different experiments. I would like to thank Dr H K Varma and Mr. Nishad, for SEM analysis. Dr. T.V. Anilkumar for help with confocal laser scanning microscopy.

I am indebted to all my colleagues at Transmission Electron Microscope(TEM). My lab members : Dr. Beena, Mrs. Susan, Mrs. Sunitha, Mr. Mir, Mrs. Resmi, Mrs. Ganga, Mr. Hadi, Dr. Manitha, Dr. Vibin, Mr. Balu, Mrs. Smitha, Mrs. Devi & Mr. Alwin are acknowledged for their support, encouragement & friendship throughout this odyssey.

My friends and teachers from within and outside the campus have helped in many different ways and are acknowledged. Cooperation from staff of various administrative departments and library of the Institute is fondly remembered. Cordial attitude and support from the student community of our campus is acknowledged

I have no words to express gratitude to my family members who provided the most precious support. I am indebted to my parents, my brother Cyril Fernandez & my sister Maria Fernandez for their endless support, encouragement, love and prayers.

God, almighty I kneel down in your presence for giving me strength, courage and for providing good health for completing this work.

TABLE OF CONTENTS

LIST OF FIGURES

LIST OF TABLES

ABBREVIATIONS

ADMSC	:Adipose Derived Mesenchymal Stem Cells
ALP	: Alkaline Pphosphatase
BCP	: Biphasic Calcium Phosphate
BMP	: Bone Morphogenetic Protein(s)
cLSM	:Confocal laser scanning microscope
CPCSEA	:Committee for the Purpose of Control and Supervision of Experiments on Animal
DAPI	: 4',6-diamidino-2-phenylindole
DMEM - HG	: Dulbecco's Modified Eagle's Medium High Glucose
DMEM - LG	: Dulbecco's Modified Eagle's Medium Low Glucose
EDTA	:Ethylenediaminetetraacetic Acid
FGF	:Fibroblast Growth Factor
FTIR	:Fourier Transform Infrared
GADMSC	:Goat adipose Derived Mesenchymal Stem Cells
GAG	:Gglycosaminoglycan
HA	:Hydroxyapatite
HASi	:Hydroxyapatite Coated with Silica
MEM	:Minimum Essential Medium
OA	:Osteoarthritis
OCD	:Osteochondral defect
PBS	:Phosphate Buffered Saline
PCL	:Polycaprolactone
PG	:Proteoglycans
PMMA	:Polymethylmethacrylate
RA	:Rheumatoid arthritis
RADMSC	:Rabbit Adipose Derived Mesenchymal Stem Cells
GADMSC	:Goat Adipose Derived Mesenchymal Stem Cells
Runx2	:Runt-related Transcription Factor 2
TE	:Tissue Engineering
μm	:Micrometers

Appendix A – Buffers & Special Reagents

A. Hexabrix Staining Protocol

Preparation of Stain: 40% Hexabrix : 60% PBS is mixed at room temperature and used immediately. Stain should be protected from light and kept at 4°C for later use.

Deformalinization of Samples: Samples can be deformalinized in PBS overnight using an orbital shaker. Three changes of PBS are used to ensure complete formalin removal from the sample prior to staining with Hexabrix.

B. Stevenel's Blue

Dissolve 1 gm methylene blue in 75 ml distilled water, and combine with 1.5 gm of potassium permanganate in 75 ml of distilled water. Place in a boiling water bath till the precipitate formed has dissolved. Filter at room temperature, and store in a dark place.

C. Van Giesons Picrofuchsin

0.1 gm of acid fuchsin is dissolved in 10 ml distilled water. Add 100 ml of saturated picric acid to this mix. Mix well and store in a reagent bottle

D. Alcian Blue 8G

Prepare a 3% Acetic acid solution (3 ml glacial acetic acid with 97 ml distilled water). Add 1gm of Alcian Blue to 100 ml of 3% acetic acid solution, adjust pH to 2.5 with glacial acetic acid.

CHAPTER 1

INTRODUCTION

1.1 Introduction & Current Scenario

Injuries to the articular cartilage tissue are common with sequela that involves continued loss of tissue with progressive worsening of the related joint function. Insults at early time points may also contribute to late-onset of related arthritis, causing a worsening of the quality of life and associated economic loss. Osteochondral lesions or defects are areas of damage where the cartilage and underlying bone are affected. This acts as a serious impediment in joint reconstruction. When untreated they do not heal, and the risk of degeneration increases with time. With an increasingly ageing population it is anticipated that the number of people affected and the resulting burden on healthcare system will increase dramatically over the years to come. Osteochondral status is intimately linked with limb alignment, meniscal status, and as well with ligamentous status. With over 40% of patients 65 years and older having symptomatic osteoarthritis (OA), it severely affects the quality of life and overall outcome (Dawson et al., 2004).

A deficiency in one part of this functional unit can have an impact on the other parts and, in the short term, can lead to a loss of performance. Lesions or damage can be caused by disease, arthritis, inflammation or trauma. Ten percent of the world population over thirty years has clinical osteoarthritis (OA of the hip or knee, with total direct costs estimated in billion dollars per year (Felson et al., 2000)

In contrast to cartilage defects where in subchondral bone is not damaged in the case of partial thickness defects or merely exposed in full thickness defects, an osteochondral defect (OCD) disrupts integrity of the chondral, subchondral bony

interface layer as well as the underlying bony tissue. Pain is the key symptom with untreated OCD (Lindén, 1976), as well as progression to OA resulting from the joint incongruence and abnormal loading of surrounding normal cartilage over limits of native biomechanical constraints (Shirazi and Shirazi-Adl, 2009). Of interest to the keen eye is the underlying problems that contribute to the formation of OCD. Subchondral bone lesions that are a trademark of damage via osteochondritis dissecans or due to Osteochondral fractures are the main contributors to lesions of the Osteochondral layer and its resulting pathologies (Menetrey et al., 2010).

In the earlier stages of OA or aggravated untreated OCD, pharmacological or physical therapy interventions are selected for the purpose of reducing pain, with slow escalation in the pain pyramid. The preliminary focus is on reduction of pain and conservation of joint function with emphasis on delaying progressive structural deterioration in the joint structures (Block, 2014). Surgical therapies, joint replacement, osteotomy are available for patients who pass certain diagnostic milestones (Marcacci et al., 2013). Current therapies vary from autologous chondrocyte implantation, subchondral drilling or microfracturing. The treatments are well established and effective for reducing pain and improving the quality of life of the patient. But treatments indicate the regeneration of mechanically inferior fibrocartilage at the defect site post treatment which undergoes wear and tear over time causing joint failure in the long term. Thus regardless of therapeutic options, there is no single option that will facilitate complete healing of the articular cartilage (Shimomura et al., 2010) (Kandel et al., 2006).

The paramount goal is to reconstruct a smoothly articulating anatomical joint surface resembling as closely as possible the normal structure of an Osteochondral unit. Current therapies have several shortcomings that are (a) integral to the use of surgical techniques and (b) nature of the tissues under reconstruction

Recently several biological approaches such as the use of tissue engineered materials have been proposed to overcome such chronic problems. In such situations, alternative tissue engineering strategies call for the application of appropriate scaffolds to deliver cells and growth factors which would simultaneously degrade keeping pace with restoration of tissue function. Application of resources scarce at

the site via external intervention would help in the resolution of the defect healing process, resulting in an uneventful healing process.

These limitations provoked a closer look at cell based methods for effectively treating cartilaginous structures (Cohen et al., 1993). Tissue Engineering has been defined as an "interdisciplinary field that applies the principles of engineering and life sciences towards the development of biological substitutes that restore, maintain, or improve tissue function" (Langer and Vacanti, 1993a).

1.2 Strategies

Thus strategies for replacing, restoring or repairing lost function can be broken down into the following goals:

(1) Identification of a suitable source of cells, followed by isolation, expansion and differentiation of ADMSCs

(2) Development of a device/scaffold to either carry or encapsulate the cells;

(3) Uniform seeding of cells onto or into the device under appropriate culture conditions (*in vitro*) ; and

(4) *in vivo* implantation of the engineered construct

1.3 Cellular Components

Mesenchymal stem cells have functioned as the pathfinders on the revolutionary path of tissue engineering, proving to be accessible, expandable and easily differentiated sources of healing in built to the living system. To rebuild an Osteochondral system the amenability of cell capacity to differentiate via osteogenic and chondrogenic lineages have to be ensured. Sourcing primary cells is hobbled by the restrictions of poor cell proliferation in native chondrocytes as well as osteoblasts. This renders moot the requirement of a plastic cell population (Bronckaers et al., 2014). The recruitment of cells from the stem cell compartment would ensure growth and regeneration of tissue *in situ* as the native tissue is avascular and not conducive to rapid growth and repair. The repair has been observed to be mediated wholly by the proliferation and differentiation of mesenchymal cells of the marrow in the case of rabbit articular cartilage healing model investigated by Shapiro *et al.,* 1993 (Shapiro

et al., 1993a). On the contrary, adipose tissue is also another appropriate cell source due to ease of access (less invasive), low donor site morbidity & relatively easy isolation procedure and has been used as a proponent in earlier studies for the repair of bone and cartilage tissues (Dragoo et al., 2003). Thus, adipose derived stem cells are poised to be a major source of cells for therapy and regeneration, taking advantage also of their immune privileged status (Kokai et al., 2014). This provides an off the shelf approach to allogenic transplants involving adipose derived stem cells, helping in the commoditization of cell dependent products, which is a major challenge in the clinical scenario.

1.4 Scaffolds

A successful tissue engineering approach involves the fabrication of scaffold surfaces that support the growth, differentiation and maturation of native tissue. In the case of Osteochondral injuries there is an inherent challenge in the need to develop a scaffold which would address the needs of the cartilage and bony surfaces simultaneously. Biphasic scaffolds with surfaces tuned to the needs of disparate tissues but brought together at the time of implantation are inherently unstable in the high demand articulating cartilage compartment (Gelinsky, 2007). There is a felt need for the development of monolithic, anchorage stable implant systems that will help in the resolution of damage to both chondral and sub chondral compartments (Schütz et al., 2014). In this context, bioactive ceramics were the scaffolds of choice as they are known to be biocompatible, porous for tissue in growth, biodegradable and above all, their composition is similar to skeletal tissues. In view of the unique nature of articular cartilage & the nature of osteochondral lesions where the cartilage & underlying bone is affected, there is a need for the development of a composite ceramic scaffold (singly or in two phases) for osteochondral defect amelioration.

1.5 Ceramics as Scaffolds

Evaluation of the role of ceramics as scaffolds for Osteochondral defects have been ongoing since 1989 (Ohgushi et al., 1989) with the latest reports indicating the combination of ceramics with exotic materials (Jiang et al., 2010a) to achieve desired material characteristics. Further use of ceramics as carrier surfaces for the

placement of scaffold free cartilage development has also been noted (Kitahara et al., 2008). The ability of the ceramic surfaces to provide a native bone identical surface for cartilage overgrowth and support has been well identified.

1.6 Animal Models

Small animal models are key to initial testing and demonstration of novel materials. New Zealand White Rabbits are a proven model with a 4mm critical size defect in the Osteochondral plate used as an experimental model to understand healing patterns associated with tissue engineering techniques (Rudert 2002). Long term survival of graft and healing patterns are better understood in a animal model that closely mimics the human gait & load bearing stride and hence the caprine model was chosen (Saw et al., 2009). Delamination, surface degradation & related issues are better resolved at a longer time point in a human mimic model.

So the interest was to utilize adipose tissue derived Mesenchymal Stem cells (ADMSCs) which are capable of differentiating into multiple lineages (Zuk, 2010a)' to determine the cytocompatibility of selected ceramic scaffolds and thereafter to assess their regenerative efficacy in a short term lapine and long term caprine osteochondral defect models.

This dissertation lays down the foundation for an unitary ceramic based, differentially capacitated cell loaded approach that leads to a translational level of Osteochondral regenerative solution. This comprises extended applications in 'Interfacial Orthopaedic Tissue Engineering' and prospective evaluation and tempering of interfacial tissue constructs.

CHAPTER 2

REVIEW OF LITERATURE

---

2. 1 Preliminary Statement

"From Hippocrates to present age, it is universally allowed that ulcerated cartilage is a trouble some thing & that once destroyed, is not repaired", quoted William Hunter in 1743, acknowledging the inadequacies of human technology to deal with cartilaginous tissues (Buchanan, 2003). A quick survey of the term osteochondral on the pre-eminent biomedical search engine PubMed (Fig. 2C 1) indicates an increase in rate of publications using the keyword "Osteochondral" from the 1940's onwards. In a world beset with problems related to coping with an aging population, increased risk of microcirculation disorders, the surge in studies is expected.

2.2 Anatomy of Cartilage and Subchondral Bone:

The **Osteochondral Complex** basically is overlying cartilage built on underlying bone compartment.

Cartilage tissue is biochemically largely comprised of water, chondrocytes, type II collagen and proteoglycan. (Yang and Temenoff, 2009). Cartilage can be discriminated into four distinct zones: the superficial, the middle, the deep and the calcified cartilage zones (Madry et al., 2010a). The zones are defined by the particular composition and the organization of cells and also extracellular matrices. The ECM material content of the layers and its orientation to cellular and non cellular components influence the mechanical properties of each zone of cartilage. Preservation of these structural adaptations is key to the true functioning of the cartilage layers in its native functional role (Bohdan et al., 2007).

Bone is a complex tissue, majority components are water, collagen type I & hydroxyapatite (HA). Collagen type I and HA provide majority of the structural support integral to the tissue's stiffness and compressive strength (Arvidson *et al.*, 2011). Compressive modulus of the underlying bone is higher than that of cartilage with the varying morphological compositions of bone and cartilage indicating the complexity of the tissue interface.

The **Osteochondral interface (Fig. 2C 2)** can be defined as the zone of interaction of calcified cartilage and underlying bone. Thus it is a harmonious intercalation of articular cartilage and underlying subchondral bone (Madry et al., 2010b). This vital region has a multifaceted architecture (Lyons et al., 2007) connecting the articular cartilage through the calcified cartilage with the subchondral bone. A classic Osteochondral interface can be illustrated in the case of the knee joint which can be described as complex, synovial, & diarthroidal. The components of the osteohcondral compartment therein can be broken down as follows.

2.3 Articular Cartilage

Articular Cartilage is highly specialized connective cartilage tissue that provides a low friction surface for joints to allow easy articulation with lack of trauma. It is characterized by a distinct lack of vascularization, low cellularity and limited metabolic activity of the matured cell population i.e. chondrocytes. The majority cell type is mature chondrocytes within this tissue and are a key & unique feature (Newman, 1998).

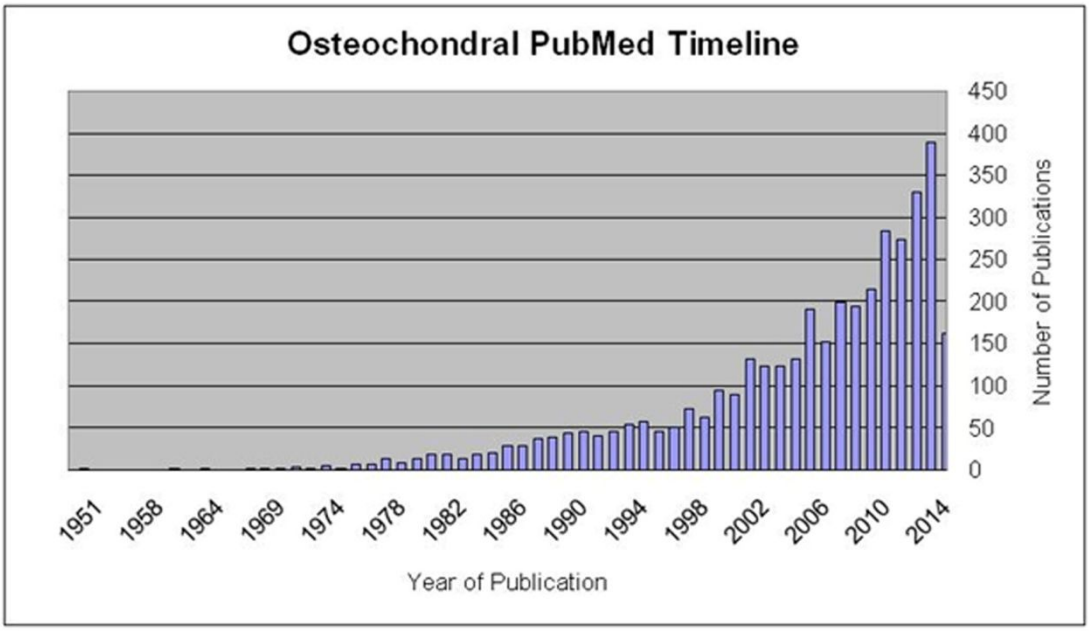

Fig. 2C 1: Frequency of Occurence of term "osteochondral" in PubMed Database

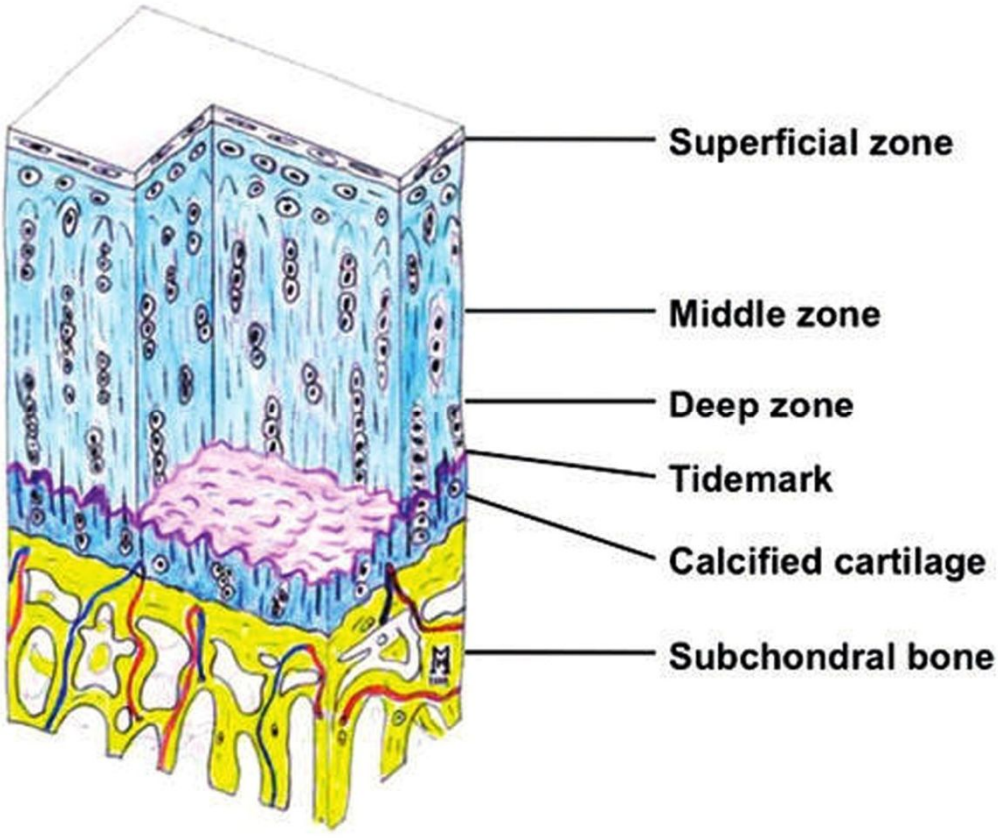

Fig. 2C 2: Diagrammatic representation of Osteochondral Interface

Type II collagen is the prevalent collagen here with proteoglycans (PG) forming the fundamental component of the extracellular matrix (ECM). PG's are negatively charged and provide a water retention property (65 – 80 % wet weight) within cartilage. This is key to the property of cartilage to undergo load dependent deformation (Minas, 2012). It has a highly anisotropic structure and has layers composed of varied cell and collagen fibril orientation. The superficial zone contains small flattened chondrocytes relative to inner layers and finds collagen fibers oriented tangentially to articular surface. Transition zone has rounded chondrocytes which synthesize collagen type II and aggrecan also in the presence of obliquely oriented collagen fibers. The deep radial zone has chondrocytes arranged in columns and collagen fibers that are perpendicular to the articular surface and parallel to each other (Becerra et al., 2010). A layer of calcified cartilage connects articular cartilage to the subchondral bone plate and is 20-25 μm thick (Hoemann et al., 2012). It is separated from articular cartilage by the tidemark a basophilic line on histological sections (Broom and Poole, 1982); (Lyons et al., 2005). The calcified cartilage regions also contain type X collagen with type II collagen fibrils extending from the non – calcified articular cartilage to the underlying calcified layers. The organization of the tissue in the above mentioned layered structure is critical to the functionality of articular cartilage which is the high fidelity reproduction of these layers and orientation of ECM fibers remain a challenge (Huey et al., 2012). A closer look at the two definite regions of the Osteochondral junction is thereby warranted.

2.3.1 Subchondral Region

The subchondral region bone is composed primarily of the subchondral bone plate and subarticular spongiosa. The few intervening spaces are closed off by the coming together of cancellous bone plates in the subchondral bone plate. This is usually thin in the normal human subchondral bone (Hunziker, 2002). In the case of OA the spaces are broader and denser. The subarticular spongiosa is formed from the gradual enlargement, elongation of the subchondral bony structures in a direction parallel to the diaphysis in deeper regions. There in the subchondral bone plate has low porosity while porosity of the subarticular spongiosa is much larger (Madry et al., 2010a).

The cement line is the junction of the calcified cartilage with the subchondral bone. This connection is of major importance in the development of osteochondral integration. This site is active remodeling with lack of collagen fiber transition (Type II and Type X collagen) from upper layers to the subchondral bone. To note, a surprisingly high number of blood vessels exist. Nerve fibers do send minute branches through canals in the subchondral bone plate into the calcified cartilage. Thereby ensuring nutrient, gas perfusion of the chondrocytes in the calcified and articular cartilage layers (Pan et al., 2009). Thus the osteochondral connection is neither impermeable nor inactive but forms a key connection in allowing mechanical, biochemical & transport interactions throughout.

Current Scenario

The treatment of cartilage and cartilage plus subchondral bone injuries has become a major interest area for doctors as the majority of lesions on this area do heal spontaneously and does predispose the joint to “early onset” secondary osteoarthritis (Habermeyer et al., 2006). This has lead to the development of several surgical interventions (Safran et al., 2008). Non-surgical interventions lack uniformity in the healing process and result in further interventions necessitated over a period of time (Shearer et al., 2002). Surveys of knee arthroscopy estimate that nearly 60% of all patients, though asymptomatic have articular cartilage defects (Curl et al., 1997). 66% patients in a survey of non-related arthroscopies had evidence of preliminary articular cartilage pathology, with 11% exhibiting localized full depth lesions that were amenable to further therapeutic interventions (Arøen et al., 2004). Prevalence is higher in the case of athletic population wherein about 36% of the survey population had full thickness chondral defects (Flanigan et al., 2010).

2.4 Focal Lesions and Natural Repair of Articular Cartilage

During traumas, shear forces lead to a separation of cartilage between the radial and the calcified layers (Levy et al., 1996). Focal defects are classified as either **chondral** or **osteochondral**.

2.4.1 Chondral lesions lie entirely within the cartilage and do not penetrate beyond the calcified zone into the subchondral bone. In these cases since access to vasculature is restricted, the lesions lack healing and are analogous to early phase osteoarthritis lesions (Mankin, 1974) (Kim et al., 1991).

2.4.2 Osteochondral defects penetrate the articular surface in depth through the vascularised subchondral bone. Mesenchymal chondroprogenitor stem cells invade the lesion, differentiate into chondrocytes and attempts to form cartilage which can be visualized (Shapiro et al., 1993b). The repair effects are only transient with observations that the repair tissue is fibrous in nature, does not have the functional properties of native hyaline cartilage, and thus results more vulnerable to the action of free radicals, metalloproteinases and catabolic cytokines including IL-1 and TNF-α (Pelletier et al., 1993) (Tyler, 1985). Osteoarthritis onset is characterized by formation of clefts and fissures on the articular surface due to matrix breakdown (Buckwalter, 1998).

Articular cartilage has intrinsic deficiencies in healing that are reinforced by its unique architecture which is reflected in biophysical function based design.

1. the mature chondrocytes have a relatively low metabolic activity and proliferation capacity and the abundant extracellular matrix may provide a barrier for their migration to the defect;
2. articular cartilage being neither vascularised nor penetrated by lymphatic vessels, there is no direct access to progenitor cells; furthermore, the supply of growth and differentiation promoting factors is ensured only by diffusion from the synovial fluid;
3. some of the proteoglycans of the matrix have anti-adherent properties and may prevent cell adhesion, further undermining any tentative repair process;

herein may also lie the difficulty of achieving a good integration between repair tissue and native cartilage;

4. Finally, articular cartilage is not innervated and thus insensitive to early injuries that can readily progress to degeneration much before evident clinical symptoms emerge.

2.4.3 Classification of Lesions

Articular cartilage lesions present with focal pain and associated inflammation with sudden onset in the case of trauma, or diffuse pain in the case of temporal degradation of structures associated with the surface. The Outerbridge Classification recognizes lesions based on their structural manifestation and depth of affected areas (Cameron et al., 2003). Cartilage lesions when mild, present as normal appearing cartilage on explorative arthroscopy, and are difficult to discern between lesion borders and normal cartilage. Mild fibrillation or discoloration of affected tissue with tissue softness exaggerated on palpation is a sign of injury. Linear cracks may present with split thickness depths and is associated with ligament injuries. Stellate cracking is the most common traumatic lesion with a divergence of normal tissue structure with central flaking. Flap tears occur when cartilage is avulsed from underlying bone, with fibrillation when entire cartilage layer to subchondral bone is not removed. Full thickness defects present with exposure of subchondral bone. Under degradative conditions, tissue undergoes diffuse degradation and presence of bone spurs, where anomalous tissue structures can be visualized.

The Outerbridge Classification takes in to account the above described traumatic presentations of articular cartilage and underlying bone to provide the following classification (Cameron et al., 2003):

2.4.4 Outerbridge Classification:

- Grade 0: normal cartilage;
- Grade I: cartilage with softening and swelling;
- Grade II: a partial-thickness defect with fissures on the surface that do not reach subchondral bone or exceed 1.5 cm in diameter;
- Grade III: fissuring to the level of subchondral bone in an area with a diameter more than 1.5 cm;
- Grade IV: exposed subchondral bone.

Total joint replacement using artificial prostheses eliminates pain and restores functionality but is limited by the lifespan of the device versus the need of the user. In particularly young users it is mandatory that alternative processes are identified by which revision surgeries with inherent risks & costs can be avoided. The complexity of articular cartilage structure and the peculiarity of its biological/biophysical features necessitate the diversified therapeutic approaches that have been developed and are being investigated to regenerate osteochondral lesions and restore joint functionality. The following is an overview of these.

2.4.5 Current Interventions:

In the late 1980's there was a wave of cartilage repair techniques that undertook the technique of marrow stimulation techniques, where in exposure of the marrow compartment in the defect region was purported to spur the healing process by tapping in to the available stem cell pool. Abrasion arthroplasty and Pridie (subchondral bone) drilling was undertaken extensively to clear lesion of damaged articular cartilage & non – viable tissues. Following this subchondral bone plate was damaged to encourage access to the marrow compartment (Gomoll, 2012).

2.4.5.1 Microfracturing

Microfracturing is the most widely used cartilage repair technique, with more than 76,000 procedures reported in 1999 in the U.S. only (Jackson et al., 2001a). The procedure, which is generally performed arthroscopically, consists in perforating the subchondral plate of (osteo) chondral defects by multiple holes, thus allowing marrow-derived mesenchymal progenitor cells to reach the lesion and form new cartilaginous matrix (W. Norman Scott MD, 2011). The technique is popular as it is easy to perform, with low morbidity & overall appeasement of clinical symptoms, however, the tissue generated after microfracturing was shown to lack the structure, composition, mechanical properties, and in most instances the durability of articular cartilage (Buckwalter and Lane, 1997a).

2.4.5.2 Autologous Periosteal Transfer

The technique consists in harvesting autologous periosteal tissue from the medial proximal tibia and suturing it into the defect, thereby introducing a new cell population along with an organic matrix (Lorentzon et al., 1998). Animal experiments and clinical practice indicates that periosteal grafts placed in articular cartilage defects can produce native cartilaginous tissue. But increasing patient age adversely affected the results (Buckwalter and Lane, 1997b) with scattered reports of not totally satisfactory outcomes (Hoikka et al., 1990).

2.4.5.3 Autologous Osteochondral Transfer

The technique, also called mosaicplasty, consists in harvesting osteochondral cylinders from a joint area of minor load and press-fitting them into predrilled holes at the defect site (Hangody et al., 2001). Based on graft integration, it was concluded that small symptomatic osteochondral or cystic lesions are appropriate indications for this technique (Minas and Nehrer, 1997). However, due to the limited availability of donor tissue and the induced morbidity at the donor site, the recommended size limit of the damaged area is only about 2 cm^2. This implies its application only in lesions graded at level III or IV on the Outerbridge Classification.

2.4.5.4 Fresh Osteochondral Allograft

The technique, used in cases of unconfined, extensive cartilage defects, consists in transplantation of osteochondral tissue from compatible donors. Clinical results indicate successful treatment of large unipolar osteochondral defects, although an unloading period of 1 year after surgery is required (Ghazavi et al., 1997). The procedure strongly depends on the access to osteochondral grafts from a sufficient number of donors, in order to minimise size mismatch between donor and recipient, and is therefore limited to few specialised centers with the main risk factors being disease transmission, need for patient compliance and existing infrastructural facilities for the procedure (Lipscomb and Masten, 2002).

2.4.5.5 Autologous Chondrocyte Implantation

Autologous chondrocyte implantation (ACI) consists in harvesting healthy articular cartilage from a minor weight bearing area of the knee joint. Chondrocytes are enzymatically isolated, expanded in monolayer culture and then reinjected under an autologous periosteal flap, which covers the cartilage defect. A pilot clinical study (Brittberg et al., 1994) was judged as good to excellent in 14/16 patients with isolated femoral condyle lesions (up to 6.5 cm^2 in size). Peterson et al (Peterson et al., 2000) reported the clinical, arthroscopic and histological results obtained for the first 101 patients that were treated with ACI.

Results (good to excellent results for 92% of isolated lesions and for 67% of multiple lesions), although the lack of comparative groups and of validated assessment methods is a noted weakness.

Biopsy samples from the graft site, harvested up to 30 months after surgery, indicated an initial formation of fibrocartilaginous tissue, which progressively remodelled and where newly synthesised type II collagen accumulated (Roberts et al., 2001). Biopises from the center of the defect do not reflect total joint integration. ACI is limited with regard to the form of graft fixation as well as delamination of flap structures post sugery with the resulting control over injected cells described as poor (Driesang and Hunziker, 2000). More advanced techniques with development

of synthetic matrices are being advanced with a keen interest on the future of this technique.

2.5 Tissue Engineering

For the ideal repair of osteochondral defects there is an integral need (Orth et al., 2013) to:

(a) Regenerate subchondral bone
(b) Facilitate zonal restoration of cartilage
(c) Mimic natural articular structure.

Tissue Engineering (TE), an interdisciplinary field of science that melds together biological components & engineering processes to facilitate the repair of damaged tissues, restoration of lost tissue function or replacement of damaged tissues provides an unique solution for addressing the challenges listed. TE would necessitate the usage of a support system, a 3-dimensional material that would conform to wound dimensions and would act as scaffolding / delivery device for appropriate building blocks as needed. Biomaterials form a group of natural, synthesized materials that when placed in a living system elicit specific and directed interactions with the system to produce a desired result (Williams, 2008).

Tissue Engineering places the onus on the success of interventions under its aegis on primarily the delivery system as well as the cells or building blocks added therein. A closer look at the demands on the system in the milieu of the osteochondral defect is thereby warranted.

2.6 Strategisation Hypothesis Development

"To identify a bioactive ceramic system to serve as a support system for Osteochondral applications in conjunction with adipose derived stem cell products"

The hypothesis statement can be further broken down in to working objectives to provide measurable milestones in the progression of the work.

Basic objectives can be defined as follows: the need to identify biomaterial structures; that will mimic native biological structures, provide ideal levels of integration into interfacial tissue, support growth & differentiation of cells and will be rapidly resorbed.

CHAPTER 3

MATERIALS & METHODS

3.1 Materials

Biphasic Calcium Phosphate (BCP) and Triphasic ceramic coated hydroxyapatite (HASi), synthesized as part of ongoing developmental programme of bioceramics in SCTIMST, Trivandrum, India, were gifted for this study to undertake a part of preclinical evaluation of these materials for osteochondral applications.

3.1.1 Material Synthesis

Materials were synthesized in house at the Bioceramics Laboratory, SCTIMST.

3.1.2 Synthesis of Triphasic Ceramic Coated Hydroxyapatite (HASi)

Hydroxyapatite powder was synthesized by wet precipitation method involving calcium nitrate and ammonium dihydrogen phosphate in the stoichiometric proportion at a pH of 11 and a temperature of 80ºC. The precipitated HA powder was freeze dried and washed with distilled water to get rid of surface impurities such as nitrate and ammonium ions. HA powder having particle size less than 125 microns was mixed with aqueous solution of poly vinyl alcohol and gluteraldehyde solution and stirred for 30 min. To the resulting frothy slurry, benzoyl peroxide dispersed in benzene and N, N- dimethyl aniline were added and stirred for thorough mixing. The resulting frothy and viscous slurry was poured into plastic moulds and allowed to dry at room temperature. After drying, the blocks were biscuit fired at 300ºC for 1h to remove the binder and then sintered at temperature between 1100°C and 1300°C for 1h to get porous HA. These blocks were then dipped in silica sol prepared by the hydrolysis of TEOS in ethanol-water system for 1 min (sol gel method) and sintered at 1200^{o}C for 2 h to get a coating of silica over HA.

3.1.3 Synthesis of Biphasic Calcium Phosphate

Biphasic Calcium Phosphate was synthesized by wet chemical *in situ* precipitation technique. Ammonium phosphate solution was added to calcium nitrate at a ratio of 1: 6. Further processing is as per Babu S et al (Sureshbabu et al.,). Here the

combination of HA and αTCP was synthesized as the second phase in this BCP composite. The materials were polished in the form of discs - 5mm diameter with 1-2mm thickness (for *in-vitro* studies) and subjected to ultrasonic cleaning (Cole Parmer, USA). Subsequently, the materials were sterilized by steam (121ºC, 15psi pressure for 15minutes) (Sureshbabu et al., 2012).

3.2 Material sterilization

Ceramic discs were polished in fixed dimensions required for each experiment. The discs were polished on a dedicated grindstone, sonicated in distilled water (Cole parmer) (3 times, 10 min each) for the complete removal of fine powders adhered over the surface. The materials were then sterilized by steam sterilization (121°C temperature and 15psi pressure for 15min) prior to *in vitro* and *in vivo* experiments.

3.3 Physicochemical Characterization

3.3.1 Elemental analysis

The BCP & HASi discs were examined under ESEM (FET Quanta 200) and the elements present in these areas (Ca, P and Si) were differentiated with Energy dispersive x-ray spectroscopy EDS- OXFORD X-ray- microanalysis software.

3.3.2 Phase analysis

The phase analysis and crystallinity checkup of BCP and HASi were done by X-ray diffraction technique (XRD). The materials were scanned between 20^{o} and 40^{o} 2 θ at a rate of 2º per minute under a step size of 0.02º using Cu-Kα1 radiation at a voltage of 40 kV and a current strength of 30 mA (Siemens D-5005).

3.3.3 Functional groups

Fourier Transform Infrared Spectroscopy (FTIR) analysis was conducted on Thermo Nicolet 5700 spectrometer and the spectra were collected in the diffuse reflectance (DRIFT) mode to determine the functional groups. BCP and HASi were powered

and mixed with optical grade KBr powder. The spectra were recorded at a resolution of 4 cm^{-1} and scanned between of 400 to 4000 cm^{-1} wave number range and average scan of 200. Pure KBr was used as the background.

3.4 Porosity studies

3.4.1 Scanning Electron Microscopy

BCP and HASi discs were gold coated in an ion sputter (Hitachi E101) and examined for the microstructure, including porosity and morphology by scanning electron microscope (SEM) (Hitachi S2400).

3.5 Isolation & Characterization of Adipose Derived Mesenchymal Stem Cells

Adipose Derived Stem Cells were isolated from the respective animal models as follows.

3.5.1 Isolation of Adipose Tissue from Rabbit

About 2g of adipose tissue retrieved from the suprascapular subcutaneous site of animal model, retrieved aspetically, was minced manually and mixed with an equal volume of 0.2% collagenase (Invitrogen) solution, digested at 37º C and filtered. The digest was centrifuged at 15º C for 10 mins at 2500 rpm & pellet re-suspended in DMEM – HG, seeded into T25cm^2 flask (NUNC) and maintained in culture with DMEM - HG containing 10% fetal bovine serum (FBS) and 50 units/ml of penicillin and 50 μg/ml of streptomycin (Gibco, Anti – Anti Mix) at 37ºC under 5% CO_2 atmosphere. Medium was first changed within sixteen hours of plating and cells were fed every three days until confluency (Fig.3C 1).

(A) NZW Rabbit

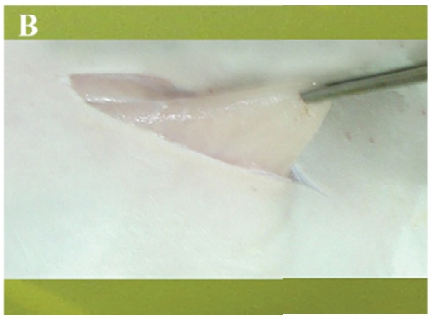

(B) Subcutaneous fat accessed

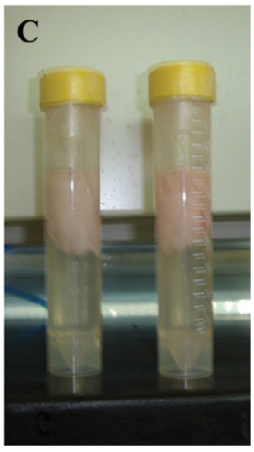

(C) Fat collected in saline + Ab

(D) Isolate is cleaned and minced

(E) Vacuum filtration after collagenase digestion

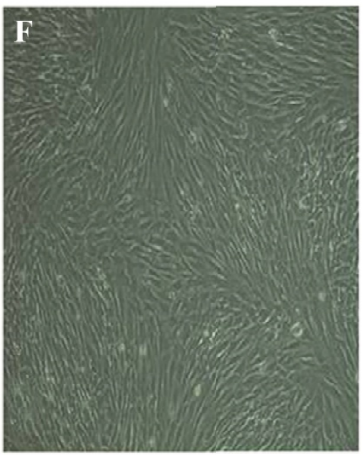

(F) Cells in TC flask (Phase contrast image)

Fig. 3C 1: Rabbit Adipose Tissue Isolation

3.5.2 Isolation of Adipose Tissue from Goat

About 5g of adipose tissue retrieved from the subcutaneous site of animal model, retrieved aspetically, was minced manually and mixed with an equal volume of 0.2% collagenase (Invitrogen) solution, digested at 37º C and filtered. The digest was centrifuged at 15º C for 10 mins at 2500 rpm & pellet re-suspended in DMEM – HG, seeded onto T25cm^2 flask (NUNC) and maintained in culture with DMEM - HG containing 10% fetal bovine serum (FBS) and 50 units/ml of penicillin and 50 μg/ml of streptomycin (Gibco, Anti – Anti Mix) at 37ºC under 5% CO_2 atmosphere. Medium was first changed within sixteen hours of plating and cells were fed every three days until confluency (Fig.3C 2).

Adipose Derived Stem Cells as ADMSC, Rabbit Adipose Derived Stem Cells are referred in text as **RADMSC** & Goat Adipose Derived Stem Cells are referred in text as **GADMSC**.

3.6 Characterization of ADMSC

ADMSCs from rabbit and goat were characterized using a common protocol, the details of which are described below.

3.6.1 Actin and Nuclear staining

ADMSCs (1 x 10^4 cells in passage 2) after culturing for 24 h on glass cover slips (Blue star India) were washed with PBS and fixed with 3.7% paraformaldehyde in Sorensen's phosphate buffer. The fixed cells after washing with PBS were permeabilised using 0.1% Triton X-100 (Sigma Chemicals) in PBS. After washing three times with PBS, cells were stained with rhodamine-phalloidin (1: 1000 in PBS) (Invitrogen) overnight in a humidifying chamber followed by staining with DAPI for 30mins (1: 100 in PBS) (Sigma Chemicals) in the dark at room temperature for determining actin filament (red) and nucleus (blue) respectively. The cells were then washed thoroughly with PBS and imaged using confocal laser scanning microscopy (Carl Zeiss 510 META).

(1) Site Preparation

(2) -(3) Accessing Subcutaneous Fat Tissue

(4) Explantation of Tissue Sample

(5) Site Closure

Fig. 3C 2: Goat Fat Isolation

3.6.2 Flow cytometric analysis of CD 34, CD 90 & CD 105.

ADMSCs ($1x10^5$ cells in passage 3) were washed with PBS; trypsinized with 0.25% trypsin-EDTA for 5 min and centrifuged at 300g for 10 min. The pellet was fixed with 3.7% paraformaldehyde in Sorensen's phosphate buffer for 5 min, washed with PBS and centrifugation at 2500 rpm for 10 min at 4°C. The pellet was blocked with 3% BSA in PBS for 30 min followed by washing with PBS and centrifugation.

Each pellet with approximately $1x10^5$ cells was then incubated with CD34 (sc-65261) (1: 50), CD 105 (sc-71042) (1:100) and CD 90 (ab225) (1: 100 in 3% BSA) (Invitrogen, India) for 1 h and the intensity of fluorescence was recorded under flow cytometry (BD Biosciences, FACS Aria). ADMSCs with secondary staining, but trypsinized, fixed and washed under the same conditions were used as the control.

3.6.3 Osteogenic Differentiation of Adipose Derived Mesenchymal Stem Cells

ADMSC's ($1x10^5$ cells in passage 3) were cultured in DMEM - HG with 10% FBS for 24 h in order to facilitate the initial cell adhesion. After 24 h, these cells were induced to differentiate into the osteoblast lineage by maintaining in osteogenic medium (DMEM-HG with 15% FBS, 10 mM β- glycerophosphate, 10^{-8} M dexamethasone, 0.05 mg/ml L-ascorbic acid (Sigma chemicals), 100 units / ml of penicillin and 100 μg / ml of streptomycin).

3.6.3.1 Collagen staining

ADMSCs after culturing in osteogenic medium for 28 days were fixed in 3.7% paraformaldehyde in Sorensen's phosphate buffer for 20 min. After washing with PBS, the cells were incubated in Bouin's solution at 56°C for 5 min; cooled in tap water at 18 - 20°C and stained with Wright's hematoxylin for 5 min. It was then washed with schott's tap water and stained with trichrome stain for collagen (Sigma chemicals) for 5 min. The cells were again washed with distilled water; incubated with 0.5% glacial acetic acid for 1 min followed by washing with PBS, clearing in xylene, mounting in DPX and viewing under Light microscope (Leica DM 6000).

3.6.3.2 Calcium staining

ADMSCs after culturing in osteogenic medium for 28 days were fixed in 3.7% paraformaldehyde in Sorensen's phosphate buffer; washed with PBS and stained with 1% alizarin red (Sigma, India) in distilled water. It was then viewed under Light microscope Leica DM 6000 imaged for alizarin red staining respectively.

3.6.3.3 Phosphorous staining

ADMSCs after culturing in osteogenic medium for 28 days were fixed in 3.7% paraformaldehyde in Sorensen's phosphate buffer; washed with distilled water; stained with 5% silver nitrate (Merck, India) in distilled water and exposed to ultraviolet light for 12 min. The cells were then thoroughly washed with distilled water, air dried, mounted with DPX (Sigma Chemicals) and viewed under Light microscope (Leica DM 6000).

3.6.4 Chondrogenic Differentiation of Adipose Derived Mesenchymal Stem Cells

ADMSCs ($1x10^6$ cells in passage 3) were cultured in DMEM – LG, trypsinized and pelleted down in 15 ml tubes (Axygen, India). The cells were further cultured in DMEM - LG containing 15% FBS supplemented with 10ng/ml TGF-β1 (Imperial), ITS Premix (BD Biosciences) 25 µg of Ascorbate & 10^{-8} M Dexamethasone (Sigma), Antibiotics (Penicillin/streptomycin) in an incubator at 37º C and 95% RH with 5% CO_2.

3.6.4.1 Paraffin Processing & Sectioning

Pellets at 28 days were washed in PBS and fixed in 3.7% paraformaldehyde (Sigma). Pellets were dehydrated in a descending series of ethanol, cleared with xylene and embedded in paraffin. Sections were cut (5µm) thickness and stained for further study.

3.6.4.2 Safranin O Staining

This is a cationic dye stain for acidic proteoglycans present in cartilage and used for visualization of cartilage structures. Paraffin sections on slides are deparaffinized and hydrated to distilled water. Stained in 0.1% Safranin O solution for 5 minutes. The sections are dehydrated, cleared with 95 % alcohol to absolute alcohol ending in xylene with 2 changes for 2 minutes each. Sections are mounted using DPX and visualized under Leica DM 6000.

3.6.3 Alcian Blue Staining

This is a mucin stain for visualization of sulfate and carobxylated acid mucopolysaccharides and sulfated glycosaminoglycans in cartilage structures. Paraffin sections on slides are deparaffinized and hydrated to distilled water. A 1% solution of Alcian Blue (Sigma) with pH adjusted to 2.5 with acetic acid is used for 30 mins. Slide is rinsed in running distilled water, dehydrated, cleared with 95 % alcohol to absolute alcohol ending in xylene with 2 changes for 2 minutes each. Sections are mounted using DPX and visualized under Leica DM 6000.

3.7 Evaluation of tissue-engineered constructs *in vitro* - Bioactive ceramics in conjunction with ADMSCs

Cells in conjunction with candidate ceramic structures were evaluated as follows.

3.7.1 Culturing ADMSC's on Ceramic Constructs

ADMSCs of passage 3 to 5 were used for culturing on BCP & HASi. Cells were trypsinized with 0.25% Trypsin EDTA and collected by 2500 rpm centrifugation for 10 mins. Cells were suspended in "T" ml of media. Cells were counted manually using haemocytometer with counter – staining by Trypan Blue for ensuring cell viability. Required number of cells (Rn) per material was calculated by the following formula. Rn/Y ml = Viable cells in haemocytometer observation / T ml (volume of cell suspension)

3.7.2 Pre- conditioning & Seeding of Cells

Discs after sterilization were pre-conditioned by 24 hr immersion in growth media prior to seeding with cells (DMEM, 10% FBS, 1% Ab). ADMSCs were then seeded on all sides of conditioned BCP and HASi placed in 48 well Tissue Culture Plate (TCP) under static condition and cultivated in DMEM with 10% FBS for 24h in order to facilitate initial cell adhesion.

After 24h, the first batch of cells on ceramic scaffolds were induced to differentiate into osteogenic lineage by providing **osteogenic** medium (α-MEM with 15% FBS, 10 mM β- glycerophosphate, 10^{-8} M dexamethasone, 0.05 mg/ml L-ascorbic acid (Sigma chemicals), 100 units / ml of penicillin and 100 μg / ml of streptomycin). The osteogenic medium change was done twice weekly.

After 24 h, the second batch of cells on ceramic scaffolds were differentiated into chondrogenic lineage by providing **chondrogenic** medium, DMEM - LG containing 15% FBS supplemented with 10ng/ml TGF-β1 (Imperial), ITS Premix (BD Biosciences) 25 μg of Ascorbate & 10^{-8} M Dexamethasone (Sigma), Antibiotics (Penicillin/streptomycin) in an incubator at 37º C and 95% RH with 5% CO_2. Medium change was carried out twice weekly.

3.8 Evaluation of Tissue Engineered Constructs – Preliminary in vitro Screening.

3.8.1 Adhesion of ADMSC

The cell-seeded materials were fixed in 1% gluteraldehyde in Sorenson phosphate buffer (pH 7.4); rinsed with PBS; dehydrated in a graded ethanol series (Merck, India) (increasing concentrations of ethanol in distilled water: 30% ethanol for 10 min - 2 changes, 50% ethanol for 10min - 2 changes, 70% ethanol for 10min - 2 changes, 90% ethanol for 15 min -2 changes and 100% ethanol for 15 min - 2 changes); critically point dried (Hitachi HCP-2), gold sputtered in vacuum (Hitachi E101) and examined by means of secondary imaging under 15 kV SEM (Hitachi S 2400).

3.8.2 Viability of ADMSC on Bioactive Scaffolds.

3.8.2.1 Acridine Orange and Ethidium Bromide Staining – Confocal Microscopy

The viability of ADMSCs at 72h on BCP & HASi was determined qualitatively by confocal laser scanning microscope (cLSM). For this, the cell-seeded materials were stained with 100 µl of acridine orange (10 µg / ml PBS) (Sigma chemicals) and ethidium bromide (15 µg / ml PBS) (Sigma chemicals) for 10 min. It was then washed with PBS, destained of excess stain in PBS for 15 mins and imaged with cLSM (Carl Zeiss LSM 510 Meta) at an excitation and emission wavelength of 480 / 526 and 518 / 605 for acridine orange and ethidium bromide respectively. The excitation of acridine orange and ethidium bromide was carried out with Argon/2 laser. Green coloured cells were marked as live and red coloured as dead.

3.8.3 Differentiation: Viability – Osteogenic

Viability of adipose derived stem cells under differentiation conditions on scaffold surfaces was evaluated.

3.8.3.1 Viability of Osteogenically Differentiated ADMSC's on Ceramic Constructs

3.8.3.1.1 Confocal Laser Scanning Microscopy

The viability of osteogenically induced ADMSC was determined qualitatively as mentioned in section **3.8.2.1**. Cells seeded on scaffold were evaluated after 72 h with confocal laser scanning microscopy.

3.8.3.1.2 Lactate Dehydrogenase Assay

The cell viability was determined quantitatively through the total activity of lactate dehydrogenase (LDH) in the cell lysates using LDH reaction buffer (Cytotox96 kit, Promega, USA) It is measured in an enzymatic reaction that occurs in two steps (1)

NAD+ is reduced to NADH/H+ by the LDH catalysed conversion of lactate to pyruvate (2) The catalyst (diaphorase) transfers H/H+ of NADH/H+ to the tetrazolium salt INT which is reduced to formazan. This leads to colour change from pale yellow to red.

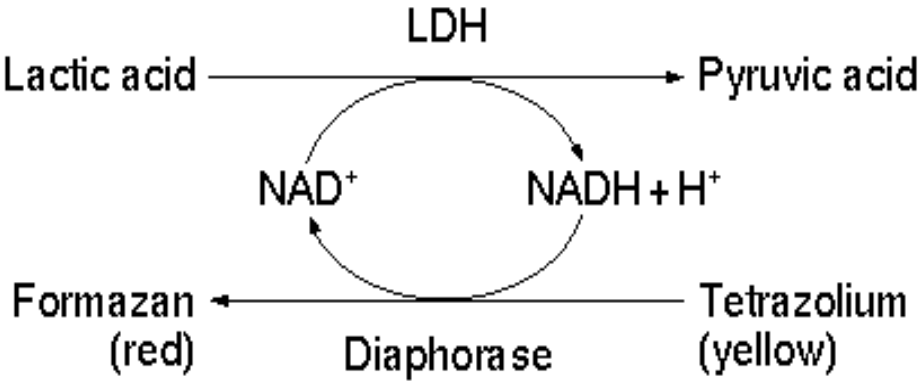

The viability of osteogenically induced ADMSCs on day 7, 14 and 21 days of culture were measured. For this, the cell-seeded materials (n=3) were washed with PBS twice and kept in -80°C until analysis. Frozen cell samples were thawed for 20 min on ice and lysed with 1% Triton X-100 (300 µl) for 50 min with sonication for 10 min. An aliquot of each cell lysate (50µl) was mixed with LDH substrate (50µl) at room temperature and the enzymatic reaction was stopped after 30 min with 0.1 M acetic acid (50µl). The absorbance was read at 492 nm (Chameleon Plate Reader). The absorbance (OD values) was correlated with cell viability using a calibration line constructed from cell suspensions with increasing concentrations of cell numbers.

3.8.3.2 Proliferation of Osteogenically Induced ADMSCs

3.8.3.2.1 Picogreen Assay

The proliferation of ADMSCs differentiated in to osteogenic lineage were determined on day 7, 14, and 21 was determined using Picogreen® dsDNA Quantitation reagent (Molecular probes). For this, the cell-seeded materials (n=3) were washed with PBS twice and kept in -80°C until analysis. Frozen cell samples were thawed for 20 min on ice and lysed with 1% Triton X-100 (300 µl) for 50 min with sonication for 10 min. The lysate (10µl) was then mixed with picogreen in Tris-EDTA buffer (190µl) for 5 min and the intensity of fluorescence was measured with a multifunction microplate reader (Chameleon) at an excitation and emission wavelength of 485 / 535 nm.

Relative fluorescence units were correlated with cell number using a calibration line constructed from cell suspensions with increasing concentrations of cell numbers.

3.8.4 Differentiation Potential of ADMSCs

3.8.4.1 Alkaline Phosphatase Activity – Biochemical Estimation

The effect of osteogenic medium on cells seeded on BCP & HASi scaffolds were determined through ALP activity, based on the hydrolysis of p-nitrophenyl phosphate (Sigma chemicals) to p-nitrophenol. For this, ADMSCs of passage number 1 to 6 were seeded ($1x10^5$ cells) separately on 6 well TCPS plates (n=3) for 7 days. The cells were washed with PBS twice and kept in -80°C until analysis. Frozen cell samples were thawed for 20 min on ice and lysed with 300µl 1% Triton X-100 for 50 min with sonication for 10 min. The cell lysate (25 µl) was added to ALP reaction buffer (125 µl) containing 1mM $MgCl_2$, 0.1 M diethanolamine and 1% Triton X-100 (pH 9.8) (Sigma chemicals) and the mixture was incubated at 37°C for 30 min. 1 M NaOH was added to stop the enzymatic reaction. After centrifugation at 16,000 g for 10 min, 170µl of each supernatant was transferred to a microtiter plate (NUNC) and the absorbance was read at 405 nm (Chameleon). A calibration line

was constructed from different concentrations of p-nitrophenol (Sigma, India). The ALP activity measured from each samples was related to the cell number in order to calculate the specific ALP activity for each sample.

The cell number was calculated by using Picogreen® dsDNA Quantitation reagent (Molecular probes). The cell lysate (10µl) prepared above was mixed with picogreen in Tris-EDTA buffer (190µl) for 5 min and the intensity of fluorescence was measured with a multifunction microplate reader (Chameleon) at an excitation and emission wavelength of 485 / 535 nm.

Relative fluorescence units were correlated with cell number using a calibration line constructed from cell suspensions with increasing concentrations of cell numbers.

3.8.4.1 Real-time PCR analysis

The expression of ALP, osteopontin and osteocalcin on osteogenically differentiated cells in 6 groups of BCP & HASi was evaluated after 7, 14, 21 and 28 days of cultivation. The RNA was isolated by TRIzol reagent (Sigma, India) as per manufacturer's instructions.

Cell-seeded materials were recovered from culture medium, washed with RNAse free water and treated with 500µl TRIzol reagent for 10 min and stored at -80°C until analysis. After thawing at room temperature, 100µl of chloroform was added for 15 min followed by centrifugation at 12,000g for 15 min at 4°C. The clear supernatant (top layer) was transferred to a fresh tube and mixed with 250µl of isopropyl alcohol for 10 min at room temperature for precipitating RNA followed by centrifugation at 12,000g for 8 min. The pellet was washed with 70% ethanol in RNase free water (Invitrogen, India) with centrifugation at 12,000g for 8 min. The pellet was air dried and added with 50µl RNase fee water and incubated at 55°C for 10 min. The yield of RNA was determined spectrophotometrically.

The first strand cDNA was then synthesized from 1 µg of total RNA, 5 µl MLV reverse transcriptase (50U / µl), 5 µl stratascript buffer (10x), 1µl RNase inhibitor (40U / µl), and 4 µl random hexamer (10pmole) and 2 µl dNTP mix (10mM)

(Invitrogen, India) for a 50µl RT reaction using the Thermal cycler (Master Cycler, Eppendorf, USA). The real-time PCR was performed using a Chromo4 system (MJ Research, USA). All reactions were carried out in a total volume of 20 µl, containing 10µl full velocity SYBR Green Master mix (Stratagene,USA), 1µl forward and 1µl reverse primer (10 picomole) and 8 µl cDNA at an annealing temperature of 50 - 55°C (depending upon the primers) over 35 cycles. The primers that were designed are listed in Table 2 (Sources are attributed in following table, conditions as per recommendation). The annealing temperatures for β actin, ALP, osteopontin and osteocalcin gene are 52, 51, 53 and 59°C respectively or as specified in each reference. For each gene, the quality and specificity was assessed by examining PCR melt-curves following real-time PCR. The results were normalized by being expressed relative to the amount of β-actin mRNA determined. The results of the expression of ALP, osteopontin and osteocalcin on day 7, 14, 21 and 28 were represented as fold increase.

Rabbit Osteogenesis		
Gene	**Sequence (5'-3')**	**Reference**
ALP	F:5' GGAC CATT CCCA CGTC TTCA C 3' R:5' CCTT GTAG CCAG GCCC ATTG 3'	(Ming et al., 2013)
Osteocalcin	F:5'CCCAGGCGCTACCTGTATCAA3' R:5' GGTCAGCCAACTCGTCACAGTC 3'	
Osteopontin	F:5'GCCGACCAAGGAAAACTCACT 3' R:5'GGCACAGGTGATGCCTAGGA3'	

Table. 1: Real – Time PCR Analysis - Primers used in Rabbit Osteogenesis Assay

Goat Osteogenesis		
Gene	**Sequence (5'-3')**	**Reference**
ALP	CGTGGCTAAGAATGTCATCATGTT TGGTGGAGCTGACCCTTGA	(Xiao et al., 2003)
Osteocalcin	GCAAAGGTGCAGCCTTTGTG GGCTCCCAGCCATTGATACAG	
Osteopontin	ACATCCAGTACCCTGATGCTACAG GGCCTTGTATGCACCATTCA	

Table 2: Real – Time PCR Analysis - Primers used in Goat Osteogenesis Assay

3.8.5 Differentiation – Viability - Chondrogenic

3.8.5.1 Viability of Chondrogenically Differentiated ADMSCs on Ceramic Constructs

Viability of adipose derived stem cells under chondrogenic differentiation conditions were evaluated as follows.

3.8.5.2 Confocal Laser Scanning Microscopy

The viability of chondrogenically induced ADMSCs was determined qualitatively as mentioned in section **3.8.2.1.** Cells seeded on scaffold were evaluated after 72 h with confocal laser scanning microscopy.

3.8.5.3 Lactate Dehydrogenase Assay

The cell viability was determined quantitatively through the total activity of lactate dehydrogenase (LDH) in the cell lysate using LDH reaction buffer (Cytotox96 kit, Promega, USA). Chondrogenically induced ADMSCs on BCP & HASi were evaluated on 7,14 & 21 days. For details refer **3.8.3.1.2**

3.8.6 Proliferation of Chondrogenically Induced ADMSCs

3.8.6.1 Picogreen Assay

The proliferation of ADMSCs differentiated in to chondrogenic lineage were determined on day 7, 14, and 21 was determined using Picogreen® dsDNA Quantitation reagent (Molecular probes). For detailed protocol refer section: **3.8.3.2.1**

3.8.7 Chondrogenic Differentiation Potential – GAG Analysis

The effect of chondrogenic medium on cells seeded on BCP & HASi scaffolds were determined through estimating the total amount of glycosamionglycans synthesized over a period of time. GAG was estimated using a Blyscan Kit from Bicolor according to manufacturer's instructions with a papain extraction step. The Blyscan Assay is a quantitative dye - binding method for the analysis of sulfated proteoglycans and glycosaminoglycans, (sGAG). The dye label used in the assay is 1, 9- dimethylmethylene blue and the dye is employed under conditions that provide a specific label for the sulfated polysaccharide component of proteoglycans or the protein free sulfated glycosaminoglycan chains.

For this, ADMSCs of passage number 3 were seeded ($1x10^5$ cells) on materials (n=3) for periods of 7, 14, 21, & 28 days. The matrices on retrieval from cell culture medium were washed with PBS and stored at – 80°C till analysis.

Papain Extraction was carried out as follows. Papain (Sigma P3125) 5 mg was added to 50 ml of a 0.2M sodium phosphate buffer, (Na2HPO4–NaH2PO4), pH 6.4 papain extraction buffer. This is referred to further as the extraction reagent.

The solution is stable at 4°C for 14 days. Discs for analysis are retrieved from the deep freezer and placed in 1 ml of extraction reagent, at 65 °C for 3 hours in a heating block. Tubes are spun down at 10,000g for 10 mins and supernatant collected for further analysis.

Sample aliquots of are normalized to 100µl with distilled water and to each tube 1.0 ml of Blyscan dye reagent is added and agitated on MixMate (Eppendorf, Germany) for 30 mins at 300 rpm. Tubes are spun down at 12,000 rpm for 10 minutes (Eppendorf 5410 R) to firmly pack the dye – sample complex within tubes. Tubes are inverted on tissue paper and drained with gentle tapping. 0.5ml of the dissociation agent is added to each tube and vortexed thoroughly (Vortex Genie, Remy India). Foam if any is settled using a quick centrifugation. 200 µl of each sample is transferred to a 96 – well plate for absorbance measurement (580 nm, Chameleon). Sample concentrations are derived from the standard curve obtained by testing kit standards.

3.8.8 Real-time PCR analysis – Chondrogenesis

The expression of Sox 9, Col2A and Aggrecan on chondrogenically differentiated cells in 6 groups of BCP & HASi was evaluated after 7, 14, 21 and 28 days of cultivation. The RNA was isolated by TRIzol reagent (Sigma, India) as per manufacturer's instructions.

Cell-seeded materials were recovered from culture medium, washed with RNAse free water and treated with 500µl TRIzol reagent for 10 min and stored at -80°C until analysis. Multiple steps of pipetting was carried out to ensure complete dissociation of cells within the construct, especially at later time points. After thawing at room temperature, 100µl of chloroform was added for 15 min followed by centrifugation at 12,000g for 15 min at 4°C. The clear supernatant (top layer) was transferred to a fresh tube and mixed with 250µl of isopropyl alcohol for 10 min at room temperature for precipitating RNA followed by centrifugation at 12,000g for 8 min. The pellet was washed with 70% ethanol in RNase free water (Invitrogen, India) with centrifugation at 12,000g for 8 min. The pellet was air dried and added with 50µl RNase fee water and incubated at 55°C for 10 min. The yield of RNA was determined spectrophotometrically.

The first strand cDNA was then synthesized from 1 µg of total RNA, 5 µl MLV reverse transcriptase (50U / µl), 5 µl stratascript buffer (10x), 1µl RNase inhibitor

(40U / µl), and 4 µl random hexamer (10pmole) and 2 µl dNTP mix (10mM) (Invitrogen, India) for a 50µl RT reaction using the Thermal cycler (Master Cycler, Eppendorf, USA). The real-time PCR was performed using a Chromo4 system (MJ Research, USA). All reactions were carried out in a total volume of 20 µl, containing 10µl full velocity SYBR Green Master mix (Stratagene,USA), 1µl forward and 1µl reverse primer (10 picomole) and 8 µl cDNA at an annealing temperature of 50 - 55°C (depending upon the primers) over 35 cycles. The primers that were designed are listed in Table 2 (Source: References are added to the table of primer sequences added below). The annealing temperatures for β actin, Sox9, Col2A and Aggrecan gene are 52, 00, 00 and 58 °C respectively or as per reference added. For each gene, the quality and specificity was assessed by examining PCR melt-curves following real-time PCR. The results were normalized by being expressed relative to the amount of β-actin mRNA determined. Results presented as Fold expression.

Rabbit Chondrogenesis			
Gene	**Sequence (5'-3')**	**Size (bp)**	**Reference**
Sox 9	(S) CACACAGCTCACTCGACCTTG (AS) TTCGGTTATTTTTAGGATCATCTCG	76	(Kim and Im, 2009)
Aggrecan	(S) CCTTGGAGGTCGTGGTGAAAGG (AS) AGGTGAACTTCTCTGGCGACGT	280	(Park et al., 2009)
Col 2 A	(S) GCACCCATGGACATTGGAGGG (AS) GACACGGAGTAGCACCATCG	366	

Table 3: Real – Time PCR Analysis - Primers used in Rabbit Chondrogenesis Assay

Goat Chondrogenesis		
Gene	**Sequence (5'-3')**	**Reference**
Sox 9	F-TTCATGAAGATGACCGACGA R-CACACCATGAAGGCGTTCAT	(Coburn et al., 2013)
Aggrecan	F-CACGATGCCTTTCACCACGAC R-TGCGGGTCAACAGTGCCTATC	
Col 2 A	F-GTGGAGCAGCAAGAGCAAGGA R-CTTGCCCCACTTACCAGTGTG	

Table 4: Real – Time PCR Analysis - Primers used in Goat Chondrogenesis Assay

Statistics

Three separate materials for each group were used for every quantitative experiment. Again from each material, all measurements were done in duplicate in order to confirm the repeatability. Each parameter is expressed as means of all values ± standard deviations. Single factor analysis of variance (ANOVA) was employed to assess the statistical significance of results. P-values less than 0.01 were considered significant.

3.9 Preliminary in – vivo Studies

Care and management of animals were conducted as per Committee for the Purpose of control and Supervision of Experiments on Animals (CPCSEA) Guidelines and Institutional Animal Ethics Committee (IAEC) approval.

3.9.1 Animal Surgical Implantation

Animal Surgery procedures were carried out at the Division of Laboratory Animal Science (Lapine) and the Division of In-Vivo Models & Testing (Caprine), BMT Wing, SCTIMST.

3.9.2 Fabrication of Ceramic Scaffolds for Implantation

Ceramic scaffolds were fabricated using a stainless steel mold in the dimensions of the critical size defect (3.5mm * 4mm). Cylinders were polished using graded sand paper, cleaned via sonication with 3 changes of water to facilitate clearance of debris.

For Caprine Defect model, molds were developed as follows (Fig. 3C 4)

(A) Prepared Scaffolds

(B) Top Down view
Scaffolds in Stainless Steel Mold

(C) Defect Unit in Stainless Steel Mold

(D) Scaffold in Stainless Steel Mold

Fig. 3C 4: Scaffold Preparation

3.9.3 Cell Loading & Differentiation on Scaffolds for Implantation

Approximately 10^6 rabbit adipose derived stem cells were seeded on scaffolds 4 days prior to implantation. Cells were placed under chondrogenic media conditions with a total of 8 medium changes between cell seeding and implantation date. Short – term studies for rabbit model were carried out for a period of 4 weeks. Group I (control),

Group II & Group III (acellular BCP & HASi) has been carried out. Long term implantation was carried out for a period of 6 months (Table below plan below).

3.9.4 Surgical Procedure

New Zealand White Rabbits (6 months) (Fig. 3C 3) were used for surgical implantation studies. The animals were pre-medicated with intramuscular injection of atropine sulphate at 0.1mg per kg body weight, xylazine hydrochloride at 0.22mg per kg body weight and ketamine hydrochloride at 11mg per kg body weight. A medial parapatellar incision was made on the knee joint and carried through the medial aspect of joint capsule. Patella is dislocated laterally until the medial femoral condyle was exposed. A surgical drill bit was used to create a 3.5mm diameter, 4mm deep defect on the femoral condyle. The HASi and BCP cylindrical scaffolds were "press fit" separately in to the defect aseptically in rabbit knee joints. The joint capsule and skin will be closed. A non-treated animal was maintained without any surgical intervention as the normal control condyle. All experiments were carried out with the approval of the Institute Animal Ethics Committee (IAEC) following the guidelines of Committee for the Purpose of Control and Supervision of Experiments on Animals (CPCSEA)

3.9.5 *Ex vivo* Evaluation

Post implantation, rabbits were housed in separate cages and took water and feed *ad libitum.* Healing was uneventful without any inflammation and after the study period of 4 weeks the animals were euthanized with an overdose of the anaesthetic thiopentone. HASi, BCP and the normal condyle control samples were retrieved and fixed in 10% neutral buffered formalin. No stress behaviors or injury related gait alteration was observed.

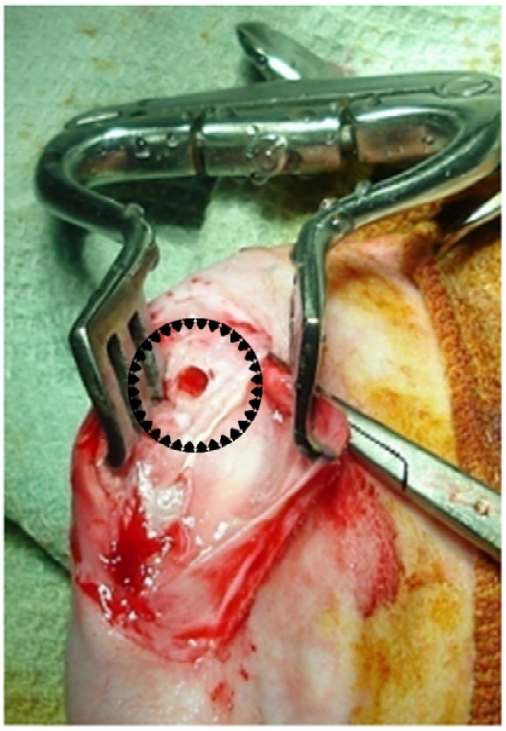

(A) Defect site preparation

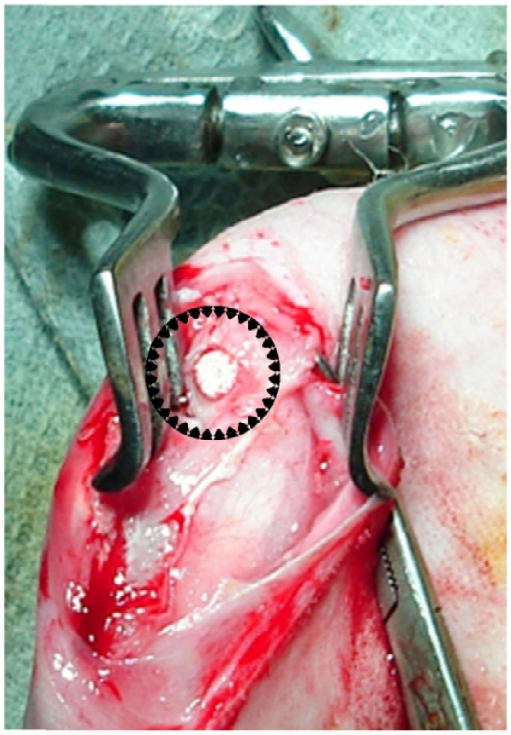

(B) Scaffold implantation

Fig. 3C 3: Surgical Procedure for Implantation – Lapine Model

3.9.6 Histological evaluation

The retrieved tissues (Group I, II, III) after four weeks of implantation were fixed in 10% neutral buffered formalin in Sorensen's phosphate buffer for 2 days. The samples were dehydrated in graded ascending series of isopropyl alcohol (FINAR, India) (70% isopropyl alcohol for 4 days; 80% isopropyl alcohol for 4 days; 96% isopropyl alcohol for 4 days; 100% isopropyl alcohol for 2 days; isopropyl alcohol: acetone (1: 1 v/v) for 1 day; 100% isopropyl alcohol for 1 day), infiltered in PMMA (Merck, India) for 6 days (2 changes) and finally embedded in PMMA with 1% benzoyl peroxide (accelerator). The plastic sections of about 100 µm were sliced using the high speed precision saw (Isomet ^{TM} 2000 Precision Saw, Buehler) and polished (Ecomet 3000, Buehler) to get a thickness of 70 - 90 µm. The PMMA sections after washing with tap water were kept in Stevenal's blue solution at 60ºC for 15 min and counter stained with van Gieson's picrofuchsin for 5 min at room temperature. The sections were then viewed under Light microscope (Leica DM 6000). Stevenal's blue stains cells and extracellular structures in a subtle gradation of blue tones and van Gieson's picrofuchsin colours collagen fibres (green or green blue), bone (orange or purple) and osteoid matrix (yellow-green) (Maniatopoulos C *et al.*, 1986).

3.9.7 Back Scatter Electron Imaging.

Composition of the ceramic insert within the joint structure was examined using Back Scattered Electron (BSE) imaging on a FEI Quanta 200. PMMA embedded sections from Group II & Group III were pasted on an aluminum stub and imaged in the back scatter mode.

3.9.8 Enhanced Contrast Micro – CT Imaging

High resolution x-ray micro-computed tomography (Micro-CT 40, SCANCO MEDICAL, Switzerland) was used to analyze the surface topology of retrieved rabbit condylar samples. Hexabrix contrast agent was used to enhance radio – opacity at 2% in phosphate buffered saline. Joints for imaging were de-formalinized

in 50 ml PBS for 16 h with six changes of buffer. Stained in 2% Hexabrix solution and imagery acquired with slice thickness and slice increment of 15 µm; energy of 70,000V and intensity of 115µA. 3 – dimensional models of the joint surfaces were reconstructed using equipment software with emphasis on visualization of non – calcified tissue surfaces.

3.9.9 Long Term Implantation Studies – Lapine Model

Long term implantation studies in a rabbit model was carried out in rabbit model as per the following implantation schedule. Two implants were placed in each animal on the inner femoral condyle of each animal.

Period of Study	**Group -1 (BCP)**	**Group - 11 (HASi)**	**Group – III (BCP+cells)**	**Group – IV (HASi+cells)**
6 months	3 animals	3 animals	3 animals	3 animals
6 months	Sham - 2 animals			

Table 5: Lapine Animal Experiment Plan

3.10 Dual – Cell Loading on Goat Model Implantation Scaffolds

For facilitating the loading of dual cell types on Goat implantation models the following protocol was used.

1. Differentiation of Cells in Monolayer Culture

Goat Adipose Derived Mesenchyhmal Stem Cells in monolayer culture (NUNC cell culture flasks) were placed in osteogenic and chondrogenic media as required.

2. Labelling of Cells for *In – Vitro* Tracking

Osteogenic cells were labeled with the PKH 26 cell membrane labeling kit from Sigma as per manufacturer's instructions. In short, The PKH26 Fluorescent Cell Linker Kits use proprietary membrane labeling technology to stably incorporate a yellow - orange fluorescent dye with long aliphatic tails (PKH26) into lipid regions of the cell membrane. Briefly, required cell number of 1E7 is trypsinized and washed in media lacking in serum and washed in calcium / magnesium free PBS to ensure non – aggregation of cells in buffer. Cells are pelleted down and resuspended in Diluent C (kit buffer) 1 ml volume. 4 µl of dye added to 1 ml of diluent C is added to the cells resuspended in Diluent C for a total volume of 2 ml. 3 min incubation at room tremperature with inverted mixing is carried out. Final volume is made up to 10 ml with complete media containing serum to stop the staining process. Cells are washed thrice in complete media to remove residual unbound dye. Cells are re-plated under standard culture conditions in osteogenic media to ascertain viability indicated by retention of adherence and staining – visibility under fluorescence microscopy (Leica DMIL).

3.11 Cell Loading on Scaffold Structures

Cells were trypsinized, pelleted at 2000 rpm at 25^{o}C for 5 mins. A high concentration cell suspension (10^{7}cells) was added to a non – adherent cell surface and incubated at 95% RH with 5% CO_2 to form pellets. Scaffold cylinders were placed on the cell pellet as illustrated (Fig. 3C 5) and inverted over second pellet to achieve complete loading of dual cell types.

The cell loaded scaffold was counterstained with Acridine Orange (as above). All cells were counterstained with Acridine Orange. Labeled cells yield a yellow signal (PKH26+Acridine Orange) in overlay mode while unlabelled cells are indicated by green signal from acridine orange uptake alone.

3.12 Evaluation of Dual – Cell Loaded Construct

Cells were visualized using overlay method on a Carl Zeiss LSM 510 META. Labeled cells (**O**steogenic **R**ed) & unlabeled cells (**C**hondrogenic **G**reen) were visualized via Z – stacking. The first 8 slices to a depth of 50um indicated the presence of chondrocyte cells alone. The scaffold to a depth of 125um had a mix of osteogenic & chondrogenic layers

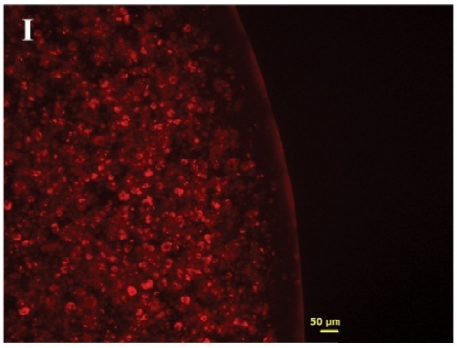

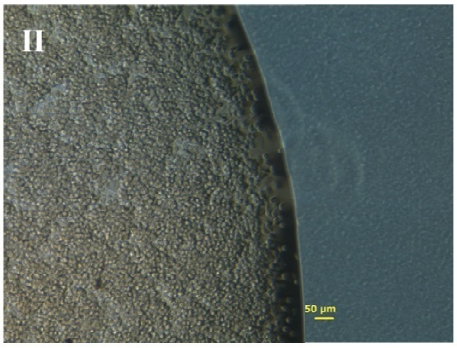

(A) Cell Spheroid Generation - OR cells (Fig. I) & CG (Fig. II) cells were fabricated into "cell spheroids" Seeded on a ceramic scaffold under dual seeding conditions.

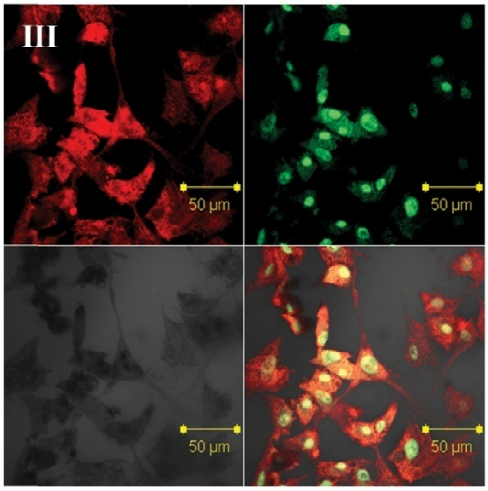

(B) Confirmation on 2D Surface - GADMSC's were stained with PKH 26 and counterstained with Acridine Orange. Cells imaged in overlay mode exhibited red cytoplasmic staining, along with generalized acridine orange staining Normal morphology of cells was confirmed using a Carl Zeiss LSM 510 META in DIC mode (Fig. III).

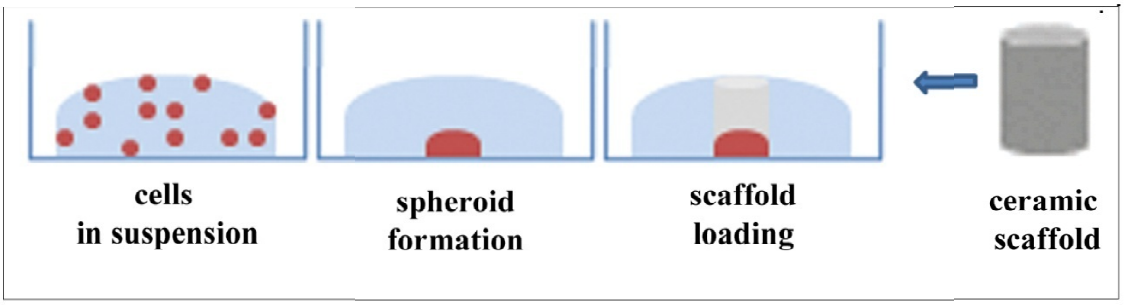

(C) Cell Loading – Schematic

Fig. 3C 5: Implant Seeding Caprine Model

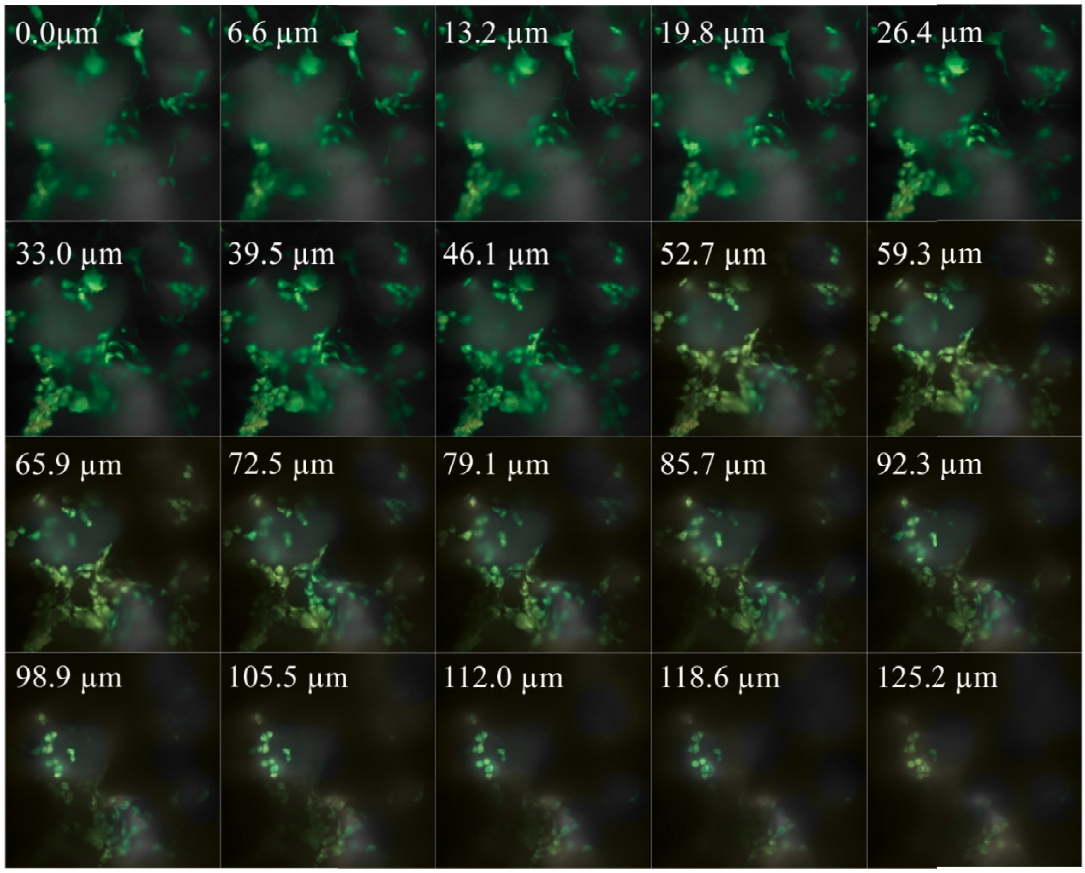

The first 8 slices to a depth of 50µm indicated the presence of CG cells alone. The scaffold to a depth of 125µm had a mix of osteogenic & chondrogenic layers. The presence of chondrogenic layers at the top will ensure integration of *in vitro* developed chondral surfaces with the surrounding joint tissue. Deeper layers of chondrogenic cells will undergo a gradual transformation to bone tissue via endochondral ossification.

Fig. 3C 5: Cell Tracking

3.13 Implantation Schedule in Goat

Period of Study	Group -1 (BCP)	Group - 11 (HASi)	Group – III (BCP+cells)	Group – IV (HASi+cells)
6 months	**3 animals**	**3 animals**	**3 animals**	**3 animals**
6 months	**Sham - 2 animals**			

Table 6: Caprine Animal Experiment Plan

3.14 Goat Implantation – Surgical Procedure

Healthy young male goats of age about 1year and weight ranging 20-30 kg will be selected. The animals will be anaesthetized and surgery will be conducted under aseptic conditions. The surgical site is prepared and painted with betadine antiseptic solution and draped.

A medial parapatellar incision will be made on the knee joint and carried through the medial aspect of joint capsule. Patella will be dislocated laterally until the medial femoral condyle was exposed. Surgical drill bits measuring 4.0mm diameter defect will be made on the condyle which will be reaching up to the depth of the bone marrow.

The scaffold with cells will be implanted in to the defect aseptically. The scaffold will be press fit in to the defect. The joint capsule and skin will be closed.

The animals will be pre-medicated with intramuscular injection of atropine sulphate at 0.1 mg per kg body weight, xylazine hydrochloride at 0.22 mg per kg body weight and ketamine hydrochloride at 11mg per kg body weight. Thiopentone sodium at 5 mg per kg body weight followed by succinyl choline at 0.02 mg per kg body weight intravenously will be given for induction of anesthesia and muscle relation respectively. The animal will be intubated immediately with size 9 portex endotracheal tube and put on ventilator. Anesthesia will be maintained with increments of 50 – 100 mg of thiopentone sodium and half the initial does of succinyl choline every 30 – 40 minutes (Fig.3C 6).

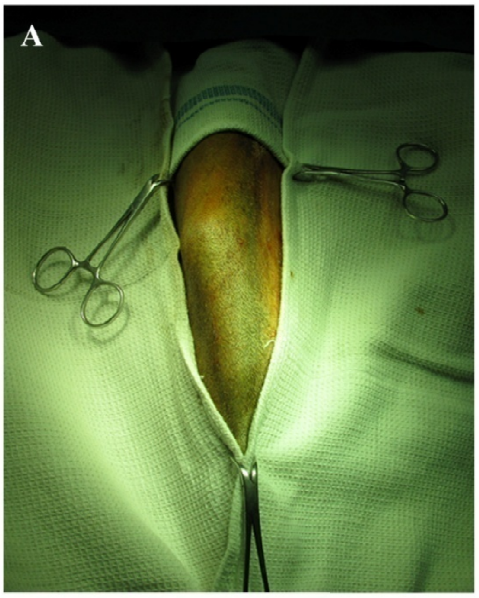

(A) Surgical site preparation

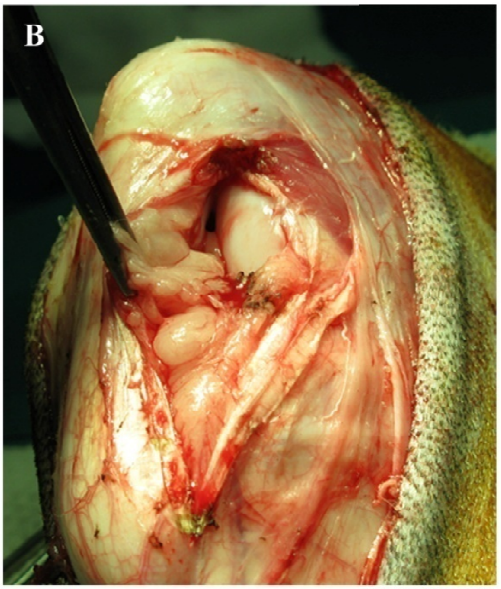

(B) Exposure of
Medial Femoral Condyle

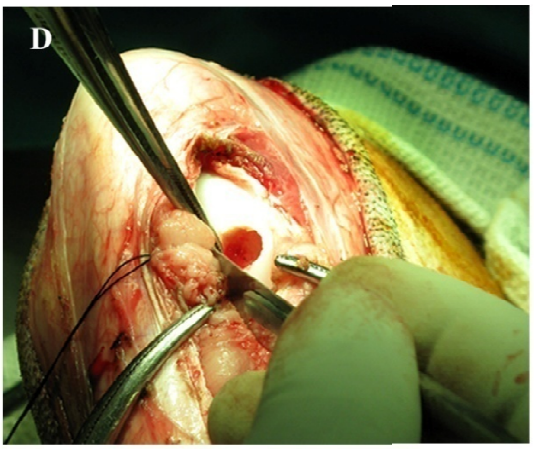

(C) & (D) Preparation of
Defect site with irrigated drilling

Fig. 3C 6: Surgical Procedure for Implantation - Caprine Model

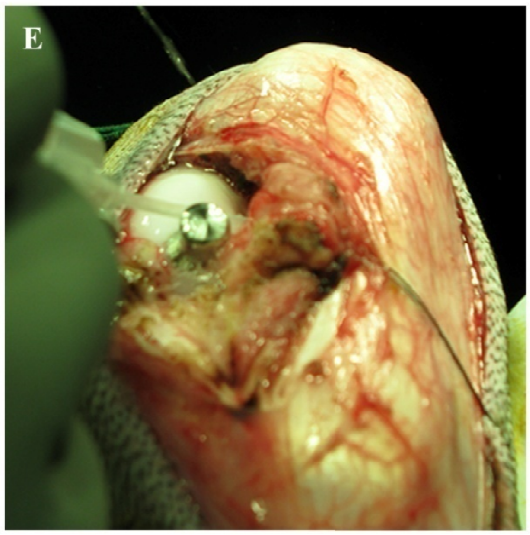

(E) Defect Dimension Verification

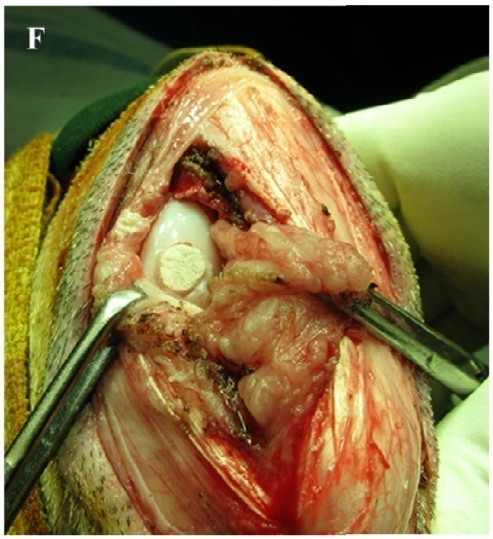

(F) Scaffold Implanted at site

(G) Wound Suturing

(H) Experimental Animal in Recovery

Fig. 3C 6: Surgical Procedure for Implantation - Caprine Model

CHAPTER 4

MATERIAL CHARACTERIZATION

Physico – Chemical Characterization of Bioactive Ceramics

4.1 Introduction

Bioactive ceramics are characterized by their superior biological activity, and resorbability than calcium phosphate ceramics. Especially in the case of silica based bioceramics, this can be mimicked by pure calcium phosphate ceramics by calibrating the phases of hydroxyapatite within the system to ensure tailored degradation based on experimental parameters. Ideally in the case of bone substitutes or in this case provision of subchondral bone replacement, degradation of material should be on par with tissue ingrowth (Hamadouche and Sedel, 2000). In this study HASi, a silica based hydroxyapatite was used in comparison with a biphasic tricalcium phosphate with varying ratios of different phases of hydroxyapatite in the osteochondral replacement role mentioned above. The goal was to utilize osteoconduction and osteointegration properties of hydroxyapatite based bioceramics to provide a stable scaffold surface for reconstruction of articular surfaces.

The specific objectives of the first phase of the study are the characterization of prepared hydroxyapatite scaffolds of HASi and BCP variety using multiple techniques prior to biological evaluation.

4.2. Physicochemical Characterization of Materials

4.2.1 Scanning Electron Microscopy

SEM provides in depth visualization of the scaffold surfaces depicting the microstructures that make up the scaffold surface as well as porosity & pore morphology data. BCP & HASi has an interconnecting pore system with pores ranging from small (50µm) to larger pores (200 - 500 µm). Porosity at this range is suitable for cell infiltration as well it has been confirmed as per (Nair et al., 2008). Topography of the material is critical to the material's interaction with cell burden (Gough et al., 2004). Appearance of the scaffolds under scanning electron microscopy indicated prevalence of multiple open pores on the surface and presence of a rough exterior surface as indicated in the case of BCP & HASi (Fig. 4C 1).

4.2.2 Elemental Analysis

Elements present in the outer layers of the BCP & HASi scaffolds were evaluated via Energy Dispersive Spectra Analysis. Presence of Silica (Si) was confirmed in the case of HASi and Ca/P detected in both samples as illustrated in the X- ray EDS spectra in the figures (Fig. 4C 2).

4.2.3 Phase Analysis

X-ray diffraction (XRD) pattern exhibited crystallinity with hydroxyapatite as the major phase in both materials. The outer coating layer in HASi showed peaks for calcium silicate, tricalcium phosphate and hydroxyapatite. In BCP the presence of α-TCP was validated against comparison to standard patterns. Presence of both HA & α-TCP indicates the biphasic nature of the scaffold. Variations within the calcium phosphate peaks have a strong effect on cellular responses hence degree of crystallinity, phase and purity are important parameters with respect to scaffold materials (Hing et al., 1999). The data was matched to the JCPDS files. The powder diffraction data number (PDF No.) for hydroxyapatite , tricalcium phosphate and calcium silicate are 09-0432, 09-0348 and 01-1029 respectively Nair et al (Nair et

al., 2009). Crystallization and phase transformation are dependent on the chemical composition and sintering temperature of green ceramic structures. Temperatures over thousand degrees centigrade has been proven to cause decomposition of phases in hydroxyapatite (Langstaff et al., 1999). Hence final verification of the component structures is necessitated. The structures delineated in the XRD pattern, confirmed via comparison to the JCPDS files indicate the presence of candidate materials in correct phase and proportion (Fig. 4C 3).

4.2.4 Functional Group Studies

The FTIR spectra obtained showed the characteristic absorption band corresponding to a hydroxyapatite phase in both samples. The characteristic triplet peak for phosphate at 962cm^{-1}, 1054cm^{-1} and 1088cm^{-1} and hydroxyl groups at 3570 cm^{-1}, was agreeable with the literature data (Walters et al., 1990).

The bands at 3571.4 cm^{-1} can be attributed to hydroxyl groups (Nair et al., 2009), whereas bands at 1190–976 cm^{-1} and 660–520 cm^{-1} correspond to phosphate groups. In HASi, the peak at 722.6 cm^{-1} corresponds to silica. But as phosphate and silica share similarly spaced vibrational modes, differentiation of peaks is a fine task. Since the absorption of hydroxyapatite is maximum as compared to α-TCP, the relevant absorption peaks are submerged. The data collected confirms the presence of the relevant peaks for hydroxyapatite across both materials (Fig. 4C 4) .

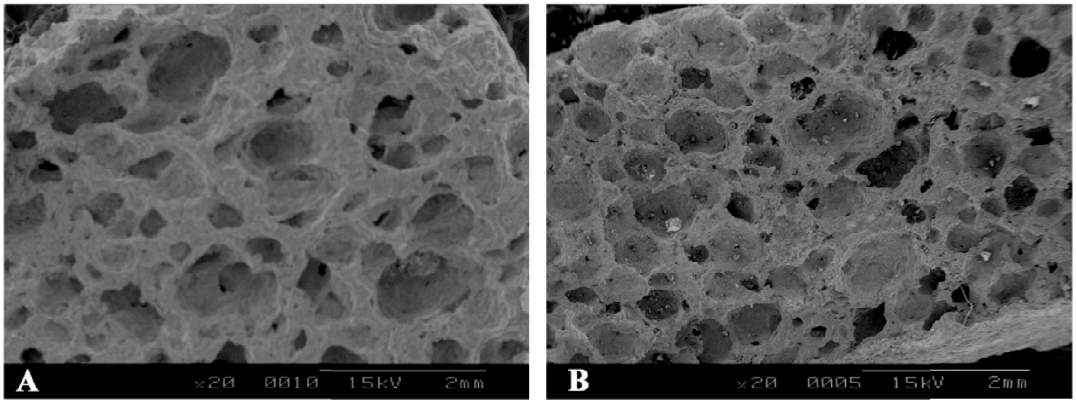

Fig. 4C 1: Scanning Electron Micrographs showing surface morphology and pore structure of (A) BCP (B) HASi

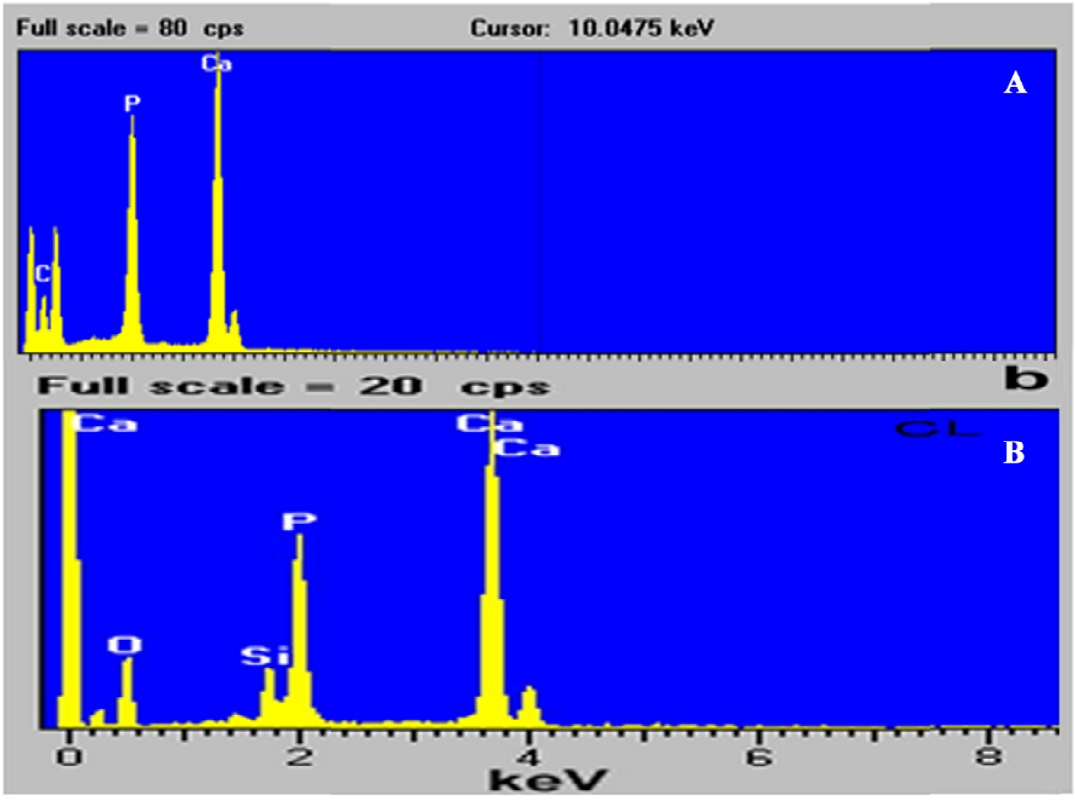

Fig. 4C 2: Energy Dispersive X - ray Analysis
(A) BCP - Native calcium & phosphate peaks visible
(B) HASi - Silica peak visible alongside native peaks

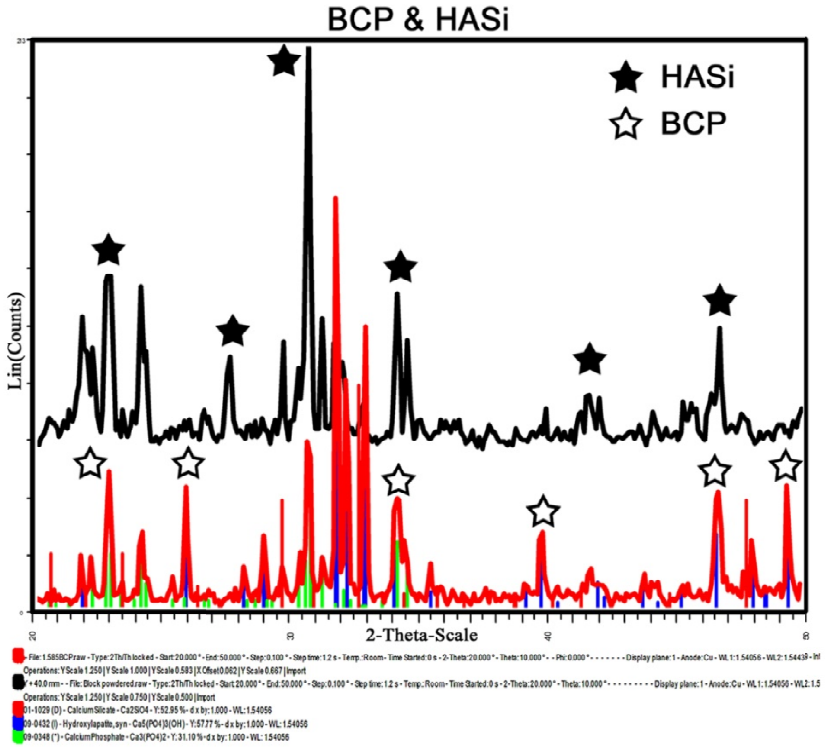

Fig. 4C 3: X-ray diffraction spectra of BCP (☆) in comparison with HASi (★)

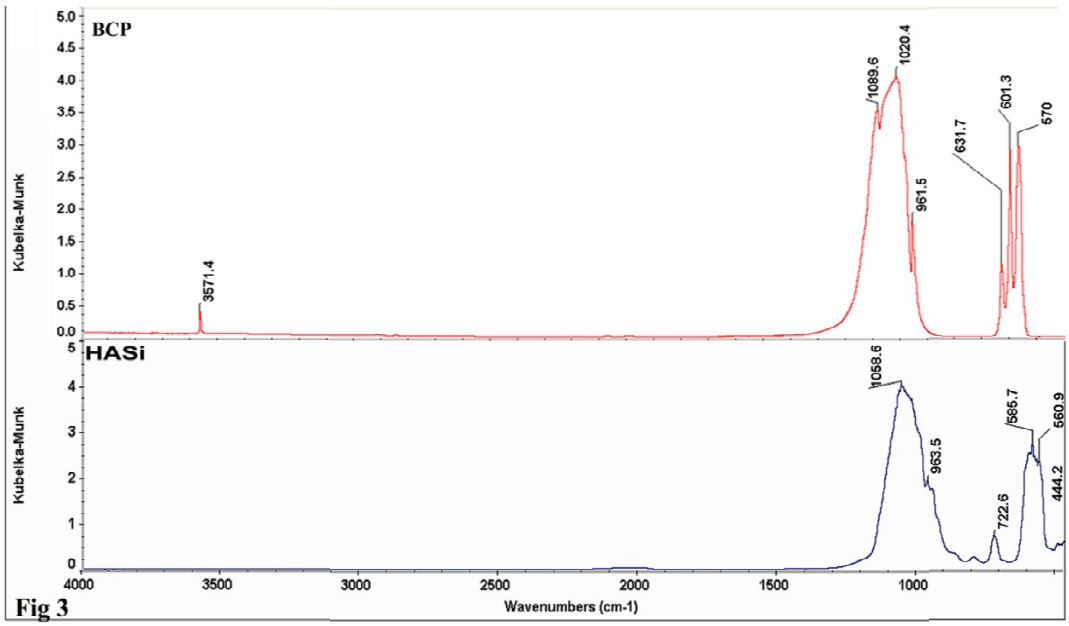

Fig. 4C 4: Fourier Transform Infrared Spectra of BCP & HASi depicting characterstic hydroxyl at 3671cm^{-1} and phosphate groups at 1020 cm^{-1}, 670 cm^{-1}. Silica peak characteristic to HASi depicted at 722.6 cm^{-1}

CHAPTER 5

Evaluation of Cell – Ceramic Constructs:

In Vitro – Adipose Derived Mesenchymal Stem Cells

5.1 Introduction

The concept of fabricating tissue engineered structures with emphasis on the restoration of normal functionality is slowly gaining acceptance. To achieve this goal it is necessary that materials, cells and processes evolved in the laboratory are to be field tested under rigorous conditions. This ensures proper process validation, provides an understanding of life cycle performance of the product in question. Prior to application key concepts of the tissue engineering triad involving scaffolds, cells and other moieties a keen understanding of their interaction and its modulation is necessitated. Keeping in mind the need for validating the selected scaffolds as well as processes in a pre-clinical pipeline two prospective models were selected for cell isolation (Chu et al., 2010a). The use of two models in conjunction enable us to offset probable effects associated with single model studies thus providing for a valid evaluation of proposed systems (Ahern et al., 2009). Comparison of cell – material interaction within model systems under *in vitro* conditions is key in understanding short – term dynamics and providing predictive information in for framing further studies (Nooeaid et al., 2012a).

The goals of the second phase of the study are as follows.

1. To isolate and characterize Adipose Derived Mesenchymal Stem Cells (ADMSCs) from goat and rabbit model systems *in vitro.*
2. Study scaffold-cell interaction and its parameters.
3. Study scaffold – cell interaction under osteogenic and chondrogenic differentiation conditions.

5.2 Isolation & Characterization of ADMSCs.

ADMSCs were isolated from the subcutaneous fat tissue of New Zealand White Rabbit and Goat as described in 3.2.1 and 3.2.2 The usage of ADMSCs has been described in several studies (Zuk, 2010b). The cells can be isolated via collagenase digestion of adipose tissue, and enriched via adhesion due to their adhesion to preferential attachment on TCPS and timed change of growth media. This has been extensively reported in rabbit (Chen et al., 2012) and goat model systems (Ren et al., 2012).

5.2.1 Isolation of Adipose Derived Stem Cells

In the current study adipose tissue, 2g was isolated aseptically from the mid- dorsal region of the rabbit. In the goat model adipose tissue 4g, was isolated from ventral side of the rib cage along the medial line. Disparity in initial isolation weight depended on amount of tissue excised and availability of free fat tissue at explant sites. Tissue was cleaned of extraneous material, minced, digested and plated post – digestion in regular growth medium in 25 cm^2 TCPS (NUNC) flasks. Cells adhered, exhibiting characteristic fibroblast morphology in the case of rabbit adipose derived stem cells (Fig. 5C 1) and in the case of goat adipose derived stem cells (Fig. 5C 2). Cells attained confluent levels of 90% of flask area within day 7 of culture in both species. Cells were harvested by removing growth media, washing of non-adherent components using sterile PBS and achieving cell dissociation with a 0.25% trypsin – EDTA solution.

ADMSC's grown on a coverslip was stained with Rhodamine conjugated Phalloidin (red) to identify actin fibre structure and DAPI (blue) to characterize nuclei. The cells exhibited spread morphology with diverse actin cytoskeletal structures as well as the presence of intact nuclear patterns. RADMSC's (Fig. 5C 3) & GADMSC's (Fig. 5C 4) were imaged using Confocal Laser Scanning Microscopy

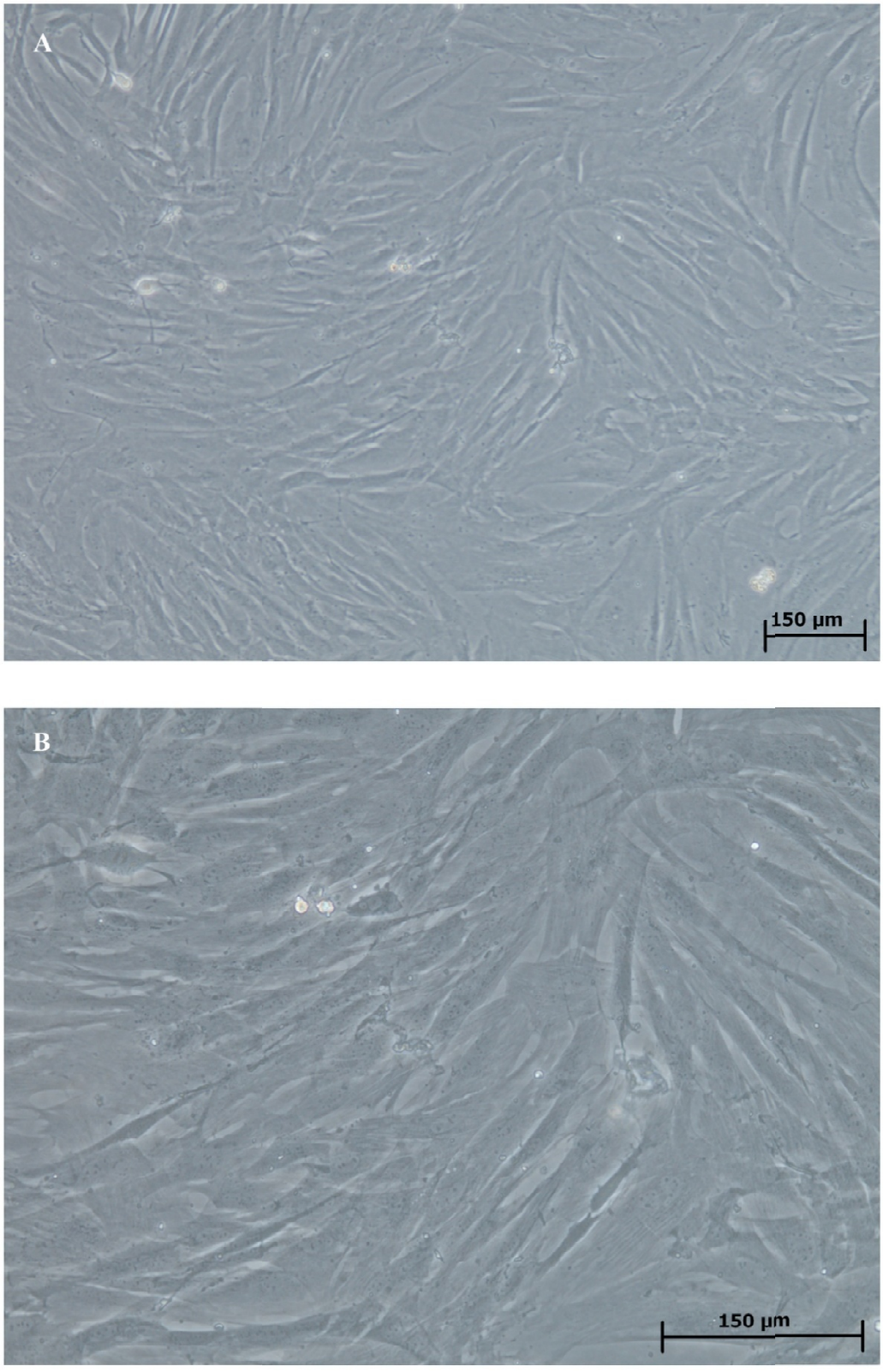

Fig. 5C 1: Phase contrast images of Rabbit Adipose Derived Stem Cells in culture (A - 10X, B - 20X)

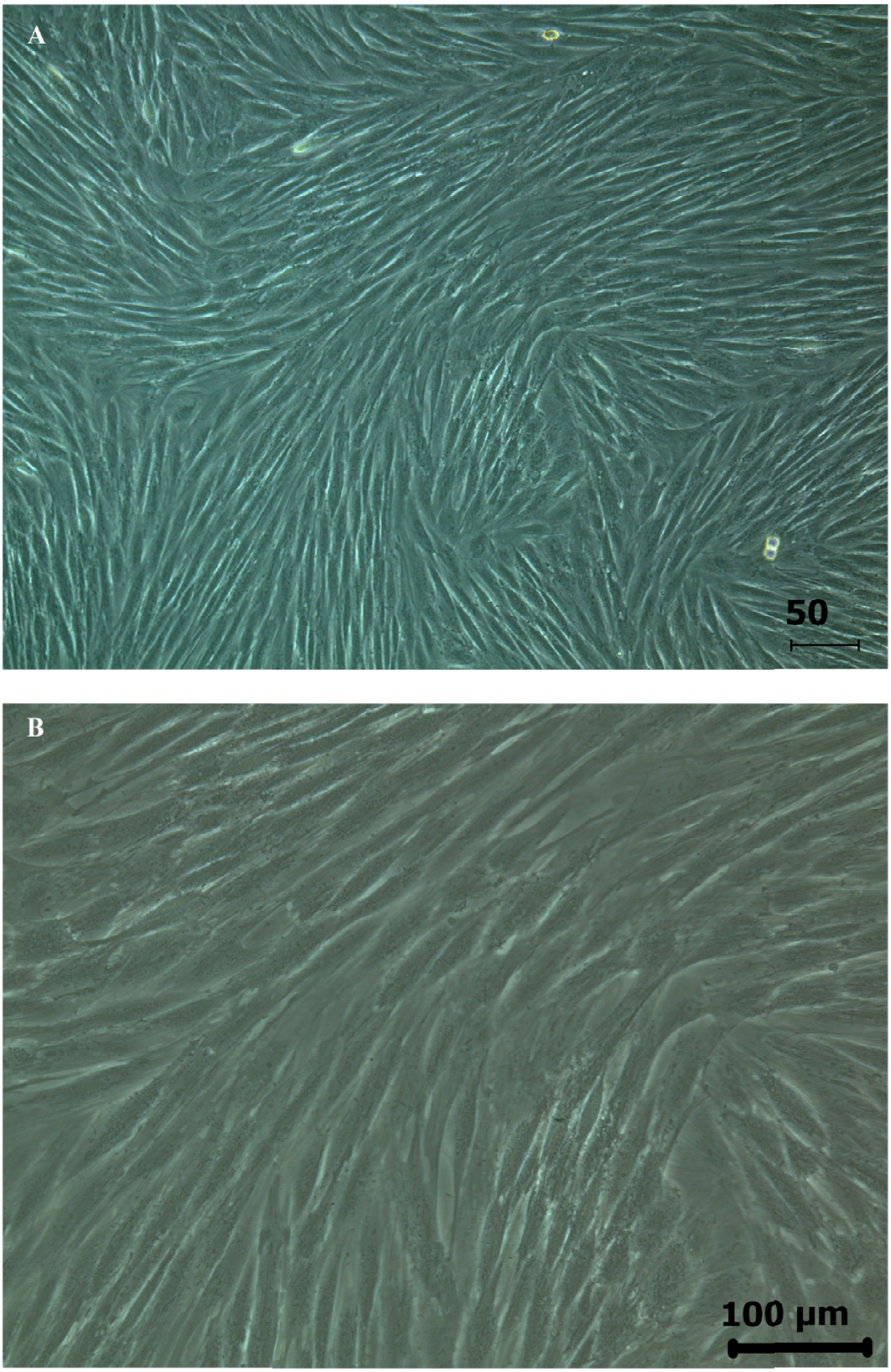

Fig. 5C 2: Phase contrast images of Goat Adipose Derived Stem Cells in culture (A - 10X, B - 20X)

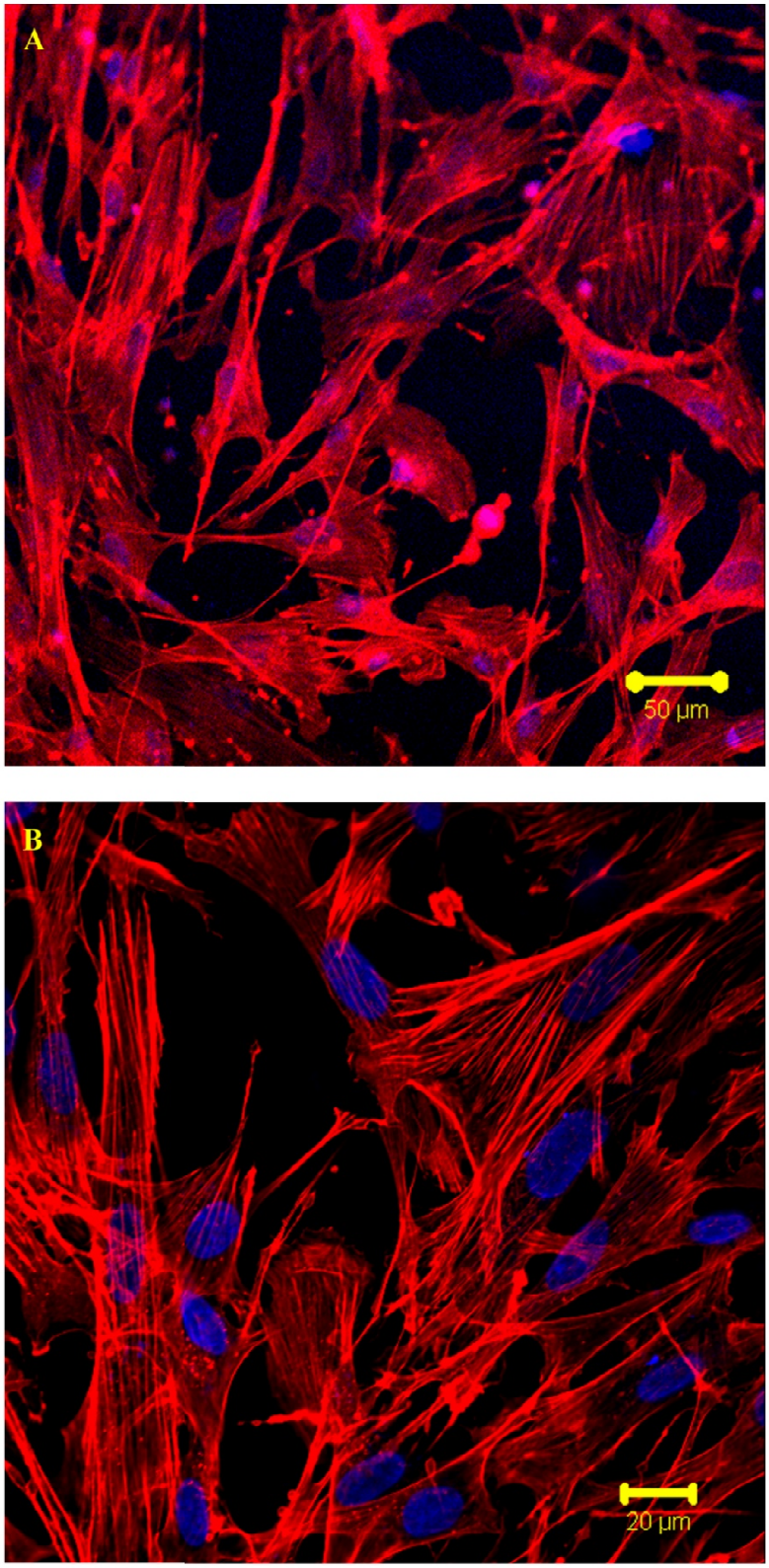

Fig. 5C 3: Confocal laser scanning micrographs of Rabbit Adipose Derived Stem cells. Actin Fibres stained red with Rhodamine Phalloidin and nucleus blue with DAPI (A - 20X, B - 40X)

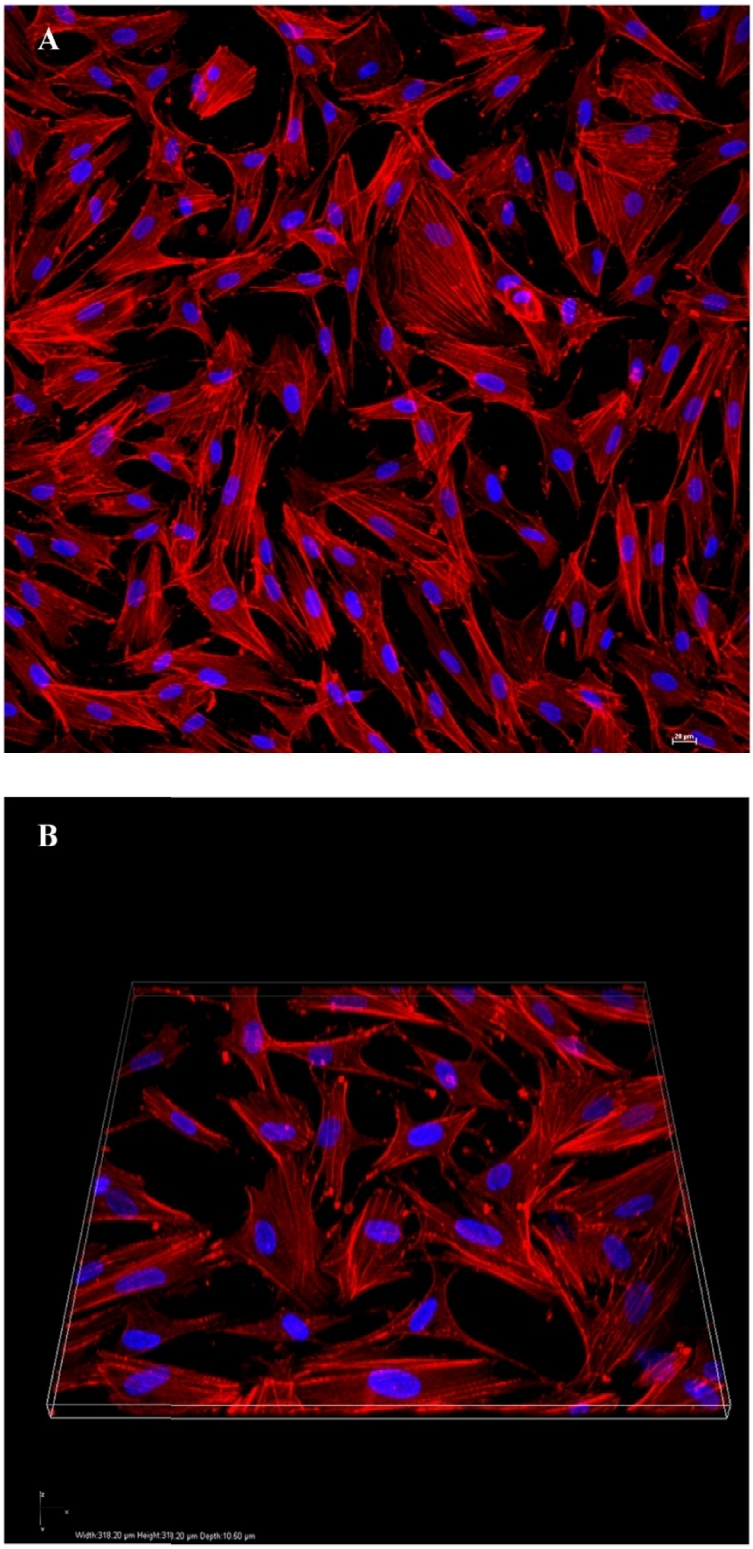

Fig. 5C 4: Confocal laser scanning micrographs of Goat Adipose Derived Stem cells. Actin Fibres stained red with Rhodamine Phalloidin and nucleus blue with DAPI (A - 20X, B - 40X, 3D - reconstruction of cell morphology)

5.2.2 Characterization of Adipose Derived Stem Cells.

Characterization of isolated cell population was carried out at Passage 4 to ensure uniformity of cell properties.

5.2.2.1 Flow Cytometric Analysis

A number of CD markers were used for evaluating the isolated adipose derived stem cells. Markers such as CD 90, CD 105 & CD 34 were used with secondary staining alone as control sample.

RADMSCs at passage 4 were stained positively for CD 105 & CD 90 with above 80% of the cells increased signal intensity (Fig. 5C 5). Cells stained with CD 34 a haematopoietic marker indicated less than 5% positive signals, indicating homogenous nature of the sample. Results obtained are consistent with observed reports from our laboratory (Mohan et al., 2013) and reported elsewhere (Arrigoni et al., 2013).

GADMSCs at passage 4 were stained positively for CD 105 & CD 90 with above 75% of the cells indicating positive signal intensity. Cells stained with CD 34 in this case indicated less than 7 % positive cells, indicating the homogenous mesenchymal nature of the sample (Fig. 5C 6) Results obtained are consistent with current published work depending on the passage chosen for study (Ren et al., 2012)

Positive staining for the mesenchymal markers with definite negative indication for the presence of haematopoeitic stem cells is key to confirming the mesenchymal nature of the stem cells (Pascucci et al., 2011).

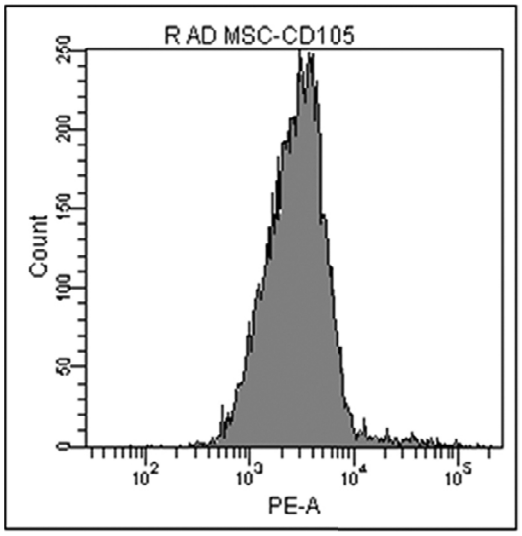

(A) CD 105 > 80% positive

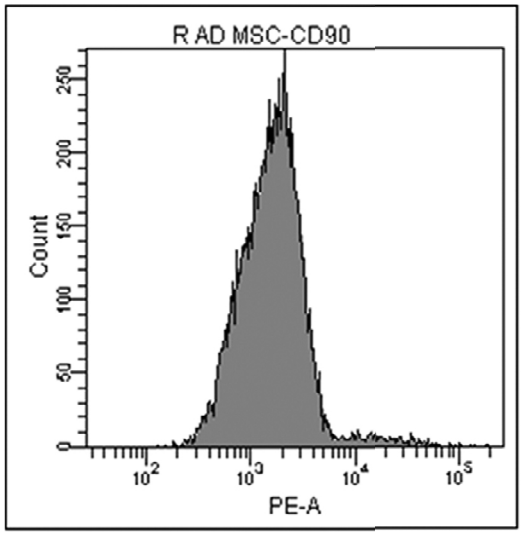

(B) CD 90 > 80% positive

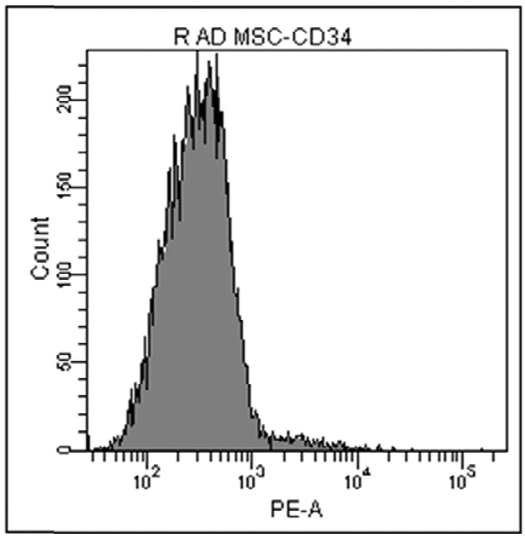

(C) CD 34 < 5% positive

Fig. 5C 5: FACS Analysis - Characterization of Rabbit Adipose Derived Stem Cells (A) CD 105 > 80% positive (B) CD 90 > 80% positive (C) CD 34 < 5% positive - Mesenchymal Stem Cell Characteristics of Cell Population is confirmed

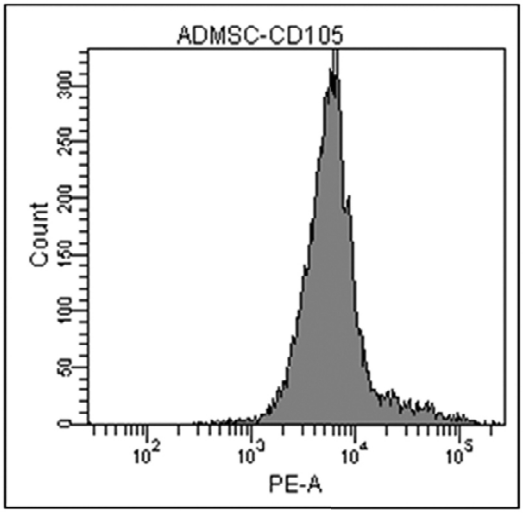

(A) CD 105 > 80% positive

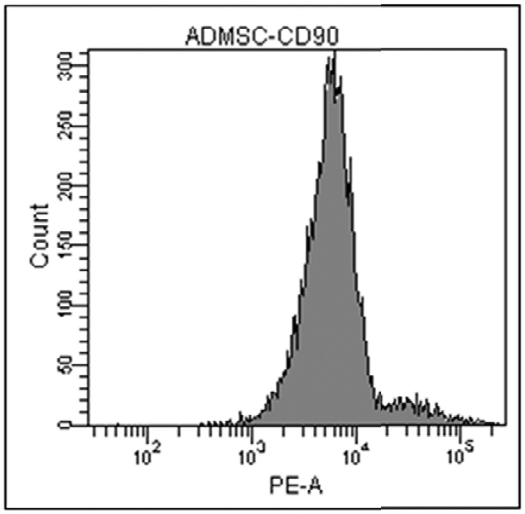

(B) CD 90 > 80% positive

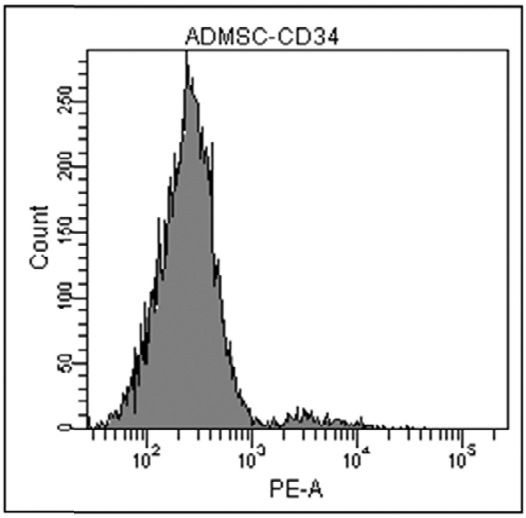

(C) CD 34 < 5% positive

Fig. 5C 6: FACS Analysis - Characterization of Goat Adipose Derived Stem Cells (A) CD 105 > 80% positive (B) CD 90 > 80% positive (C) CD 34 < 5% positive - Mesenchymal Stem Cell Characteristics of Cell Population is confirmed

5.2.2.2 Differentiation Studies of Adipose Derived Stem Cells

RADMSCs and GADMSCs were differentiated into osteogenic and chondrogenic lineages *invitro* and evaluated for identifying differentiation characteristics as well as deposition of representative extracellular matrix.

Chondrogenic medium used was DMEM - LG containing 15% FBS supplemented with 10ng/ml TGF-β1 (Imperial), ITS Premix (BD Biosciences: final content: final concentrations: 6.25 µg/mL bovine insulin, 6.25 µg/mL transferrin, 6.25 µg/mL selenous acid, 5.33 µg/mL linoleic acid, and 1.25 mg/mL bovine serum albumin) 25 µg of Ascorbate & 10^{-8} M Dexamethasone (Sigma)antibiotics (Penicillin/streptomycin) in an incubator at 37º C and 95% RH with 5% CO_2. Chondrogenesis is characterized by the production of a matrix rich in collagen, proteoglycans and glycosaminoglycans. Upregulation of collagen synthesis genes as well as those of component ECM molecules are observed.

TGF-β1 is key in inducing chondrogenesis with characteristics that include depression of mitogenic activity, increase in expression of Sox 9, Col II, Aggrecan & deposition of chondrogenic extra cellular matrix(Tuli et al., 2003) (Xu et al., 2008). Ascorbic acid is involved in the procollagen hydroxylation as part of the matrix secretion but also requires the activation of ERK signalling to initiate this process (Temu et al., 2010). TGF-β1 and ITS+ in tandem stimulates cell growth and protein synthesis while dexamethasone at higher concentrations has a negative effect on extra cellular matrix synthesis, especially proteoglycan synthesis and accumulation (Awad et al., 2003). The combination of components added to media stimulates the induction, maintenance and maturation of chondrogenic structures (Leboy et al., 1989) (Solchaga et al., 2011).

RADMSCs and GADMSCs grown under pellet culture conditions were sectioned and stained to demonstrate the characteristic chondrogenic extra cellular matrix materials via differential staining. Alcian Blue is a polyvalent basic dye that stains acidic mucosubstances and acetic mucins. (Ogawa et al., 2004) including glycaosaminoglycans.. Staining in dark blue to light blue hues are indicative of chondrogenic extra cellular matrix synthesis. Presence of proteoglycans is stained

dark red by the use of Safranin O as indicated (Naumann et al., 2002) here (Fig. 5C 7 & 8).

Through adding osteogenic supplements as indicated here: DMEM - HG containing 15% FBS supplemented with 10 mM β- glycerophosphate, 10^{-8} M dexamethasone and 0.05 mg/ml L-ascorbic acid (Sigma) antibiotics (Penicillin/streptomycin) in an incubator at 37º C and 95% RH with 5% CO_2 induction of osteogenesis of isolated adipose derived stem cells is possible. This is characterized by the secretion of collagen, increase in expression of ALP, osteocalcin and also in the formation of a mineralized extra cellular matrix (Kern et al., 2006).

Adipose derived stem cells were seeded on coverslips, and osteogenic medium added with regular medium changes twice a week for three weeks. At the end of 21 days assessment of the secreted extracellular matrix identified the presence of collagen networks as identified here in (Fig. 5C 9 & 10) with Trichrome staining. Abundant mineralized collagen staining was observed under von Kossa staining and presence of deposited calcium identified with alizarin red staining. Presence of characteristic extra cellular matrix components and deposition indicates the differentiation of the adipose derived stem cells towards osteogenic lineage (Kern et al., 2006).

Ascorbic acid has been shown to be necessary for the collagen synthesis and induction of osteogeneis in vitro (Maehata et al., 2006). It also regulates ALP activity and protein synthesis in osteoblast cell cultures (Son et al., 2007). With beta – glycerophosphate, it serves as a source of phosphate ions for mineralization (zur Nieden et al., 2003). Dexamethasone has also been associated with the initiation of Wnt signalling, a secreted glycoprotein that exerts concentration dependent effect on cell fate (de Boer et al., 2004). Wnt basically acts on Beta – catenin, causing nuclear translocation of the substrate leading to an increase in expression of Runx2 and ALP (Hamidouche et al., 2008).

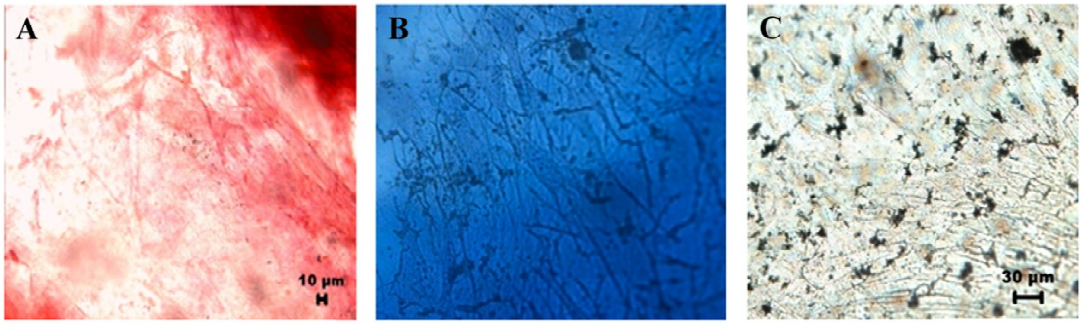

Fig. 5C 7: Rabbit Adipose Derived Stem Cells differentiated to Osteogenic lineage

(A) Alizarin Red staining for calcium deposition
(B) Masson's Trichome staining for collagen deposition
(C) Von Kossa staining for calcium deposition

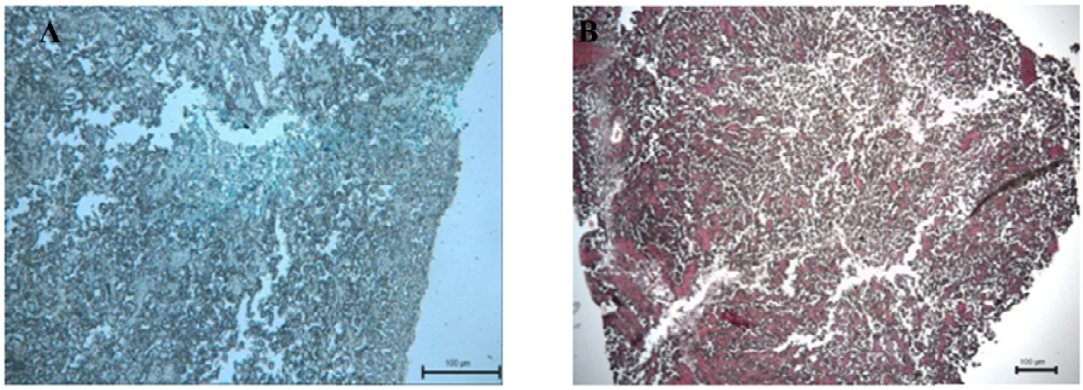

Fig. 5C 8: Rabbit Adipose Derived Stem Cells differentiated to Chondrogenic lineage

(A) Alcian Blue staining for glycosaminoglycans
(B) Safranin O staining for proteoglycans

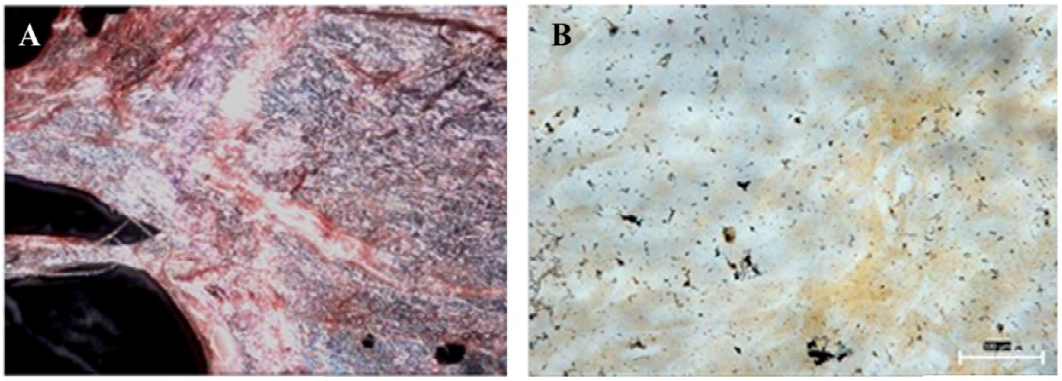

Fig. 5C 9: Goat Adipose Derived Stem Cells differentiated to Osteogenic lineage

(A) Alizarin Red staining for calcium deposition
(B) Von Kossa staining for calcium deposition

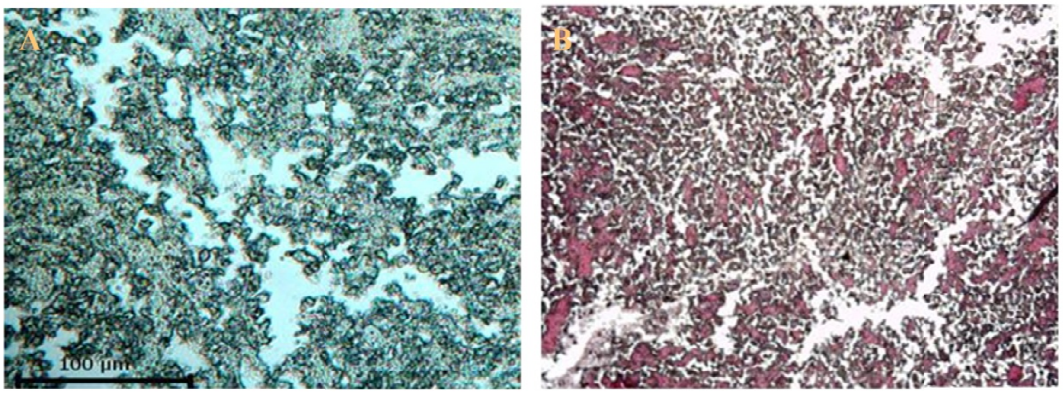

Fig. 5C 10: Goat Adipose Derived Stem Cells differentiated to Chondrogenic lineage

(A) Alcian Blue staining for glycosaminoglycans
(B) Safranin O staining for proteoglycans

5.3 Assessing Cell – Ceramic Interaction: Adipose Derived Stem Cells on Scaffold Structures

Material – cell interaction plays a major role in the development, sustenance and success of any tissue engineered product. It is necessary to evaluate scaffold structures at short time intervals in conjunction with candidate cell components to understand the same. Fabrication of adipose – derived stem cell constructs in combination with BCP & HASi was carried out as follows. The materials prior to cell seeding were soaked in growth medium prior to cell seeding for 16 hrs. The materials in soaking gain a layer of serum proteins facilitating recognition of adhesion moieties by cells as well as the generation of an amorphous layer of calcium phosphate which may stimulate cell proliferation (Kizuki et al., 2003). Cells in close interaction with ceramic surfaces were assessed with scanning electron microscopy & confocal laser scanning microscopy.

5.3.1 Adhesion of Adipose Derived Stem Cells on BCP & HASi Scaffolds

Pre-conditioned discs (3mm * 1mm) were seeded with approximately $1*10^5$ cells and fixed in glutaraldehyde after 72 hours and processed for evaluation via scanning electron microscopy. The images of rabbit adipose derived stem cells and goat adipose derived stem cells (Fig. 5C SEM) indicate consistent cell adhesion and spreading on scaffold surfaces indicating ability to mediate with material surfaces.

As per published observations, initial phases of cell adhesion involve a spherical entity that further flattens in close apposition with a preferred material surface, with later appearance of nuclear prominence (Malik et al., 1992). Adhesion of cells on material surfaces in the initial contact phase is mediated by the presence of serum proteins viz fibronectin and vitronectin which show preferential adsorption on ceramic surfaces(Anselme et al., 2000) (Anselme, 2000). Extensive cell spreading on the surface of the HASi scaffolds observed in both goat & rabbit adipose derived stem cells indicate a consistent cell response to the silica content of HASi. The presence of the silinol (Si – OH) on the surface may prove to provide an anchor for irreversible binding of favourable proteins from serum in media (Lobel and Hench, 1998). BCP & HASi surfaces provoked characteristic cell phenomenology of

adhesion, with cellular processes in close contact with material surfaces, with pores remaining open (Bagambisa and Joos, 1990). Pore occlusion may lead to nutrient starvation within the core of fabricated tissue engineered constructs.

The pore sizes of the scaffold surfaces observed qualitatively to range from 200 – 500 μm are ideal for the ingrowth of cellular components, providing a suitable growth surface for the candidate cell population seeded within (Ducheyne and Qiu, 1999). The ability of material surface properties to elicit desired cell responses is well enabled here, with the overarching goal of providing a stable growth surface to a cartilage overburden within the milieu of an osteochondral defect defined by the ability of the material to encourage bony anchorage (Ohgushi and Caplan, 1999).

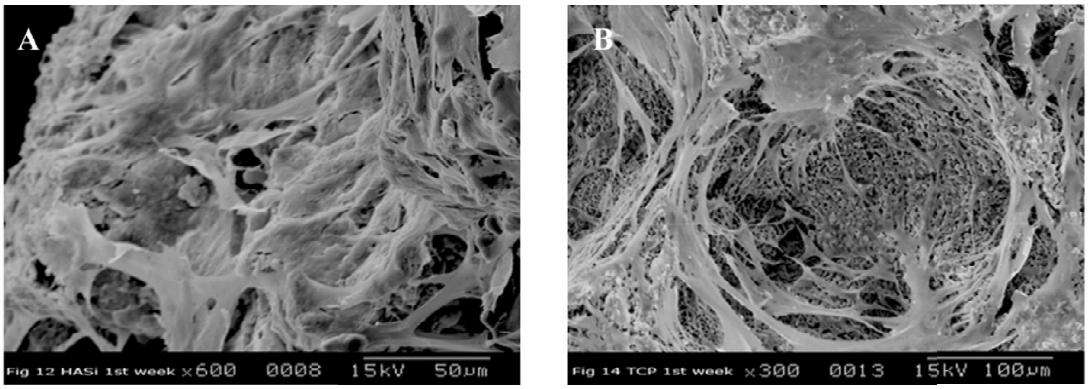

Fig. 5C SEM (1) Scanning Electron Micrographs: Rabbit Adipose Derived Stem Cells on Ceramic Scaffolds. (A) BCP (B) HASi - cells exhibit characteristic morphology

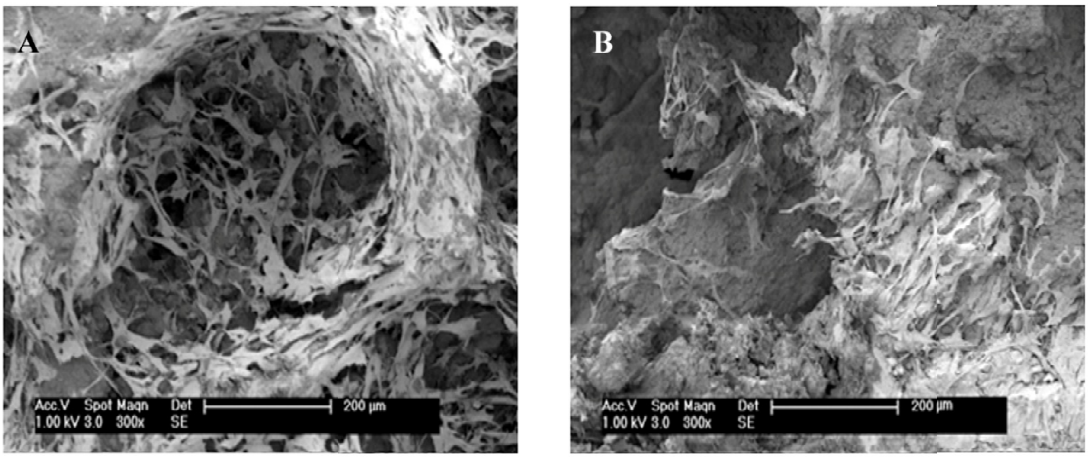

Fig. 5C SEM (2) Scanning Electron Micrographs: Goat Adipose Derived Stem Cells on Ceramic Scaffolds. (A) BCP (B) HASi - Cells spread over scaffold surfaces with no pore bridging

5.3.2 Viability of Adipose Derived Stem Cells on BCP & HASi Scaffolds

Viability of cells on scaffold was measured qualitatively via a one step staining process utilizing a combination of acridine orange and ethidium bromide staining. Acridine orange is a green fluorescent dye permeant to living cells and intercalates in DNA. Ethidium bromide intercalates with DNA to provide orange fluorescence where it is able to permeate via damaged membranes (Liegler et al., 1995) (Waring, 1965).

Adipose derived stem cells from goat (Fig. 5C 11) & rabbit (Fig. 5C 12) were seeded on BCP & HASi discs and evaluated at 72 hrs via confocal laser scanning microscopy, with viable cells visible as green and non – viable cells indicated in orange. Scaffolds on evaluation were rimmed with viable green cells indicating the ability of scaffold surfaces to maintain cell integrity & membrane impermeability. This indicates lack of factors that defeat cell integrity and support of rapidly proliferating cellular components within the microstructures of the ceramic scaffolds.

5.4 Viability & Proliferation of Adipose Derived Stem Cells under Differentiation Conditions

Adipose Derived Stem Cells isolated from goat & rabbit sources prior to transplantation are placed under appropriate differentiation conditions to evaluate cell response and effect of differentiation media and conditions on cell viability & proliferation. To ascertain more information, adipose derived stem cells from candidate cell sources under differentiation conditions are evaluated qualitatively via confocal laser scanning microscopy and quantitatively via biochemical and gene expression studies

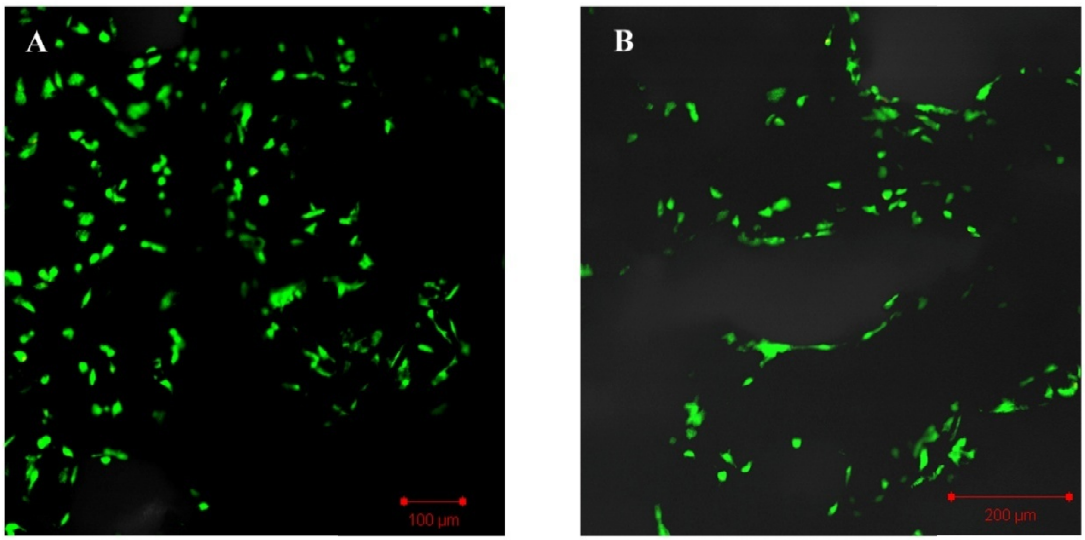

Fig. 5C 11:Live Dead imaging of Rabbit Adipose Derived Stem Cells on Ceramic Scaffolds: Confocal Laser Scanning Micrographs (A) BCP (B) HASi; Acridine orange stains the live cells green and Ethidium bromide stains the dead cells red

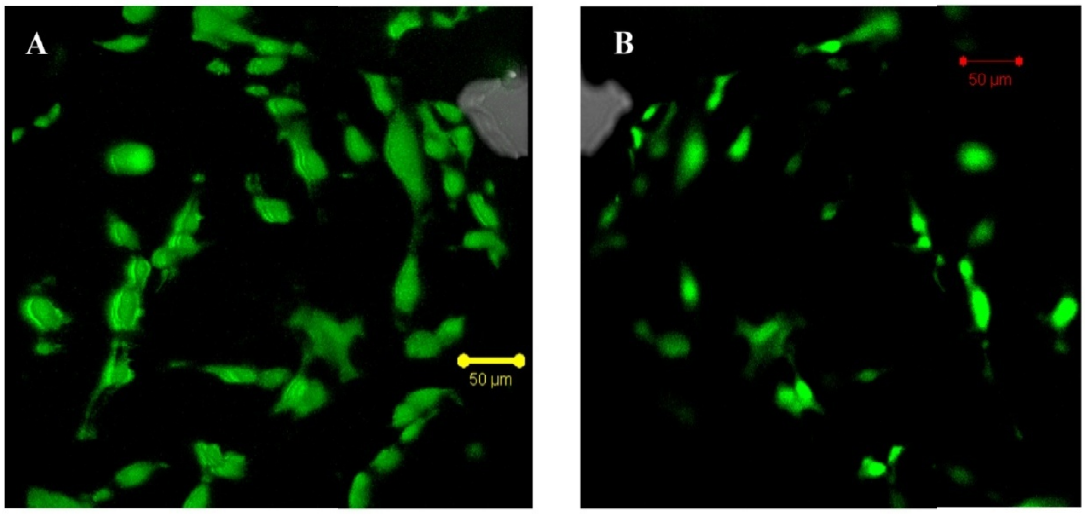

Fig. 5C 12:Live Dead imaging of Goat Adipose Derived Stem Cells on Ceramic Scaffolds: Confocal Laser Scanning Micrographs (A) BCP (B) HASi; Acridine orange stains the live cells green and Ethidium bromide stains the dead cells red

5.4.1 Evaluation of Osteogenic Differentiation Conditions: Scaffolds & Adipose Derived Stem Cells

RADMSCs and GADMSCs were seeded on ceramic discs and evaluated for cell proliferation, viability, ALP estimation and gene expression studies.

5.4.1.1 Viability of Adipose Derived Stem Cells on BCP & HASi Scaffolds under Osteogenic Conditions

On day 3 of exposure to osteogenic medium, GADMSCs (Fig. 5C 13) and RADMSCs (Fig. 5C 14) were evaluated via confocal laser scanning microscopy. Viable cells containing acridine orange, fluorescing green was visible on the scaffold surfaces. Negligible signals of ethidium bromide uptake were observed. Cells spread on the surface of HASi scaffolds in close apposition, with individual cell morphologies undistinguishable. Dexamethasone induced changes in cell morphology as reported in earlier studies over a long term were not observed (Mauney et al., 2004).

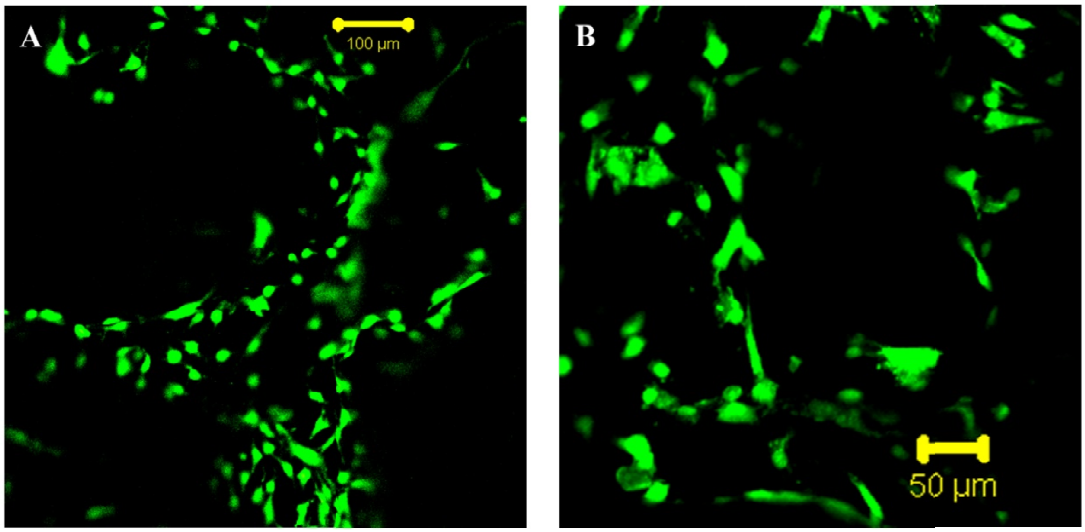

Fig. 5C 13:Live Dead imaging of Goat Adipose Derived Stem Cells on Ceramic Scaffolds (day 3 under osteogenic conditions): Confocal Laser Scanning Micrographs - (A) BCP (B) HASi; Acridine orange stains the live cells green and Ethidium bromide stains the dead cells red.

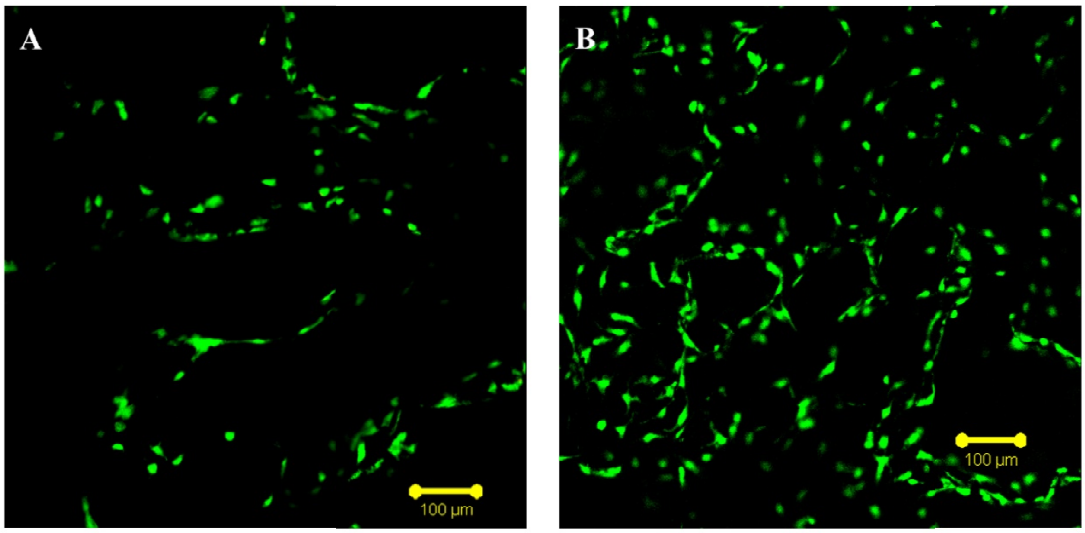

Fig. 5C 14:Live Dead imaging of Rabbit Adipose Derived Stem Cells on Ceramic Scaffolds (day 3 under osteogenic conditions): Confocal Laser Scanning Micrographs - (A) BCP (B) HASi; Acridine orange stains the live cells green and Ethidium bromide stains the dead cells red.

5.4.1.2 Viability of Adipose Derived Stem Cells on BCP & HASi Scaffolds under Osteogenic Conditions – 21 day observations

LDH assay was carried out to evaluate the viability of the adipose derived stem cell constructs in conjunction with the ceramic constructs by extending the period of observation upto 28 days. Empirically LDH analysis is rooted in the estimation of "leakage" or LDH present in culture medium due to the damaged nature of cell membranes (Decker and Lohmann-Matthes, 1988). To better understand viability levels, LDH analysis was carried out by lysing intact cells at designated time periods (Sepp et al., 1996). LDH within cell lysate estimated would provide a directly proportional measure of the viability of constructs under evaluation.

LDH analysis at 7, 14, & 21 days indicates a steady increase in viability of cells in both rabbit (Fig. 4C 15) & (Fig. 4C 16) goat groups. Cells seeded on the HASi scaffolds had a ($p<0.01$) significantly higher viability at all time points compared to the BCP group. This was reflected in cells of both candidate sources, indicating a cross – species effect of silica on the increased viability of cells (Hakki et al., 2013). The presence of an alkanizing effect of bioglass based ceramics has been lined to increased osteogenic cell activity in silica containing ceramics (Silver et al., 2001). The consistent increase in cell viability was maintained till observations were terminated at day 21. The HASi based scaffold systems are able to provide a higher viability maintenance over the study period across both animal groups while BCP based scaffold systems are able to support viability albeit at lower levels across groups.

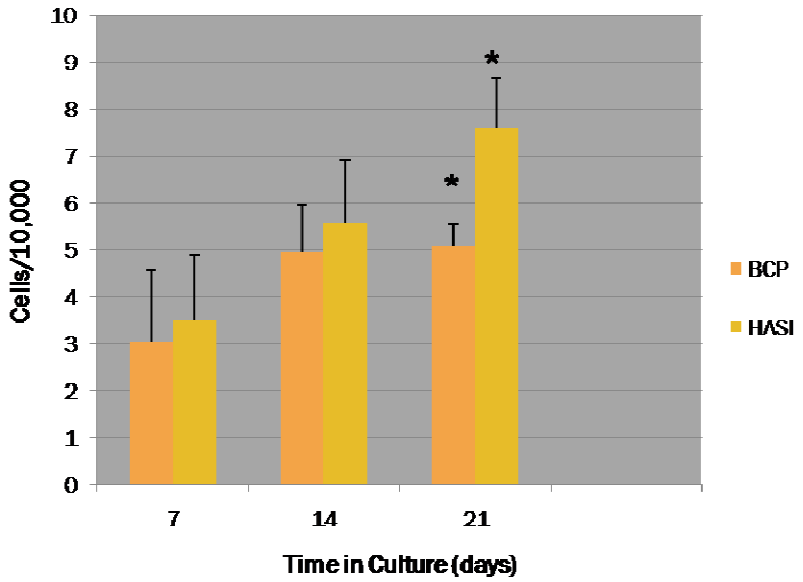

Fig. 5C 15: LDH assay of the viability of RADMSCs cultured on BCP and HASi under osteogenic conditions. Cells on HASi showed significantly higher viability (*) cells on BCP by day 21 ($p<0.001$).

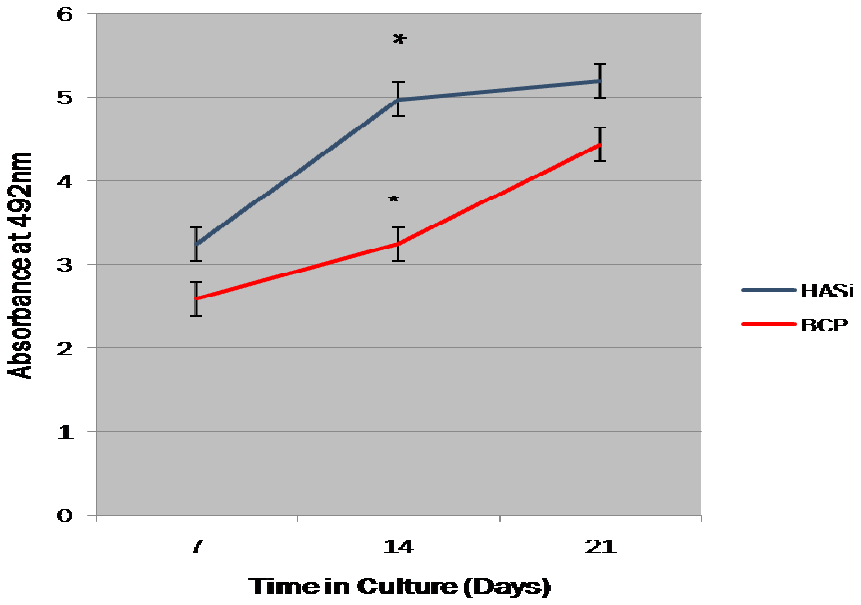

Fig. 5C 16: LDH assay of the viability of GADMSCs cultured on BCP and HASi under osteogenic conditions. Cells on HASi showed significantly higher viability (*) cells on BCP by day 14 ($p<0.001$).

5.4.1.3 Proliferation of Adipose Derived Stem Cells on BCP & HASi Scaffolds under Osteogenic Conditions – 21 day observations

Proliferation of RADMSCs and GADMSCs were quantified by picogreen assay (Ng et al., 2005) which is a widely accepted model of determining cellular proliferation with a DNA binding dye (Murakami and McCaman, 1999). Adipose derived stem cells seeded on BCP & HASi from both candidate cell sources were evaluated at day 7, 14 & 21. The results indicate a steady increase in cell proliferation across BCP & HASi in the case of RADMSC (Fig. 5C 17) & GADMSC (Fig. 5C 18) groups. There is a ($p< 0.01$) significant increase in cell proliferation from day 14 to day 21 in HASi groups. Proliferation is however maintained across groups indicating scaffold amenability to supporting osteogenic differentiation of rabbit & goat adipose derived stem cells over a period of 21 days.

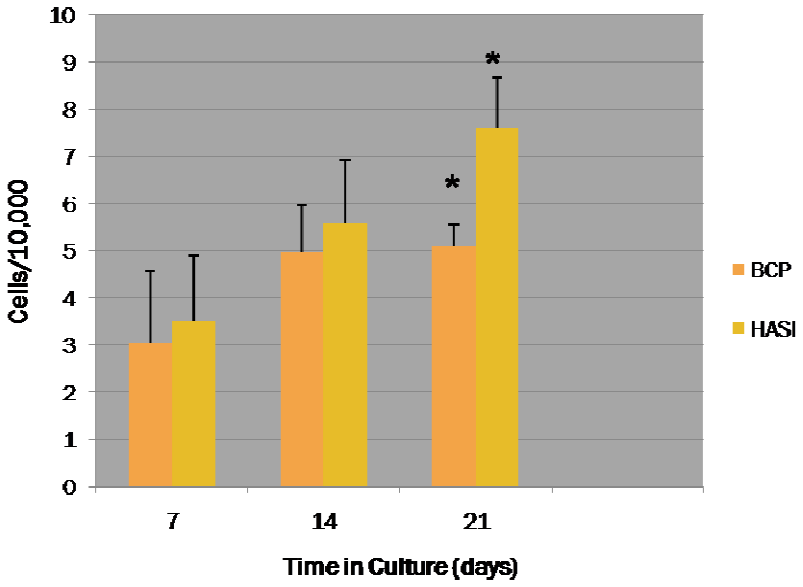

Fig. 5C 17: Picogreen assay of the proliferation of of RADMSCs cultured on BCP and HASi under osteogenic conditions. Cells on HASi showed significantly higher viability (*) cells on BCP by day 21 ($p<0.001$).

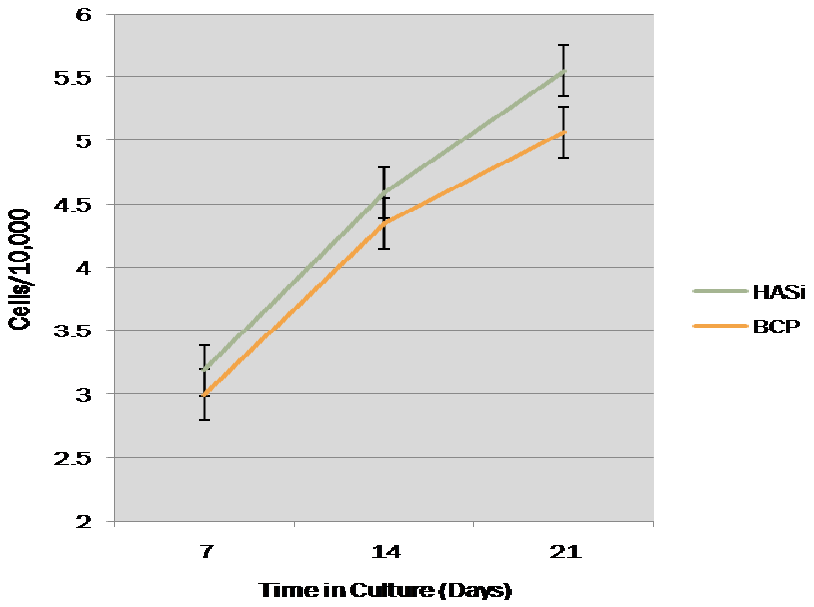

Fig. 5C 18: Picogreen assay of the proliferation of of GADMSCs cultured on BCP and HASi under osteogenic conditions. Cells on HASi compared to BCP indicated no significant difference in viability over 21 days.

The open architecture of the scaffold structures would contribute directly to the increase in cell proliferation (Kruyt et al., 2003). This is in turn made possible by the developing process of the ceramics. Presence of silica has been postulated to be the stimulating factor in development and maintenance of high cell proliferation over a period of 21 days. Hydrogels with nanospheres of silica with embedded nanospheres have been shown to enhance adherence as well as promote cellular activity (Gaharwar et al., 2013). The presence of tricalcium phosphate a highly soluble phase of hydroxyapatite as a ready source of calcium ions would promote cellular activity across groups. Cells in resting phase of G0 could be stimulated by calcium to enter the cell cycle, linking cellular activity to bioavailability of calcium based on scaffold properties.

5.4.1.4 Specific Alkaline Phosphatase Activity of Adipose Derived Stem Cells on BCP & HASi Scaffolds under Osteogenic Conditions – 21 day observations

ALP is an essential enzyme for mineralization, present in cells at early stage of osteogenesis. The enzyme presence & functionality is required for initialization of differentiation as well as promoting mineralized matrix synthesis (zur Nieden et al., 2003) (Stein et al., 1990). The transcription and expression of ALP is part of the days 5 to 14 of early osteogensis, after this initial peak the levels decrease indicating increasing maturation of induced osteogenesis (Aubin, 2001). In this study in the case of RADMSC's & GADMSC's. a species independent effect of osteogenic medium on cell differentiation can be observed with increase in ALP expression from day 7 to day 14. HASi indicates a significantly higher level of ALP, correlated to higher cell viability over the same period in the LDH assay also. Decrease in ALP levels is ascertained from day 14 onwards indicating onset of maturation in the synthesized bone matrix. Exposure to bioceramic contact directly or in extract form has been shown to increase osteogenic activity in ADSC's over time (Lee et al., 2013a). Expression of ALP in earlier stages has been liked to improved osteogeneis activity under implant conditions, leading to improved material – tissue interaction.

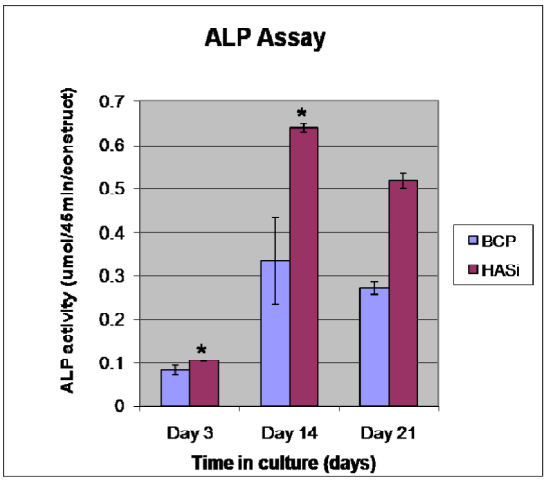

Fig: 5C 19: The specific ALP activity of RADMSC cells cultured on BCP and HASi - biochemical estimation. The ALP activity was determined, based on the hydrolysis of p-nitrophenyl phosphate to p-nitrophenol. Activity was significantly higher on HASi (*) than BCP ($p<0.001$).

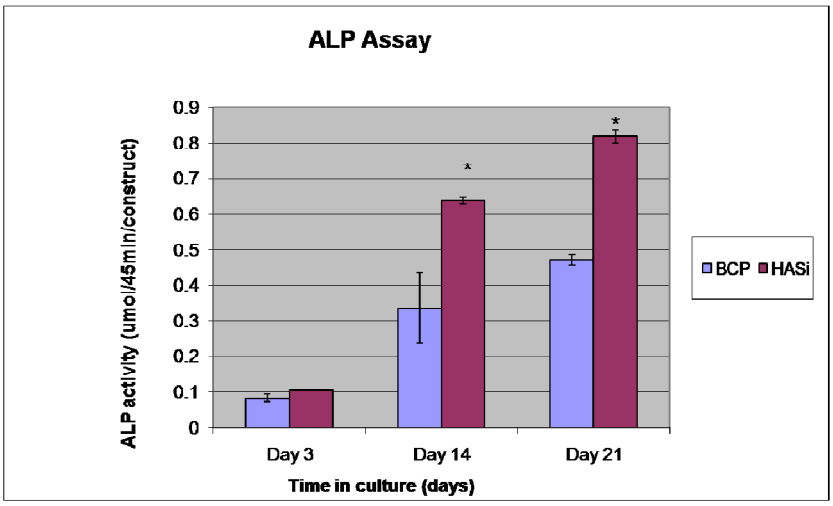

Fig: 5C 20: The specific ALP activity of GADMSC cells cultured on BCP and HASi - biochemical estimation. The ALP activity was determined, based on the hydrolysis of p-nitrophenyl phosphate to p-nitrophenol. Activity was significantly higher on HASi (*) than BCP ($p<0.001$).

5.4.1.5 Expression of ALP, Osteocalcin & Osteopontin

Real – Time PCR anlaysis of ALP, Osteocalcin & Osteopontin was carried out to evaluate osteogenic delineation of cells on scaffolds. Rabbit and Goat cells were evaluated on BCP & HASi scaffolds as indicated in materials & methods.

ALP levels across species increased from 7 to 14 days, with peak activity at 14 days and tapering off to the 4 week level. Significant difference in osteocalcin expression is reflected in rabbit cells seeded on BCP compared to cells on HASi (Fig. 5C 21 – 23). Although osteopontin expression is relatively in sync with overall osteogenic induction. In goat cells under osteogenic conditions, seeded on BCP & HASi scaffolds, expression of osteocalcin increased when expressed as fold expression with relation to time in culture (Fig. 5C 24 – 26). Osteopontin expression in this case peaks in the case of BCP at 2nd week, indicating early maturation. In HASi, peak levels of osteopontin are in the 3rd week of culture. This indicates the ability of the cells to undergo phased differentiation and achieve maturation depending on material properties.

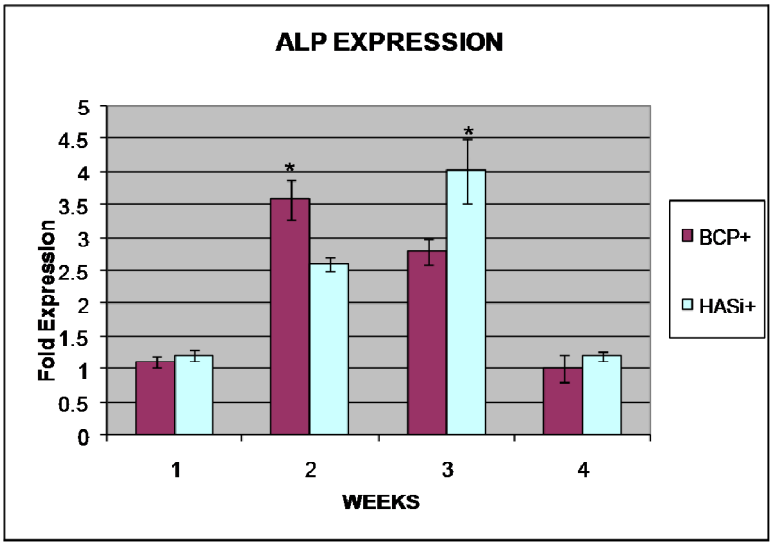

Fig. 5C 21: Real – Time PCR Analysis of the expression of ALP on RADMSCs cultured on BCP & HASi over a period of 4 weeks under osteogenic conditions. HASi showed significant increase in expression (*) than BCP ($p<0.001$) only at late phase of week 3.

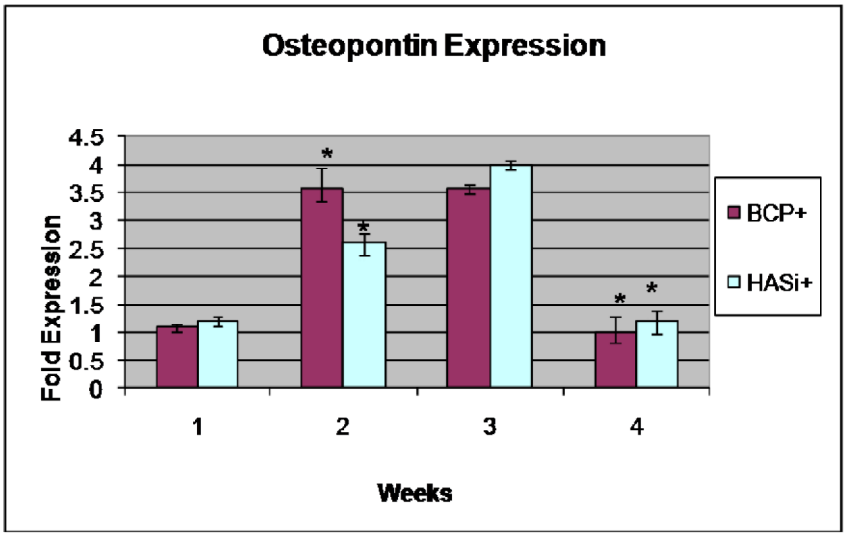

Fig. 5C 22: Real – Time PCR Analysis of the expression of Osteopontin on RADMSCs cultured on BCP & HASi over a period of 4 weeks osteogenic conditions. HASi showed significant increase in expression (*) than BCP ($p<0.001$).

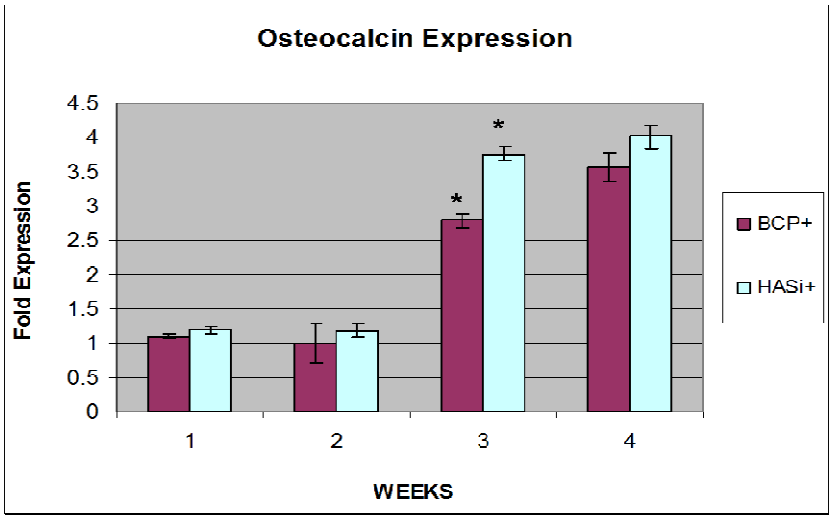

Fig. 5C 23: Real – Time PCR Analysis of the expression of Osteocalcin on RADMSCs cultured on BCP & HASi over a period of 4 weeks osteogenic conditions. HASi showed significant increase in expression (*) than BCP ($p<0.001$).

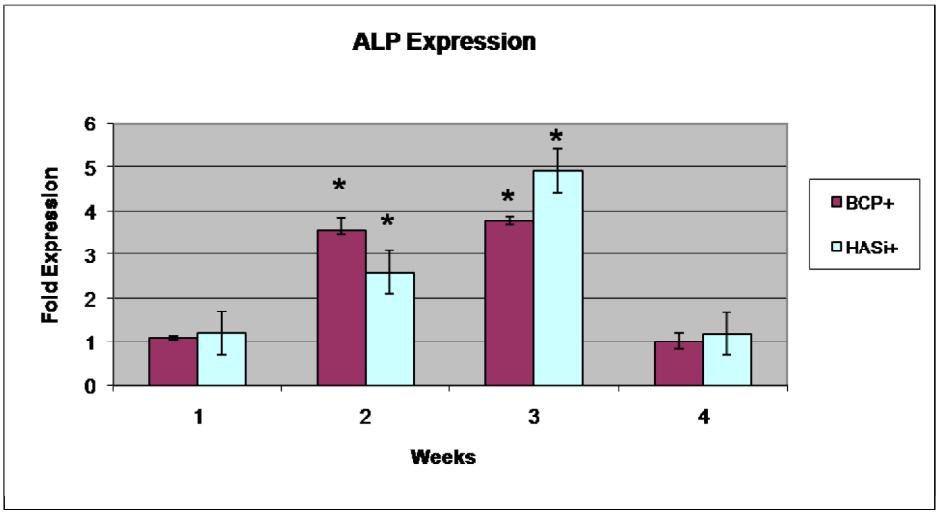

Fig. 5C 24: Real – Time PCR Analysis of the expression of ALP on GADMSCs cultured on BCP & HASi over a period of 4 weeks osteogenic conditions. BCP at three weeks and HASi at 4 weeks showed significant increase in expression (*).

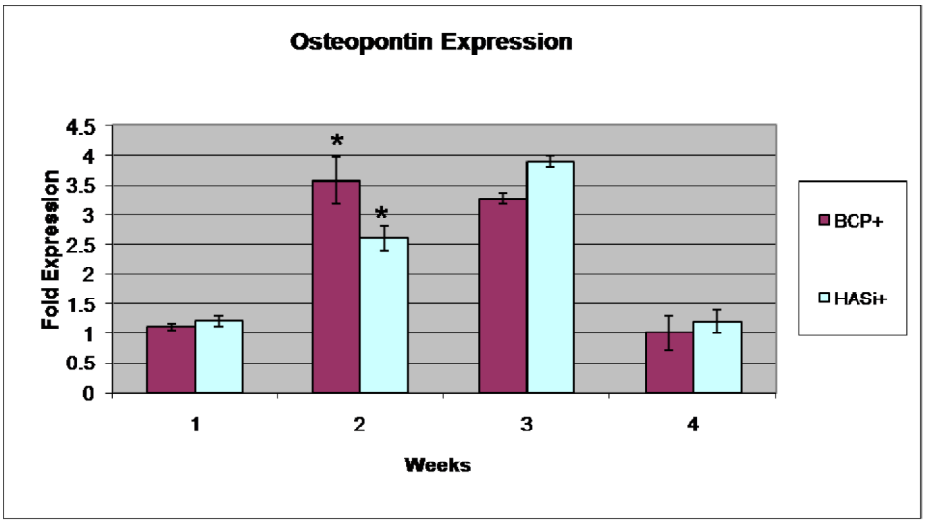

Fig. 5C 25: Real – Time PCR Analysis of the expression of Osteopontin on GADMSCs cultured on BCP & HASi over a period of 4 weeks osteogenic conditions. BCP and HASi at 2 weeks showed significant increase in expression (*).

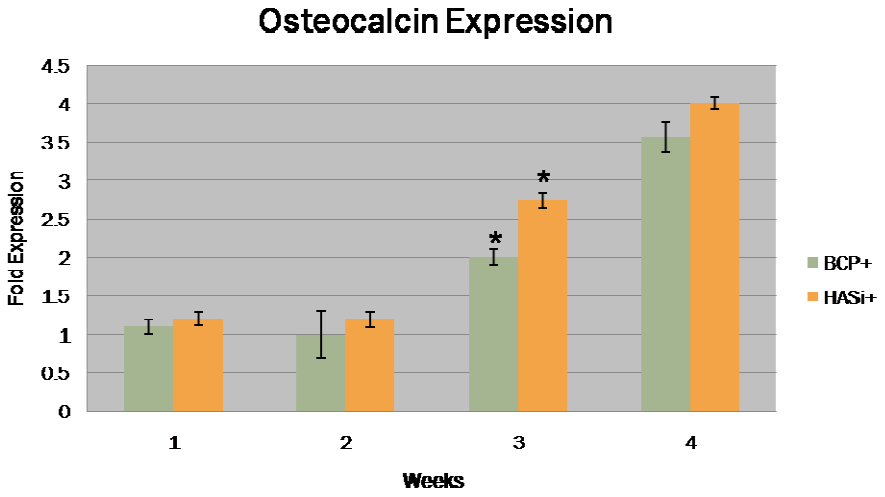

Fig. 5C 26: Real – Time PCR Analysis of the expression of Osteocalcin on GADMSCs cultured on BCP & HASi over a period of 4 weeks. HASi showed significant increase in expression (*) than BCP ($p<0.001$). at week three of osteogenic conditions.

The expression of ALP indicates initiation and tapering off is indicative of bone cell maturation. It is an early marker of osteogenic development and is a hallmark of

osteogenic initiation and calcification regulator (Jung et al., 2010) (Tsai et al., 2012). Strong consistent expression of ALP indicates the effectiveness of the osteogenic medium regimen followed. Also the expression of ALP in sync with the maturation cycles of normal bone (Borovecki et al., 2007) indicates normal development of stem cells to osteogenic lineage on the novel bioceramic scaffold systems.

Osteopontin is a late marker for maturing osteoblasts with expression increasing with relation to time spent in culture. ADSCs cultured on bioceramics have shown an innate ability to express heightened levels of RunX2 (Lee et al., 2013b), which in turn actively stimulates the early marker (ALP) as well as late markers (Osteocalcin, Osteopontin) for osteogenesis. The use of osteogenic medium with appropriate inducers compiled with quick resorbing nature of BCP causing a higher flux of calcium ion presence as well as stimulation of cell proliferation by silica would contribute optimized levels of osteogenic gene expression.

Pre- osteoblastic to osteoblastic evolution of cell types can be traced via their expression of characteristic gene products. Higher expression of osteogenic related gene products on HASi based scaffolds could be attributed to related reports of silica content in scaffold materials that promote osteogenic activity(Xynos et al., 2000a), (Xynos et al., 2000b). Depending on availability of calcium sources and current levels in local cell milieu, compared to levels of ionic availability of silica plays a key role in upregulation of desired gene products (Xynos et al., 2001).

The timely cascade type expression of ALP, Osteopont and Osteocalcin in goat and rabbit ADMSC based scaffold systems under osteogenic conditions indicates initiation & commitment to the osteoblastic lineage of the stem cell sources. Further evaluation of scaffold performance is possible under *in vivo* conditions.

5.4.2 Evaluation of Chondrogenic Differentiation Conditions: Scaffolds & Adipose Derived Stem Cells

RADMSCs and GADMSCs were seeded on ceramic discs and evaluated for cell proliferation, viability, GAG estimation and gene expression studies.

5.4.2.1 Viability of Adipose Derived Stem Cells on BCP & HASi Scaffolds under Chondrogenic Conditions

On day 3 of exposure to chondrogenic medium, GADMSCs (Fig. 5C 27) and RADMSCs (Fig. 5C 28) were evaluated via confocal laser scanning microscopy.

Cells on scaffold were observed to be fluorescing green, indicating viable nature of cells under chondrogenic growth medium conditions. Nil signals of orange / red fluorescence indicating presence of dead / pre- apoptotic cells were observed.

Cells were observed in the case of Goat and Rabbit ADMSCs to be spread closely on the surface at 72 hrs of culture time. Variations based on serum conditions prescribed to stess were not observed (Kyllönen et al., 2013). Viability of cells indicates acceptance of chondrogenic medium conditions, as non – viable medium composition results in failure of continued chondrogenesis (Indrawattana et al., 2004). Cells were observed to be regularly shaped and attached to the surface, but have not achieved spherical morphology of mature chondroblastic structures as time in culture is restricted (Wu et al., 2014).

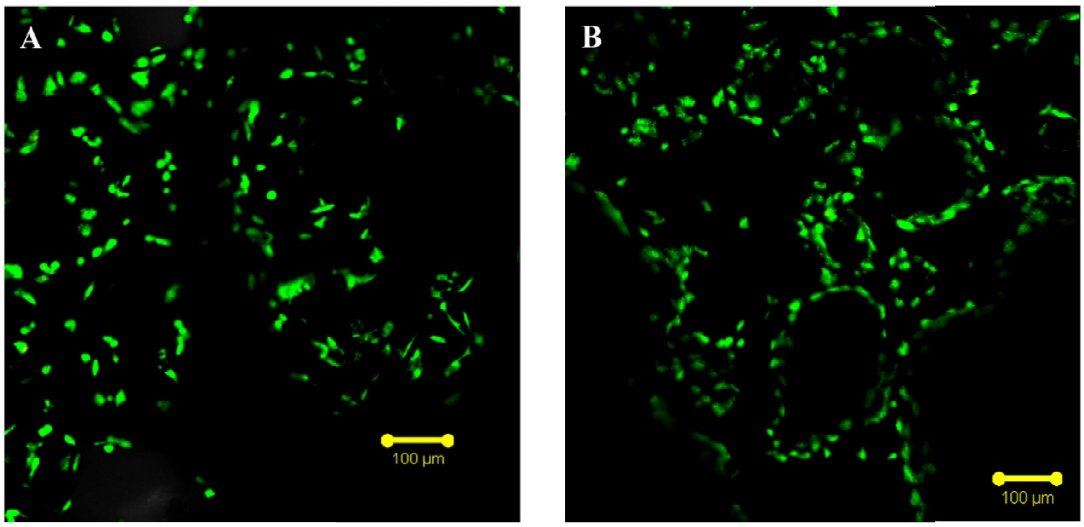

Fig. 5C 27: Live Dead imaging of Goat Adipose Derived Stem Cells on Ceramic Scaffolds (day 3 under chondrogenic conditions): Confocal Laser Scanning Micrographs - (A) BCP (B) HASi; Acridine orange stains the live cells green and Ethidium bromide stains the dead cells red.

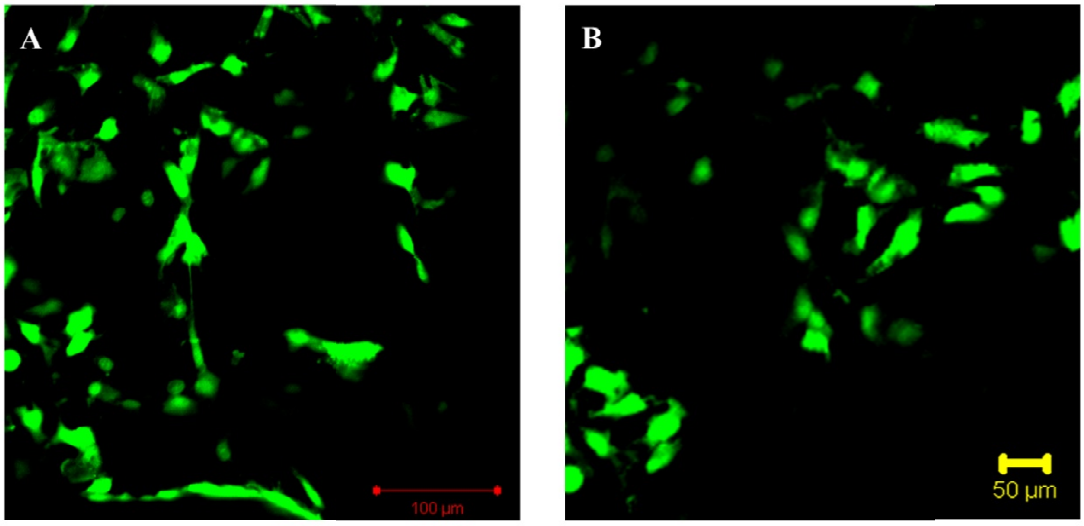

Fig. 5C 28:Live Dead imaging of Rabbit Adipose Derived Stem Cells on Ceramic Scaffolds (day 3 under chondrogenic conditions): Confocal Laser Scanning Micrographs - (A) BCP (B) HASi; Acridine orange stains the live cells green and Ethidium bromide stains the dead cells red.

5.4.2.2 Viability of Adipose Derived Stem Cells on BCP & HASi Scaffolds under Chondrogenic Conditions – 21 day observations

LDH assay was carried out to evaluate the viability of the adipose derived stem cell constructs in conjunction with the ceramic constructs by extending the period of observation upto 28 days. As mentioned in **4.4.2.1**, the analysis here is based on estimable LDH contained within viable cellular structures (Sepp et al., 1996) and not as per cell leakage (Decker and Lohmann-Matthes, 1988).

LDH analysis at 7, 14, & 21 days indicates a steady increase in viability of cells in both goat (Fig. 5C 29) & (Fig. 5C 30) rabbit groups. A dip in cell population viability at the two week mark is observed, but viability is at highest points at 21 days when observation is terminated. A temporary reduction in viability may be due to changes in the microenvironment due to quicker dissolution of alkaline calcium products from BCP breakdown, where in modifications of cell substrate chemical structures have been proven to affect total cell viability (Curran et al., 2006). Viability is also co-related to the amount of extra-cellular matrix generated over time, which in the coming sections are shown to increase in direct proportion to time spent in culture (Ogawa et al., 2010).

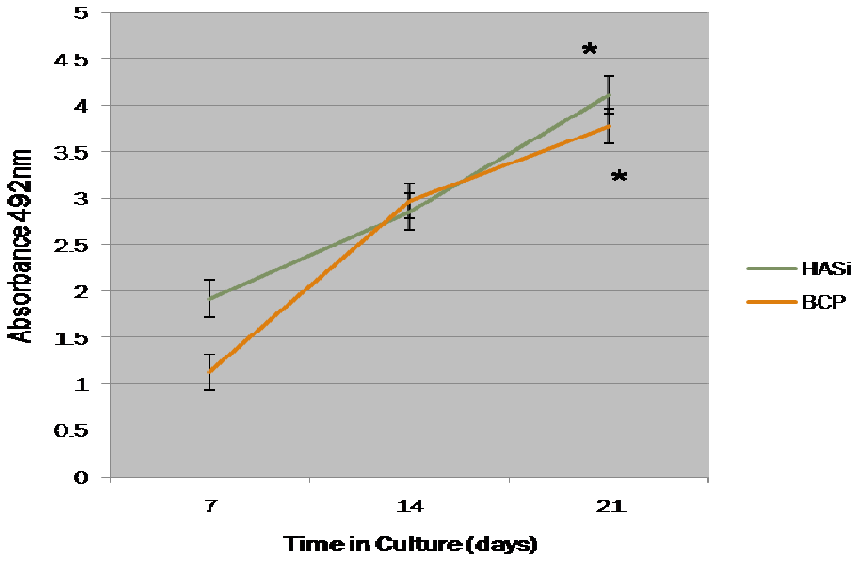

Fig. 5C 29: LDH assay of the viability of GADMSCs cultured on BCP and HASi under chondrogenic conditions. No significant difference was observed over 21 days

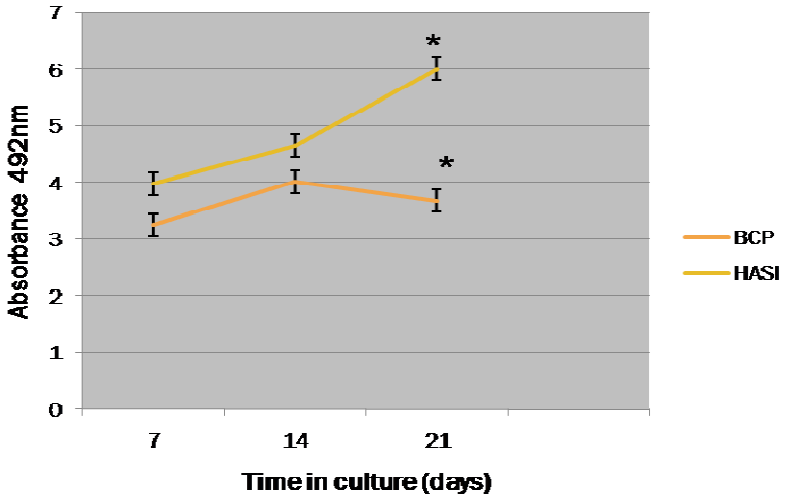

Fig. 5C 30: LDH assay of the viability of RADMSCs cultured on BCP and HASi under chondrogenic conditions. Cells on HASi showed significantly higher viability (*) cells on BCP by day 21 ($p<0.001$). Drop in viability conversant with differentiation is observed.

HASi scaffolds supported ($p<0.01$) significantly higher viability at all time points compared to the BCP group. This was reflected in cells of both candidate sources. Increased viability may be attributed to effect of silica on the increased viability of cells (Hakki et al., 2013), leading to the use of silica based nanofibers as viable carriers for cartilage tissue engineering (Buchtová et al., 2013).

The HASi based scaffold systems are able to provide a higher viability maintenance over the study period across both animal groups while BCP based scaffold systems are able to support viability albeit at lower levels across groups.

5.4.2.3 Proliferation of Adipose Derived Stem Cells on BCP & HASi Scaffolds under Chondrogenic Conditions – 21 day observations

Proliferation of RADMSCs and GADMSCs were quantified by picogreen assay, as proliferation plays a major role in the acceptance, integration and maintenance of any long term tissue engineered product. Picogreen an accepted DNA binding model system was used here (Ng et al., 2005) (Murakami and McCaman, 1999). The cell

seeded scaffold systems of goat (Fig. 5C 31) and rabbit (Fig. 5C 32) were evaluated at day 7, 14 & 21. In both systems, under chondrogenic conditions there was steady increase in cell proliferation over time in culture. Continued cell proliferation under differentiation conditions indicate ongoing compatibility with media and lack of cell loss under stress, this is designed for in modern tissue engineering applications (Hamid et al., 2014). Cell proliferation is mostly optimized for (Zhou et al., 2014) as implant functionality and success of terminal applications depend on the ability of the scaffold to maintain sustained growth.

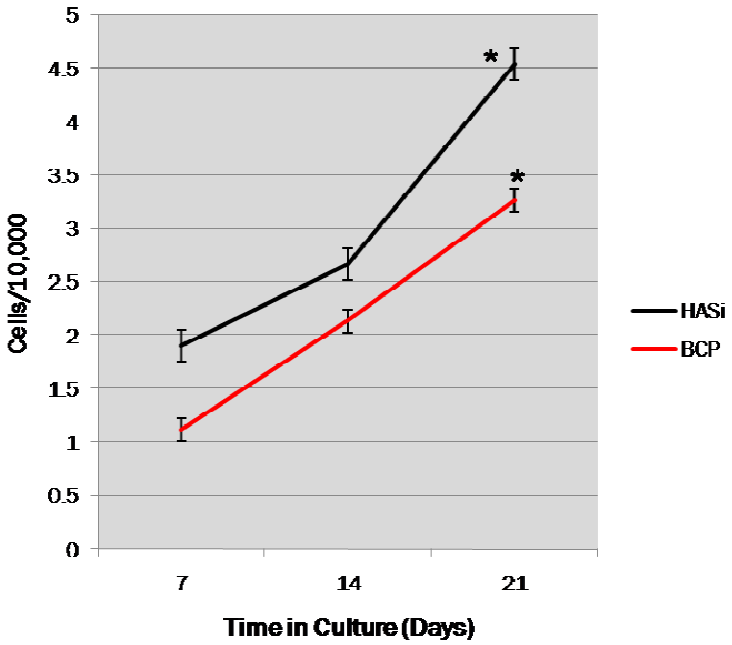

Fig. 5C 31: Picogreen assay of the proliferation of of GADMSCs cultured on BCP and HASi under chondrogenic conditions. Cells on HASi compared to BCP indicated significant (*) difference in viability over 21 days ($p<0.001$).

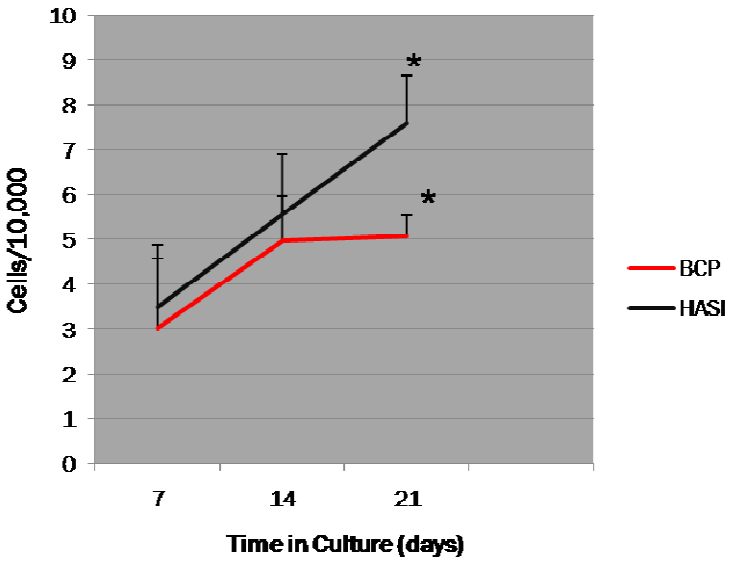

Fig. 5C 32: Picogreen assay of the proliferation of of RADMSCs cultured on BCP and HASi under chondrogenic conditions. Cells on HASi compared to BCP indicated significant difference in proliferation over 21 days ($p<0.001$) (*).

Increase in cell proliferation under chondrogenesis is promoted via compressive stress application (Wang et al., 2013), which is not applied in this case. But scaffold specific stimuli would play a major role in stimulation of cell proliferation. The ability of scaffolds that promote proliferation coupled with chondrogenesis are proved to function better under real world conditions (Awad et al., 2004). Appropriate cell response depend on surface to cell interaction, which when positive is indicated by improve cell viability and proliferation. This in turn affects the rate and quality of new tissue formation, starting from initial tissue adherence (Boyan et al., 1996). The modified apatite surfaces are therein proven to be plausibly effective in maintaining a differentiating population of stem cells over a period of 21 days.

5.4.2.4 Total GAG Estimation: Adipose Derived Stem Cells on BCP & HASi Scaffolds under Chondrogenic Conditions – 21 day observations

In articular cartilage GAG's are the most common ECM components ranging from chondroitin sulphate, keratin sulphate, dermatan sulphate and heparan sulphate.

Aggrecan and collagen type II are synthesiszed by chondrocytes and is the load bearing component. GAG estimation was carried out by an accepted (Totonelli et al., 2012)(Maghsoudlou et al., 2013) kit based system using a DMMB dye method.

Total GAG estimation was carried out on goat and rabbit cell seeded scaffold structures and evaluated after a 21 day period. In goat (Fig. 5C 33) and rabbit (Fig. 5C 34) statistically signification increase in GAG synthesis was observed over time. Slight increase in silica coated scaffolds was observed. Prior observations have indicated that the more cell clusters, as well as micro-environment changes within silica coated based bioglass structures have stimulated the production of extra cellular matrix, GAG abundantly. The ability of the scaffold systems to support GAG synthesis over time indicates firm activation of chondrogenesis pathways on the cells seeded on the support structures (Helen and Gough, 2008).

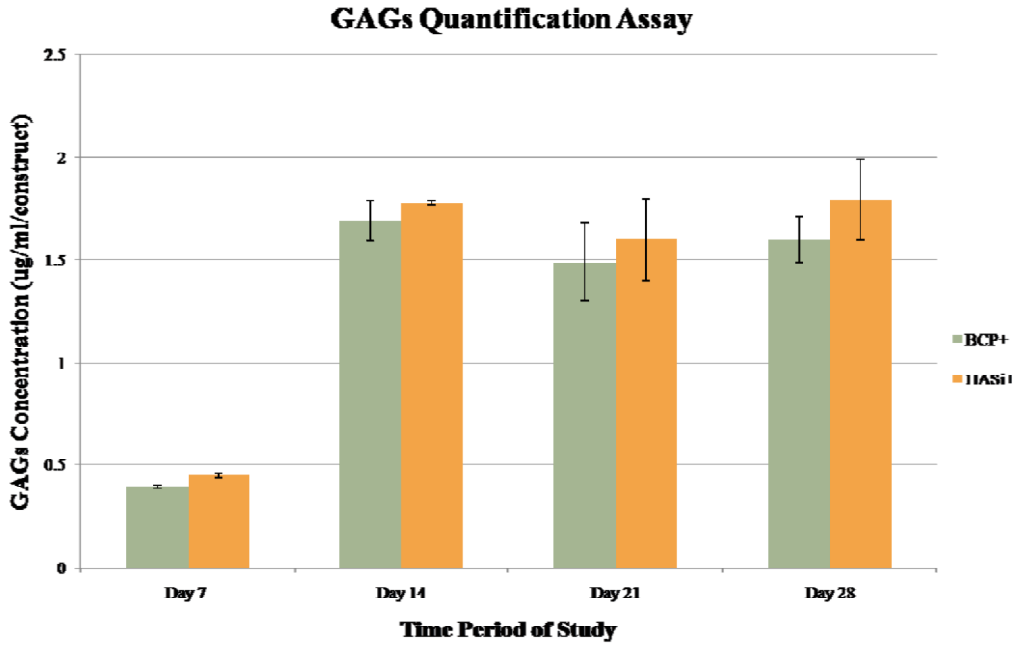

Fig. 5C 33: GAG Estimation: Blyscan Assay estimation of glycosaminoglycans synthesized by GADMSCs on BCP & HASi scaffolds under chondrogenic conditions. No significant difference between scaffolds over a period of 28 days was observed.

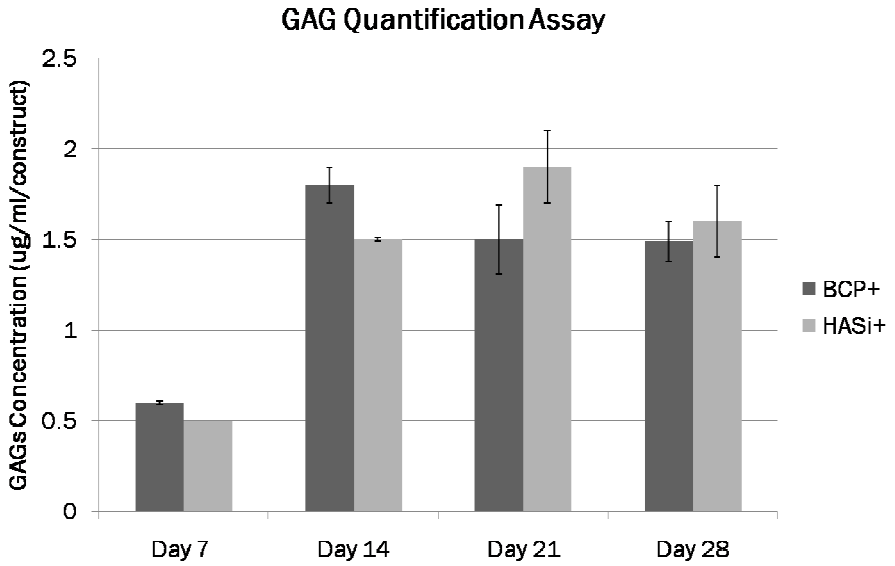

Fig. 5C 34: GAG Estimation: Blyscan Assay estimation of glycosaminoglycans synthesized by RADMSCs on BCP & HASi scaffolds under chondrogenic conditions. No significant difference between scaffolds over a period of 28 days was observed.

5.4.2.5 Expression of Sox 9, Col 2A & Aggrecan on Ceramic Scaffolds

Three genes were selected for expression analysis on samples drawn from goat & rabbit adipose derived stem cells seeded on ceramic scaffold structures. To understand the intiation, maintenance & maturation of stem cells into chondrogenic lineage under defined conditions these candidate genes were selected. In goat adipose derived stem cells placed on ceramic scaffolds the results (Fig. 5C 35 - 37) indicated expression of key chondrocytic genes. Rabbit samples (Fig. 5C 38 - 40) also indicated effectiveness of chondrogenic regimen by vital increase in fold expression of key chondrocytic genes assayed.

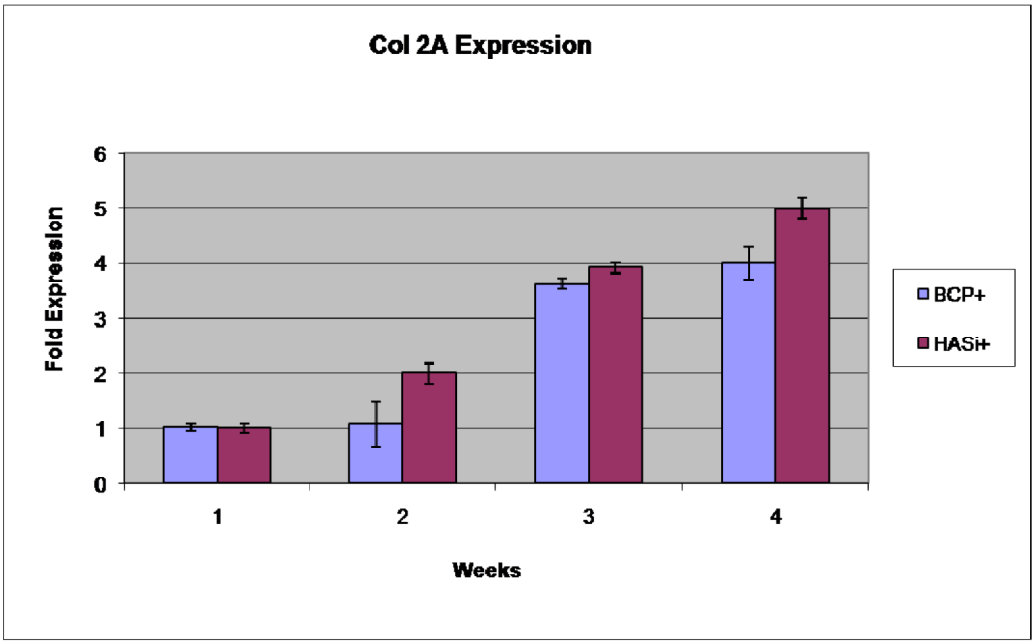

Fig 5C 35: Real – Time PCR Analysis of the expression of Col 2A by GADMSCs cultured on BCP & HASi cultured under chondrogenic conditions for 28 days. No significant difference in expression was observed.

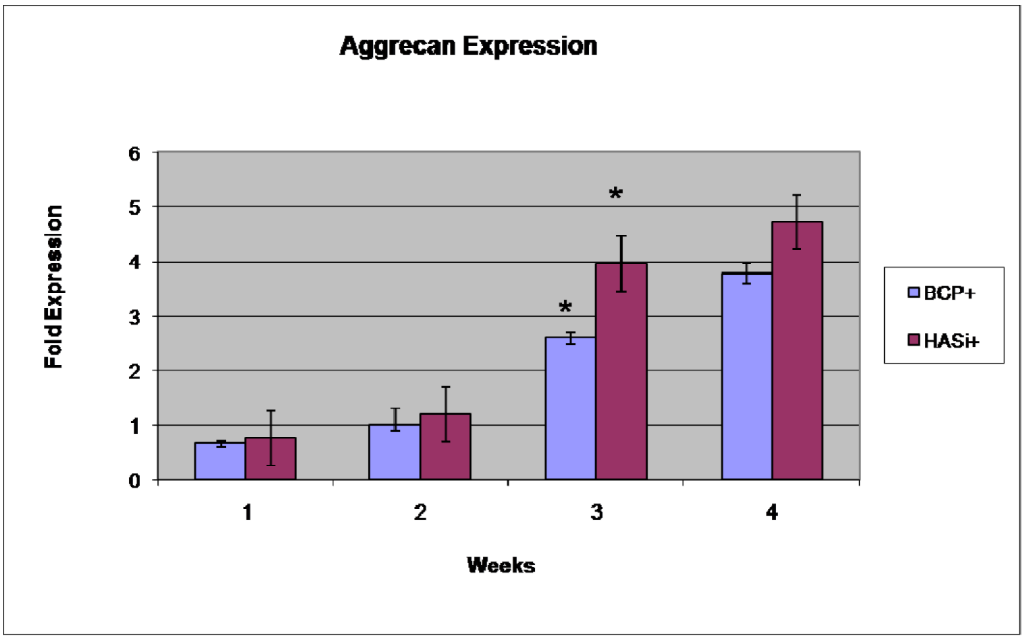

Fig. 5C 36: Real – Time PCR Analysis of the expression of Aggrecan by GADMSCs cultured on BCP & HASi cultured under chondrogenic conditions for 28 days. Cells on HASi compared to BCP indicated significant difference in expression at 21 days ($p<0.001$) (*).

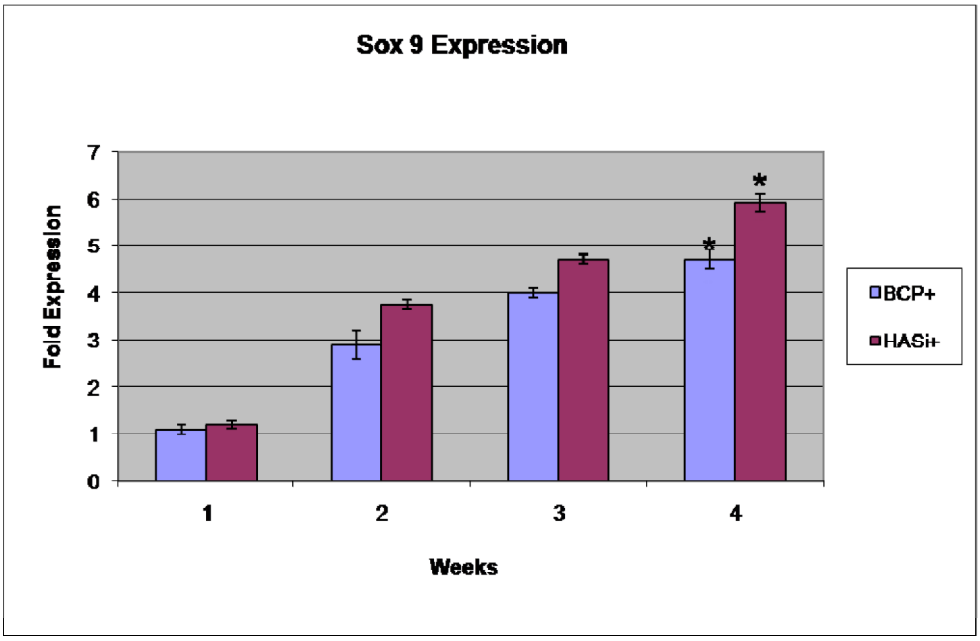

Fig. 5C 37: Real – Time PCR Analysis of the expression of Sox 9 by GADMSCs cultured on BCP & HASi cultured under chondrogenic conditions for 28 days. Cells on HASi compared to BCP indicated significant difference in expression at 28 days ($p<0.001$) (*).

Chondrogenesis is a defined pathway that occurs as a result of mesenchymal stem cell condensation and differentiation into chondroprogenitor cell population (Goldring, 2012), cells may further undergo hypertrophy to undergo endochondral ossification in the osteogenic pathway. The regulation of stem cell condensation, cells derived to resting chondrocytes in articular cartilage, initiation of hypertrophy are an interplay of events subject to regulation by fibroblast growth factor (FGF), TGF (Wu et al., 2007), BMP (Yoon et al., 2006) & Wnt signaling pathways (Lefebvre and Smits, 2005). Sox 9 is one of the earliest markers expressed in mesenchymal condensations and is the key transcriptional factor in chondrocyte differentiation (Lefebvre et al., 1998).

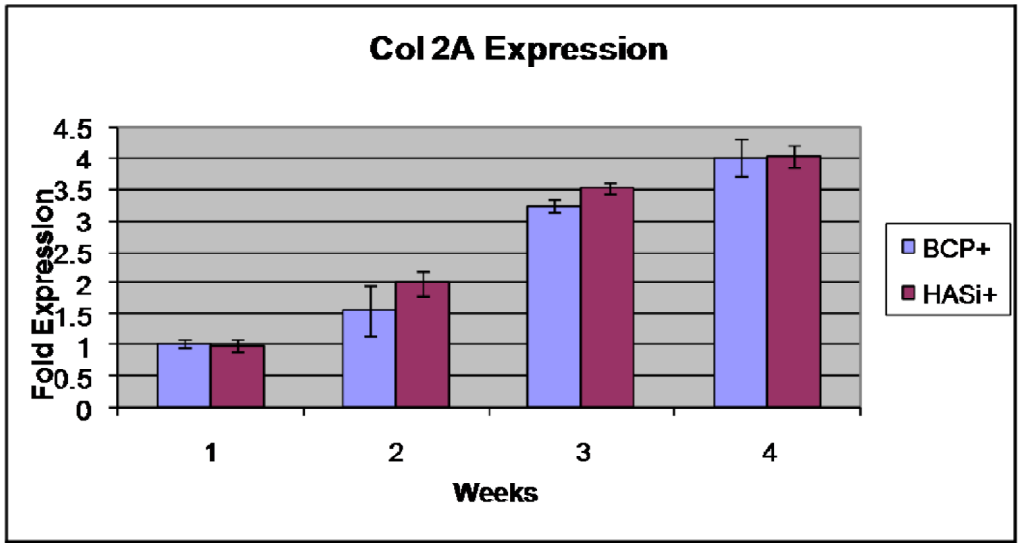

Fig 5C 38: Real – Time PCR Analysis of the expression of Col 2A by RADMSCs cultured on BCP & HASi cultured under chondrogenic conditions for 28 days. No significant difference in expression was observed.

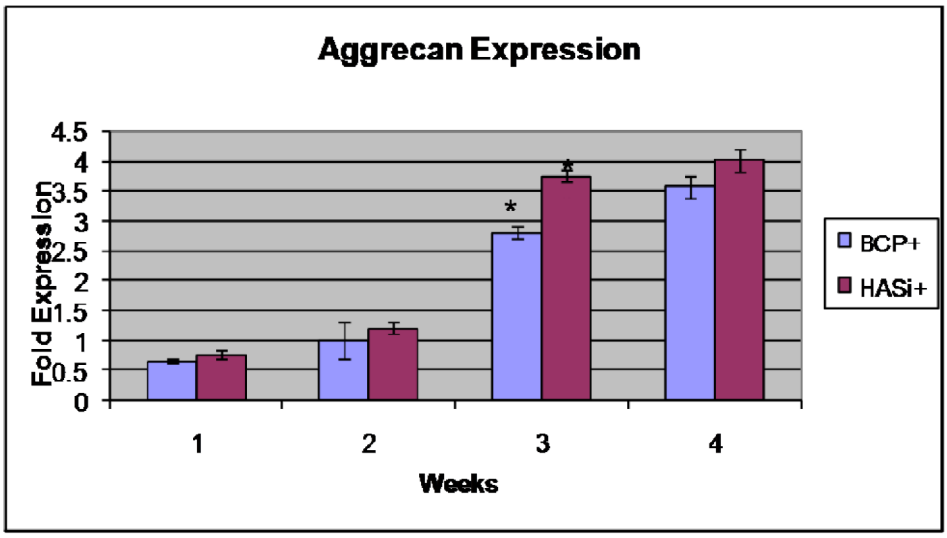

Fig. 5C 39: Real – Time PCR Analysis of the expression of Aggrecan by RADMSCs cultured on BCP & HASi cultured under chondrogenic conditions for 28 days. Cells on HASi compared to BCP indicated significant difference in expression at 21 days ($p<0.001$) (*).

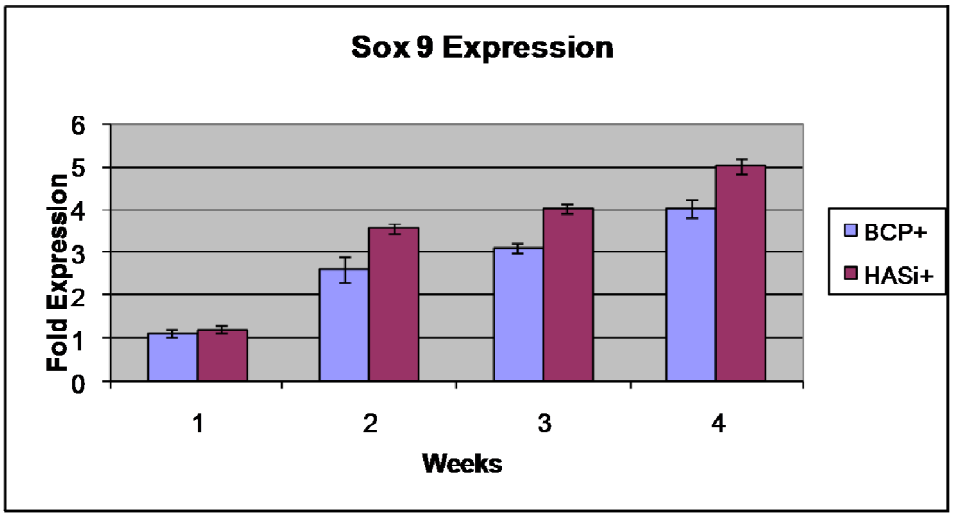

Fig. 5C 40: Real – Time PCR Analysis of the expression of Sox 9 by RADMSCs cultured on BCP & HASi cultured under chondrogenic conditions for 28 days. No significant difference in expression was observed.

Sox9, in concert with L-Sox5 and Sox6, regulates cartilage formation and maintains the chondrocyte phenotype in the mature cartilage by activating expression of several cartilage-specific genes, including genes for the types II, IX and XI collagen (*Col2a1, Col9a1 and Col11a1*), aggrecan (*Acan*) and COMP (*Comp*) (Huang et al., 2001); (Ng et al., 1997). The selected genes are therefore in sync with understanding initialization and maintenance of chondrogenesis via Sox 9 expression, and maturation via aggrecan and collgen type II expression.

Differentiation step	Extracellular matrix markers	Regulatory markers		Growth and differentiation factors
Chondrogenic Mesenchymal cells	*Col1a1*	*Sox9, Runx2*		Shh, TGF-β
Prechondrocytes	*Ncam1, Tnc*	*Sox9, Sox5, Sox6*	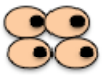	TGF-β Wnt-3A, Wnt7A FGF-2,4,8,10 BMP-2,4,7
Early chondroblasts	*Col2a1, Acan, Crtl*	*Sox9, Sox5, Sox6*		
Columnar chondroblasts	*Col2a1, Acan, Crtl1 Comp, Crtm*	*Sox9, Sox5, Sox6*		IGF-1 FGF-2/ FGFR2 BMP-2,4,7,14
Prehypertrophic chondrocytes	*Col2a1, Acan, Crtl1 Comp, Crtm*	*Pthr1, Ihh*	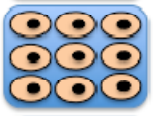	FGF-18,FGFR-3 BMP-2,7
Hypertrophic chondrocytes	*Col10a1*	*Runx2, Runx3*	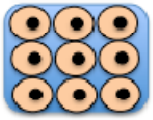	VEGF FGF-2,FGF-R1 Wnt14/β-catenin
Terminal chondrocytes	*Mmp13, Spp1*	*Runx2, c-Maf*		

Modified from Lefebvre & Smits (2005)

CHAPTER: 6

DEMONSTRATION OF CELL – CERAMIC CONSTRUCTS IN LAPINE & CAPRINE MODELS

6.1 Demonstration in Lapine & Caprine Models

Testing the mettle of a tissue engineered scaffold involves trials in selected in vivo models under controlled conditions. This helps collate information regarding material – tissue interaction as well in understanding the performance of cell – ceramic constructs in tissue milieu. Small animal models are widely used keeping in mind the ease of use as well as cost control issues. Large animal models are selected for pre – clinical data acquisition as well as understanding scaffold performance under increased loading conditions (Chu et al., 2010b). Defect sizes and placement are also crucial, with emphasis on the use of load bearing defect areas on the condylar surface of the femur or the tibial plateau to validate high stress environments (Chu et al., 2010c).

Restoration of the joint surface has to be validated in a suitable model. This in turn depends on the question being asked, hypothesis being tested and finally the availability of suitable models (Reinholz et al., 2004). In this study the high load bearing, large osteochondral defects in the medial femoral condyles of the lapine and caprine model were selected for optimal evaluation (Shao et al., 2006a).

Demonstration of *in-vivo* performance of the fabricated osteochondral grafts have been carried out as follows:

1. **Short – Term Implantation Study in Rabbit Model**
2. **Long – Term Implantation Study in Rabbit Model**
3. **Long – Term Implantation Study in Goat Model**

6.2 Short Term Implantation Studies in Rabbit Osteochondral model – *in vivo*

Post implantation, rabbits were housed in separate cages and took water and feed *ad libitum.* Healing was uneventful without any inflammation and after the study period of 4 weeks. Healing pattern of test animals with implanted samples was uneventful with BCP & HASi implanted animals. Experimental animals regained pre-operative gait performance as implant area healing rendered locomotion pain free, with no observation of repetitive or stress behaviours recorded.

6.2.1 *Ex vivo* Evaluation

Gross examination revealed no fibrous tissue formation or anomalies within the joint structure. Retrieved rabbit implant samples on macroscopic examination indicated an overburden on the ceramic scaffolds *in situ*

6.2.2 Histology – Poly Methylmethacrylate (PMMA) Embedding: Van Gieson's Picrofuschin – Stevenal's Blue Staining.

Post-processing & staining examination revealed a Stevenal's blue stained area over the yellow Van Gieson's stained area. Stevenal's blue staining of the control condyle section indicated hyaline cartilage formations with vertically aligned chondrocytes. Van Gieson's staining below the same indicated healthy trabecular bone conditions.

Similarly the ceramic surface in the test samples (Fig. 6C 1A & 2B) revealed the beginning of formation of an unorganized cartilage matrix over the surface stained by Stevenal's blue. The ceramic implant has been over grown by the matrix and integrated into the joint tissue. Presence of matrix overlay indicates the acceptance of the material into the joint milieu. In the BCP scaffold implanted condyle a definite lack of organization in the deposition, accretion of cells in the cartilage layer can be identified on comparison with the control section (Fig. 6C 2C). The aggregate over the HASi scaffold appears to be more cellular in nature, with less accumulation of extracellular matrix. The un-organized appearance of the cartilage over growth is contingent to the short duration of observation of the study which may reorganize with time. Preliminary integration with surrounding tissue indicates scaffold acceptance in the joint milieu (Nooeaid et al., 2012b).

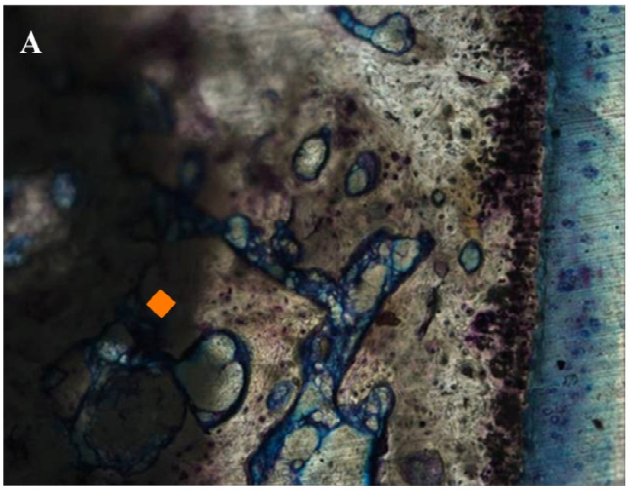

(A) BCP – demonstrating cellular overgrowth.

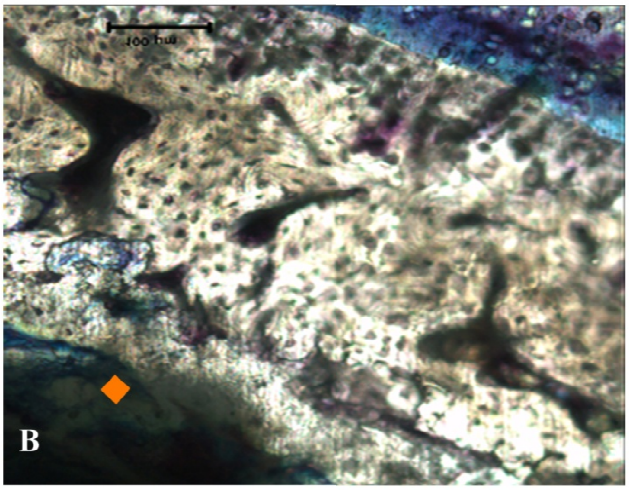

(B) HASi – demonstrating integration into condylar tissue

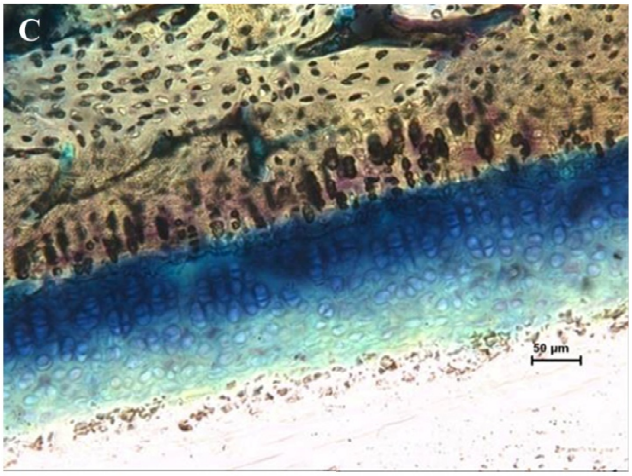

(C) Control – demonstrates native stage of condylar tissue

Fig. 6C 1: Polymethylmethacrylate embedded rabbit condylar longitudinal sections retrieved 4 weeks post implantation and demonstrated with Stevenal's blue & Van Gieson's Picrofucshin differential stain (cells - blue; bone – yellow) ◆ - indicates remnant scaffold structures.

6.2.3 Back Scatter Electron Imaging.

To further understand the interaction of the scaffold with the surrounding bone tissue, BSE imaging was carried out. The (Fig. 6C 2) indicates the ceramic scaffold in white, with the surrounding / infiltrating bone surfaces in gray. The image clearly highlights the steady deterioration of the scaffold and the simultaneous in-growth of bone within the scaffolds. Pronounced osteointegration of the scaffold can be observed in the case of the HASi scaffold, the ceramic has been well assimilated in to the newly formed trabecular bone structure. With BCP, the original scaffold morphology was retained, with bone infiltration proceeding from the outer edges of the ceramic via the pores. Ingrowth of bone will help in the stabilization of scaffold material within the defect area. Prevention of micro movements will help organization of proper cartilage architecture as it is understood that such movements & wear particle debris can accelerate the process of fibrous tissue capsule formation and related loosening of surrounding bone (F. H.R. De Man et al., 2005).

6.3 Long Term Implantation Study in Rabbit Model

Cell – seeded BCP & HASi scaffolds were placed in the medial femoral condyle of New Zealand White Rabbits, with bare scaffolds as control. The cell – seeded scaffolds were implanted for a period of 6 months and retrieved post – euthanasis.

6.3.1 *Ex – vivo* Evaluation

Healing in all cases of implanted rabbit was uneventful, with animals gaining weight at normal levels. Cases of infection or loss of animals due to secondary reasons was not observed.

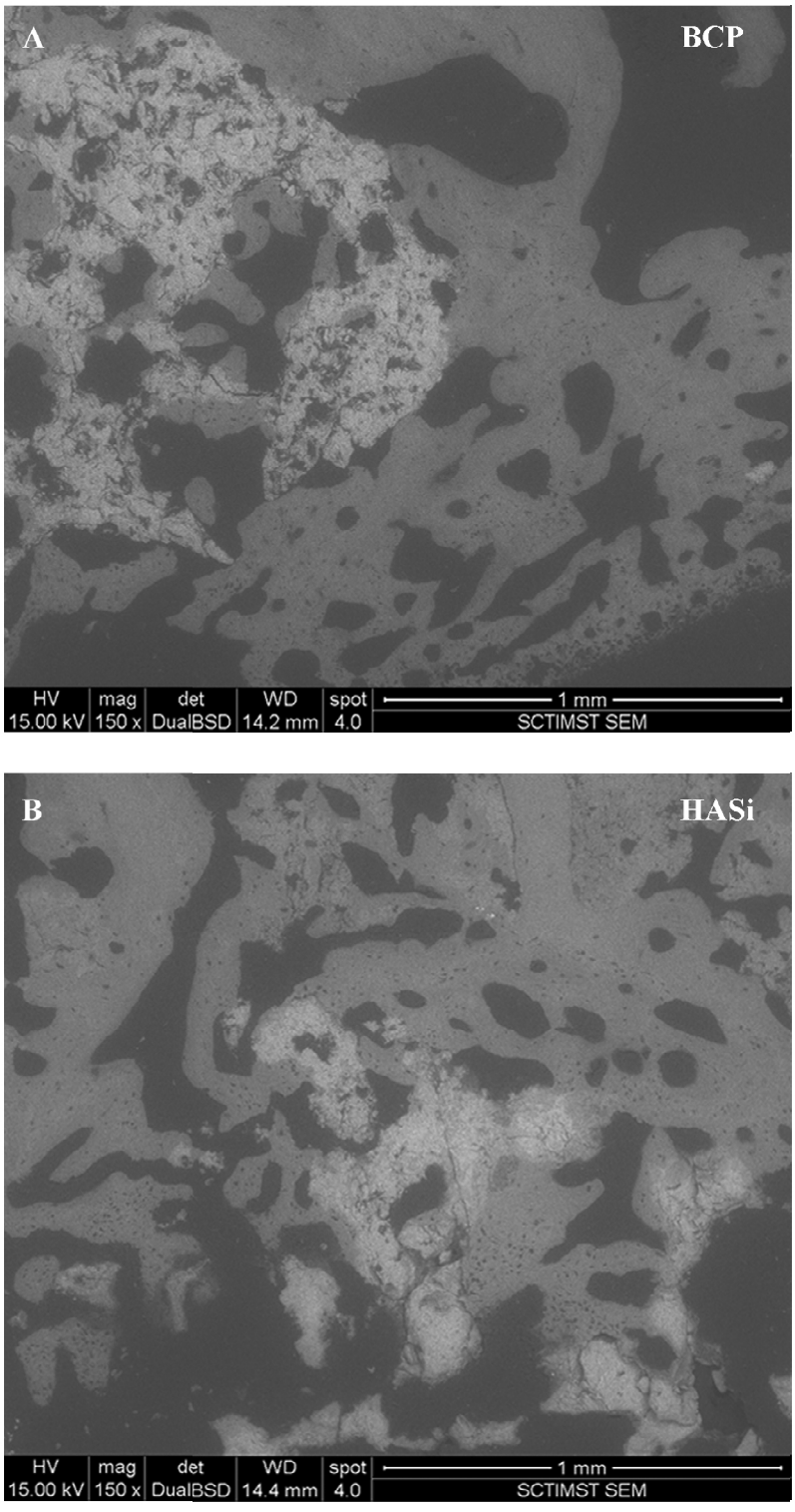

Fig. 6C 2: Back Scatter Electron Micrographs of (A) BCP – 150 X image indicating ingrowth of bony trabeculae via pore network (B) HASi – 150 X image indicating integration into newly formed trabecular bone with remnants of ceramic isolated within bone islands.

6.3.2 Gross Examination

Gross examination of retrieved implants indicated lack of abnormal morphology within the joint structures. Retrieved material alone implant structures were visible in the case of HASi and BCP (Fig. 6C 3) under a layer of translucent tissue covering. On the contrary in the case of fabricated osteochondral constructs a covering of clear cartilage structure is visible in gross morphology (Fig. 6C 4). Absence of nicks, presence of intact cartilage layer on extra – condylar surfaces within the retrieved knee joint is observed. Gross examination therefore confirms lack of disturbance in joint integrity by implant placement.

6.3.3 Micro-computed Tomography for 3 –D Surface Reconstruction Imaging

Micro-computed Tomography makes non – destructive 3D imaging and quantification of micro-structural morphology at high resolution. Contemporarily soft tissues such as muscles & cartilage are undetectable by the x – ray imaging used in micro – CT, due to their low Hounsfeld number (Reeves et al., 2012). This results in low attenuation and reduced visibility under imaging conditions. This has been resolved to a certain extent by the use of a technique that relies on the equilibrium partitioning of an ionic – contrast agent termed as EPIC - µCT. This provides an option for in-situ analysis of bone – cartilage interfaces during development, degeneration, repair or in the assessment of performance of tissue engineered scaffold structures (Renders et al., 2014).

Hexabrix is a sterile, non-pyrogenic, aqueous solution intended for use as a diagnostic radiopaque medium. It contains 39.3% w/v N-(2-hydroxyethyl)-2,4,6-triiodo-5-[2-[2,4,6-triiodo-3-(N-methylacetamido)-5-(methylcarbamoyl) benzamido] acetamido]-isophthalamic acid, compounded with 1-deoxy-1-(methylamino)-D-glucitol (1:1) and 19.6% w/v sodium N-(2-hydroxyethyl)-2,4,6 triiodo-5-[2-[2,4,6-triiodo-3-(N-methylacetamido)-5-(methylcarbamoyl) benzamido] acetamido]-isophthalamate. It is a clear, colorless to pale yellow liquid supplied in nitrogen charged containers. Staining was carried out via a gift of the contrast agent from the manufacturer Guerbet incorporated.

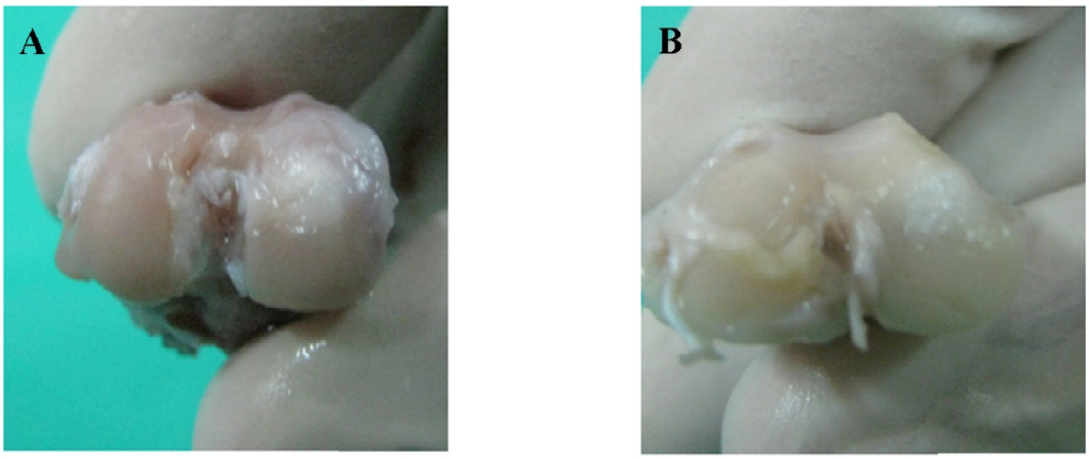

Fig. 6C 3: Gross View - Acellular Scaffold Implantation - 6 months

(A) HASi - material clearly visible below tissue layer
(B) BCP - irregular surface tissue formation

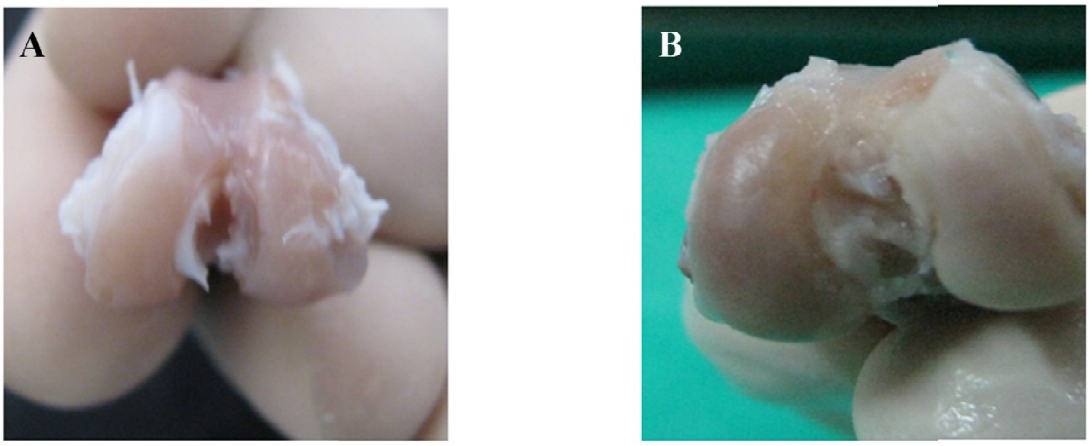

Fig. 6C 4: Gross View - Cell loaded Scaffold Implantation - 6 months

(A) HASi+C - scaffold smooth under gross view
(B) BCP+C - reorganization of articular surface is smooth and regular

Sham Defect at 6 months - Incomplete Defect Resurfacing

Micro – CT reconstruction of the 3D surfaces of the rabbit femoral condyle 6 months after implantation indicates a smooth exterior characterized by near complete reconstruction of the implant sites in BCP & HASi (Fig. 5C 5) based constructs. Comparison of non – implanted areas with the topography of implant sites provides a clear reference to the complete re- organization of the repair tissue. The non – altered morphology visible in Hexabrix stained repair tissue is indicative of the ability of the cell seeded scaffolds to induce healing in defect sites. EPIC - µCT based reconstruction of joint morphology is reflected in the quality of repair with high precision and accuracy (Xie et al., 2009) confirmed by further analysis.

Non – destructive assessment of the joint structures via EPIC - µCT also contributes information about signal density related to levels of sulfated glycosaminoglycan content and distribution (Xie et al., 2010). The high spatial resolution of the technique, as reflected in the scans ability to image soft tissue structures closely related to the joint is also indicative of the quality of repair. The uptake of the non – ionic contrast agent relative to sGAG content as indicated by the signal density from non – implant areas as well as repair areas qualifies the repair induced by cell loaded scaffold structures. The need to calibrate the use of contrast agent at sufficient strength, logistical difficulty in ensuring stain uptake are limitations in the use of this method in all experimental procedures (Renders et al., 2014).

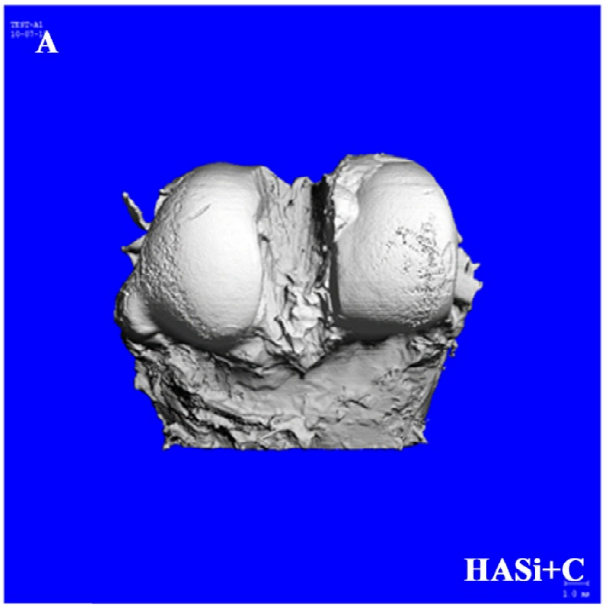

(A) HASi+C - complete re-organization of femoral condyle surface observed

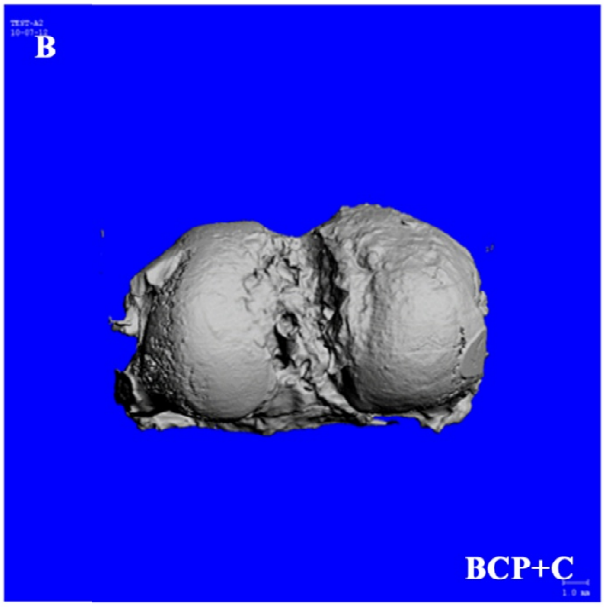

(B) BCP+C - Smooth articular surfaces on evaluation indicated complete healing at 6 months

Fig. 6C 5: Micro - CT Evaluation of Hexabrix Stained Femoral Condyles - 6 months post-implantation.
Note visualization of soft tissue structures along with joint architecture.

6.3.4 Histological Evaluation of Retrieved Implants

Retrieved femoral condyles were processed, embedded in PMMA, sectioned, ground and stained with Stevenel's Blue & Van Gieson's Picrofuchsin. The stained sections retrieved for BCP & HASi (Fig. 6C 6) indicate bone in yellow, with the cartilage overburden delineated in light shades of blue depending on the staining.

Stevenel's Blue developed originally by L Stevenel in 1918 to stain human parasites is solution comprising of 2% potassium permanganate and aqueous methylene blue (1.3%). Staining is carried out at 60 degrees Celsius (del Cerro et al., 1980). Stevenel's blue stains osteoid tissue shades of blue, with the calcification front, haversian systems, osteocytes, cartilage and lamella all clearly visible.

Van Gieson's staining (Kiernan, 2008) at equilibrium stains cytoplasmic elements yellow, with high affinity between cytoplasmic proteins and acid fuchsin. Protein concentrations at different levels and uptake of picric acid within the stained area has been correlated. Staining of non – collagen proteins via various pathways is carried out, with dye binding to collagen by hydrogen bonds (Prentø, 1993).

A 24 week study period was chosen at the farther end of the study spectrum for small animal models with emphasis on the evaluation of long term functionality of the regenerative and integrative properties of the scaffold. The interval is well chosen especially when novel investigations are being implemented (Han et al., 2003). The cellularity of the regenerated cartilage can be observed as islands in the Stevenel's stained cartilage levels, indicating recovery of the damaged area as well as continued maintenance. Degeneration of cartilage structures due to failure of transplanted cells due to apoptosis (Lee et al., 2007) is common concern in the development of successful tissue engineered grafts. The uniform cellular nature as well as integration observed in the joint structure evinced by the bony structures underlying the cartilage overburden indicates parametric healing under the stressful conditions of the loading defect area. There is also the marked absence of inadequate fixation to adjacent tissues, evidenced by areas of marked fibrous tissue development, which is cause of long term implant failure (Nehrer et al., 1999).

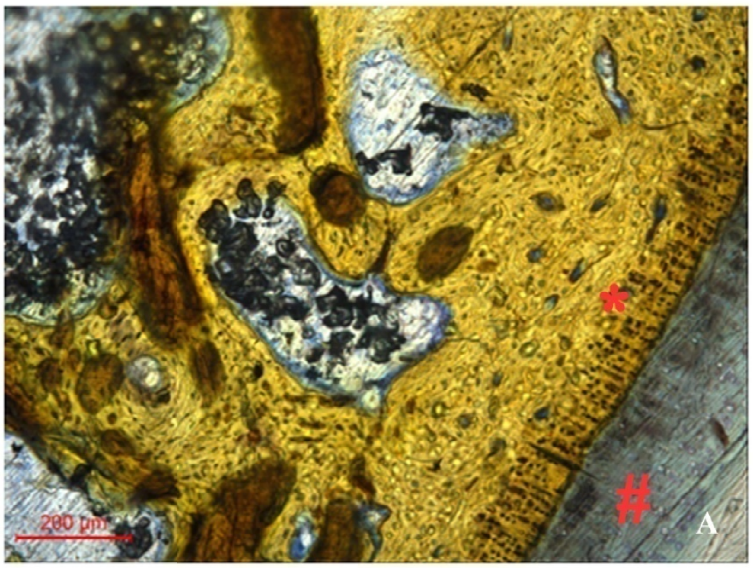

(A) HASi+C - reorganization of subchondral architecture. Tidemark of replicating cartilage layers indicated(*). Articular cartilage layer demonstrates characteristic re-organization(#), indicates complete resolution of defect area.

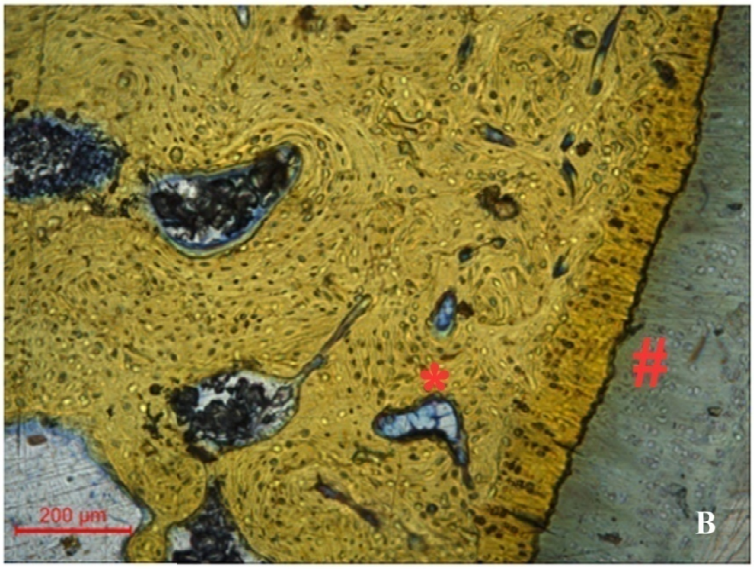

(B) BCP+C - reorganization of subchondral architecture with pockets of re-organizaing tissue(*). Articular cartilage tidemark formation with irregular subchondral surfaces observed(#)

Fig. 6C 6: Polymethylmethacrylate embedded rabbit condylar longitudinal sections retrieved 24 weeks post implantation and demonstrated with Stevenal's blue & Van Gieson's Picrofucshin differential stain (cells - blue; bone – yellow).

The tissue developed is consistent across the defect area indicating healthy tissue regeneration augmented by cells on the stimulatory scaffolds, long term decrease in tissue thickness and variability in size has been implicated in joint failure (Chu et al., 1997). Cellular tensegrity has been maintained, where in continuous structures perform as a whole rather than dependent on compressional continuity amidst themselves (Ingber, 1993). Canine studies have shown that transplanted chondrocytes undergo a sequential pattern of healing, with proliferation within six weeks, transitioning between 7 to 12 weeks and remodeling between twelve weeks and three years (Breinan et al., 1998). The remodeling stage is crucial for this study here, as it has been conclusively demonstrated that fabricated tissue constructs undertake integration with surrounding cartilage and subchondral bone within this time frame (Breinan et al., 1998). The ability of calcium phosphate based ceramics to serve as subchondral supports with integrative powers have been proven (Tanaka et al., 2005) (Shao et al., 2006b). The long term results in Shao et al noted degradatory changes in the cartilage structures that were enmeshed in PCL fibers. The 6 month implantation in case of biphasic ceramic scaffolds or silica coated hydroxyapatite scaffolds have shown a keen lack of degradative changes at this critical time point. By 12 weeks most ceramic structures in the osteochondral region have been understood to undergo degradation, here there are some tissue voids within the van Gieson stained regions, indicating reservoirs of scaffold material. This material remains in close apposition with the tissue and does not contraindicate the long term benefits of the scaffold usage. BMP – 2 treatments have indicated bony plug formation in osteochondral defects, thereby predicating the use of hydroxyapatite scaffolds with osteoinduction properties in such a location. Here in this study, the ability of BCP & HASi to maintain a differentiating population of stem cells under chondrogenic conditions and promote the reconstruction of the tissue structures in a osteochondral defect region have been conclusively demonstrated. The quality of tissue indicated by its lack of fibrous tissue formation and non – cellularity in the upper layers of regenerated cartilage indicates the formation of hyaline like cartilage tissue within the defect structures.

Hyaline like cartilage tissue formation is a key point in the success of osteochondral graft structures, especially with differentiated stem cell components (Naumann et al., 2004).

The transplanted structures indicated no evidence of immunerejection or inflammatory reaction, indicating compatibility with local tissue structures (Blanco et al., 1998).

6.4 Long - Term Implantation Studies in Goat Osteochondral Model – i*n vivo*

Dual cell type seeded fabricated osteochondral grafts were placed in defects created in the medial femoral condyle of a healthy goat. The grafts were maintained for a period of 6 months and retrieved post – euthanasia.

6.4.1 Ex – vivo Evaluation

Healing was uneventful in all cases and no loss of animals to secondary infection or other reasons was reported. Normal gait pattern was observed in all experimental animals with no observations of anomalous locomotion or related complications. Animals remained healthy in gross appraisal during autopsy at graft retrieval.

6.4.2 Gross Examination

Retrieved condyles under gross examination indicated characteristic smooth, clear surface morphology, indicating lack of complications or pitting in articular surfaces due to initiation of matrix breakdown. No extraneous tissue, nodules or adhesions were observed from the surgery or suture sites indicating an uneventful healing process. Joint integrity was judged to be ideal under the retrieval conditions. Differences between the sham, material & fabricated osteochondral implant structures are visible as indicated in Fig. 6C 7 panels.

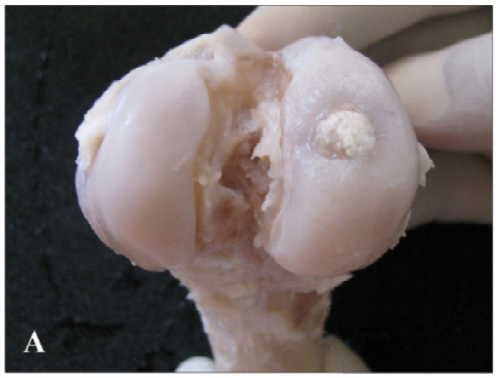

(A) Acellular BCP – Scaffold retains integrity, with poor to nil resurfacing

(B) Acellular HASi – Scaffold surface not visible, poor resurfacing with visible defects

(C) Cell – Loaded BCP – Smooth reorganization with slightly dimpled cartilage overburden

(D) Cell – Loaded HASi – Smooth reorganization with characteristic smooth exterior integral to smooth articular cartilage surfaces

(E) Sham Defect – note incomplete resurfacing of articular cartilage surface with pronounced depression and loss of total wound architecture

Fig. 6C 7: Gross Images of Goat Femoral Condyle 6 month Implantation Period.

6.4.3 Histological Evaluation of Retrieved Implants

Full thickness defects of 6 *6 mm in the Spanish goat have been indicated to be critical sized, evoking incomplete healing (Jackson et al., 2001b). The defects at critical size used in our defect model system using the Indian goat are in line with these findings, non – healing wounds of this size undergo progressive, deleterious changes in both surface tissue as well as surrounding osteoid tissues.

In animal models where the material was implanted as such, lacking in the dual – cell fabrication technique, the material retention at 6 months as well as its presence is noted even on gross imaging of the condylar surfaces. The samples when imaged microscopically (Fig. 6C 8) in the case of BCP based systems indicates a breakdown in the wound margin with collapse of the cartilage overburden. This indicates partial failure in the ability of the scaffold to provide sub – chondral support, whereas it demonstrates optimal bone bonding in the bony layer. Invagination of the wound surface has already been reported as a classic sign of deleterious wound healing (Jackson et al., 2001b). The acellular HASi implant stimulated initial stages of overburden development, but with lack of maturation structures in Fig. 6C 8, long term effects would be unpredictable. In comparison with the drilled sham, there is maintenance of wound architecture and provision of an integral subchondral support structure in both cases. The presence of a healthy sub-chondral layer is the basis of true cartilage health (Orth et al., 2013). Variations in sub-chondral bone quality has been implicated in osteoarthritis (Orth et al., 2014), occurrence of intra-lesionary bony overgrowth (Shive et al., 2014), and does not play a role in the preservation of allograft quality (Pennock et al., 2006). The evolution of an ideal sub-chondral layer, with capabilities for suitable cartilage support is currently the task of articular cartilage research the world over (Schütz et al., 2014).

In the dual – cell configuration of fabricated osteochondral grafts a high cell density has been used as there is emphasis on higher cell numbers favoring chondrogenesis (Troken et al., 2007) (Concaro et al., 2008). The role of differentiated cells has been debated since the inception of stem cell loaded structures for osteochondral therapy but theories that sustain the multiple scenarios are not yet in vogue. Dual – Cell

loading is a cutting edge technique with not many reported studies, with emphasis on material derivations (Angele et al., 1999) or on the use of varying levels or types of growth factors aimed at cell recruitment in situ(Kim et al., 2013). Use of novel, yet currently inaccessible technologies have been advocated (Shim et al., 2012) but our emphasis was on the development and practical use of available techniques & adaptation of routine methods in novel formats.

The retrieved implants wherein dual – cell fabricated constructs had been implanted indicate the total re-organization of the cartilage overburden (Fig. 6C 9). The cellular organization within the defect structure, re-organized at the end of the 6 month period is indicative of the functionality of cell – delivery in this method. The presence of optimally differentiated cells play a role in direct lay down of extra cellular matrix as well as in paracrine stimulation of surrounding tissues to ensure inclusive healing within the defect (Wu et al., 2011). Temporal changes in adipose – derived stem cells differentiated in to the chondrogenic & osteogenic lineage (Mitchell et al., 2006) would also play a role in the qualitative healing observed in the tissue sections. In some cases even when surface integration is ideal there is degradatory changes in the sub chondral bone leading to long term damage (Pallante-Kichura et al., 2013). Pallante – Kichura also reports cysts, lesions in subchondral or deep areas with structure and content varied across sites. The location of these defects may cause asymptomatic damage via signaling pathways or impaired nutrient supply to the chondral layer resulting in osteoarthritic joint failure (Raub et al., 2013).

Retention of scaffold material is also a major challenge. Herein within the acellular control groups there is massive material retention, while in the cell mediated groups there is lack of material presence within the defect area. Scaffold free techniques are being tested to overcome the inherent mechanical incompatibilities of materials & local tissue milieu (Brehm et al., 2006). Anchoring of scaffolds on the articular cartilage surface is also of importance, as methods are still being assessed for optimal efficiency (Drobnic et al., 2006), although the thickness of cartilage in large animal / human models lends itself to suture fixation; long term adverse effects are being reported (Hunziker and Stähli, 2008).

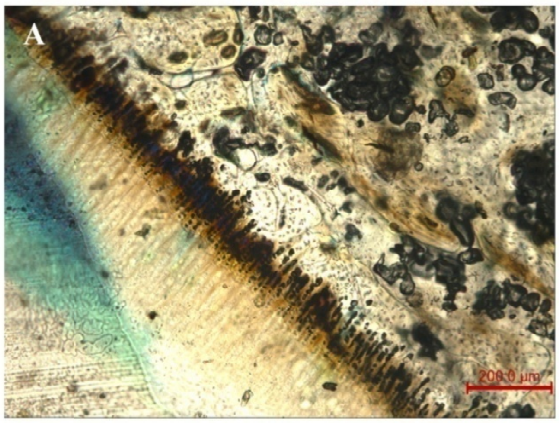

(A) BCP - incomplete re-organization of cartilage layer. Cellular structures & extracellular matrix organization is poor.

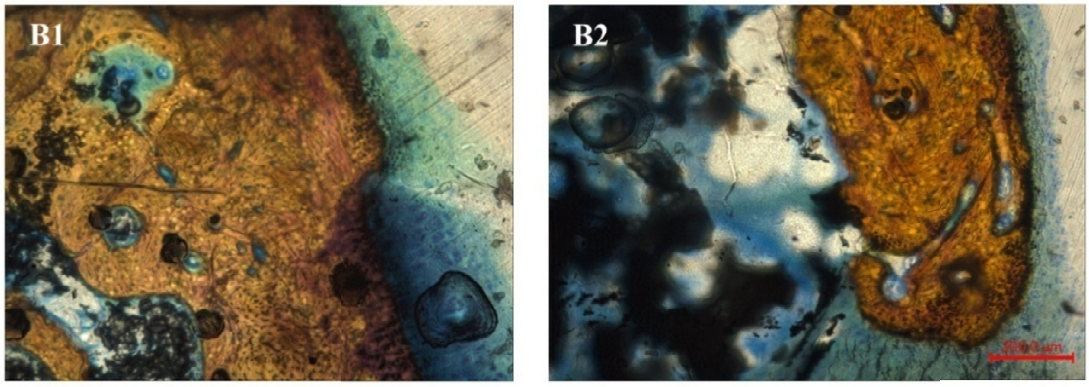

(B) HASi – loss of wound architecture, invagination of irregularly organized repair tissue within defect area.

Fig. 6C 8: Polymethylmethacrylate embedded Goat condylar samples (acellular constructs) longitudinal sections retrieved 24 weeks post implantation and demonstrated with Stevenal's blue & Van Gieson's Picrofucshin differential stain (cells - blue; bone – yellow)

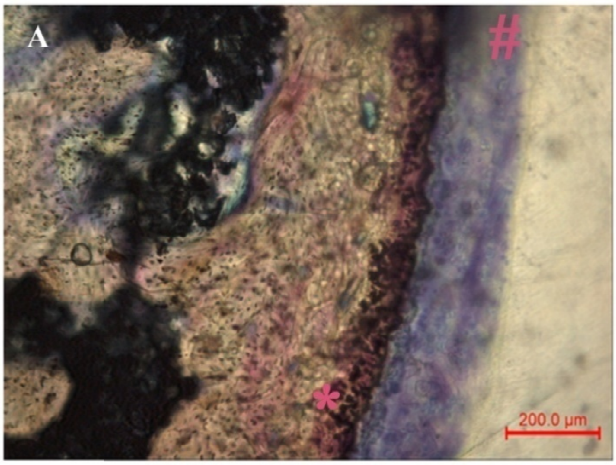

(A) BCP+C - complete re-organization of cartilage layer. Cellular structures & extracellular matrix organization is poor #. Defect margin not completely re-organized *

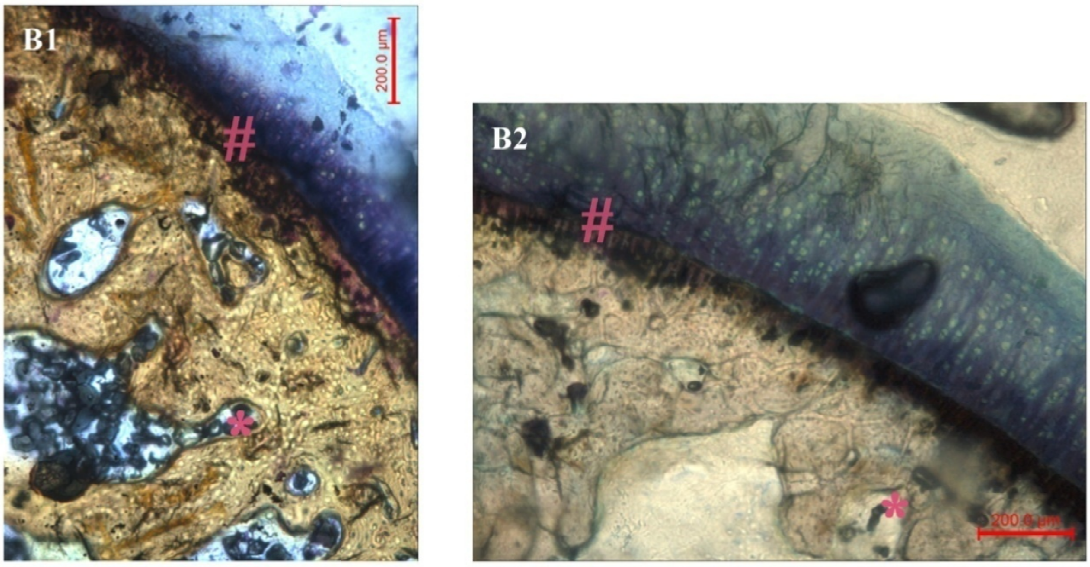

(B) HASi+C – re-organization of cartilage tidemark is emergent. Articular cartilage overburden is clearly demarcated in to cellular # and acellular matrix zones. Few pockets of ongoing bone regeneration are visualized *

Fig. 6C 9: Polymethylmethacrylate embedded Goat condylar samples (cell loaded constructs) longitudinal sections retrieved 24 weeks post implantation and demonstrated with Stevenal's blue & Van Gieson's Picrofucshin differential stain (cells - blue; bone – yellow).

The development of a novel peg – hole design using a stainless sizing device ex-vivo for preparing the scaffolds as well as *in vivo* for preparation of defect sites helped in ensuring optimal fit of the scaffold to drilled defects in the femoral condyle, ensuring anchorage and prompt integration which is crucial to long term survival & positive performance characteristics (Patent - 1998) (Farmer et al., 2001). Fixation of the scaffold was un-aided in any other way, with the goat ambulatory post – surgery with load bearing activity regained fully within 7 days, and release into communal pen on removal of external sutures. This probably facilitated and enhanced scaffold activity, but has limitations on being replicated in the clinical scenario.

The medial site of the femoral condyle in the goat was chosen keeping in mind the load bearing nature of the region and demand for stringent implant performance. The variation in elastic moduli and biomechanical load contributes to thicker cartilage structures at this site (Andriacchi et al., 2009) (Koo et al., 2005). Variations in the elastic moduli at different areas within the femoral condyle was already demonstrated in 1994 (Athanasiou et al., 1994), emphasizing the need for stringency in model selection. In case biomechanical stimuli are postulated as contributors to the healing process, the site could explain differences observed between implantations in differing sites using similar scaffold – cell combinations. Improvement in quality of life has been a certainty in this investigation (Fig. 6C 10).

Fig. 6C 10: Quality of Life
Goat demonstrating complete Range of Motion Post - Recovery

CHAPTER 7

SUMMARY AND CONCLUSION

7.1 Problem Statement

Osteochondral defects are caused by trauma, disease or degenerative conditions like rheumatoid or osteoarthritis. This causes degradation of joint function, progressive loss of the articular cartilage surface and loss of quality of life for the affected population. Current therapies for osteochondral defect involve the removal of damaged tissue alone in abrasion arthroplasty, with micro-fracture technique involving the generation of cracks in the subchondral bone to promote cartilage healing. The use of cartilage transplantation, from autologous or allologous donors are being explored. Osteochondral plug transplantation where suitably sized viable plugs are harvested from non – weight bearing regions of articular surfaces to replace damaged regions is also being practiced. Cutting edge technologies involve chondrocyte transplantation which involves ex – vivo expansion of chondrocytes harvested from the joint structure and re-implanted with a periosteal or polymer patch to cover the defect region. Therapies have been hamstrung by lack of complete effectiveness in the past (Gross et al., 1983) and current scenario with lack of uniformity across prescribed treatments, as well as disparate response to treatment (Dhinsa and Adesida, 2012).

Replacing damaged osteochondral structures are a complex task as it ivolves the identification of a suitable matrix that transcends two tissue types (bone, cartilage), has to support three distinct cell populations (osteoplast, chondrocytes & cell in calcifieds/growth plate) and be able to tolerate the loading demands placed on articular cartilage in primary locomotion based joints. Such a matrix would encompass the ability to integrate with cartilage & bony tissue while providing a niche for the survival of cellular components and stimulating direct appropriate extracellular matrix generation. Such complexities would entail the creation of a

novel line of scaffold structures that would be tailor made to specifications as mentioned.

Tissue engineering (TE) has the potential to become an alternative to current therapeutic interventions. TE functions as the intersection of biological tools, engineering sciences & material technology. At the therapeutic level applications of Tissue Engineering in Regenerative Medicine involves the use of cells, growth factors & scaffolds to repair, replace or regenerate damaged areas of tissue (Langer and Vacanti, 1993b). The selection of the biomaterial component is a critical step that determines the ultimate success of the engineered graft. It must provide an appropriate environment (porosity, chemical composition, surface topography, degradation etc) for the attachment, proliferation and function of cells. It should also have an appropriate interconnected pore network to facilitate the inflow of nourishment to the cells implanted within the tissue-engineered construct or cells that invaded from local host environment. Scaffolds ideally should be biodegradable and tissue regeneration should be in par with material degradation (Ishaug et al., 1997).

Diverse groups of materials have been explored as scaffolds for osteochondral tissue engineering. Polymers, natural scaffolds, decellularized biological units and calcium phosphate based ceramics have been utilized in multiple formats with mixed results (Schütz et al., 2014) (Giannoni et al., 2012). Chemically defined, synthesized calcium phosphate based chemicals are of rising interest given their osteointegrative capacities providing a stable anchorage for optimal subchondral support (Gao et al., 2001) (Jiang et al., 2010b). Hydroxyapatite based scaffolds are of interest as their properties can be tailored, due to their chemically defined nature and the elimination of immune recognition or disease transmission. Silica based modification increases bone apposition as well as material degradation (Mastrogiacomo et al., 2007). Links between the presence of silica and its increase in cell health parameters, increase in bone mineralization and, stimulation of nourishment via vasculogenesis (Hing et al., 1999) lead to its incorporation in the development of the osteochondral scaffold. Tailored biphasic calcium phosphate scaffolds with a defined nature of degradation

at par with overburden formation (Sureshbabu et al., 2012) is also tested for compatibility in the osteochondral defect site.

The osteochondral compartment is lacking in proliferating cells, with a lack of vascularity precluding the sourcing of cells from the circulatory compartment. Presence of abundant extra cellular matrix tied to the functionality of the articular compartment hampers cell mobility within the defect area. These reasons hinder the migration and proliferation of cells within the defect area or migratory cells from other areas from participating in the healing process. The regeneration of the defect site can therefore be revitalized by providing a pool of suitably differentiated stem cell population on a suitable scaffold. This would serve to deliver the required repair machinery and scaffolding for ensuring maintenance of wound architecture as well as supporting an appropriate healing process. Adipose derived stem cells are reported to be an easily accessible, numerous, capable of differentiation in to required lineages (Mahmoudifar and Doran, 2013) to enable the fabrication of a cell – ceramic composite that improves osteochondral repair. Cells can be induced to differentiate into osteoblast cells by providing biochemical supplements (dexamethasone, L-ascorbic acid and β glycerophosphate) in defined concentrations in their external milieu (Jaiswal et al., 1997). Cells can also be further delineated from native condition by exposure to defined levels of (dexamethasone, L-ascorbic acid, ITS, TGF – β1) to differentiate into chondrogenic lineage (Ronzière et al., 2010) (Hagmann et al., 2013).

7.2 Objective of the Study

The objective of this study has been three fold: (a) To identify & characterize suitable scaffold systems using multi – potential cells as a tool in Osteochondral reconstruction. (b) Demonstration of the viability of such scaffold – cell combination units in a lapine model (c) Pre – Clinical analysis using a large animal model for successful long term testing.

Bioceramic constructs HASi & BCP (expand) were identified for this purpose and characterized. The fabrication of tissue engineered constructs using these ceramic systems focused on the role of Si^{+} ions in stimulating the cellular reconstruction and

using tailored biphasic ceramic systems to identify a suitable scaffold degradation for integration at the defect site. Stem cells from adipose tissue identified as an easily accessible, rich source of multi-potential cells were used to fabricate tissue engineered ceramics. The focus of the study was based on demonstrating the cytocompatibility of the scaffolds for both cell types followed by their ability to facilitate compatibility, integration and overburden re-organization at the defect site in suitable animal models and osteointegration *in vivo*.

7.3 Processes & Investigations

The objective of the entire study was divided into three phases: (1) Physicochemical characterization of bioactive ceramics & in vitro evaluation with required cell – components (2) Evaluation of tissue-engineered constructs in a lapine model (3) Evaluation of tissue-engineered constructs in a caprine model.

Bioactive ceramics Biphasic Calcium Phosphate (BCP) and Triphasic ceramic coated hydroxyapatite (HASi) was selected as materials, which was gifted by Bioceramics Laboratory, SCTIMST. Elemental components post – synthesis was confirmed via EDS. The phase composition and functional groups in the materials were determined by XRD and FT-IR respectively. The porosity of HA and HASi was assessed by SEM by scanning surface topography.

BCP and HASi were polished in the form of discs of 3 mm diameter and 1 mm thickness for fabricating tissue-engineered constructs *in vitro*. In the first part, ADMSCs of rabbit and goat origin were cultured separately on HA and HASi. The mesenchymal origin of stem cells isolated from adipose tissue was determined through markers like CD34 and CD44 and also through their ability to differentiate into osteogenic & chondrogenic lineages.

Cellular responses under differentiation conditions were evaluated in terms of adhesion (SEM); viability (acridine orange / ethidium bromide staining by cLSM and LDH assay); proliferation (picogreen assay); morphology (SEM). Differentiation into osteogenic lineage was confirmed via respective mineralized ECM staining as well as estimation of ALP & osteognenic gene expression. Evaluation for total GAG

synthesis & chondrogenic gene expression was carried to estimate chondrogenic differentiation.

Primarily acellular structures (bare materials) were evaluated in a short- term study using the rabbit model. The retrieved constructs were evaluated via Stevenal's blue and van Gieson's picrofuchsin staining & Back Scatter Electron Analysis.

Tissue engineered constructs in comparison with acellular structures were validated *in vivo* in the medial femoral condyle of a lapine model utilizing the critical size defect in that specie. Care & management of animals were conducted as per the guidelines of IAEC & CPCSEA. Re-organization of overburden, integration with surrounding tissue was evaluated at the end of 12 and 24 weeks of implantation via Stevenal's blue and *van* Gieson's Picrofuchsin staining., combined with Micro – CT analysis of surface reconstruction.

The utility of dual – cell seeded scaffolds was evaluated via implantation in a goat model for 24 weeks. This also utilized a critical size defect as the model and experiments were carried out under the approval of IAEC & CPCSEA. Osteochondral integration and regeneration was assessed under gross evaluation as well as via sectioning of PMMA embedded samples for histology (Stevenal's blue and *van* Gieson's Picrofuchsin staining).

7.4 Summary of Results

Objective of the first phase was to undertake characterization of BCP & HASi as plausible Osteochondral support structures.

In HASi outer coated layer showed XRD peaks for calcium silicate and TCP phases. While in the case of BCP classic crystalline peaks of hydroxyapatite was demonstrated. SEM depicted the interconnected porous nature of BCP and HASi with the pore size in the range of 50 - 500µm.

The objective of the second phase was to evaluate the performance of candidate scaffold structures along with adipose derived stem cells from rabbit & goat models. This would help in the final fabrication of Osteochondral constructs for implantation

studies. Adipose derived stem cells under osteogenic differentiation conditions on BCP & HASi indicated the presence of a viable, proliferating cell population. Further analysis via ALP estimation and gene expression confirmed the definite delineation of cells into the osteogenic lineage with steady maturation of the cell population. This confirmed the ability of the candidate scaffolds to maintain an osteogenic population of cells. Adipose derived stem cells under chondrogenic differentiation conditions on BCP & HASi indicated the presence of a viable, proliferating cell population. Further analysis via GAG estimation and gene expression confirmed the definite delineation of cells into the chondrogenic lineage with steady maturation of the cell population. This confirmed the ability of the candidate scaffolds to maintain a population of cells necessitated in the Osteochondral compartment.

The third phase of the study focused on the *in vivo* demonstration of cell – ceramic products in two different animal models. The site of the defect was common, selected as the medial femoral condyle a load bearing site commonly used for Osteochondral defect demonstration.

The first part involved the demonstration of acellular scaffold material at the selected defect area in the lapine model. The ability of the scaffold to integrate well with the joint surface was demonstrated, although the overburden developed was clearly ill – organized.

The second part involved the demonstration of Osteochondral constructs loaded with differentiated rabbit adipose derived stem cells in to the selected site at critical size defect levels. The re-organization of the cartilage layer was clearly hyaline like thereby resulting in the organization of the articular cartilage surface. The re-organization identified via micro – computed tomographical reconstruction depicted a smooth articular surface. Sections stained via Stevenel's blue and van Gieson's Picrofuchsin provided conclusive proof of the success of implanted tissue engineered substrates in achieving wound resolution.

The third part involving demonstration of dual – cell seeded scaffold structures in a long term caprine model. The results here in indicated superior performance of the

cell seeded BCP & HASi scaffolds over the acellular candidates. The performance as well as quality of motion of the animal was maintained over an extended period of time.

Conclusions

BCP & HASi was gifted from the Bioceramics Laboratory with novel methods of preparation (Sureshbabu et al., 2011) (Venugopal et al., 2012). The scaffolds thus prepared were demonstrated to contain the defined material phases as evidenced by EDS, XRD & FT – IR data.

The cytocompatible nature of the scaffolds was confirmed by its interaction with adipose derived stem cells from goat & rabbit. Stem cell properties were verified for cells isolated from the adipose tissue of goat & rabbit by differentiation in to osteogenic and chondrogenic lineages. Further confirmed by the use of relevant antibodies in FACS analysis of the isolated cell population.

The addition of osteogenic supplements in defined concentrations (10 mM β-glycerophosphate, 10-8 M dexamethasone, 0.05 mg/ml L-ascorbic acid) resulted in the differentiation of adipose derived stem cells towards the osteogenic lineage culminating in biomineralisation. Adding chondrogenic medium; 15% FBS supplemented with 10ng/ml TGF-β1 (Imperial), ITS Premix (BD Biosciences) 25 µg of Ascorbate & 10^{-8} M Dexamethasone (Sigma), results in the synthesis of chondrogenic extracellular matrix components as well as elevated expression of chondrogenic genes.

Further assays demonstrated the capability of the cells to colonize, remain viable & demonstrate long term proliferation within the scaffold structures. Unlike cases where post – differentiation cellular viability is depressed, observations indicate ability of the Si^{+} coated HASi as well as the biphasic calcium phosphate to maintain cell populations under optimal conditions. The success of any tissue engineered

product depends keenly on the performance of its cellular components, and the ability of the scaffolds to maintain differentiated cell populations is well understood.

The highly interconnected porous nature of ceramic materials (50-500 μm pore size) in par with the appropriate chemical composition improved the migration and distribution of cells towards the internal voids of the material. The response of rabbit and goat cells in terms of viability, morphology and proliferation was approximately same on BCP and HASi, implying the comparability between these two species for in vivo studies.

In – vivo performance analysis of the scaffolds via comparison between cellular and acellular structures implied the ability of the cell loaded scaffolds in rabbit & goat model to resolve defect site injury, completely integrate with joint area and achieve homeostasis with material degeneration & complete the life cycle of the developed product.

The ability of the (acellular) material alone, to achieve integration with the intra – chondral structures illustrate the suitability of using a ceramic material to provide stable sub-chondral structures for the development of ideal cartilage overburden. The plugs thus developed may also be parlayed into methods for utilization in resurfacing sites of Osteochondral plug harvest as a preliminary evaluation method.

Optimal performance by cell loaded scaffolds in contrast to the non – directional regeneration observed in the acellular structures places emphasis on the ability of the cell machinery delivered to the site to perform required functions over critically long periods of time. The ability of the cell – material combinations herein termed as fabricated Osteochondral composites has to be further understood in terms of cell concentration versus delivery timelines compared to defect creation.

Future investigations

Osteochondral Tissue Engineering has innate potential to be developed further into a therapeutic intervention which would surpass the current standard of care. The current study has undertaken a comprehensive analysis of material systems from

synthesis level, via various biological testing routes to finally ensure compliance with current demands on an osteochondral regenerative system.

The current program of analysis has been able to comprehensively address many issues related to clinical acceptance. To fully exploit the potential of this indigenous technology to provide affordable, acceptable clinical therapy a few further concerns are to be addressed.

The assessment of plastic sections via immunohistochemistry is a challenge that has not been met in this program. Further efforts to refine the evaluation of archival samples using acceptable methods would be a right step in data mining the repository of information that we hold.

Future applications would definitely require the functional analysis of scaffolds with stem cells derived from human adipose tissue. Demonstration of scaffold capacity for further acceptance using human adipose derived stem cells can be carried out via the use of immuno-deficient mice models (SCID/NOD) in conjunction with extensive *in vitro* analyses.

Technical refinements would pave the path for human application with emphasis on the replacement of bovine serum, animal derived components in media with chemically defined media components. This would ensure control of quality & composition within a tightly regulated circle from synthesis to application enabling finer control of all aspects. Cell products in line with current national /international guidelines may be generated within a GMP facility to ensure clinical acceptance as well as ensure data veracity on a global scale.

The ability to synthesize an *in vitro* model of the Osteochondral system could prove to be beneficial in the testing & verification of drugs / therapeutic moieties that affect osteogenic, chondrogenic or events at the interface of osteo – chondral tissues. Developing three dimensional systems for understanding tissue response would help us mimic real world conditions within the Osteochondral interface and better guide in the beneficial manipulation of the same.

REFERENCES

Ahern BJ, Parvizi J, Boston R, Schaer TP (2009) Preclinical animal models in single site cartilage defect testing: a systematic review. Osteoarthritis Cartilage **17**: 705–713. doi:10.1016/j.joca.2008.11.008.

Andriacchi TP, Koo S, Scanlan SF (2009) Gait mechanics influence healthy cartilage morphology and osteoarthritis of the knee. J. Bone Joint Surg. Am. **91 Suppl 1**: 95–101. doi:10.2106/JBJS.H.01408.

Angele P, Kujat R, Nerlich M, Yoo J, Goldberg V, Johnstone B (1999) Engineering of Osteochondral Tissue with Bone Marrow Mesenchymal Progenitor Cells in a Derivatized Hyaluronan-Gelatin Composite Sponge. Tissue Eng. **5**: 545–553. doi:10.1089/ten.1999.5.545.

Anselme K (2000) Osteoblast adhesion on biomaterials. Biomaterials **21**: 667–681.

Anselme K, Bigerelle M, Noel B, Dufresne E, Judas D, Iost A, Hardouin P (2000) Qualitative and quantitative study of human osteoblast adhesion on materials with various surface roughnesses. J. Biomed. Mater. Res. **49**: 155–166.

Arøen A, Løken S, Heir S, Alvik E, Ekeland A, Granlund OG, Engebretsen L (2004) Articular cartilage lesions in 993 consecutive knee arthroscopies. Am. J. Sports Med. **32**: 211–215.

Arrigoni E, de Girolamo L, Di Giancamillo A, Stanco D, Dellavia C, Carnelli D, Campagnol M, Domeneghini C, Brini AT (2013) Adipose-derived stem cells and rabbit bone regeneration: histomorphometric, immunohistochemical and mechanical characterization. J. Orthop. Sci. Off. J. Jpn. Orthop. Assoc. **18**: 331–339. doi:10.1007/s00776-012-0349-y.

Arvidson K, Abdallah BM, Applegate LA, Baldini N, Cenni E, Gomez-Barrena E, Granchi D, Kassem M, Konttinen YT, Mustafa K, Pioletti DP, Sillat T, Finne-Wistrand A (2011) Bone regeneration and stem cells. J. Cell. Mol. Med. **15**: 718–746. doi:10.1111/j.1582-4934.2010.01224.x.

Athanasiou KA, Agarwal A, Dzida FJ (1994) Comparative study of the intrinsic mechanical properties of the human acetabular and femoral head cartilage. J. Orthop. Res. Off. Publ. Orthop. Res. Soc. **12**: 340–349. doi:10.1002/jor.1100120306.

Aubin JE (2001) Regulation of osteoblast formation and function. Rev. Endocr. Metab. Disord. **2**: 81–94.

Awad HA, Halvorsen Y-DC, Gimble JM, Guilak F (2003) Effects of Transforming Growth Factor β1 and Dexamethasone on the Growth and Chondrogenic Differentiation of Adipose-Derived Stromal Cells. Tissue Eng. **9**: 1301–1312. doi:10.1089/10763270360728215.

Awad HA, Quinn Wickham M, Leddy HA, Gimble JM, Guilak F (2004) Chondrogenic differentiation of adipose-derived adult stem cells in agarose, alginate, and gelatin scaffolds. Biomaterials **25**: 3211–3222. doi:10.1016/j.biomaterials.2003.10.045.

Bagambisa FB, Joos U (1990) Preliminary studies on the phenomenological behaviour of osteoblasts cultured on hydroxyapatite ceramics. Biomaterials **11**: 50–56. doi:10.1016/0142-9612(90)90052-R.

Becerra J, Andrades JA, Guerado E, Zamora-Navas P, López-Puertas JM, Reddi AH (2010) Articular cartilage: structure and regeneration. Tissue Eng. Part B Rev. **16**: 617–627. doi:10.1089/ten.TEB.2010.0191.

Blanco FJ, Guitian R, Vázquez-Martul E, de Toro FJ, Galdo F (1998) Osteoarthritis chondrocytes die by apoptosis. A possible pathway for osteoarthritis pathology. Arthritis Rheum. **41**: 284–289. doi:10.1002/1529-0131(199802)41:2<284::AID-ART12>3.0.CO;2-T.

Block JA (2014) Osteoarthritis: OA guidelines: improving care or merely codifying practice? Nat. Rev. Rheumatol. doi:10.1038/nrrheum.2014.61.

De Boer J, Siddappa R, Gaspar C, van Apeldoorn A, Fodde R, van Blitterswijk C (2004) Wnt signaling inhibits osteogenic differentiation of human mesenchymal stem cells. Bone **34**: 818–826. doi:10.1016/j.bone.2004.01.016.

Bohdan P, Baraa Z, Yusuf K (2007) Guided cartilage regeneration using resorbable template. Eplasty **8**: e5.

Borovecki F, Pecina-Slaus N, Vukicevic S (2007) Biological mechanisms of bone and cartilage remodelling--genomic perspective. Int. Orthop. **31**: 799–805. doi:10.1007/s00264-007-0408-8.

Boyan BD, Hummert TW, Dean DD, Schwartz Z (1996) Role of material surfaces in regulating bone and cartilage cell response. Biomaterials **17**: 137–146.

Brehm W, Aklin B, Yamashita T, Rieser F, Trüb T, Jakob RP, Mainil-Varlet P (2006) Repair of superficial osteochondral defects with an autologous scaffold-free cartilage construct in a caprine model: implantation method and

short-term results. Osteoarthr. Cartil. OARS Osteoarthr. Res. Soc. **14**: 1214–1226. doi:10.1016/j.joca.2006.05.002.

Breinan HA, Minas T, Barone L, Tubo R, Hsu H-P, Shortkroff S, Nehrer S, Sledge CB, Spector M (1998) Histological Evaluation of the Course of Healing of Canine Articular Cartilage Defects Treated with Cultured Autologous Chondrocytes. Tissue Eng. **4**: 101–113. doi:10.1089/ten.1998.4.101.

Brittberg M, Lindahl A, Nilsson A, Ohlsson C, Isaksson O, Peterson L (1994) Treatment of deep cartilage defects in the knee with autologous chondrocyte transplantation. N. Engl. J. Med. **331**: 889–895. doi:10.1056/NEJM199410063311401.

Bronckaers A, Hilkens P, Martens W, Gervois P, Ratajczak J, Struys T, Lambrichts I (2014) Mesenchymal stem/stromal cells as a pharmacological and therapeutic approach to accelerate angiogenesis. Pharmacol. Ther. doi:10.1016/j.pharmthera.2014.02.013.

Broom ND, Poole CA (1982) A functional-morphological study of the tidemark region of articular cartilage maintained in a non-viable physiological condition. J. Anat. **135**: 65–82.

Buchanan WW (2003) William Hunter (1718–1783). Rheumatology **42**: 1260–1261. doi:10.1093/rheumatology/keg003.

Buchtová N, Réthoré G, Boyer C, Guicheux J, Rambaud F, Vallé K, Belleville P, Sanchez C, Chauvet O, Weiss P, Le Bideau J (2013) Nanocomposite hydrogels for cartilage tissue engineering: mesoporous silica nanofibers interlinked with siloxane derived polysaccharide. J. Mater. Sci. Mater. Med. **24**: 1875–1884. doi:10.1007/s10856-013-4951-0.

Buckwalter JA (1998) Articular cartilage: injuries and potential for healing. J. Orthop. Sports Phys. Ther. **28**: 192–202. doi:10.2519/jospt.1998.28.4.192.

Buckwalter JA, Lane NE (1997a) Athletics and Osteoarthritis. Am. J. Sports Med. **25**: 873–881. doi:10.1177/036354659702500624.

Buckwalter JA, Lane NE (1997b) Athletics and Osteoarthritis. Am. J. Sports Med. **25**: 873–881. doi:10.1177/036354659702500624.

Cameron ML, Briggs KK, Steadman JR (2003) Reproducibility and reliability of the outerbridge classification for grading chondral lesions of the knee arthroscopically. Am. J. Sports Med. **31**: 83–86.

Del Cerro M, Cogen J, del Cerro C (1980) Stevenel's Blue, an excellent stain for optical microscopical study of plastic embedded tissues. Microsc. Acta **83**: 117–121.

Chen L, Peng EJ, Zeng XY, Zhuang QY, Ye ZQ (2012) Comparison of the proliferation, viability, and differentiation capacity of adipose-derived stem cells from different anatomic sites in rabbits. Cells Tissues Organs **196**: 13–22. doi:10.1159/000330796.

Chu CR, Dounchis JS, Yoshioka M, Sah RL, Coutts RD, Amiel D (1997) Osteochondral repair using perichondrial cells. A 1-year study in rabbits. Clin. Orthop. 220–229.

Chu CR, Szczodry M, Bruno S (2010a) Animal models for cartilage regeneration and repair. Tissue Eng. Part B Rev. **16**: 105–115. doi:10.1089/ten.TEB.2009.0452.

Chu CR, Szczodry M, Bruno S (2010b) Animal models for cartilage regeneration and repair. Tissue Eng. Part B Rev. **16**: 105–115. doi:10.1089/ten.TEB.2009.0452.

Chu CR, Szczodry M, Bruno S (2010c) Animal Models for Cartilage Regeneration and Repair. Tissue Eng. Part B Rev. **16**: 105–115. doi:10.1089/ten.teb.2009.0452.

Coburn JM, Bernstein N, Bhattacharya R, Aich U, Yarema KJ, Elisseeff JH (2013) Differential Response of Chondrocytes and Chondrogenic-Induced Mesenchymal Stem Cells to C1-OH Tributanoylated N-Acetylhexosamines. PLoS ONE **8**: e58899. doi:10.1371/journal.pone.0058899.

Cohen S, Baño MC, Cima LG, Allcock HR, Vacanti JP, Vacanti CA, Langer R (1993) Design of synthetic polymeric structures for cell transplantation and tissue engineering. Clin. Mater. **13**: 3–10.

Concaro S, Nicklasson E, Ellowsson L, Lindahl A, Brittberg M, Gatenholm P (2008) Effect of cell seeding concentration on the quality of tissue engineered constructs loaded with adult human articular chondrocytes. J. Tissue Eng. Regen. Med. **2**: 14–21. doi:10.1002/term.60.

Curl WW, Krome J, Gordon ES, Rushing J, Smith BP, Poehling GG (1997) Cartilage injuries: a review of 31,516 knee arthroscopies. Arthrosc. J. Arthrosc. Relat. Surg. Off. Publ. Arthrosc. Assoc. N. Am. Int. Arthrosc. Assoc. **13**: 456–460.

Curran JM, Chen R, Hunt JA (2006) The guidance of human mesenchymal stem cell differentiation in vitro by controlled modifications to the cell

substrate. Biomaterials **27**: 4783–4793. doi:10.1016/j.biomaterials.2006.05.001.

Dawson J, Linsell L, Zondervan K, Rose P, Randall T, Carr A, Fitzpatrick R (2004) Epidemiology of hip and knee pain and its impact on overall health status in older adults. Rheumatol. Oxf. Engl. **43**: 497–504. doi:10.1093/rheumatology/keh086.

Decker T, Lohmann-Matthes M-L (1988) A quick and simple method for the quantitation of lactate dehydrogenase release in measurements of cellular cytotoxicity and tumor necrosis factor (TNF) activity. J. Immunol. Methods **115**: 61–69. doi:10.1016/0022-1759(88)90310-9.

Dhinsa BS, Adesida AB (2012) Current clinical therapies for cartilage repair, their limitation and the role of stem cells. Curr. Stem Cell Res. Ther. **7**: 143–148.

Dragoo JL, Samimi B, Zhu M, Hame SL, Thomas BJ, Lieberman JR, Hedrick MH, Benhaim P (2003) Tissue-engineered cartilage and bone using stem cells from human infrapatellar fat pads. J. Bone Joint Surg. Br. **85**: 740–747.

Driesang IM, Hunziker EB (2000) Delamination rates of tissue flaps used in articular cartilage repair. J. Orthop. Res. Off. Publ. Orthop. Res. Soc. **18**: 909–911. doi:10.1002/jor.1100180609.

Drobnic M, Radosavljevic D, Ravnik D, Pavlovcic V, Hribernik M (2006) Comparison of four techniques for the fixation of a collagen scaffold in the human cadaveric knee. Osteoarthr. Cartil. OARS Osteoarthr. Res. Soc. **14**: 337–344. doi:10.1016/j.joca.2005.11.007.

Ducheyne P, Qiu Q (1999) Bioactive ceramics: the effect of surface reactivity on bone formation and bone cell function. Biomaterials **20**: 2287–2303.

F. H.R. De Man, W. Tigchelaar, R. K. Marti, C. J.F. Van Noorden, H. M. Van der Vis (2005) Effects of Mechanical Compression of a Fibrous Tissue Interface on Bone with or without High-Density Polyethylene Particles in a Rabbit Model of Prosthetic Loosening. J. Bone Jt. Surg. Am. **87**: 1522–1533. doi:10.2106/JBJS.D.01882.

Farmer JM, Martin DF, Boles CA, Curl WW (2001) CHONDRAL AND OSTEOCHONDRAL INJURIES: Diagnosis and Management. Clin. Sports Med. **20**: 299–320. doi:10.1016/S0278-5919(05)70308-2.

Felson DT, Lawrence RC, Dieppe PA, Hirsch R, Helmick CG, Jordan JM, Kington RS, Lane NE, Nevitt MC, Zhang Y, Sowers M, McAlindon T,

Spector TD, Poole AR, Yanovski SZ, Ateshian G, Sharma L, Buckwalter JA, Brandt KD, Fries JF (2000) Osteoarthritis: New Insights. Part 1: The Disease and Its Risk Factors. Ann. Intern. Med. **133**: 635 –646.

Flanigan DC, Harris JD, Trinh TQ, Siston RA, Brophy RH (2010) Prevalence of chondral defects in athletes' knees: a systematic review. Med. Sci. Sports Exerc. **42**: 1795–1801. doi:10.1249/MSS.0b013e3181d9eea0.

Gaharwar AK, Rivera C, Wu C-J, Chan BK, Schmidt G (2013) Photocrosslinked nanocomposite hydrogels from PEG and silica nanospheres: structural, mechanical and cell adhesion characteristics. Mater. Sci. Eng. C Mater. Biol. Appl. **33**: 1800–1807. doi:10.1016/j.msec.2012.12.099.

Gao J, Dennis JE, Solchaga LA, Awadallah AS, Goldberg VM, Caplan AI (2001) Tissue-engineered fabrication of an osteochondral composite graft using rat bone marrow-derived mesenchymal stem cells. Tissue Eng. **7**: 363–371. doi:10.1089/10763270152436427.

Gelinsky M (2007) Biphasic, but monolithic scaffolds for the therapy of osteochondral defects. Int. J. Mater. Res. Former. Z. Fuer Met. 747–753. doi:10.3139/146.101520.

Ghazavi MT, Pritzker KP, Davis AM, Gross AE (1997) Fresh osteochondral allografts for post-traumatic osteochondral defects of the knee. J. Bone Joint Surg. Br. **79**: 1008–1013.

Giannoni P, Lazzarini E, Ceseracciu L, Barone AC, Quarto R, Scaglione S (2012) Design and characterization of a tissue-engineered bilayer scaffold for osteochondral tissue repair. J. Tissue Eng. Regen. Med. doi:10.1002/term.1651.

Goldring MB (2012) Chondrogenesis, chondrocyte differentiation, and articular cartilage metabolism in health and osteoarthritis. Ther. Adv. Musculoskelet. Dis. **4**: 269–285. doi:10.1177/1759720X12448454.

Gomoll AH (2012) Microfracture and augments. J. Knee Surg. **25**: 9–15.

Gough JE, Notingher I, Hench LL (2004) Osteoblast attachment and mineralized nodule formation on rough and smooth 45S5 bioactive glass monoliths. J. Biomed. Mater. Res. A **68**: 640–650. doi:10.1002/jbm.a.20075.

Gross AE, McKee NH, Pritzker KP, Langer F (1983) Reconstruction of skeletal deficits at the knee. A comprehensive osteochondral transplant program. Clin. Orthop. 96–106.

Habermeyer P, Magosch P, Luz V, Lichtenberg S (2006) Three-dimensional glenoid deformity in patients with osteoarthritis: a radiographic analysis. J. Bone Joint Surg. Am. **88**: 1301–1307. doi:10.2106/JBJS.E.00622.

Hagmann S, Moradi B, Frank S, Dreher T, Kämmerer PW, Richter W, Gotterbarm T (2013) Different culture media affect growth characteristics, surface marker distribution and chondrogenic differentiation of human bone marrow-derived mesenchymal stromal cells. BMC Musculoskelet. Disord. **14**: 223. doi:10.1186/1471-2474-14-223.

Hakki SS, Bozkurt BS, Ozcopur B, Gandolfi MG, Prati C, Belli S (2013) The response of cementoblasts to calcium phosphate resin-based and calcium silicate-based commercial sealers. Int. Endod. J. **46**: 242–252. doi:10.1111/j.1365-2591.2012.02122.x.

Hamadouche M, Sedel L (2000) Ceramics in orthopaedics. J. Bone Joint Surg. Br. **82**: 1095–1099.

Hamid Q, Wang C, Snyder J, Sun W (2014) Surface modification of SU-8 for enhanced cell attachment and proliferation within microfluidic chips. J. Biomed. Mater. Res. B Appl. Biomater. doi:10.1002/jbm.b.33223.

Hamidouche Z, Haÿ E, Vaudin P, Charbord P, Schüle R, Marie PJ, Fromigué O (2008) FHL2 mediates dexamethasone-induced mesenchymal cell differentiation into osteoblasts by activating Wnt/beta-catenin signaling-dependent Runx2 expression. FASEB J. Off. Publ. Fed. Am. Soc. Exp. Biol. **22**: 3813–3822. doi:10.1096/fj.08-106302.

Han CW, Chu CR, Adachi N, Usas A, Fu FH, Huard J, Pan Y (2003) Analysis of rabbit articular cartilage repair after chondrocyte implantation using optical coherence tomography. Osteoarthr. Cartil. OARS Osteoarthr. Res. Soc. **11**: 111–121.

Hangody L, Feczkó P, Bartha L, Bodó G, Kish G (2001) Mosaicplasty for the treatment of articular defects of the knee and ankle. Clin. Orthop. S328–336.

Helen W, Gough JE (2008) Cell viability, proliferation and extracellular matrix production of human annulus fibrosus cells cultured within PDLLA/Bioglass® composite foam scaffolds in vitro. Acta Biomater. **4**: 230–243. doi:10.1016/j.actbio.2007.09.010.

Hing KA, Best SM, Tanner KE, Bonfield W, Revell PA (1999) Quantification of bone ingrowth within bone-derived porous hydroxyapatite implants of varying density. J. Mater. Sci. Mater. Med. **10**: 663–670.

Hoemann CD, Lafantaisie-Favreau C-H, Lascau-Coman V, Chen G, Guzmán-Morales J (2012) The cartilage-bone interface. J. Knee Surg. **25**: 85–97.

Hoikka VE, Jaroma HJ, Ritsilä VA (1990) Reconstruction of the patellar articulation with periosteal grafts. 4-year follow-up of 13 cases. Acta Orthop. Scand. **61**: 36–39.

Huang W, Chung U, Kronenberg HM, Crombrugghe B de (2001) The chondrogenic transcription factor Sox9 is a target of signaling by the parathyroid hormone-related peptide in the growth plate of endochondral bones. Proc. Natl. Acad. Sci. **98**: 160–165. doi:10.1073/pnas.98.1.160.

Huey DJ, Hu JC, Athanasiou KA (2012) Unlike bone, cartilage regeneration remains elusive. Science **338**: 917–921. doi:10.1126/science.1222454.

Hunziker EB (2002) Articular cartilage repair: basic science and clinical progress. A review of the current status and prospects. Osteoarthr. Cartil. OARS Osteoarthr. Res. Soc. **10**: 432–463. doi:10.1053/joca.2002.0801.

Hunziker EB, Stähli A (2008) Surgical suturing of articular cartilage induces osteoarthritis-like changes. Osteoarthr. Cartil. OARS Osteoarthr. Res. Soc. **16**: 1067–1073. doi:10.1016/j.joca.2008.01.009.

Indrawattana N, Chen G, Tadokoro M, Shann LH, Ohgushi H, Tateishi T, Tanaka J, Bunyaratvej A (2004) Growth factor combination for chondrogenic induction from human mesenchymal stem cell. Biochem. Biophys. Res. Commun. **320**: 914–919. doi:10.1016/j.bbrc.2004.06.029.

Ingber DE (1993) Cellular tensegrity: defining new rules of biological design that govern the cytoskeleton. J. Cell Sci. **104**: 613–627.

Ishaug SL, Crane GM, Miller MJ, Yasko AW, Yaszemski MJ, Mikos AG (1997) Bone formation by three-dimensional stromal osteoblast culture in biodegradable polymer scaffolds. J. Biomed. Mater. Res. **36**: 17–28.

Jackson DW, Simon TM, Aberman HM (2001a) Symptomatic articular cartilage degeneration: the impact in the new millennium. Clin. Orthop. S14–25.

Jackson DW, Lalor PA, Aberman HM, Simon TM (2001b) Spontaneous repair of full-thickness defects of articular cartilage in a goat model. A preliminary study. J. Bone Joint Surg. Am. **83-A**: 53–64.

Jaiswal N, Haynesworth SE, Caplan AI, Bruder SP (1997) Osteogenic differentiation of purified, culture-expanded human mesenchymal stem cells in vitro. J. Cell. Biochem. **64**: 295–312.

Jiang J, Tang A, Ateshian GA, Guo XE, Hung CT, Lu HH (2010a) Bioactive stratified polymer ceramic-hydrogel scaffold for integrative osteochondral repair. Ann. Biomed. Eng. **38**: 2183–2196. doi:10.1007/s10439-010-0038-y.

Jiang J, Tang A, Ateshian GA, Guo XE, Hung CT, Lu HH (2010b) Bioactive stratified polymer ceramic-hydrogel scaffold for integrative osteochondral repair. Ann. Biomed. Eng. **38**: 2183–2196. doi:10.1007/s10439-010-0038-y.

Jung G-Y, Park Y-J, Han J-S (2010) Effects of HA released calcium ion on osteoblast differentiation. J. Mater. Sci. Mater. Med. **21**: 1649–1654. doi:10.1007/s10856-010-4011-y.

Kandel RA, Grynpas M, Pilliar R, Lee J, Wang J, Waldman S, Zalzal P, Hurtig M, CIHR-Bioengineering of Skeletal Tissues Team (2006) Repair of osteochondral defects with biphasic cartilage-calcium polyphosphate constructs in a sheep model. Biomaterials **27**: 4120–4131. doi:10.1016/j.biomaterials.2006.03.005.

Kern S, Eichler H, Stoeve J, Klüter H, Bieback K (2006) Comparative analysis of mesenchymal stem cells from bone marrow, umbilical cord blood, or adipose tissue. Stem Cells Dayt. Ohio **24**: 1294–1301. doi:10.1634/stemcells.2005-0342.

Kiernan JA (2008) Histological and Histochemical Methods: Theory and Practice. Scion Publishing Limited, January.

Kim HK, Moran ME, Salter RB (1991) The potential for regeneration of articular cartilage in defects created by chondral shaving and subchondral abrasion. An experimental investigation in rabbits. J. Bone Joint Surg. Am. **73**: 1301–1315.

Kim H-J, Im G-I (2009) Chondrogenic differentiation of adipose tissue-derived mesenchymal stem cells: greater doses of growth factor are necessary. J. Orthop. Res. Off. Publ. Orthop. Res. Soc. **27**: 612–619. doi:10.1002/jor.20766.

Kim K, Lam J, Lu S, Spicer PP, Lueckgen A, Tabata Y, Wong ME, Jansen JA, Mikos AG, Kasper FK (2013) Osteochondral tissue regeneration using a bilayered composite hydrogel with modulating dual growth factor release kinetics in a rabbit model. J. Control. Release Off. J. Control. Release Soc. **168**: 166–178. doi:10.1016/j.jconrel.2013.03.013.

Kitahara S, Nakagawa K, Sah RL, Wada Y, Ogawa T, Moriya H, Masuda K (2008) In vivo maturation of scaffold-free engineered articular cartilage on hydroxyapatite. Tissue Eng. Part A **14**: 1905–1913. doi:10.1089/ten.tea.2006.0419.

Kizuki T, Ohgaki M, Katsura M, Nakamura S, Hashimoto K, Toda Y, Udagawa S, Yamashita K (2003) Effect of bone-like layer growth from culture medium on adherence of osteoblast-like cells. Biomaterials **24**: 941–947.

Kokai LE, Marra K, Rubin JP (2014) Adipose stem cells: biology and clinical applications for tissue repair and regeneration. Transl. Res. J. Lab. Clin. Med. **163**: 399–408. doi:10.1016/j.trsl.2013.11.009.

Koo S, Gold GE, Andriacchi TP (2005) Considerations in measuring cartilage thickness using MRI: factors influencing reproducibility and accuracy. Osteoarthr. Cartil. OARS Osteoarthr. Res. Soc. **13**: 782–789. doi:10.1016/j.joca.2005.04.013.

Kruyt MC, de Bruijn JD, Wilson CE, Oner FC, van Blitterswijk CA, Verbout AJ, Dhert WJA (2003) Viable osteogenic cells are obligatory for tissue-engineered ectopic bone formation in goats. Tissue Eng. **9**: 327–336. doi:10.1089/107632703764664792.

Kyllönen L, Haimi S, Mannerström B, Huhtala H, Rajala KM, Skottman H, Sándor GK, Miettinen S (2013) Effects of different serum conditions on osteogenic differentiation of human adipose stem cells in vitro. Stem Cell Res. Ther. **4**: 17. doi:10.1186/scrt165.

Langer R, Vacanti JP (1993a) Tissue engineering. Science **260**: 920–926.

Langer R, Vacanti JP (1993b) Tissue engineering. Science **260**: 920–926.

Langstaff S, Sayer M, Smith TJ, Pugh SM, Hesp SA, Thompson WT (1999) Resorbable bioceramics based on stabilized calcium phosphates. Part I: rational design, sample preparation and material characterization. Biomaterials **20**: 1727–1741.

Leboy PS, Vaias L, Uschmann B, Golub E, Adams SL, Pacifici M (1989) Ascorbic acid induces alkaline phosphatase, type X collagen, and calcium deposition in cultured chick chondrocytes. J. Biol. Chem. **264**: 17281–17286.

Lee H-R, Kim H-J, Ko J-S, Choi Y-S, Ahn M-W, Kim S, Do SH (2013a) Comparative Characteristics of Porous Bioceramics for an Osteogenic Response In Vitro and In Vivo. PLoS ONE **8**. doi:10.1371/journal.pone.0084272.

Lee H-R, Kim H-J, Ko J-S, Choi Y-S, Ahn M-W, Kim S, Do SH (2013b) Comparative Characteristics of Porous Bioceramics for an Osteogenic Response In Vitro and In Vivo. PLoS ONE **8**. doi:10.1371/journal.pone.0084272.
http://www.ncbi.nlm.nih.gov/pmc/articles/PMC3877265/.

Lee JH, Prakash KVB, Pengatteeri YH, Park SE, Koh HS, Han CW (2007) Chondrocyte apoptosis in the regenerated articular cartilage after allogenic chondrocyte transplantation in the rabbit knee. J. Bone Joint Surg. Br. **89-B**: 977–983. doi:10.1302/0301-620X.89B7.18983.

Lefebvre V, Li P, de Crombrugghe B (1998) A new long form of Sox5 (L-Sox5), Sox6 and Sox9 are coexpressed in chondrogenesis and cooperatively activate the type II collagen gene. EMBO J. **17**: 5718–5733. doi:10.1093/emboj/17.19.5718.

Lefebvre V, Smits P (2005) Transcriptional control of chondrocyte fate and differentiation. Birth Defects Res. Part C Embryo Today Rev. **75**: 200–212. doi:10.1002/bdrc.20048.

Levy AS, Lohnes J, Sculley S, LeCroy M, Garrett W (1996) Chondral delamination of the knee in soccer players. Am. J. Sports Med. **24**: 634–639.

Liegler TJ, Hyun W, Yen TS, Stites DP (1995) Detection and quantification of live, apoptotic, and necrotic human peripheral lymphocytes by single-laser flow cytometry. Clin. Diagn. Lab. Immunol. **2**: 369–376.

Lindén B (1976) The incidence of osteochondritis dissecans in the condyles of the femur. Acta Orthop. Scand. **47**: 664–667.

Lipscomb MF, Masten BJ (2002) Dendritic cells: immune regulators in health and disease. Physiol. Rev. **82**: 97–130. doi:10.1152/physrev.00023.2001.

Lobel KD, Hench LL (1998) In vitro adsorption and activity of enzymes on reaction layers of bioactive glass substrates. J. Biomed. Mater. Res. **39**: 575–579.

Lorentzon R, Alfredson H, Hildingsson C (1998) Treatment of deep cartilage defects of the patella with periosteal transplantation. Knee Surg. Sports Traumatol. Arthrosc. Off. J. ESSKA **6**: 202–208. doi:10.1007/s001670050100.

Lyons TJ, Stoddart RW, McClure SF, McClure J (2005) The tidemark of the chondro-osseous junction of the normal human knee joint. J. Mol. Histol. **36**: 207–215. doi:10.1007/s10735-005-3283-x.

Lyons TJ, Stoddart RW, McClure SF, McClure J (2007) Lectin and other histochemical studies of the articular cartilage and the chondro-osseous junction of the normal human knee joint. J. Mol. Histol. **38**: 13–23. doi:10.1007/s10735-006-9071-4.

Madry H, van Dijk CN, Mueller-Gerbl M (2010a) The basic science of the subchondral bone. Knee Surg. Sports Traumatol. Arthrosc. Off. J. ESSKA **18**: 419–433. doi:10.1007/s00167-010-1054-z.

Madry H, van Dijk CN, Mueller-Gerbl M (2010b) The basic science of the subchondral bone. Knee Surg. Sports Traumatol. Arthrosc. Off. J. ESSKA **18**: 419–433. doi:10.1007/s00167-010-1054-z.

Maehata Y, Takamizawa S, Ozawa S, Kato Y, Sato S, Kubota E, Hata R-I (2006) Both direct and collagen-mediated signals are required for active vitamin D3-elicited differentiation of human osteoblastic cells: roles of osterix, an osteoblast-related transcription factor. Matrix Biol. J. Int. Soc. Matrix Biol. **25**: 47–58. doi:10.1016/j.matbio.2005.09.001.

Maghsoudlou P, Georgiades F, Tyraskis A, Totonelli G, Loukogeorgakis SP, Orlando G, Shangaris P, Lange P, Delalande J-M, Burns AJ, Cenedese A, Sebire NJ, Turmaine M, Guest BN, Alcorn JF, Atala A, Birchall MA, Elliott MJ, Eaton S, Pierro A, Gilbert TW, De Coppi P (2013) Preservation of micro-architecture and angiogenic potential in a pulmonary acellular matrix obtained using intermittent intra-tracheal flow of detergent enzymatic treatment. Biomaterials **34**: 6638–6648. doi:10.1016/j.biomaterials.2013.05.015.

Mahmoudifar N, Doran PM (2013) Osteogenic differentiation and osteochondral tissue engineering using human adipose-derived stem cells. Biotechnol. Prog. **29**: 176–185. doi:10.1002/btpr.1663.

Malik MA, Puleo DA, Bizios R, Doremus RH (1992) Osteoblasts on hydroxyapatite, alumina and bone surfaces in vitro: morphology during the first 2 h of attachment. Biomaterials **13**: 123–128.

Mankin HJ (1974) The reaction of articular cartilage to injury and osteoarthritis (second of two parts). N. Engl. J. Med. **291**: 1335–1340. doi:10.1056/NEJM197412192912507.

Marcacci M, Filardo G, Kon E (2013) Treatment of cartilage lesions: what works and why? Injury **44 Suppl 1**: S11–15. doi:10.1016/S0020-1383(13)70004-4.

Mastrogiacomo M, Papadimitropoulos A, Cedola A, Peyrin F, Giannoni P, Pearce SG, Alini M, Giannini C, Guagliardi A, Cancedda R (2007) Engineering of bone using bone marrow stromal cells and a silicon-stabilized tricalcium phosphate bioceramic: evidence for a coupling between bone formation and scaffold resorption. Biomaterials **28**: 1376–1384. doi:10.1016/j.biomaterials.2006.10.001.

Mauney JR, Blumberg J, Pirun M, Volloch V, Vunjak-Novakovic G, Kaplan DL (2004) Osteogenic differentiation of human bone marrow stromal cells on partially demineralized bone scaffolds in vitro. Tissue Eng. **10**: 81–92. doi:10.1089/107632704322791727.

Menetrey J, Unno-Veith F, Madry H, Van Breuseghem I (2010) Epidemiology and imaging of the subchondral bone in articular cartilage repair. Knee Surg. Sports Traumatol. Arthrosc. Off. J. ESSKA **18**: 463–471. doi:10.1007/s00167-010-1053-0.

Minas T (2012) A primer in cartilage repair. J. Bone Joint Surg. Br. **94**: 141–146. doi:10.1302/0301-620X.94B11.30679.

Minas T, Nehrer S (1997) Current concepts in the treatment of articular cartilage defects. Orthopedics **20**: 525–538.

Ming WZ, Yu LJ, Xin LR, Hao L, Yong G, Lu L, Chang ZX, Zheng ZX (2013) Bone formation in rabbit cancellous bone explant culture model is enhanced by mechanical load. Biomed. Eng. OnLine **12**: 35. doi:10.1186/1475-925X-12-35.

Mitchell JB, McIntosh K, Zvonic S, Garrett S, Floyd ZE, Kloster A, Di Halvorsen Y, Storms RW, Goh B, Kilroy G, Wu X, Gimble JM (2006) Immunophenotype of human adipose-derived cells: temporal changes in stromal-associated and stem cell-associated markers. Stem Cells Dayt. Ohio **24**: 376–385. doi:10.1634/stemcells.2005-0234.

Mohan BG, Suresh Babu S, Varma HK, John A (2013) In vitro evaluation of bioactive strontium-based ceramic with rabbit adipose-derived stem cells for bone tissue regeneration. J. Mater. Sci. Mater. Med. **24**: 2831–2844. doi:10.1007/s10856-013-5018-y.

Murakami P, McCaman MT (1999) Quantitation of Adenovirus DNA and Virus Particles with the PicoGreen Fluorescent Dye. Anal. Biochem. **274**: 283–288. doi:10.1006/abio.1999.4282.

Nair MB, Varma HK, John A (2009) Triphasic ceramic coated hydroxyapatite as a niche for goat stem cell-derived osteoblasts for bone regeneration and repair. J. Mater. Sci. Mater. Med. **20 Suppl 1**: S251–258. doi:10.1007/s10856-008-3598-8.

Naumann A, Dennis JE, Aigner J, Coticchia J, Arnold J, Berghaus A, Kastenbauer ER, Caplan AI (2004) Tissue engineering of autologous cartilage grafts in three-dimensional in vitro macroaggregate culture system. Tissue Eng. **10**: 1695–1706. doi:10.1089/ten.2004.10.1695.

Naumann A, Dennis JE, Awadallah A, Carrino DA, Mansour JM, Kastenbauer E, Caplan AI (2002) Immunochemical and Mechanical Characterization of Cartilage Subtypes in Rabbit. J. Histochem. Cytochem. **50**: 1049–1058. doi:10.1177/002215540205000807.

Nehrer S, Spector M, Minas T (1999) Histologic analysis of tissue after failed cartilage repair procedures. Clin. Orthop. 149–162.

Newman AP (1998) Articular cartilage repair. Am. J. Sports Med. **26**: 309–324.

Ng KW, Leong DTW, Hutmacher DW (2005) The Challenge to Measure Cell Proliferation in Two and Three Dimensions. Tissue Eng. **11**: 182–191. doi:10.1089/ten.2005.11.182.

Ng LJ, Wheatley S, Muscat GE, Conway-Campbell J, Bowles J, Wright E, Bell DM, Tam PP, Cheah KS, Koopman P (1997) SOX9 binds DNA, activates transcription, and coexpresses with type II collagen during chondrogenesis in the mouse. Dev. Biol. **183**: 108–121. doi:10.1006/dbio.1996.8487.

Zur Nieden NI, Kempka G, Ahr HJ (2003) In vitro differentiation of embryonic stem cells into mineralized osteoblasts. Differ. Res. Biol. Divers. **71**: 18–27. doi:10.1046/j.1432-0436.2003.700602.x.

Nooeaid P, Salih V, Beier JP, Boccaccini AR (2012a) Osteochondral tissue engineering: scaffolds, stem cells and applications. J. Cell. Mol. Med. **16**: 2247–2270. doi:10.1111/j.1582-4934.2012.01571.x.

Nooeaid P, Salih V, Beier JP, Boccaccini AR (2012b) Osteochondral tissue engineering: scaffolds, stem cells and applications. J. Cell. Mol. Med. **16**: 2247–2270. doi:10.1111/j.1582-4934.2012.01571.x.

Ogawa R, Mizuno H, Watanabe A, Migita M, Shimada T, Hyakusoku H (2004) Osteogenic and chondrogenic differentiation by adipose-derived stem cells harvested from GFP transgenic mice. Biochem. Biophys. Res. Commun. **313**: 871–877.

Ogawa T, Akazawa T, Tabata Y (2010) In vitro proliferation and chondrogenic differentiation of rat bone marrow stem cells cultured with gelatin hydrogel microspheres for TGF-beta1 release. J. Biomater. Sci. Polym. Ed. **21**: 609–621. doi:10.1163/156856209X434638.

Ohgushi H, Goldberg VM, Caplan AI (1989) Repair of bone defects with marrow cells and porous ceramic. Experiments in rats. Acta Orthop. Scand. **60**: 334–339.

Ohgushi H, Caplan AI (1999) Stem cell technology and bioceramics: From cell to gene engineering. J. Biomed. Mater. Res. **48**: 913–927. doi:10.1002/(SICI)1097-4636(1999)48:6<913::AID-JBM22>3.0.CO;2-0.

Orth P, Cucchiarini M, Kohn D, Madry H (2013) Alterations of the subchondral bone in osteochondral repair--translational data and clinical evidence. Eur. Cell. Mater. **25**: 299–316; discussion 314–316.

Orth P, Cucchiarini M, Wagenpfeil S, Menger MD, Madry H (2014) PTH [1-34]-induced alterations of the subchondral bone provoke early osteoarthritis. Osteoarthritis Cartilage **22**: 813–821. doi:10.1016/j.joca.2014.03.010.

Pachence JM, Frenkel S, Menche D (1998) Fixation method for the attachment of wound repair materials to cartilage defects. February 3.

Pallante-Kichura AL, Cory E, Bugbee WD, Sah RL (2013) Bone cysts after osteochondral allograft repair of cartilage defects in goats suggest abnormal interaction between subchondral bone and overlying synovial joint tissues. Bone **57**: 259–268. doi:10.1016/j.bone.2013.08.011.

Pan J, Zhou X, Li W, Novotny JE, Doty SB, Wang L (2009) In situ measurement of transport between subchondral bone and articular cartilage. J. Orthop. Res. Off. Publ. Orthop. Res. Soc. **27**: 1347–1352. doi:10.1002/jor.20883.

Park JS, Yang HN, Woo DG, Chung H-M, Park K-H (2009) In vitro and in vivo chondrogenesis of rabbit bone marrow-derived stromal cells in fibrin matrix mixed with growth factor loaded in nanoparticles. Tissue Eng. Part A **15**: 2163–2175. doi:10.1089/ten.tea.2008.0532.

Pascucci L, Curina G, Mercati F, Marini C, Dall'Aglio C, Paternesi B, Ceccarelli P (2011) Flow cytometric characterization of culture expanded multipotent mesenchymal stromal cells (MSCs) from horse adipose tissue: Towards the definition of minimal stemness criteria. Vet. Immunol. Immunopathol. **144**: 499–506. doi:10.1016/j.vetimm.2011.07.017.

Pelletier JP, DiBattista JA, Roughley P, McCollum R, Martel-Pelletier J (1993) Cytokines and inflammation in cartilage degradation. Rheum. Dis. Clin. North Am. **19**: 545–568.

Pennock AT, Robertson CM, Wagner F, Harwood FL, Bugbee WD, Amiel D (2006) Does Subchondral Bone Affect the Fate of Osteochondral Allografts During Storage? Am. J. Sports Med. **34**: 586–591. doi:10.1177/0363546505281815.

Peterson L, Minas T, Brittberg M, Nilsson A, Sjögren-Jansson E, Lindahl A (2000) Two- to 9-year outcome after autologous chondrocyte transplantation of the knee. Clin. Orthop. 212–234.

Prentø P (1993) Van Gieson's picrofuchsin. The staining mechanisms for collagen and cytoplasm, and an examination of the dye diffusion rate model of differential staining. Histochemistry **99**: 163–174.

Raub CB, Hsu SC, Chan EF, Shirazi R, Chen AC, Chnari E, Semler EJ, Sah RL (2013) Microstructural remodeling of articular cartilage following defect repair by osteochondral autograft transfer. Osteoarthr. Cartil. OARS Osteoarthr. Res. Soc. **21**: 860–868. doi:10.1016/j.joca.2013.03.014.

Reeves T, Mah P, McDavid W (2012) Deriving Hounsfield units using grey levels in cone beam CT: a clinical application. Dentomaxillofacial Radiol. **41**: 500–508. doi:10.1259/dmfr/31640433.

Reinholz GG, Lu L, Saris DBF, Yaszemski MJ, O'Driscoll SW (2004) Animal models for cartilage reconstruction. Biomaterials **25**: 1511–1521.

Ren Y, Wu H, Zhou X, Wen J, Jin M, Cang M, Guo X, Wang Q, Liu D, Ma Y (2012) Isolation, expansion, and differentiation of goat adipose-derived stem cells. Res. Vet. Sci. **93**: 404–411. doi:10.1016/j.rvsc.2011.08.014.

Renders G a. P, Mulder L, Lin AS, Langenbach GEJ, Koolstra JH, Guldberg RE, Everts V (2014) Contrast-enhanced microCT (EPIC-μCT) ex vivo applied to the mouse and human jaw joint. Dento Maxillo Facial Radiol. **43**: 20130098. doi:10.1259/dmfr.20130098.

Roberts S, Hollander AP, Caterson B, Menage J, Richardson JB (2001) Matrix turnover in human cartilage repair tissue in autologous chondrocyte implantation. Arthritis Rheum. **44**: 2586–2598.

Ronzière MC, Perrier E, Mallein-Gerin F, Freyria A-M (2010) Chondrogenic potential of bone marrow- and adipose tissue-derived adult human mesenchymal stem cells. Biomed. Mater. Eng. **20**: 145–158. doi:10.3233/BME-2010-0626.

Safran MR, Kim H, Zaffagnini S (2008) The use of scaffolds in the management of articular cartilage injury. J. Am. Acad. Orthop. Surg. **16**: 306–311.

Saw K-Y, Hussin P, Loke S-C, Azam M, Chen H-C, Tay Y-G, Low S, Wallin K-L, Ragavanaidu K (2009) Articular cartilage regeneration with autologous marrow aspirate and hyaluronic Acid: an experimental study in a goat model. Arthrosc. J. Arthrosc. Relat. Surg. Off. Publ. Arthrosc. Assoc. N. Am. Int. Arthrosc. Assoc. **25**: 1391–1400. doi:10.1016/j.arthro.2009.07.011.

Schütz K, Despang F, Lode A, Gelinsky M (2014) Cell-laden biphasic scaffolds with anisotropic structure for the regeneration of osteochondral tissue. J. Tissue Eng. Regen. Med. doi:10.1002/term.1879.

Sepp A, Binns RM, Lechler RI (1996) Improved protocol for colorimetric detection of complement-mediated cytotoxicity based on the measurement of cytoplasmic lactate dehydrogenase activity. J. Immunol. Methods **196**: 175–180.

Shao XX, Hutmacher DW, Ho ST, Goh JCH, Lee EH (2006a) Evaluation of a hybrid scaffold/cell construct in repair of high-load-bearing osteochondral defects in rabbits. Biomaterials **27**: 1071–1080. doi:10.1016/j.biomaterials.2005.07.040.

Shao X, Goh JCH, Hutmacher DW, Lee EH, Zigang G (2006b) Repair of large articular osteochondral defects using hybrid scaffolds and bone marrow-derived mesenchymal stem cells in a rabbit model. Tissue Eng. **12**: 1539–1551. doi:10.1089/ten.2006.12.1539.

Shapiro F, Koide S, Glimcher MJ (1993a) Cell origin and differentiation in the repair of full-thickness defects of articular cartilage. J. Bone Joint Surg. Am. **75**: 532–553.

Shapiro F, Koide S, Glimcher MJ (1993b) Cell origin and differentiation in the repair of full-thickness defects of articular cartilage. J. Bone Joint Surg. Am. **75**: 532–553.

Shearer C, Loomer R, Clement D (2002) Nonoperatively Managed Stage 5 Osteochondral Talar Lesions. Foot Ankle Int. **23**: 651–654. doi:10.1177/107110070202300712.

Shim J-H, Lee J-S, Kim JY, Cho D-W (2012) Bioprinting of a mechanically enhanced three-dimensional dual cell-laden construct for osteochondral tissue engineering using a multi-head tissue/organ building system. J. Micromechanics Microengineering **22**: 085014. doi:10.1088/0960-1317/22/8/085014.

Shimomura K, Ando W, Tateishi K, Nansai R, Fujie H, Hart DA, Kohda H, Kita K, Kanamoto T, Mae T, Nakata K, Shino K, Yoshikawa H, Nakamura N (2010) The influence of skeletal maturity on allogenic synovial mesenchymal stem cell-based repair of cartilage in a large animal model. Biomaterials **31**: 8004–8011. doi:10.1016/j.biomaterials.2010.07.017.

Shirazi R, Shirazi-Adl A (2009) Computational biomechanics of articular cartilage of human knee joint: effect of osteochondral defects. J. Biomech. **42**: 2458–2465. doi:10.1016/j.jbiomech.2009.07.022.

Shive MS, Restrepo A, Totterman S, Tamez-Peña J, Schreyer E, Steinwachs M, Stanish WD (2014) Quantitative 3D MRI reveals limited intra-lesional bony overgrowth at 1 year after microfracture-based cartilage repair. Osteoarthr. Cartil. OARS Osteoarthr. Res. Soc. **22**: 800–804. doi:10.1016/j.joca.2014.03.020.

Silver IA, Deas J, Erecińska M (2001) Interactions of bioactive glasses with osteoblasts in vitro: effects of 45S5 Bioglass, and 58S and 77S bioactive glasses on metabolism, intracellular ion concentrations and cell viability. Biomaterials **22**: 175–185.

Solchaga LA, Penick KJ, Welter JF (2011) Chondrogenic Differentiation of Bone Marrow-Derived Mesenchymal Stem Cells: Tips and Tricks. Methods Mol. Biol. Clifton NJ **698**: 253–278. doi:10.1007/978-1-60761-999-4_20.

Son E, Do H, Joo H-M, Pyo S (2007) Induction of alkaline phosphatase activity by L-ascorbic acid in human osteoblastic cells: a potential role for CK2 and Ikaros. Nutr. Burbank Los Angel. Cty. Calif **23**: 745–753. doi:10.1016/j.nut.2007.06.013.

Stein GS, Lian JB, Owen TA (1990) Bone cell differentiation: a functionally coupled relationship between expression of cell-growth- and tissue-specific genes. Curr. Opin. Cell Biol. **2**: 1018–1027.

Sureshbabu S, Komath M, Varma HK In Situ Formation of Hydroxyapatite – Alpha Tricalcium Phosphate Biphasic Ceramics with Higher Strength and Bioactivity. J. Am. Ceram. Soc. doi:10.1111/j.1551-2916.2011.04987.x. http://onlinelibrary.wiley.com/doi/10.1111/j.1551-2916.2011.04987.x/abstract.

Sureshbabu S, Komath M, Varma HK (2011) In Situ Formation of Hydroxyapatite – Alpha Tricalcium Phosphate Biphasic Ceramics with Higher Strength and Bioactivity. J. Am. Ceram. Soc. n/a. doi:10.1111/j.1551-2916.2011.04987.x.

Sureshbabu S, Komath M, Varma HK (2012) In Situ Formation of Hydroxyapatite – Alpha Tricalcium Phosphate Biphasic Ceramics with Higher Strength and Bioactivity. J. Am. Ceram. Soc. **95**: 915–924. doi:10.1111/j.1551-2916.2011.04987.x.

Tanaka T, Komaki H, Chazono M, Fujii K (2005) Use of a biphasic graft constructed with chondrocytes overlying a beta-tricalcium phosphate block in the treatment of rabbit osteochondral defects. Tissue Eng. **11**: 331–339. doi:10.1089/ten.2005.11.331.

Temu TM, Wu K-Y, Gruppuso PA, Phornphutkul C (2010) The mechanism of ascorbic acid-induced differentiation of ATDC5 chondrogenic cells. Am.

J. Physiol. - Endocrinol. Metab. **299**: E325–E334. doi:10.1152/ajpendo.00145.2010.

Totonelli G, Maghsoudlou P, Garriboli M, Riegler J, Orlando G, Burns AJ, Sebire NJ, Smith VV, Fishman JM, Ghionzoli M, Turmaine M, Birchall MA, Atala A, Soker S, Lythgoe MF, Seifalian A, Pierro A, Eaton S, De Coppi P (2012) A rat decellularized small bowel scaffold that preserves villus-crypt architecture for intestinal regeneration. Biomaterials **33**: 3401–3410. doi:10.1016/j.biomaterials.2012.01.012.

Troken A, Marion N, Hollister S, Mao J (2007) Tissue engineering of the synovial joint: the role of cell density. Proc. Inst. Mech. Eng. [H] **221**: 429–440.

Tsai M-T, Lin D-J, Huang S, Lin H-T, Chang WH (2012) Osteogenic differentiation is synergistically influenced by osteoinductive treatment and direct cell-cell contact between murine osteoblasts and mesenchymal stem cells. Int. Orthop. **36**: 199–205. doi:10.1007/s00264-011-1259-x.

Tuli R, Tuli S, Nandi S, Huang X, Manner PA, Hozack WJ, Danielson KG, Hall DJ, Tuan RS (2003) Transforming growth factor-beta-mediated chondrogenesis of human mesenchymal progenitor cells involves N-cadherin and mitogen-activated protein kinase and Wnt signaling cross-talk. J. Biol. Chem. **278**: 41227–41236. doi:10.1074/jbc.M305312200.

Tyler JA (1985) Chondrocyte-mediated depletion of articular cartilage proteoglycans in vitro. Biochem. J. **225**: 493–507.

Venugopal B, Fernandez FB, Babu SS, Harikrishnan VS, Varma H, John A (2012) Adipogenesis on biphasic calcium phosphate using rat adipose-derived mesenchymal stem cells: in vitro and in vivo. J. Biomed. Mater. Res. A **100**: 1427–1437. doi:10.1002/jbm.a.34082.

W. Norman Scott MD (2011) Insall & Scott Surgery of the Knee: Expert Consult - Online and Print, 5e 5 edition. Philadelphia, PA: Churchill Livingstone, November 2.

Walters MA, Leung YC, Blumenthal NC, LeGeros RZ, Konsker KA (1990) A Raman and infrared spectroscopic investigation of biological hydroxyapatite. J. Inorg. Biochem. **39**: 193–200.

Wang Y, Wang J, Bai D, Song J, Ye R, Zhao Z, Lei L, Hao J, Jiang C, Fang S, An S, Cheng Q, Li J (2013) Cell proliferation is promoted by compressive stress during early stage of chondrogenic differentiation of rat BMSCs. J. Cell. Physiol. **228**: 1935–1942. doi:10.1002/jcp.24359.

Waring MJ (1965) Complex formation between ethidium bromide and nucleic acids. J. Mol. Biol. **13**: 269–282.

Williams DF (2008) On the mechanisms of biocompatibility. Biomaterials **29**: 2941–2953. doi:10.1016/j.biomaterials.2008.04.023.

Wu L, Leijten JCH, Georgi N, Post JN, van Blitterswijk CA, Karperien M (2011) Trophic effects of mesenchymal stem cells increase chondrocyte proliferation and matrix formation. Tissue Eng. Part A **17**: 1425–1436. doi:10.1089/ten.TEA.2010.0517.

Wu X, Shi W, Cao X (2007) Multiplicity of BMP signaling in skeletal development. Ann. N. Y. Acad. Sci. **1116**: 29–49. doi:10.1196/annals.1402.053.

Wu Y-N, Law JBK, He AY, Low HY, Hui JHP, Lim CT, Yang Z, Lee EH (2014) Substrate topography determines the fate of chondrogenesis from human mesenchymal stem cells resulting in specific cartilage phenotype formation. Nanomedicine Nanotechnol. Biol. Med. doi:10.1016/j.nano.2014.04.002.

Xiao Y, Qian H, Young WG, Bartold PM (2003) Tissue engineering for bone regeneration using differentiated alveolar bone cells in collagen scaffolds. Tissue Eng. **9**: 1167–1177. doi:10.1089/10763270360728071.

Xie L, Lin ASP, Guldberg RE, Levenston ME (2010) Nondestructive assessment of sGAG content and distribution in normal and degraded rat articular cartilage via EPIC-microCT. Osteoarthr. Cartil. OARS Osteoarthr. Res. Soc. **18**: 65–72. doi:10.1016/j.joca.2009.07.014.

Xie L, Lin ASP, Levenston ME, Guldberg RE (2009) Quantitative assessment of articular cartilage morphology via EPIC-microCT. Osteoarthr. Cartil. OARS Osteoarthr. Res. Soc. **17**: 313–320. doi:10.1016/j.joca.2008.07.015.

Xu Y, James AW, Longaker MT (2008) Transforming growth factor-beta1 stimulates chondrogenic differentiation of posterofrontal suture-derived mesenchymal cells in vitro. Plast. Reconstr. Surg. **122**: 1649–1659. doi:10.1097/PRS.0b013e31818cbf44.

Xynos ID, Hukkanen MVJ, Batten JJ, Buttery LD, Hench LL, Polak JM (2000a) Bioglass ®45S5 Stimulates Osteoblast Turnover and Enhances Bone Formation In Vitro: Implications and Applications for Bone Tissue Engineering. Calcif. Tissue Int. **67**: 321–329. doi:10.1007/s002230001134.

Xynos ID, Edgar AJ, Buttery LDK, Hench LL, Polak JM (2000b) Ionic Products of Bioactive Glass Dissolution Increase Proliferation of Human Osteoblasts and Induce Insulin-like Growth Factor II mRNA Expression and Protein Synthesis. Biochem. Biophys. Res. Commun. **276**: 461–465. doi:10.1006/bbrc.2000.3503.

Xynos ID, Edgar AJ, Buttery LDK, Hench LL, Polak JM (2001) Gene-expression profiling of human osteoblasts following treatment with the ionic products of Bioglass® 45S5 dissolution. J. Biomed. Mater. Res. **55**: 151–157. doi:10.1002/1097-4636(200105)55:2<151::AID-JBM1001>3.0.CO;2-D.

Yang PJ, Temenoff JS (2009) Engineering orthopedic tissue interfaces. Tissue Eng. Part B Rev. **15**: 127–141. doi:10.1089/ten.teb.2008.0371.

Yoon BS, Pogue R, Ovchinnikov DA, Yoshii I, Mishina Y, Behringer RR, Lyons KM (2006) BMPs regulate multiple aspects of growth-plate chondrogenesis through opposing actions on FGF pathways. Dev. Camb. Engl. **133**: 4667–4678. doi:10.1242/dev.02680.

Zhou Y, Yu D, Zhu H (2014) Optimization of culture condition of human bone marrow stromal cells in terms of purification, proliferation, and pluripotency. In Vitro Cell. Dev. Biol. Anim. doi:10.1007/s11626-014-9778-6.

Zuk PA (2010a) The Adipose-derived Stem Cell: Looking Back and Looking Ahead. Mol Biol Cell **21**: 1783–1787. doi:10.1091/mbc.E09-07-0589.

Zuk PA (2010b) The Adipose-derived Stem Cell: Looking Back and Looking Ahead. Mol Biol Cell **21**: 1783–1787. doi:10.1091/mbc.E09-07-0589.

Society For Biomaterials

Adipogenesis on biphasic calcium phosphate using rat adipose-derived mesenchymal stem cells: *In vitro* and *in vivo*

Balu Venugopal,[1] Francis. B. Fernandez,[1] Suresh S. Babu,[2] V. S. Harikrishnan,[3] Harikrishna Varma,[2] Annie John[1]

[1]Division of Implant Biology (TEM Laboratory), Biomedical Technology Wing, Sree Chitra Tirunal Institute for Medical Sciences and Technology, Trivandrum 695012, Kerala, India
[2]Bioceramic Laboratory, Biomedical Technology Wing, Sree Chitra Tirunal Institute for Medical Sciences and Technology, Trivandrum 695012, Kerala, India
[3]Division of Laboratory Animal Science, Biomedical Technology Wing, Sree Chitra Tirunal Institute for Medical Sciences and Technology, Trivandrum 695012, Kerala, India

Received 25 August 2011; revised 14 December 2011; accepted 10 January 2012
Published online in Wiley Online Library (wileyonlinelibrary.com). DOI: 10.1002/jbm.a.34082

Abstract: Developing adipose tissue-engineered construct to mend soft tissue defects arising from traumatic injury, tumor resections, and maxillofacial abnormalities is of prime importance in plastic and reconstructive surgical procedures. It is apparent that the clinical outcome of classic techniques like adipose tissue transplantation is unpredictable, with graft resorption, lack of vascularization, and impaired functionality. In this prospective, the concept of tissue engineering was adopted to fabricate a combination product with biphasic calcium phosphate (BCP) and rat adipose-derived mesenchymal stem cells (ASCs) toward the development of an adipose tissue construct. BCP, a combination of hydroxyapatite and α-tricalcium phosphate, was characterized for its physiochemical properties, and ASCs were characterized for their stemness. The cell–ceramic interactions were demonstrated *in vitro*, whereas adipogenesis was picturesquely depicted by Nile red-stained multilocular adipocyte-like cells. Subsequently, the three-dimensional cell–ceramic-engineered construct was implanted in the rat dorsal muscle for a period of 3 weeks to demonstrate the efficacy of the tissue construct *in vivo*. Interestingly, the histology of the postimplanted tissue construct revealed the distribution of chicken wire net-like fat cells within the vicinity of the construct. The efficacy of cell transplantation via the scaffold was traced using fluorescent *in situ* hybridization by labeling the Y chromosome. Thus, the ceramic-based construct may be a good option for reconstruction therapies. © 2012 Wiley Periodicals, Inc. J Biomed Mater Res Part A: 00A:000–000, 2012.

Key Words: adipose tissue engineering, calcium phosphate, rat model, mesenchymal stem cells, adipogenesis, fluorescent *in situ* hybridization

How to cite this article: Venugopal B, Fernandez Francis. B., Babu SS, Harikrishnan VS, Varma H, John A. 2012. Adipogenesis on biphasic calcium phosphate using rat adipose-derived mesenchymal stem cells: In vitro and in vivo. J Biomed Mater Res Part A 2012:00A:000–000.

INTRODUCTION

Soft tissue defects contribute significantly to cosmetic and reconstructive surgeries for attaining the normal tissue contour. These defects mainly result from deep burns, traumatic injury, tumor resection, congenital defects, or aging process. According to the American Society of Plastic Surgeons, 12.5 million cosmetic procedures and around 5.2 million reconstructive plastic surgical procedures were performed in the United States in 2009 and are increasing at a rate of 5% every year.[1]

Current treatment methods for soft tissue augmentation include mature fat transplantation, use of synthetic materials, injectable composite systems, and *de novo* adipogenesis.[2] However, all these methodologies have many limitations, including donor-site morbidity, deformity, tissue resorption, ischemia, poor vascularization, unsatisfactory long-term outcome, and toxicity of the implants.[3,4] Tissue engineering with a triad partnership of the scaffold, cells, and growth factors[5] offers a new concept toward the treatment of damaged or diseased tissues. This combination results in a functional tissue construct, which is expected to be a replica of the native, healthy tissue exhibiting similar biochemical and biomechanical properties. Fat tissue engineering is now widely accepted, as the engineered adipose construct imparts shape and required volume for the augmented soft tissue.[6] A tissue-engineered adipose substitute promotes regeneration, rather than repair, which helps in the prevention of scar tissue formation and thereby

Additional Supporting Information may be found in the online version of this article.
Correspondence to: A. John; e-mail: ajkari@sctimst.ac.in or karippacheril@gmail.com
Contract grant sponsor: SCTIMST

maintains the normal contour. Aiming toward an ideal adipose tissue construct, different scaffolds and cell types are in the research pipeline. Choi et al.[4] demonstrated adipogenesis in rat model via attachment of Mesenchymal Stem Cells (MSC) to injectable poly (D,L-lactic-co- glycolic acid) spheres aiming at scar-free transplantation. Flynn et al.[7] used an adipose tissue construct with decellularized human placenta and crosslinked hyaluronan seeded with human adipose-derived mesenchymal stem cells (ASCs) to establish adipose tissue regeneration. However, most of the clinical applications of bioceramics as scaffolds relate to the repair of skeletal systems composed of bones, joints, and teeth or to augment hard tissue. Bioactive glass ceramics and calcium phosphate ceramics such as hydroxyapatite (HA), β-tricalcium phosphate (β-TCP), or biphasic calcium phosphate (BCP) have been reported to reconstruct bone defects.[8] They are biocompatible, resorbable, and osteoconductive, and their porous nature offers better cell adhesion and proliferation, encouraging tissue regeneration.[9]

Therefore, it was of interest to investigate the use of an in-house synthesized BCP consisting of HA and α-TCP composite scaffolds for the development of an engineered adipose tissue construct in conjunction with rat adipose-derived mesenchymal stem cells (rASCs). Adipose-derived stem cells (ASCs) have become the major focus because of its easy access and abundance.[10] It also exhibits high proliferation capacity and strong differentiation potential toward adipogenic lineage.[11] Focusing on the maxillofacial reconstruction for mandibular and maxillary reconstruction therapies, the scaffold of choice will be a hard one that could support the load in the maxillofacial area. Several reconstruction strategies in the past have been attempted, including free tissue transfer and various flap models, aiming at re-establishing their aesthetic and functional outputs in the maxillofacial area.[12] Herein, an attempt has been made to demonstrate soft tissue regeneration on a ceramic porous scaffold that would simultaneously fill tissue voids to maintain esthetics and as well integrate in to the native tissue structure. Therefore, this will primarily apply to small perimeter defects, whereas large perimeter defects could be repaired with the assistance of axial vascularization of large grafts *in situ*.[13] Nevertheless, the porous nature of the scaffold could promote nutrient transfer and angiogenic in-growth to support the *de novo* tissue. In this study, the *in vitro*-fabricated cell–ceramic construct implanted in the dorsal muscle of rat model for a period of 3 weeks demonstrated the efficacy of the engineered construct in the generation of adipose tissue in an *in vivo* environment. Although little is known on the mechanism of adipogenesis on a ceramic-based scaffold, this construct may find its application in maxillofacial abnormalities.

MATERIALS AND METHODS

Materials

BCP, a bioactive ceramic, is the scaffold of choice for fabrication of an adipose tissue-engineered construct. All cell culture reagents including medium were purchased from GIBCO™ Invitrogen. Stains and chemical and molecular reagents were purchased from Sigma Aldrich, unless otherwise mentioned.

Biphasic calcium phosphate (BCP)

The bioactive ceramic used for this study was BCP, which was synthesized by wet chemical *in situ* precipitation technique. BCP is a synthetic composite of 40% α-TCP and 60% HA (w/w). BCP is synthesized by the addition of ammonia solution to an acidified aqueous solution containing calcium and phosphate ions in 1.6:1 mole ratio, resulting in a powder that is filtered out immediately and calcined at 300°C. The calcined mass was powdered in a planetary mill (Fritseh GMBH, Germany) and then dispersed in a polymer binder in the presence of a surfactant, finally crosslinked to form a jelly mass. The gel is dried, cut into circular disc, and sintered (Okay Raising-Hearth electric furnace with PID, India) at 1200°C. The sintered discs were then finely shaped by grinding to form discs of 5 mm diameter with 1–2 mm thickness and subjected to ultrasonic cleaning (Cole Parmer). Subsequently, the materials were sterilized by steam (121°C, 15 psi pressure for 15 min).

Surface morphology. BCP scaffolds were gold coated in an ion sputter unit (E101-Hitachi, Japan) before examination, and the surface morphology, porosity, and pore size were evaluated using the scanning electron microscopy (SEM; S2400-Hitachi).

Chemical composition. The chemical composition of the BCP was analyzed by Fourier transform infrared spectroscopy (FTIR) technique (Thermo Nicolet 5700 Spectrometer) using diffuse reflectance (DRIFT) accessory. The sintered discs were powdered and mixed with IR-grade KBr powder, and the spectrum was taken using pure KBr as background. The sample was scanned from 4000 to 400 cm^{-1}, and the spectrum was taken at a resolution of 4 cm^{-1} with an average scan of 64.

Phase purity and crystallinity. The phase analysis and crystallinity of BCP sample were done by powder X-ray diffraction analysis (Siemens D-5005 X-ray Diffractometer, Germany). The sintered samples were powdered and analyzed using Cu Kα radiation by scanning through an angle of 20°–50° at a scanning range of 2°/min at a step size of 0.02°. The pattern was taken at a voltage of 40 kV and a current strength of 30 mA. Materials were identified by comparing the data with the PDF files.

Adipose-derived mesenchymal stem cells

MSCs were isolated from the subcutaneous fat pad of male Sprague Dawley rats. Adipose tissue (3–5 g) was collected, digested with collagenase, and filtered (180-μ*M* Nylon filter; Millipore). The filtrate was pelleted by centrifugation and plated in 25-cm^2 flasks (Nunc) and maintained in medium at 37°C, 5% CO_2, and 95% RH. The medium used was Dulbecco's modified Eagle medium–high glucose supplemented with 10% fetal bovine serum and 1% antibiotics (hereafter referred to as growth medium). Primary cultures at 80%

confluency were trypsinized using 0.25% trypsin and were passaged. All the experiments including isolation of cells and implantation were carried out as per the guidelines of the Institutional Animal Ethics Committee and the committee for the purpose of control and supervision of experiments on animals.

Cell–scaffold interaction *in vitro*

The BCP scaffolds were conditioned in growth medium at 37°C overnight. rASCs (1×10^4) were seeded per scaffold for all the studies. ASCs were allowed to adhere onto the scaffold surface before flooding the discs with growth medium and maintained at 37°C, 5% CO_2, and 95% RH for the respective days in culture. The adhesion, proliferation, and viability of rASCs on ceramic discs were studied.

Cell adhesion studies. Cells on BCP scaffolds after 3 days in culture were fixed in 3% glutaraldehyde (EM Sciences) and processed for SEM analysis with ascending grades of ethanol (Merck, India), critically point dried (HCP2-Hitachi) to remove moisture, and coated with gold in an ion sputter unit (E101-Hitachi). Samples were viewed using SEM (S2400-Hitachi).

Biochemical evaluation for cell proliferation and viability. The proliferation and viability of rASCs on days 3 and 6 in growth medium were determined using Picogreen® dsDNA Quantitation reagent (Molecular Probes) and lactate dehydrogenase (LDH) reaction buffer (Cytotox 96 kit; Promega), respectively. Cell-seeded materials ($n = 3$) were washed with phosphate buffer saline (PBS) lysed with 1% Triton X-100. The proliferation and viability were done as per protocol detailed by Nair et al.[14] The intensity of fluorescence for picogreen (PG) assay (Ex 485 nm/Em 535 nm) was measured with a multifunction microplate reader (HIDEX Chameleon, Finland). For LDH assay, the absorbance was read at 492 nm (HIDEX Chameleon). In both the cases, the relative fluorescence and absorbance units were correlated with cell number using a calibration line constructed from cell suspensions with increasing concentrations of cell numbers.[14]

Confocal microscopic evaluation for cell viability. The viability of rASCs after 3 days in culture was qualitatively determined by confocal laser scanning microscopy (cLSM, LSM 510 Meta; Carl Zeiss) using acridine orange (10 μg/mL) and ethidium bromide (15 μg/mL). The excitation was carried out with Argon 2 laser. Viable cells take up acridine orange (Ex 502 nm/Em 526 nm) giving green fluorescence, whereas dead cells take up ethidium bromide (Ex 518 nm/Em 605 nm) and fluoresces red.

Adipogenic induction of rASCs

For adipocyte differentiation, two kinds of media were used: (a) the induction medium prepared with added supplements to growth medium for a final working concentration of 0.5 m*M* isobutylmethylxanthine (IBMX), 1 μ*M* dexamethasone, 50 μ*M* indomethacin (Unicare India), and 5 μg/mL Insulin (Sun Pharmaceuticals, India); and (b) the maintenance medium is the growth medium supplemented with a final concentration of 10 μg/mL insulin. Adipogenic induction is given for 48 h, and then the cells are maintained in the maintenance medium.

Demonstration of adipogenesis *in vitro*

Nile red staining. Adipogenic-induced rASCs after 21 days in culture on cover slips were fixed in 3.7% paraformaldehyde (SD Fine Chem, India) and stained with Nile red at a final working concentration of 0.5 μg/mL in 4:1 glycerol water mixture. Cells were then stained with 4′,6′-diamidino-2-phenylindole (DAPI) (1 μg/mL) to visualize the nucleus. Nile red stained the intracellular lipids in cytoplasm. Nile red (Ex 485 nm/Em 525 nm) and DAPI (Ex 345 nm/Em 455 nm) were viewed under cLSM.

Biochemical estimation of triglycerides. The triglyceride (TG) content of a known number of induced ASCs was estimated at days 7, 14, and 21 with TG estimation kit (Agappe Diagnostics, India). The adipogenic-induced cell pellet was lysed by ultrasonication (Cole Parmer). About 100 μL of cell lysate in PBS was estimated as per kit instructions and read at 550 nm with spectrophotometer (HIDEX Camilion). Non-induced cells cultured for 21 days were used as reference control. When compared with the provided blank and standard, final TG levels were calculated as follows:

$$\text{TG concentration} = \frac{\text{Absorbance of the sample}}{\text{Absorbance of the standard}} \times 200$$

Demonstration of adipogenesis on BCP scaffold by confocal microscopy. Induced rASCs on the BCP scaffolds cultured for 21 days were fixed with 3.7% paraformaldehyde and stained with Nile red. The scaffolds were washed twice with distilled water to remove the excess stains on the scaffold and were observed under cLSM.

***In vivo* demonstration of adipogenesis**

The BCP discs seeded with 1×10^4 rASCs were cultured 4 days *in vitro* before implantation. The implantation was carried out on six female Sprague Dawley rats (4 months old, 190–210 g) for a period of 21 days. All the experiments were conducted as per guidelines of the Institute Animal Ethics Committee.

Rats were anesthetized with ketamine at 70 mg/kg body weight and xylazine at 5 mg/kg body weight as intramuscular injection. In each rat, the cell-seeded BCP scaffolds were placed in the dorsal muscular region and secured *in situ* with the help of sterile 3–0 nonabsorbable braided silk sutures (Ethicon). Skin incision was also closed using 3–0 braided sutures on simple interrupted pattern.

Histology. The retrieved cell-seeded construct 21 days post-implantation was fixed in 10% neutral buffered formalin. The explanted "Cell–BCP" constructs of three rats were embedded in polymethylmethacrylate (PMMA) for histological analysis. In rest of the explanted sections, the ceramic discs

were carefully pulled out from the surrounding tissue, and the surrounding tissue was embedded in paraffin. The pulled out Cell–BCP construct was analyzed using SEM.

For PMMA processing, the cell–ceramic construct was dehydrated with graded series of isopropanol (Nice Chemicals, India) and embedded in PMMA. The plastic sections of about 180 μm were sliced with a linear precision saw (Isomet™ 5000 Precision Saw, Buehler, Germany), and thereafter fine polished (Ecomet® 3000, Buehler, Germany) and were stained with hematoxylin and eosin (H&E). The finely polished sections of cell-seeded BCP was immersed in acid alcohol, stained with hematoxylin (Electron Microscopy Sciences) and eosin, and viewed under the light microscope (Leica DM 6000, Germany).

For paraffin processing, the fixed samples were washed with tap water, dehydrated in graded ascending series of acetone (Merck), infiltrated with xylene (Merck) in Leica TP-1020 Histokinette (Germany), and embedded in paraffin wax (SLEE MP3/P1 Paraffin wax embedder). Thin sections (5 μm) were cut using the microtome (Leica RM2255, Germany). The sections were kept at 37°C overnight.

Fluorescence in situ hybridization. Fluorescence *in situ* hybridization (FISH) was used to detect the Y chromosome positive cells with rat Y/12 chromosome paint (Star-FISH, Cat no: CA-1631-BF; Cambio, Cambridge, UK) according to the manufacturer's instructions. Paraffin-embedded sections from the surrounding regions around the implant perimeter after removal of the implant were deparaffinized with xylene incubated in 1*M* sodium thiocyanate for 10 min at 80°C, washed in PBS, permeabilized with 0.4% pepsin (Himedia, India) in 0.1*M* HCl (Merck) for 10 min at 37°C. The reaction was quenched in 0.2% glycine in double concentration PBS, and the sections were rinsed in PBS, postfixed in 4% paraformaldehyde, in PBS, dehydrated through graded alcohols, and air dried. The sections were then incubated with fluorescein isothiocyanate (FITC)-labeled Y chromosome paint (Star-FISH) at 60°C for 10 min, and then, the temperature was set to 37°C overnight. Following hybridization, a series of washes were performed at 37°C with 50% deionized formamide (Sisco Research Labs, India) in 2× sodium chloride–sodium citrate (SSC) for 15 min; 2× SSC for 15 min; and 4× SSC containing 0.1 mL 10% Tween 20 for 10 min. The slides were washed in PBS, and the sections were mounted using DAPI. All slides were analyzed with cLSM. The Y Chromosome paint was validated using rat testes.[15]

H&E staining for paraffin-embedded section. The consecutive sections were deparaffinized with xylene (three changes, 10 min each), rehydrated in descending grade of ethanol, washed in tap water, stained with Harris' hematoxylin, differentiated and blued. It was then rinsed with tap water counterstained with 1% eosin, dehydrated in ethanol, cleared in xylene, mounted in DPX (Merck), and viewed under light microscope (Leica DM 6000). Rat skin was also processed and stained with H&E in the same condition to study the fat architecture.

Immunohistochemistry for CD31. Deparaffinized sections were incubated with 10 m*M* sodium citrate buffer for 20 min at 92°C. Immunohistochemistry (IHC) was carried out with Super Sensitive™ Polymer–HRP Detection System (Biogenex) as per the manufacturer's instructions. The primary antibody used was PECAM 1 (CD31; Santa Cruz). The complex is then made visible by treatment with a chromogenic substrate diaminobenzidine (DAB). Nuclei were visualized with hematoxylin, and sections were dehydrated and mounted in DPX.

STATISTICAL ANALYSIS

All values are presented as mean ± standard deviation. Comparison and statistical relevance among experimental groups were assessed using Student's *t*-test and considered statistically significant if $p < 0.05$. Statistical analysis was done using graph pad software.

RESULTS

Material characterization

The ceramic BCP was analyzed for their physicochemical and morphological characteristics by SEM, XRD, and FTIR methods.

Surface morphology. Scanning electron micrographs revealed the rough surface topography of the BCP scaffold. It exhibited a three-dimensional (3D) structure with interconnected micropores and macropores having pore sizes ranging from 120 to 150 μm [Fig. 1(A)].

Chemical composition. The FTIR spectrum of sintered BCP is represented in Figure 1(B), projecting the characteristic peaks of synthetic HA that corresponds to all the functional groups depicted by their vibrational frequency values. The peaks observed at 3671.4 cm^{-1} (stretching mode υ_S) and 630 cm^{-1} (liberating mode υ_L) correspond to the hydroxyl stretch in the spectra of BCP sample. All the theoretically predicted vibrational modes for phosphate group were present in the prepared BCP. The triply degenerated asymmetric peaks are seen at around 1090 and 1020 cm^{-1}, and the nondegenerative stretching mode of P—O bond is observed at 961 cm^{-1}. The peaks around 601 and 570 cm^{-1} are due to the bending modes of O—P—O bond. Because the absorption of HA is maximum when compared with α-TCP, the absorption peaks of TCP were submerged.

Phase purity and crystallinity. X-ray diffraction pattern of the sintered BCP [Fig. 1(C)] was compared with the existing powder diffraction data files in order to assess the phase and crystallinity of the prepared ceramic and was found to be well matched with the PDF files of HA and α-TCP. The black-colored scan pattern corresponds to the prepared BCP, and the comparison with the standard patterns reveals the presence of α-TCP, which matches with PDF #29-0359 denoted by blue lines and that of HA (PDF #09-0432) by red lines. The presence of both HA and α-TCP indicated the biphasic nature of the composite. The sharp peaks observed

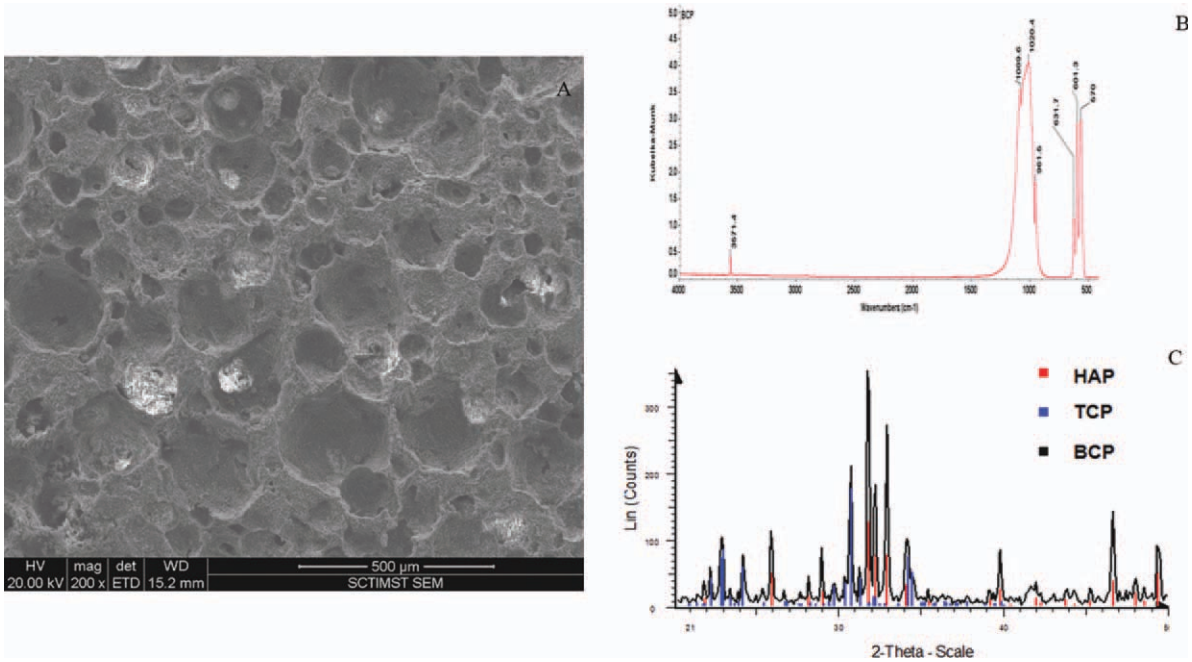

FIGURE 1. Material characterization. A: Scanning electron micrograph displaying the microporous and macroporous structures of biphasic calcium phosphate (BCP). B: FTIR spectrum of BCP depicting characteristic hydroxyl (3671 cm^{-1}) and phosphate groups (1020–670 cm^{-1}). C: Demonstration of crystallinity using XRD pattern; BCP (black) in comparison with hydroxyapatite (HA, red) and α-tricalcium phosphate (α-TCP, blue) in PDF database. [Color figure can be viewed in the online issue, which is available at wileyonlinelibrary.com.]

in the pattern indicated the well-crystallized nature of BCP. The absence of other projected patterns demonstrated the purity of the composite with HA and α-TCP as the individual components. The characterization of these materials for microstructure, phase purity, crystallinity, and functional groups are all necessary to meet the stringent requirements for use as medical implants.

Rat adipose-derived mesenchymal stem cells

Primary cultures of rASCs were isolated based on its property of plastic adherence.[16] Most of the nonadherent cells were washed out during the first medium change. Thereafter, these fibroblastic cells exhibited extensive proliferation and reached confluency within 4–6 days in the growth medium [Fig. 2(A)].

Material–cell interaction *in vitro*

Scaffolds in direct contact with ASCs and SEM. Phase contrast microscopic evaluation showed excellent cell proliferation potential in the immediate neighborhood of the scaffold BCP [Fig. 2(B)]. The cells 3 days postseeding on the scaffold displayed normal fibroblastic morphology. The initial adhesion of rASCs on the BCP evaluated 48 h postseeding by SEM [Fig. 2(C)] showed a well-distributed cell population with fibroblastic morphology.

Biochemical evaluation for proliferation and viability. When comparing the relative fluorescence unit with a known number of cells, an increase in cell number was seen over time on the BCP scaffolds. Thus, the PG assay indicated a well-proliferating cell population with pronounced difference

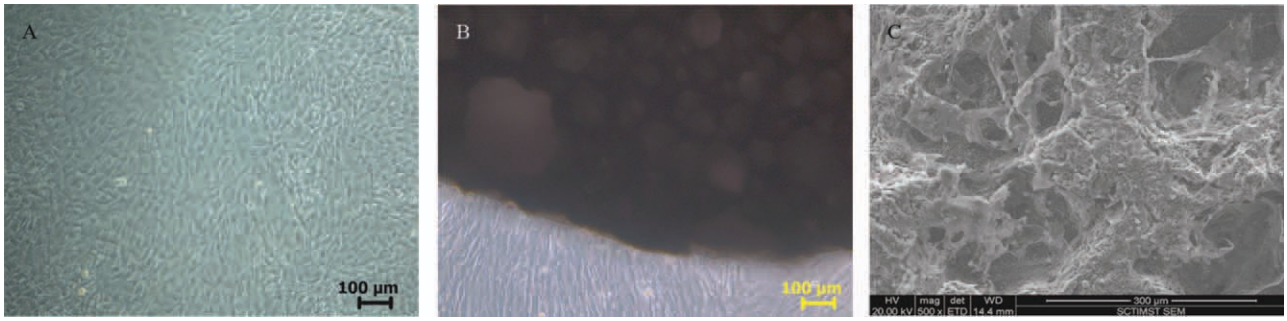

FIGURE 2. Cell material interaction. A: Phase contrast micrograph of a monolayer of rat adipose-derived mesenchymal stem cells (rASCs, passage 4) exhibiting the fibroblast morphology. B: Phase contrast micrograph of rASCs in direct contact with biphasic calcium phosphate (BCP) exhibiting normal fibroblast morphology. C: Scanning electron micrograph of rASCs adhered on BCP. [Color figure can be viewed in the online issue, which is available at wileyonlinelibrary.com.]

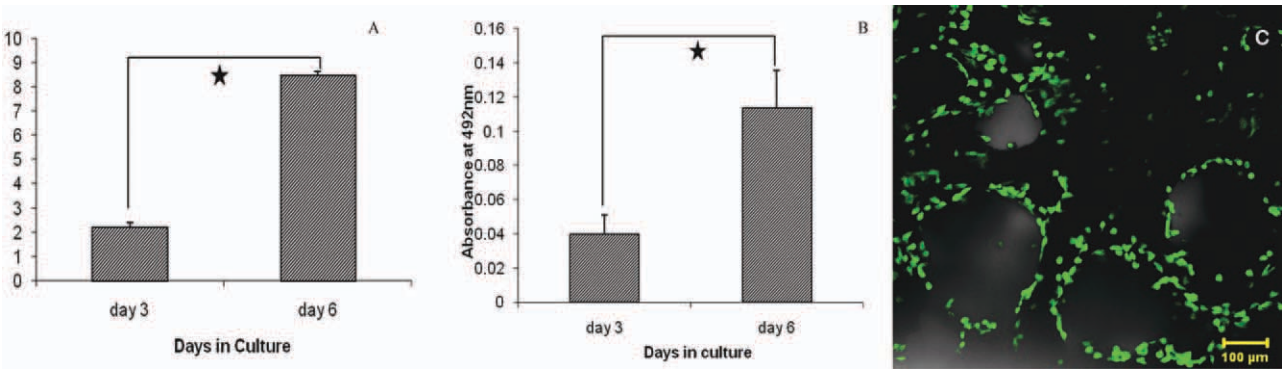

FIGURE 3. Cell material interaction. A: Picogreen assay for proliferation of rat adipose-derived mesenchymal stem cells (rASCs) on biphasic calcium phosphate (BCP). B: Lactate dehydrogenase assay for viability of rASCs on BCP (*$n = 3$; mean $\pm$ SD; Student's t-test, p value < 0.05). C: Confocal micrograph showing viable rASCs on BCP. [Color figure can be viewed in the online issue, which is available at wileyonlinelibrary.com.]

between the number of cells on the scaffold in days 3 and 6 [Fig. 3(A)]. LDH estimation clearly indicated a viable cell population on the BCP scaffold with an increase in the number of viable cells corresponding to cell proliferation over time [Fig. 3(B)]. Viability is indicated by the increased assessment of LDH in rASCs on day 6 when compared with that on day 3. For both PG and LDH assays, the data were expressed as mean and standard deviation. Student's *t*-test was conducted, and the *p* value obtained was found to be <0.05 and was statistically significant.

Qualitative assessment for viability: ASCs on BCP scaffolds. rASCs seeded on BCP were observed for viability after 48 h in culture. Live cells take up acridine orange, a nucleic acid selective cell permeable fluorescent cationic dye that fluoresces green (525 nm); ethidium bromide is a nucleic acid intercalating agent that fluoresces with a red-orange color (620 nm) and is excluded from intact cell, and therefore, dead cells fluoresce red. Appreciable number of cells was found viable on BCP [Fig. 3(C)] after 48 h in culture and was homogenously distributed and rimmed around the macropores.

Evaluation of adipogenesis *in vitro*

Demonstration using Nile red. Nile red-stained cell population is demonstrated in Figure 4(A), with evident lipid accumulation. Instead of characteristic unilocular fat droplets, multilocular lipid-containing vesicles were observed in the cytoplasm [Fig. 4(A), inset]. Induced ASCs showed typical adipocyte morphology, in which the cells attain a spherical shape [Fig. 4(B)] rather to the fibroblastic morphology. Nile red staining was further modified to determine the location of the nucleus in the cell by counter staining with DAPI. Nucleus took up a blue color, and the cytoplasm fluoresce red [Fig. 4(C)]. Most of the cell displayed a peripheral or cornered nucleus depicting typical adipocyte morphology.

Biochemical estimation for TGs. The TG accumulation quantitatively estimated at three different time intervals for a constant number of induced rASCs displayed an increase in TG content when compared with the noninduced control cell population. There was a promotion in lipid accumulation from days 7 to 21, leading to the formation of a lipophilic environment in the induced stem cell population (Fig. 5). TG accumulation of noninduced cells cultured for 21 days was used as reference control.

Demonstration of adipogenesis on BCP by confocal microscopy. The cell-seeded BCP scaffold stained with Nile red was observed using confocal microscope, which showed evident lipid accumulated cells on the ceramic scaffold and

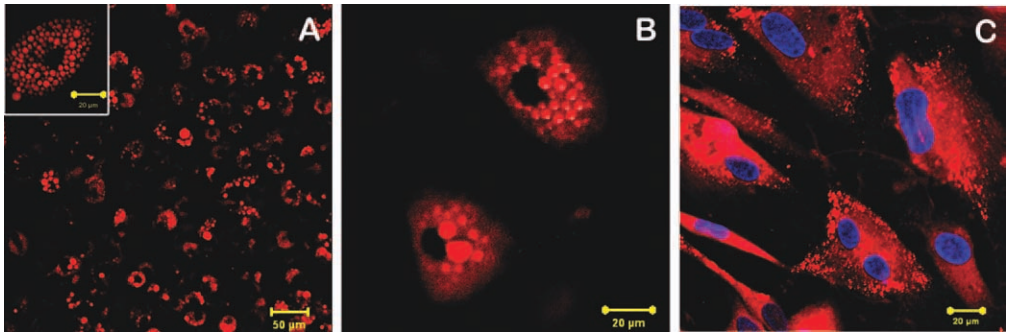

FIGURE 4. Confocal micrograph of rat adipose-derived mesenchymal stem cells (rASCs) differentiated to adipogenic lineage *in vitro*. A: Nile red-stained oil droplets (red colored) in rASCs. Inset shows a single rASC with numerous small red lipid globular structures. B: Magnified image of induced rASCs displaying spherical morphology with red globules within the cell. C: Induced rASCs stained with DAPI and Nile red depicting the nucleus along with the lipid globules. [Color figure can be viewed in the online issue, which is available at wileyonlinelibrary.com.]

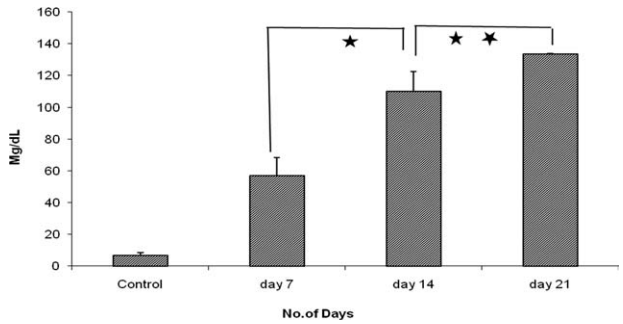

FIGURE 5. Biochemical estimation of triglycerides in induced rat adipose-derived mesenchymal stem cell (rASC) population cultured for a period of 7, 14, and 21 days. Noninduced cells (21 days in culture) were used as the reference control. (*, **Data are expressed as mean ± SD ($n = 3$) and the p value < 0.05 using Student's t-test).

was uniformly distributed throughout. The differentiated cells take up Nile red, a lipophilic fluorescent dye that fluoresces red. Differentiated cells were found both on the surface [Fig. 6(A)] and on the rim of the pores [Fig. 6(B)]. The depth code in Figure 6(C) showed differentiated cells within the pores up to a depth of 60 μm.

In vivo demonstration of adipogenesis

The gross and histological observation of the retrieved tissue showed no signs of inflammation or any kind of immune response. The scaffold also proved to be cytocompatible under *in vivo* conditions.

Histology of PMMA-embedded section. The induced cell-seeded sections stained with H&E demonstrated a faint network of "empty" spaces similar to the morphology of fat cells [Fig. 7(A)], along with muscle architecture. The fat-like cells appeared as elliptical globules, the nucleus was stained blue and the adjacent muscles stained pink. The cell-seeded constructs depicted a network of adipocyte-like cells [Fig. 7(B)] in and around the ceramic scaffolds with a prominent cytoplasm and the nucleus pushed aside to a corner. Adipocyte-like phenotype cells within the scaffolds resembled the characteristic subcutaneous fat pad design of the rat skin (Supporting Information Image S1).

FISH. The paraffin-embedded sections stained with rat Y chromosome paint conjugated with FITC and biotin showed the presence of male donor cells within the female rat muscle [Fig. 8(A,B)]. DAPI stain displayed the nucleus where the Y chromosome paint was shown to be present within the nucleus. Imaging was done using cLSM in which the FITC conjugated probe (Ex 488 nm/Em 520 nm) bound to the Y chromosome of the male cells fluoresce red within the blue background provided by DAPI (Ex 345 nm/Em 455 nm) that makes the nucleus fluoresce blue.

Histology of paraffin-embedded sections. H&E-stained sections [Fig. 8(C)] demonstrated a network of fat-like cells similar to those observed in PMMA-embedded sections. The cellular architecture of the H&E-stained cells was found similar to that of adipocytes. The presence of CD31 marker on the endothelial cells was confirmed by the brown precipitate formed by the DAB reaction [Fig. 8(D)]. Neoangiogenesis was found within the implant region indicated by incipient capillary formation, evident from IHC staining of CD31.

DISCUSSION

This study was focused on the fabrication of an adipose tissue construct using a ceramic composite BCP in conjunction with ASCs induced to the adipogenic lineage and to assess the efficacy of the cell–ceramic construct in supporting adipogenesis *in vitro* and *in vivo* in a rat model. Here, the combination of HA and α-TCP synthesized as the second phase was to attain a tunable bioresorbable characteristic of BCP to aid in faster resorption and remodeling when compared with the commonly found biphasic ceramics with HA and β-TCP. The composite is highly uniform with respect to the distribution of both phases by adopting an *in situ* preparation protocol. As the concept of induction and support of adipogenesis on BCP was successfully achieved and not reported elsewhere, this preliminary study may hopefully open up avenues in the field of hard and soft tissue reconstruction.

ASCs isolated from the subcutaneous fat pad of male rats were characterized to ensure their stemness and mesenchymal origin. Adipose tissue is an ideal source of ASCs

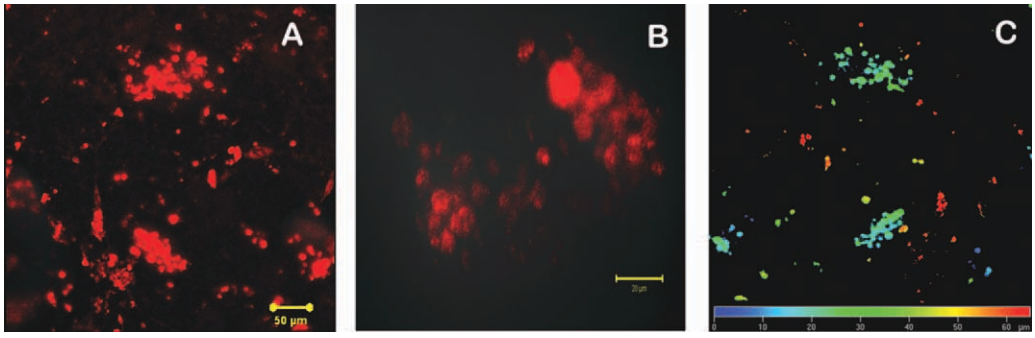

FIGURE 6. Confocal micrograph of lipid globules of induced rat adipose-derived mesenchymal stem cell (rASCs) on biphasic calcium phosphate (BCP) stained with Nile red. A: Cell distribution on BCP. B: Nile red-stained lipid globules of adipocytes within the pores of BCP. C: Depth-coded micrograph showing distribution of cells up to a depth of 60 μm within the BCP. [Color figure can be viewed in the online issue, which is available at wileyonlinelibrary.com.]

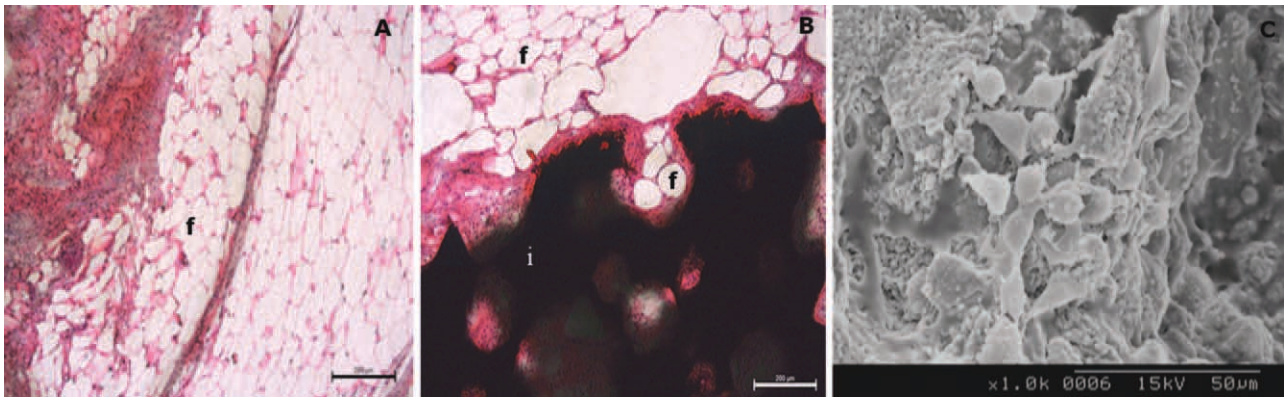

FIGURE 7. Microscopic analysis of cell–ceramic construct retrieved 21 days postimplantation: (A and B) PMMA-embedded sections stained with H&E. A: Vacuolated fat-like cells within the muscle tissue. B: Fat-like cells present within the vicinity of the implant along with fat cell formation within the scaffold pores. C: Scanning electron micrograph of the cell ceramic construct showing the spherical morphology of cells on the implant (f: fat-like cells; i: implant). [Color figure can be viewed in the online issue, which is available at wileyonlinelibrary.com.]

that is easily available, accessible, readily expandable,[8] and display multilineage differentiation potential.[16] The ASCs were found positive for the mesenchymal surface positive markers CD105 (Endoglin) and CD44 (hyaluronate)[17]; (data not shown). Furthermore, the stemness was confirmed by exploiting their multilineage differentiation potential by differentiating them to adipogenic, osteogenic, and chondrogenic lineages when stimulated within respective microenvironments (data not shown).

Scaffold structure indicated a porous and rough surface topography favorable for cell adhesion and proliferation with cozy niches for cell habitat. Simultaneously, the porous interconnections facilitated easy nutrient and macromolecule transport [Fig. 1(A)]. BCP is essentially a mixture of

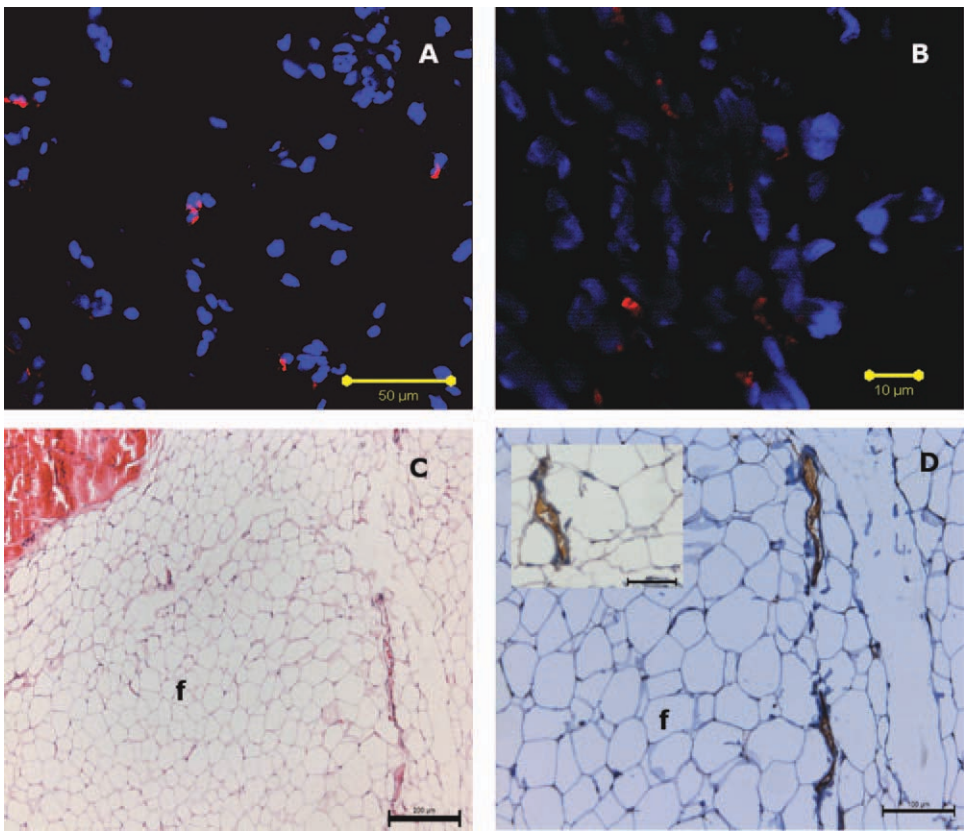

FIGURE 8. Microscopic evaluation of paraffin-embedded section of the surrounding tissue after removal of the implant 21 days postimplantation. A: Fluorescent *in situ* hybridization (FISH) of the surrounding tissue showing the presence of male donor cells by selectively staining the Y chromosomes. B: Magnified image of FISH. C: Paraffin-embedded section stained with H&E depicting fat-like phenotype. D: Consecutive section demonstrating neoangiogenesis within the regenerated area; IHC with CD31. [Color figure can be viewed in the online issue, which is available at wileyonlinelibrary.com.]

calcium and phosphorus and mimics the natural environment as they include the major elements of the human body. Physicochemical characterizations revealed the nature, surface morphology, chemical groups,[18,19] crystallinity, and purity of the scaffolds that supported cell adhesion, proliferation, and viability. Cell adhesion on the scaffolds evaluated by SEM displayed ideal cell–material compatibility, and similar observation has been reported with human MSCs seeded on ceramic discs.[20] The adhesion of cells on materials is very important as it influences their ability to proliferate and differentiate and depends on the initial adsorption of serum proteins such as vitronectin and fibronectin[21] whose strong affinity with ceramic substrates has been reported.[22] Thus, the attachment, adhesion, and spreading of cells belong to the first phase of cell–material interaction that further influences the capacity of cells to proliferate/differentiate on the scaffold. The proliferation potential and the presence of viable cells signal the effect of scaffold in promoting cellular organization and behavior. Therefore, the 3D structural topography of BCP with its interconnected pores and larger surface area enhances the proliferation potential of the ASCs, thus proving the scaffold to be cytocompatible and cell friendly, ensuring the stability and integrity of the construct.

Adipogenic differentiation is achieved by supplementing the medium with dexamethasone, IBMX, indomethacin, and insulin.[3,8,23–25] Dexamethasone is a synthetic glucocorticoid,[26] and glucocorticoids are known to elevate the intracellular c-cyclic adenosine monophosphate (c-AMP) level,[27] which could favor adipocyte formation. Dexamethasone reduces the expression of preadipocyte factor-1 (pref-1), a negative regulator of adipogenesis,[23] and activates CCAAT/enhancer binding protein alpha (C/EBPα), a major transcription factor inducing adipocyte differentiation.[26] IBMX and indomethacin can inhibit phosphodiesterase activity by inhibiting c-AMP degradation and accelerate the differentiation of preadipose cell lines and primary preadipocytes.[25] IBMX has been shown to increase the expression of CCAAT/enhancer binding protein beta (C/EBPβ), and this is required for subsequent peroxisome proliferator-activated receptor (PPARG) expression and adipocyte differentiation.[26] High concentrations of insulin can also be used in combination with these inducing agents.[28,29] In such an inductive environment, the induced cells on and within the ceramic composite may in turn generate their own growth factors, probably influenced by the physical and chemical stimuli emanated from the underlying 3D ceramic scaffold. In addition to harboring the necessary growth factors and secretory molecules, the continuous supply of required nutrients along the interconnected pores will also supplement a favorable inductive environment for the surrounding stem cells to migrate from the vicinity of the implant toward the 3D construct and to differentiate toward the specific lineage, promoting *in situ* regeneration.

The regulation of the adipocyte gene occurs primarily at the transcription level[23] where PPARG expression induces the exit of cells from the cell cycle, which is the primary prerequisite for adipocyte differentiation,[26] and triggers the expression of other adipocyte-specific genes. After growth arrest, the preadipocytes receive an appropriate combination of mitogenic and adipogenic signals to continue through subsequent differentiation steps. The induction of stem cells to adipocyte phenotype results in significant changes in cell morphology, cytoskeletal components, and secretory factors. Adipogenic differentiation is accompanied by a dramatic increase in collagen type I to IV along with lamilin and fibronectin.[23]

Induction of differentiation at confluence results in drastic changes in the fibroblast morphology due to lipid accumulation. Confocal micrographs picturesquely displayed excellent adipocyte morphology with peripheral blue DAPI-stained nucleus and Nile red-stained intracellular lipid globules in the cytoplasm as demonstrated by Pittenger.[25] Interestingly, the increase in TG content of the cytoplasm was quantitatively estimated at different time intervals revealing lipogenesis within the induced ASCs.[30] This states that lipogenesis is a process that is continuous in induced ASCs resulting in the accumulation of TG using the substrates available in the medium *in vitro*. Initially, TGs are formed as small globules at the initial stage of adipogenesis, and later, these globules collate together to form bigger lipid vacuole,[23] which is denoted by an increase in TG accumulation on day 21. From the confocal micrographs of adipocytes on the scaffolds, it is very evident that BCP can support adipogenesis *in vitro* even though ceramics are generally considered as bone substitutes.

In vivo implantation studies of the cell–ceramic construct in the dorsal muscle region of rats demonstrated the efficacy of ceramic scaffolds in adipose tissue regeneration. Dorsal muscular region is a suitable ectopic region for implantation where normal fat tissue is absent. Adipogenesis in rat model showed *de novo* formation of adipocytes at sites of implantation and was assessed in terms of histology. Fat cells or adipocytes are large (up to 200 μm in size) and contain major lipid inclusions. In mature adipocytes, characteristic unilocular fat globules occupied the cytoplasm with the nucleus pushed to the periphery and thereby formed a thin rim surrounding the lipid droplets, resulting in a "signet ring" appearance. The fat is usually dissolved in routine processing, leaving a large, empty vacuole. The loss of lipid leads to a "chicken wire" appearance. The FISH with the Y chromosome paint supported the transplantation efficiency, viability, and migration of donor cells to the tissue around the implant perimeter in female rats 21 days postimplantation by selectively labeling the Y chromosome of the male donor cells. Since the tissue from the implant perimeter was taken from paraffin-embedded blocks for FISH analysis (as FISH analysis was not possible with PMMA sections, the ceramic implant was removed and the surrounding tissue was taken for paraffin processing), the Y chromosome signals were weak and minimum as the cell–ceramic construct has been removed. However, this could substantiate the fact that the presence of differentiated cells on the ceramic implant may have migrated to the surrounding region where the autologous group of stem cells also participate in the regeneration process. H&E staining of paraffin-embedded sections

showed a network of fat cells in the ectopic region, and these cells showed striking similarity in cellular architecture with the subcutaneous fat pad of rat skin. This process may probably have been triggered by the inductive environment offered by the adipose tissue construct, and these differentiated cells displayed adipocyte morphology as revealed from the light micrographs of H&E [Fig. 8(C)]. Scanning electron micrograph of the retrieved cell-seeded construct 21 days postimplantation showed cells with spherical architecture on the BCP disc, and this supported the fact that the ceramic composite provided a favorable environment for adipogenic differentiation [Fig. 7(C)]. Data from histology, SEM, and FISH demonstrated the fact that the cells implanted via the carrier BCP survived the *in vivo* environment and differentiated into adipocytes forming a well-established network of fat cells. Neovascularization visualized in the H&E sections and demonstrated by IHC [Fig. 8(D)] observed in the vicinity of the fat-like cells can help in the formation of functional microvascular network with red blood cell perfusion. Development of the capillary network is crucial to ensure adipose tissue remodeling, and lack of vascularization may promote adipose tissue loss as in the conventional fat graft transplantations which have become a failure. This underlines a crucial link between adipose cells and the capillary network. Adipose lineage cells have shown to release potent angiogenic factors such as monobutyril, vascular endothelial growth factor, and leptin,[31] which may be harbored within the ceramic implant to help in the formation of a capillary network for the survival of the induced rASCs.

Applications of this compact scaffold for soft tissue reconstruction along the lines of adipogenesis on a ceramic composite may open up avenues in the areas where a bone–fat interface plays a major role. This construct is intended to find its application in maxillofacial reconstruction therapies, in which a hard scaffold could support the load of the mandibular and maxillary regions playing the dual role of withstanding stress along with supporting adipogenesis. MSCs also claim the advantage that all craniofacial structures has a mesenchymal origin.[32] Osteogenesis and adipogenesis are assumed to be inversely related as both tend to interfere others differentiation pathway.[16] Calcium ions are also known to inhibit adipogenesis.[25] Still it is a hairline boundary that exists between the osteogenic and adipogenic commitment pathways, and there are reports for the coexistence of adipogenic and osteogenic markers.[33] This ceramic scaffold supporting adipogenesis in the biological milieu has potential applications in maxillofacial tissue engineering. The porous nature of the ceramic scaffold makes it ideal for small perimeter defects because the cell construct can rely on fluid diffusion and blood perfusion.[13] In case of large tissue voids, suboptimal vascularization limits the survival of the *in vivo* implant tissue construct,[34] which necessitates the need of axial vascularization.[13]

The histological and microscopic analysis of the Cell–BCP construct, basically a calcium phosphate composite, have shown excellent *de novo* regeneration of fat tissue in rat model as well as *in vitro*, not reported elsewhere. Moreover, HA fillers are now in practice for esthetic treatment and has been demonstrated to induce collagen deposition,[35] a favorable sign to promote adipogenesis. The cell–ceramic construct that supported adipogenesis could be a candidate with potential applications in facial, plastic, and reconstructive therapies.

CONCLUSION

In this study, an attempt has been made to use rASCs in combination with bioactive ceramic–BCP for the application of soft tissue augmentation/regeneration. The 3D BCP characterized for its physiochemical properties displayed ideal cell–material interactions *in vitro*, and the cell–ceramic-engineered construct promoted adipose tissue regeneration in the rat model. Thus, the adipose tissue construct fabricated has far reaching benefits in the field maxillofacial reconstruction. In such applications, when the ceramic is expected to degrade, the regenerated adipose tissue would maintain the contour and aesthetics of the lost tissue.

ACKNOWLEDGMENTS

The authors acknowledge the Director SCTIMST, Head BMT for facilities provided to carry out the work; Dr. Anil Kumar and Mr. Thulasidharan for cLSM and histology; and Mr. M. A. Sanoj for SEM. Dr. Sachin J Shenoy for technical advice. Mr. Manoj for animal care.

REFERENCES

1. 2010 Report of the 2009 Statistics National Clearinghouse of Plastic Surgery Statistics. The American Society of Plastic Surgeons 2010. Available at: http://plasticsurgery.org. Accessed on 4 May, 2011.
2. Gomillion CT, Burg K. Stem cells and adipose tissue engineering. Biomaterials 2006;27:6052–6063.
3. Hong L, Peptan IA, Colpan A, Daw JL. Adipose tissue engineering by human adipose-derived stromal cells. Cells Tissues Organs 2006;183:133–140.
4. Choi YS, Park SN, Suh H. Adipose tissue engineering using mesenchymal stem cells attached to injectable PLGA spheres. Biomaterials 2005;26:5855–5863.
5. Langer R, Vacanti JP. Tissue engineering. Science 1993;260: 920–926.
6. Patrick CW, Jr. Adipose tissue engineering: The future of breast and soft tissue reconstruction following tumor resection. Semin Surg Oncol 2000;19:302–311.
7. Flynn L, Prestwich GD, Semple JL, Woodhouse KA. Adipose tissue engineering with naturally derived scaffolds and adipose-derived stem cells. Biomaterials 2007;28:3834–3842.
8. Guéhennec L, Layrolle P, Daculsi G. A review of bioceramics and fibrin sealant. Eur Cells Mater 2004;8:1–11.
9. Teixeira S, Ferraz MP, Monteiro FJ. Biocompatibility of highly macroporous ceramic scaffolds: Cell adhesion and morphology studies. J Mater Sci: Mater Med 2008;19:855–859.
10. Zuk PA, Zhu M, Mizuno H, Huang J, Futrell JW, Katz AJ, Benhaim P, Lorenz HP, Hedrick MH. Multilineage cells from human adipose tissue: Implications for cell-based therapies. Tissue Eng 2001;7: 211–228.
11. Zuk PA, Zhu M, Ashjian P, De Ugarte DA, Huang JI, Mizuno H, Alfonso ZC, Fraser JK, Benhaim P, Hedrick MH. Human adipose tissue is a source of multipotent stem cells. Mol Biol Cell 2002;13: 4279–4295.
12. Chen WL, Ye JT, Yang ZH, Huang ZQ, Zhang DM, Wang K. Reverse facial artery-submental artery mandibular osteomuscular flap for the reconstruction of maxillary defects following the removal of benign tumors. Head Neck 2009;31:725–731.
13. Kneser U, Schaefer DJ, Polykandriotis E, Horch RE. Tissue engineering of bone: The reconstructive surgeon's point of view. J Cell Mol Med 2006;10:7–19.

14. Nair MB, Varma HK, John A. Triphasic ceramic coated hydroxyapatite as a niche for goat stem cell-derived osteoblasts for bone regeneration and repair. J Mater Sci: Mater Med 2009;20: S251–S258.
15. Evans CH, Liu FJ, Glatt V, Hoyland JA, Kirker-Head C, Walsh A, Betz O, Wells JW, Betz V, Porter RM, Saad FA, Gerstenfeld LC, Einhorn TA, Harris MB, Vrahas MS. Use of genetically modified muscle and fat grafts to repair defects in bone and cartilage. Gene tissue grafts for bone and cartilage repair. Eur Cells Mater 2009;18:96–111.
16. Gimble JM, Guilak F, Nuttall ME, Sathishkumar S, Vidal M, Bunnell BA. In vitro differentiation potential of mesenchymal stem cells. Transfus Med Hemother 2008;35:228–238.
17. Ogwa R. The importance of adipose-derived stem cells and vascularized tissue regeneration in the field of tissue transplantation. Curr Stem Cell Res Ther 2006;1:13–20.
18. Gibson IR, Rehman IU, Best SM, Bonfield W. Characterization of the transformation from Ca-deficient apatite to β-tricalcium phosphate. J Mater Sci: Mater Med 2000;11:533–539.
19. Koutsopoulos S. Synthesis and characterization of hydroxyapatite crystals: A review study on the analytical methods. J Biomed Mater Res 2002;62:600–612.
20. Douglas T, Liu Q, Humpe A, Wiltfang J, Sivananthan S, Warnke PH. Novel ceramic bone replacement material ceraBalls® seeded with human mesenchymal stem cells. Clin Oral Implants Res 2010;21:262–267.
21. Anselme K. Osteoblast adhesion on biomaterials. Biomaterials 2000;21:667–681.
22. Zreiqat H, Evans P, Howlett C. Effect of surface chemical modification on bioceramic on phenotype of human bone derived cells. J Biomed Mater Res 1999;44:389–396.
23. Niemela S, Miettinen S, Sarkanen JR, Ashammakhi N. Adipose tissue and adipocyte differentiation: Molecular and cellular aspects and tissue engineering applications. In: Ashammakhi N, Reis R, Chiellini F, editors. Topics in Tissue Engineering, Vol. 4. 2008. University of Oulu.
24. Mauney JR, Nguyen T, Gillen K, Kirker-Head C, Gimble JM, Kaplan DL. Engineering adipose-like tissue in vitro and in vivo utilizing human bone marrow and adipose-derived mesenchymal stem cells with silk fibroin 3D scaffolds. Biomaterials 2007;28:5280–5290.
25. Pittenger MF. Adipogenic differentiation of human mesenchymal stem cells. U.S. Pat. 5,827,740, 1998.
26. Gregoire FM, Smas CM, Sul HS. Understanding adipocyte differentiation. Physiol Rev 1998;78:783–809.
27. Ailhaud G, Grimaldi P, Négrel R. Cellular and molecular aspects of adipose tissue development. Annu Rev Nutr 1992;12:207–233.
28. Reusch JE, Colton LA, Klemm DJ. CREB activation induces adipogenesis in 3T3–L1 cells. Mol Cell Biol 2000;20:1008–1020.
29. Rosen ED, Spiegelman BM. Molecular regulation of adipogenesis. Annu Rev Cell Dev Biol 2000;16:145–171.
30. Miki H, Yamauchi T, Suzuki R, Komeda K, Tsuchida A, Kubota N, Terauchi Y, Kamon J, Kaburagi Y, Matsui J, Akanuma Y, Nagai R, Kimura S, Tobe K, Kadowaki T. Essential role of insulin receptor substrate 1 (IRS-1) and IRS-2 in adipocyte differentiation. Mol Cell Biol 2001;21:2521–2532.
31. Moon MH, Kim SY, Kim YJ, Kim SJ, Lee JB, Bae YC, Sung SM, Jung JS. Human adipose tissue-derived mesenchymal stem cells improve postnatal neovascularization in a mouse model of hindlimb ischemia. Cell Physiol Biochem 2006;17:279–290.
32. Mao JJ, Giannobile WV, Helms JA, Hollister SJ, Krebsbach PH, Longaker MT, Shi S. Craniofacial tissue engineering by stem cells. J Dent Res 2006;85:966–979.
33. Ponce ML, Koelling S, Kluever A, Heinemann DE, Miosge N, Wulf G, Frosch KH, Schütze N, Hufner M, Siggelkow H. Coexpression of osteogenic and adipogenic differentiation markers in selected subpopulations of primary human mesenchymal progenitor cells. J Cell Biochem 2008;104:1342–1355.
34. Vacanti CA, Vacanti JP. Bone and cartilage reconstruction with tissue engineering approaches. Otolaryngol Clin North Am 1994;27:263–276.
35. Marmur ES, Phelps R, Goldberg DJ. Clinical, histologic and electron microscopic findings after injection of a calcium hydroxylapatite filler. J Cosmet Laser Ther 2004;6:223–226.

Short-term studies using ceramic scaffolds in lapine model for osteochondral defect amelioration

2012 Biomed. Mater. 7 035005

(http://iopscience.iop.org/1748-605X/7/3/035005)

IOP Publishing Biomedical Materials

Biomed. Mater. **7** (2012) 035005 (8pp) doi:10.1088/1748-6041/7/3/035005

Short-term studies using ceramic scaffolds in lapine model for osteochondral defect amelioration*

F B Fernandez, Sachin Shenoy, S Suresh Babu, H K Varma and Annie John

Biomedical Technology Wing, Sree Chitra Tirunal Institute for Medical Sciences and Technology, Poojapura, Thiruvananthapuram—695012, Kerala, India

E-mail: ajkari@sctimst.ac.in (Annie John)

Received 30 October 2011
Accepted for publication 2 February 2012
Published 9 March 2012
Online at stacks.iop.org/BMM/7/035005

Abstract

This study was undertaken to glean preliminary information on the role of triphasic ceramic coated hydroxyapatite (HASi) and biphasic (alpha-tricalcium phosphate and hydroxyapatite based) calcium phosphate (BCP) for the development of osteochondral constructs. The proposed constructs were tested for performance *in vitro* with rabbit adipose-derived mesenchymal stem cells (RADMSCs) and further analysed *in vivo* in a lapine model for osteochondral defect amelioration. Desirable scaffolding architecture ensuring favourable conditions for cell attachment, nutrient exchange and neo-tissue organization was achieved by the synthesis of porous ceramic blocks and characterizations were carried out using x-ray diffraction and Fourier transform infrared spectroscopy. The cytocompatibility of the scaffold–cell combination product was evaluated using microscopy techniques that proved the scaffold to be non-cytotoxic and favourable for cell growth and proliferation. Short-term implantation studies were conducted with bare cylindrical HASi and BCP scaffolds, press fit deep into the bony bed of the median femoral condyles of the rabbit, which resulted in favourable specific *in vivo* response of *de novo* cartilage-like cells on the surface and sub-surface bony trabeculae. The generated pilot data will help to assess the severity of proposed procedures before embarking on scaled-up efforts.

(Some figures may appear in colour only in the online journal)

1. Introduction

Injuries to the articular cartilage tissue are common with sequela that involves continued loss of tissue with progressive worsening of the related joint function. Insults at early time points may also contribute to late-onset of related arthritis, causing a worsening of the quality of life and associated economic loss. Osteochondral lesions or defects are areas of damage where the cartilage and underlying bone are affected. Osteochondral status is intimately linked with limb alignment, meniscal status and ligamentous status. A deficiency in one part of this functional unit can have an impact on the other parts and, in the short term, can lead to a loss of performance. Lesions or damage can be caused by disease, arthritis, inflammation or trauma. Ten per cent of the world population over 30 years of age has had clinical osteoarthritis (OA) of the hip or knee, with total direct costs estimated in billion dollars per year [1]—'The blessing of living long is scripted by the burden of aging'. Current therapies vary from autologous chondrocyte implantation, subchondral drilling to microfracturing. Treatments indicate the regeneration of mechanically inferior fibrocartilage at the defect site post-treatment, which undergoes wear and tear over time causing joint failure in the long term.

* Part of this work was presented at the international conference of *BIO 2011-Biomaterials and Implants. Prospects and Possibilities in the New Millennium* at the CGCRI Kolkata, India, July 21–23, 2011.

In such situations, alternative tissue engineering strategies call for the application of appropriate scaffolds to deliver cells and growth factors which would simultaneously degrade keeping pace with restoration of tissue function. In this context, bioactive ceramics were the scaffolds of choice as they are known to be biocompatible, porous for tissue ingrowth, biodegradable and above all, their composition is similar to that of skeletal tissues. In view of the unique nature of articular cartilage and the nature of osteochondral lesions where the cartilage and underlying bone are affected, there is a need for the development of a composite ceramic scaffold (singly or in two phases) for osteochondral defect amelioration. Evaluation of the role of ceramics as scaffolds for osteochondral defects has been ongoing since 1989 [2] with the latest reports indicating the combination of ceramics with exotic materials [3] to achieve desired material characteristics. Further use of ceramics as carrier surfaces for the placement of scaffold-free cartilage development has also been noted [4]. The ability of the ceramic surfaces to provide a native bone identical surface for cartilage overgrowth and support has been well identified. The recruitment of cells from the stem cell compartment would ensure growth and regeneration of tissue *in situ* as the native tissue is avascular and not conducive to rapid growth and repair. The repair has been observed to be mediated wholly by the proliferation and differentiation of mesenchymal cells of the marrow in the case of a rabbit articular cartilage healing model investigated by Shapiro *et al* (1993) [5]. Adipose tissue is an appropriate cell source due to ease of access, low donor site morbidity and relatively easy isolation procedure and has been used as a proponent in earlier studies for the repair of bone and cartilage tissues [6]. Therefore, the interest was to utilize adipose tissue-derived mesenchymal stem cells (ADMSCs) which are capable of differentiating into multiple lineages [7], to determine the cytocompatibility of selected ceramic scaffolds and thereafter to assess their regenerative efficacy in a lapine osteochondral defect model.

The aim of the study was to act as a pilot to generate preliminary data using ceramics as osteochondral scaffolds and to assess the severity of proposed procedures before embarking on large scale attempts.

2. Materials and methods

All cell culture reagents including medium were purchased from GIBCO^{TM} Invitrogen Inc., USA. Stains, chemical and molecular reagents were purchased from Sigma Aldrich, unless otherwise mentioned.

2.1. Isolation and expansion of rabbit ADMSCs

Approximately 2 g of adipose tissue retrieved aspetically from the subcutaneous site of New Zealand White (NZW) Rabbit was minced manually and mixed with an equal volume of 0.2% collagenase (Invitrogen) solution, digested at 37 °C and filtered. The digest was centrifuged at 15 °C for 10 min at 2500 rpm and pellet re-suspended in DMEM-HG, seeded onto T25cm^2 flask (NUNC) and maintained in culture with DMEM-HG containing 10% foetal bovine serum and 50 units ml^{-1} of penicillin and 50 μg ml^{-1} of streptomycin (Gibco, Anti–Anti Mix) at 37 °C under 5% CO_2 atmosphere. The medium was first changed within 16 h of plating and cells were fed every 3 days until confluency (figure 1).

2.2. Material preparation

In-house (Bioceramics Laboratory, SCTIMST, Trivandrum, India) developed bioactive ceramics—triphasic ceramic coated hydroxyapatite (HASi) and biphasic calcium phosphate (BCP)—were the scaffold materials of choice in this study.

2.2.1. Triphasic ceramic coated hydroxyapatite (HASi). Hydroxyapatite (HA) powder was synthesized by a wet precipitation method involving calcium nitrate and ammonium dihydrogen phosphate in a stoichiometric proportion, under basic medium. The precipitated HA powder was freeze-dried to generate free flowing powder which was compacted with a pore former and compressed to form discs sintered at 1200 °C. Silica coated HA was prepared by treating HA discs further with a silica sol, with excess sol removed, dried and sintered at 1200 °C to form the triphasic ceramic coated hydroxyapatite (HASi).

2.2.2. Biphasic calcium phosphate. BCP was synthesized by a wet chemical *in situ* precipitation technique. Ammonium phosphate solution was added to calcium nitrate at a ratio of 1:6. Further processing is performed as per Suresh Babu *et al* [8]. Here the combination of HA and α-tricalcium phosphate (TCP) was synthesized as the second phase in this BCP composite. The materials were polished in the form of discs—5 mm diameter with 1–2 mm thickness (for *in vitro* studies)—and subjected to ultrasonic cleaning (Cole Parmer, USA). Subsequently, the materials were sterilized by steam (121 °C, 15 psi pressure for 15 min).

2.3. Material characterization

2.3.1. X-ray diffraction. Ceramic sample powders of HASi and BCP were scanned between 20° and 40° 2θ at a rate of 2° min^{-1} under a step size of 0.02° using Cu Kα1 radiation at a voltage of 40 kV and a current strength of 30 mA (Siemens D-5005). Materials were identified by comparing the data with the JCPDS files.

2.3.2. Fourier transform infrared spectroscopy. Ceramic sample powders of HASi and BCP were pelleted separately with KBr powder and analysed on a Thermo Nicolet (Madison, WI) 5700 spectrometer. Spectra were collected in the diffuse reflectance (DRIFT) mode at a resolution of 4 cm^{-1} and scanned between 400 and 4000 cm^{-1} wave number range and with an average scan of 200.

2.3.3. Scanning electron microscopy. HASi and BCP discs were stuck to the stub with an adhesive tape and sputter coated with gold (Hitachi E101), and visualized under a scanning electron microscope (SEM) (Hitachi S2400).

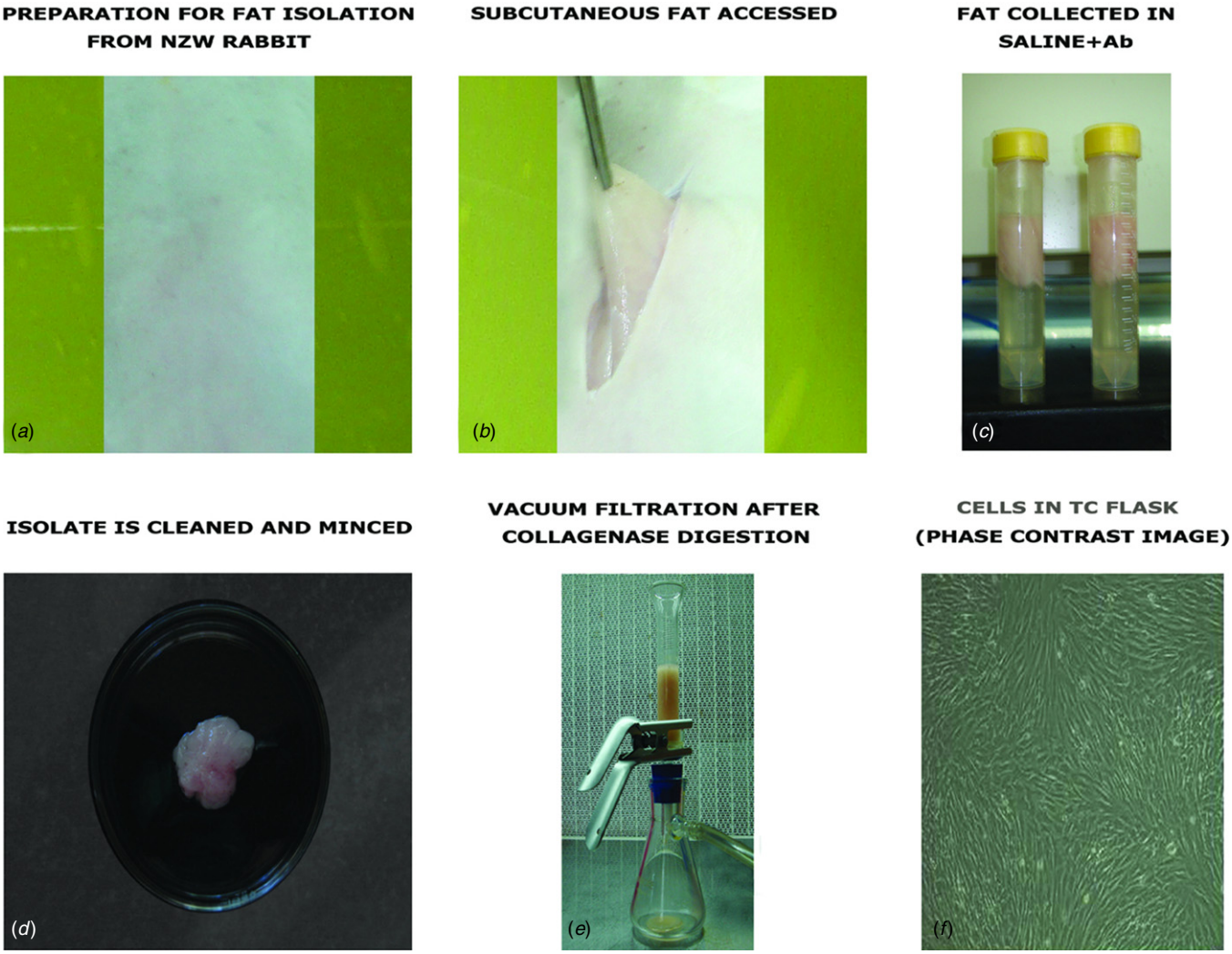

Figure 1. Isolation of RADMSCs: workflow chart of RADMSC. (*a*) Access of subcutaneous fat pad, (*b*) collected samples, (*c*) cleaned and minced fat sample, (*d*) filtration and post-processing and (*e*) phase contrast image of confluent RADMSC in culture—day 7.

2.4. Cytocompatibility—in vitro

Rabbit adipose-derived mesenchymal stem cells (RADMSCs) were seeded on sterilized scaffold surfaces of HASi and BCP discs (3 mm diameter). SEM and confocal laser scanning microscope (CLSM—Carl Zeiss 510 META) imaging was carried out to view cell–material interaction and thereby to assess cytocompatibility.

2.4.1. Scanning electron microscopy. RADMSCs were seeded on the bioactive ceramics HASi and BCP at a concentration of 10^4 cells and maintained in DMEM-HG for a period of 1 week. The cell-seeded ceramic scaffolds were then fixed in 3% gluteraldehyde, dehydrated in ascending grades of ethanol, critical point dried (Hitachi HCP-2), sputtered with gold (Hitachi E101) and examined under a SEM (Hitachi S2400). Cell morphology and cell sheet development, and pore coverage over the bioactive ceramic scaffolds were studied to understand the compatibility of the scaffold and cell type.

2.4.2. Cell viability—live–dead assay. In order to evaluate the efficacy of the scaffolds in maintaining cell viability over time a live–dead assay using acridine orange and ethidium bromide (Sigma) was performed. RADMSCs (10^4 cells cm^{-2}) were loaded on each ceramic scaffold and maintained in culture for 3 days. The scaffold was washed in PBS and incubated with 100 μl dye mixture for 30 min. Excess stain was removed with PBS and the scaffold was viewed under a CLSM (Carl Zeiss 510 META). Live cells were determined by the uptake of acridine orange (502/526) (green fluorescence) and the exclusion of ethidium bromide (518/605) (red fluorescence) stain [9].

2.5. Implantation studies in rabbit osteochondral model—in vivo

NZW rabbits (6 months) were used for surgical implantation studies. The animals were pre-medicated with intramuscular injection of atropine sulfate at 0.1 mg per kg body weight, xylazine hydrochloride at 0.22 mg per kg body weight and ketamine hydrochloride at 11 mg per kg body weight. Thiopentone sodium at 5 mg per kg body weight followed by succinyl choline at 0.02 mg per kg body weight was given intravenously for induction of anaesthesia and muscle

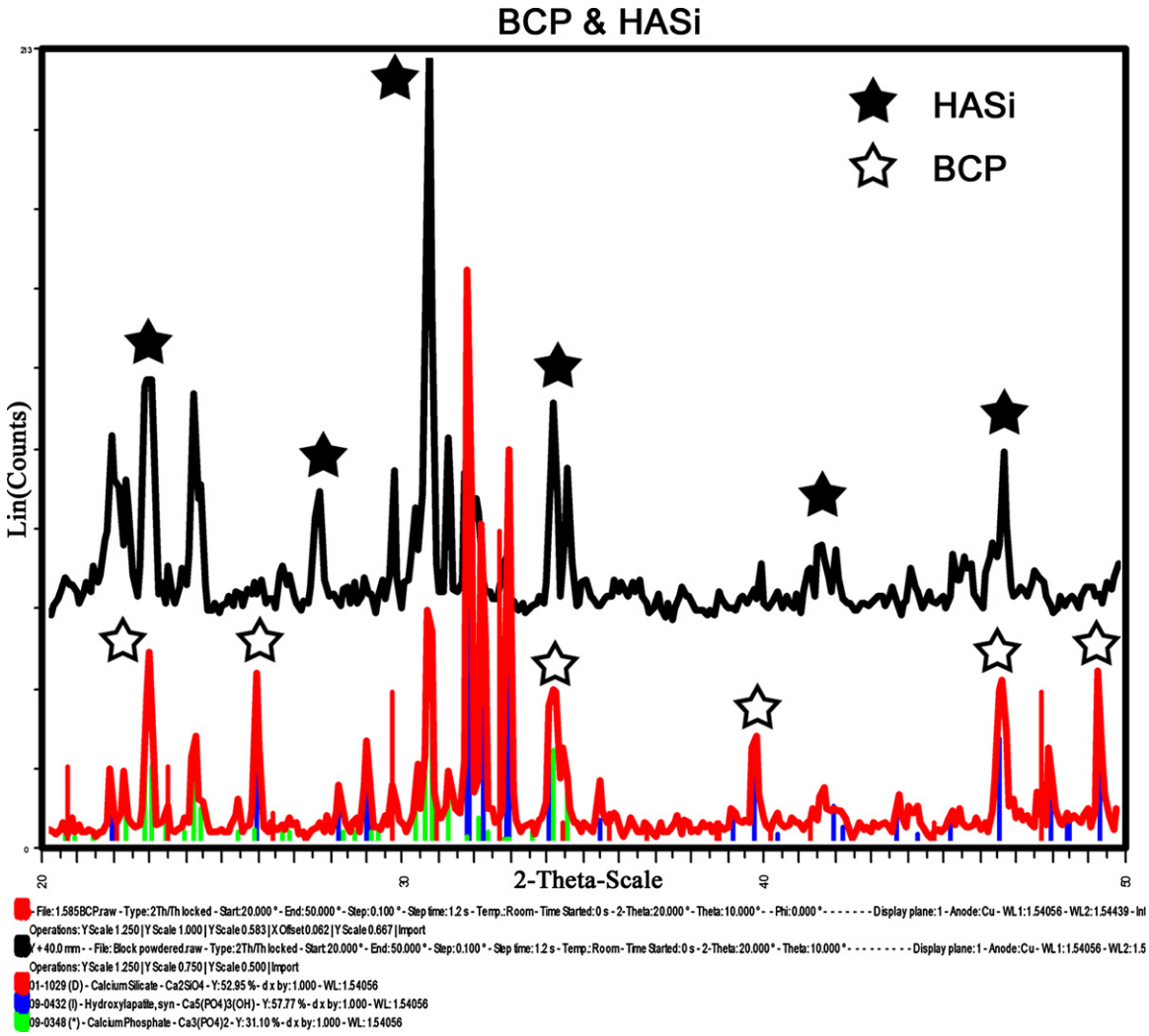

Figure 2. X-ray diffraction spectra of BCP (open ☆) in comparison with HASi (full ★).

relaxation, respectively. A medial parapatellar incision was made on the knee joint and carried through the medial aspect of joint capsule. The patella was dislocated laterally until the medial femoral condyle was exposed. A surgical drill bit was used to create a 3.5 mm diameter, 4 mm deep defect on the femoral condyle. The HASi and BCP cylindrical scaffolds were 'press fit' separately into the defect aseptically in rabbit knee joints. The joint capsule and skin were closed. A non-treated animal was maintained without any surgical intervention as the normal control condyle. All experiments were carried out with the approval of the Institute Animal Ethics Committee following the guidelines of Committee for the Purpose of Control and Supervision of Experiments on Animals.

2.5.1. Ex vivo evaluation. Post-implantation, rabbits were housed in separate cages and took water and fed *ad libitum.* Healing was uneventful without any inflammation and after the study period of 4 weeks the animals were euthanized with an overdose of the anaesthetic thiopentone. The HASi, BCP and normal condyle control samples were retrieved and fixed in 10% neutral buffered formalin.

2.5.2. Histology—polymethylmethacrylate embedding. For polymethylmethacrylate (PMMA) processing the ceramic was processed *in situ* within the condylar region of the knee. It was dehydrated with ascending graded series of isopropanol (Nice Chemicals, India) and embedded in PMMA. Plastic sections of about 180 μm were sliced with a linear precision saw (Isomet^{TM} 5000 Precision Saw, Buehler) and thereafter fine polished (Ecomet® 3000, Buehler) to a thickness of 90–100 μm and stained with van Gieson's picrofuchsin and Stevenal's blue.

2.5.3. Van Gieson–Stevenal's blue staining. PMMA sections were washed in running tap water and kept in a Stevenal's blue solution at 60 °C for 15 min and counter stained with van Gieson's picrofuchsin [10].

2.5.4. Back scatter electron imaging. The composition of the ceramic insert within the joint structure was examined using back scattered electron (BSE) imaging on a FEI Quanta 200. The PMMA embedded sections were stuck on an aluminium stub and imaged in the back scatter mode.

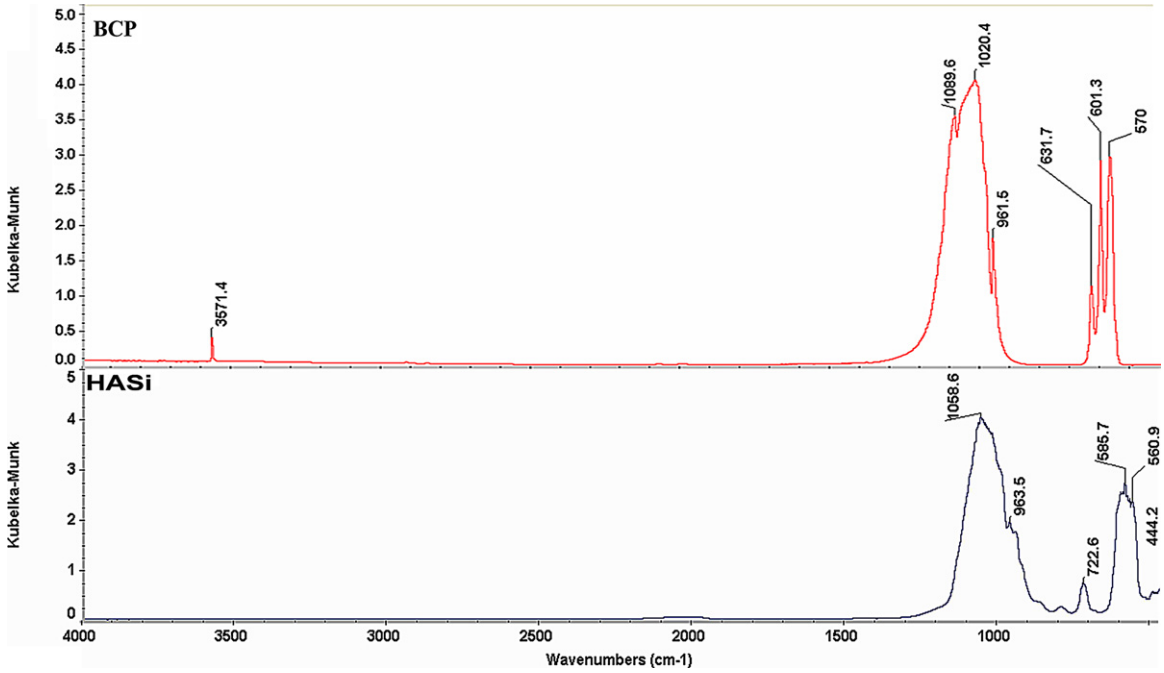

Figure 3. FTIR spectra of BCP and HASi depicting characteristic hydroxyl at 3571 cm^{-1} and phosphate groups at 1020 and 670 cm^{-1}. Silica peak characteristic to HASi depicted at 722.6 cm^{-1}.

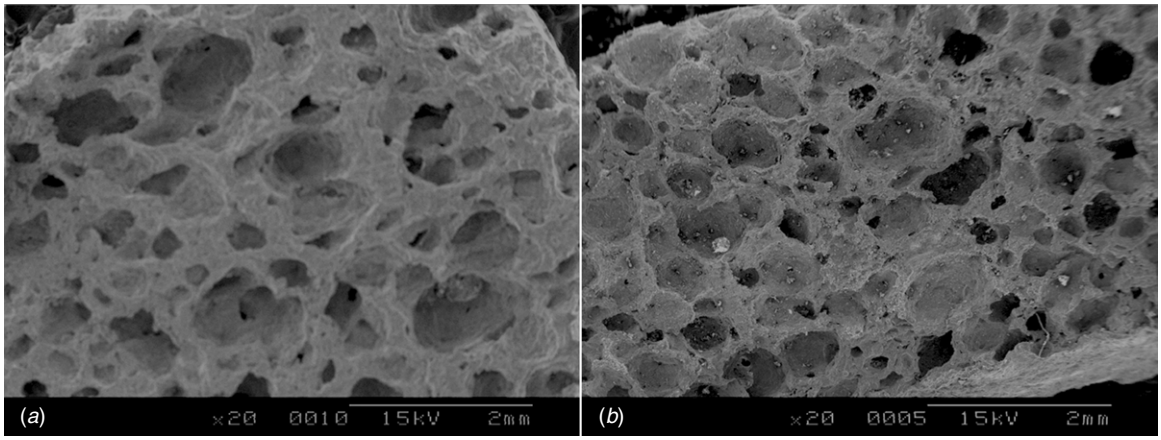

Figure 4. SEM showing surface morphology and pore structure of (*a*) BCP and (*b*) HASi.

3. Results and discussion

Damage to the articular tissue is common in adults and may lead to OA as a result of the poor regenerative capacity of the tissue [11]. The long-term consequences can be relieved by approaching cartilage injury with the holistic appeal of treating the injured tissue as a single unit—cartilage + bone approach. This helps in tissue recovery and at the same time assists in the quick restoration of nutrient flow via the bony layer and also ensuring that support structures are maintained without damage. The bare ceramic scaffold approach in the *in vivo* model based on *in vitro* cytocompatibility addresses this concern.

The XRD pattern exhibited crystallinity with HA as the major phase in both materials. The outer coating layer in HASi showed peaks for calcium silicate, TCP and HA. In BCP the presence of α-TCP was validated against standard patterns. The presence of both HA and α-TCP indicates the biphasic nature of the scaffold. The data were matched to the JCPDS files (figure 2). The powder diffraction data numbers (PDF no) for HA, TCP and calcium silicate are 09-0432, 09-0348 and 01-1029, respectively, as per Nair *et al* [9]. The FTIR spectra obtained showed the characteristic absorption band corresponding to a HA phase in both samples. The bands at 3571.4 cm^{-1} can be attributed to hydroxyl groups [9], whereas the bands at 1190–976 and 660–520 cm^{-1} correspond to phosphate groups. In HASi, the peak at 722.6 cm^{-1} corresponds to silica. Since the absorption of HA is maximum as compared to α-TCP, the relevant absorption peaks are submerged and the data collected confirm the presence of the relevant peaks for HA across both materials (figure 3).

The SEM images depicted an elaborate porous interconnected architecture (50–500 μm pore sizes) ideal for

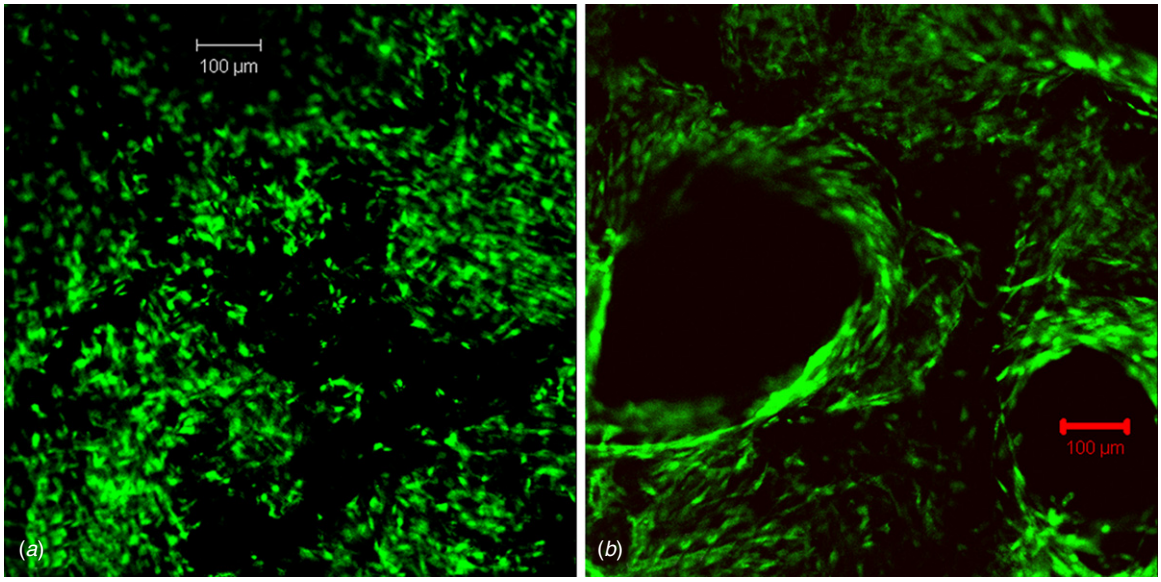

Figure 5. CLSM for the viability of RADMSC on (*a*) BCP and (*b*) HASi; acridine orange stains the live cells green and ethidium bromide stains the dead cells red.

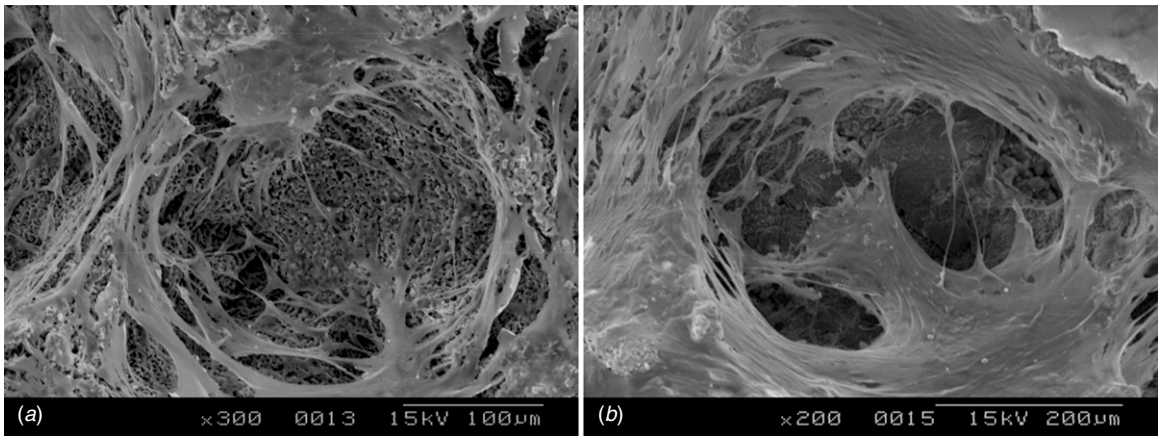

Figure 6. SEMs of (*a*) BCP and (*b*) HASi of cell–ceramic construct 3 days post-seeding indicating cellular architecture/cell–scaffold interactions.

the infiltration of cells into the internal voids of HASi and BCP (figure 4). Interconnected pores would help in the infiltration and maintenance of cells in pores by appropriate nutrient flow. The images also show an open system of pores on the surface indicating a surface suitable for material–tissue interaction. This allows for tissue ingrowth into the scaffold in the bone layer contributing to increased stability [12].

Viability assays proved the enhanced cytocompatibility of the materials in sustaining cell growth on HASi and BCP. Green live cells were seen rimmed at the edges of the pores as well as on the flat surfaces between the pores. Earlier studies have used the CLSM to monitor the structural and functional characteristics of 3D tissue engineered constructs [13]. The cells are grown and well spread on the surface with no pore occlusion and bridging (figure 5).

Cells attached, adhered and spread out (cell phenomenology) in varying degrees on the surface of both the ceramic scaffolds as identified with SEM (figure 6). A successful orthopaedic implant requires a surface that is not only non-toxic but also one that allows the phenomenological behaviour of bone cells [14]. Cells on HASi and BCP rimmed the outer edges of the pores and cell extensions bridged across the pores without pore occlusion forming a web-like cellular pattern. Filamentous extensions of the cells also traversed across the surface gripping firmly by focal adhesions. Knitted cell sheets were also observed in a few areas forming a canopy over the material. Cells that adhered and proliferated are expected to organize the ECM to convey signals (mechanical and chemical) influencing shape, actin cytoskeleton organization and transcription activity and subsequently to engineer a functional tissue [15]. Filamentous extension of cell to cell contacts was observed indicating a healthy cell population [16] on the surface and within the pores of the ceramic scaffolds. HASi portrayed cell sheet-like development on the surface where cells and extracellular matrix have joined to form a continuous smooth surface that extends within the scaffold surfaces (figure 6(*b*)). Cells on BCP can be visualized as discrete units as they spread deep into the pores on the scaffold (figure 6(*a*)).

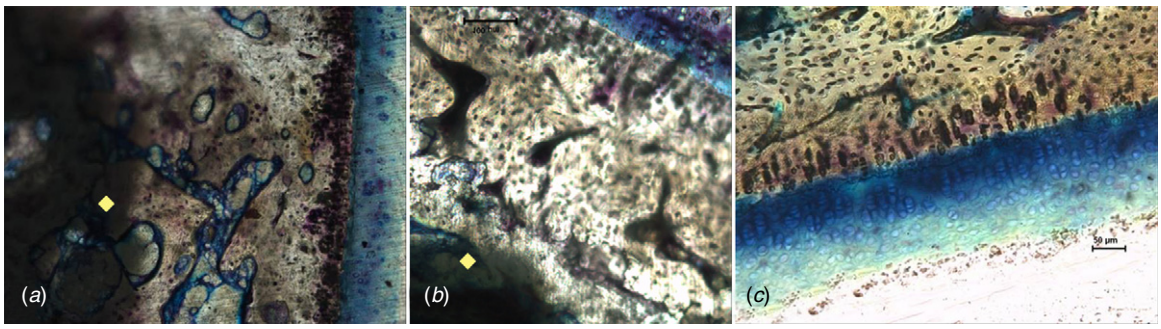

Figure 7. PMMA embedded rabbit condylar longitudinal sections retrieved 4 weeks post-implantation and demonstrated with Stevenal's blue and van Gieson's picrofuchsin differential stain (cells—blue; bone—yellow). (*a*) BCP—demonstrates cellular overgrowth. (*b*) HASi—demonstrates integration into condylar tissue. (*c*) Control—demonstrates native stage of condylar tissue.

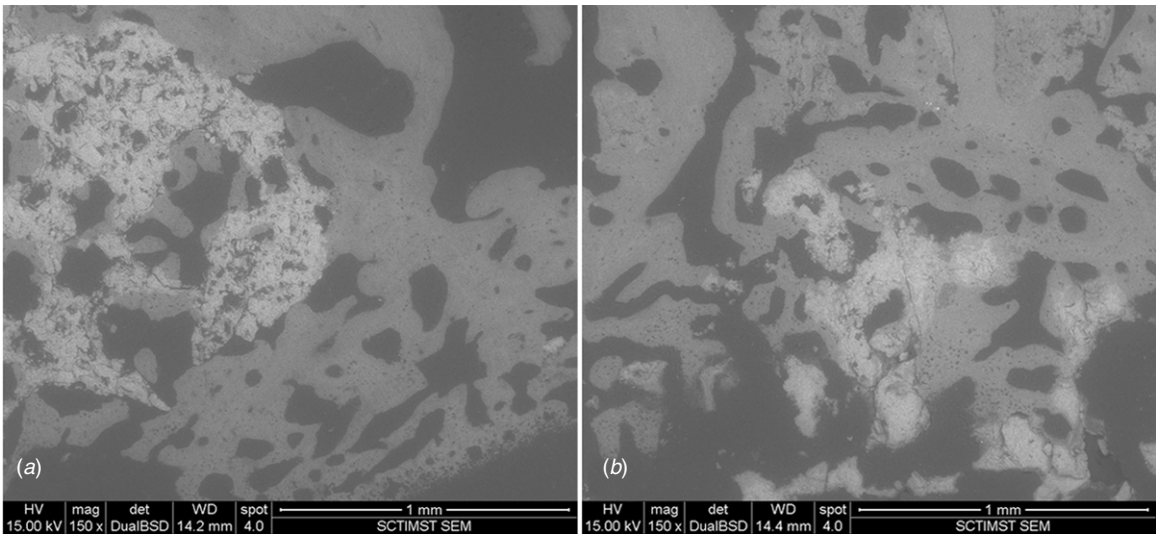

Figure 8. BSE micrographs of (*a*) BCP 150 × image indicating ingrowth of bony trabeculae via pore network and (*b*) HASi 150 × image indicating integration into newly formed trabecular bone with remnants of ceramic isolated within bone islands.

The cells are interconnected by cell to cell extensions to establish uniform coverage. In both cases the pore is open encouraging further colonization of the scaffold by cells, incursion of nutrient material and further integration of the cell–scaffold interface.

The healing pattern of test animals with implanted samples was uneventful with BCP and HASi implanted animals. Gross examination revealed no fibrous tissue formation or anomalies within the joint structure. Retrieved rabbit implant samples on macroscopic examination indicated an overburden on the ceramic scaffolds *in situ*. Post-processing and staining examination revealed a Stevenal's blue stained area over the yellow van Gieson's stained area. Stevenal's blue staining of the control condyle section indicated hyaline cartilage formations with vertically aligned chondrocytes. Van Gieson's staining below the same indicated healthy trabecular bone conditions.

Similarly the ceramic surface in the test samples (figures 7(*a*) and (*b*)) revealed the beginning of formation of an unorganized cartilage matrix over the surface stained by Stevenal's blue. The ceramic implant has been overgrown by the matrix and integrated into the joint tissue. The presence of matrix overlay indicates the acceptance of the material into the joint milieu. In the BCP scaffold implanted condyle (figure 7(*a*)) a definite lack of organization in the deposition, and accretion of cells in the cartilage layer can be identified on comparison with the control section (figure 7(*c*)). The aggregate over the HASi scaffold appears to be more cellular in nature, with less accumulation of extracellular matrix (figure 7(*b*)). The unorganized appearance of the cartilage overgrowth is contingent to the short duration of observation of the study which may most likely reorganize with time.

To further understand the interaction of the scaffold with the surrounding bone tissue, BSE imaging was carried out. The ceramic scaffold is indicated in white, with the surrounding/infiltrating bone surfaces in grey (figure 8). The image clearly highlights the steady deterioration of the scaffold and the simultaneous ingrowth of bone within the scaffolds. Pronounced osteointegration of the scaffold can be observed in the case of the HASi scaffold (figure 8(*b*)); the ceramic has been well assimilated into the newly formed trabecular bone structure. With BCP, the original scaffold morphology was retained, with bone infiltration proceeding from the outer edges of the ceramic via the pores (figure 8(*a*)). Ingrowth of bone will help in the stabilization of scaffold material within the defect area. Prevention of micro movements will help

organization of proper cartilage architecture as it is understood that such movements and wear particle debris can accelerate the process of fibrous tissue capsule formation and related loosening of surrounding bone [17].

HASi has already been reported to induce cell growth and replication [9]. Thereby the ability of the scaffold to stimulate cell replication and healing may prove helpful in providing a scaffold-alone approach to osteochondral defect amelioration. Initial data from the study conducted indicate the slow resorption of the BCP scaffold over time compared to the HASi scaffold. The better healing capacity of the bone may be a favourable attribute to speed up cartilage regeneration as the defect is extended to the underlying (vascularized) bone [18]. In addition, the ease of integration of the materials into the underlying bone layer will increase the cartilage integrity with time. Integration of the material with both tissue types enhances healing and induces a concomitant regeneration of tissue with the enhanced underlying bony structures [19].

4. Conclusion

Triphasic ceramic coated hydroxyapatite (HASi) and BCP proved to be non-cytotoxic and cytocompatible on assessment with RADMSCs. *In vivo* short-term lapine studies also indicate the suitability of the same to develop a monolithic integrated scaffold that will provide adequate integration to foster cartilage resurfacing with time. The current results favour further investigation of the same using a larger cohort and a focus on the use of compatible stem cells identified to stimulate healing. The preliminary study of short-term duration is indicative of the favourable properties of the developed ceramic scaffolds and further possibilities of making this attempt successful.

Acknowledgments

The authors gratefully acknowledge The Director and The Head BMT Wing SCTIMST for the facilities to carry out this study, Dr T V Anilkumar for cLSM, Mr R Sreekumar for SEM; Department of Biotechnology, Govt of India for Project Support of Tissue Engineering (ANCETE) and CSIR are gratefully acknowledged for Fellowship for FBF.

References

[1] Felson D T *et al* 2000 Osteoarthritis: new insights. Part 1: the disease and its risk factors *Ann. Intern. Med.* **133** 635–46

[2] Ohgushi H, Goldberg V M and Caplan A I 1989 Repair of bone defects with marrow cells and porous ceramic. Experiments in rats *Acta Orthop. Scand.* **60** 334–9

[3] Jiang J, Tang A, Ateshian G A, Guo X E, Hung C T and Lu H H 2010 Bioactive stratified polymer ceramic–hydrogel scaffold for integrative osteochondral repair *Ann. Biomed. Eng.* **38** 2183–96

[4] Kitahara S *et al* 2008 *In vivo* maturation of scaffold-free engineered articular cartilage on hydroxyapatite *Tissue Eng.* A**14** 1905–13

[5] Shapiro F, Koide S and Glimcher M J 1993 Cell origin and differentiation in the repair of full-thickness defects of articular cartilage *J. Bone Joint Surg. Am.***75** 532–53

[6] Dragoo J L *et al* 2003 Tissue-engineered cartilage and bone using stem cells from human infrapatellar fat pads *J. Bone Joint Surg. Br.***85** 740–7

[7] Zuk P A 2010 The adipose-derived stem cell: looking back and looking ahead *Mol. Biol. Cell* **21** 1783–7

[8] Suresh Babu S, Komath M and Varma H K 2012 *In situ* formation of hydroxyapatite—alpha tricalcium phosphate biphasic ceramics with higher strength and bioactivity *J. Am. Ceram. Soc.* (online, cited 29 January 2012) (available from http://onlinelibrary.wiley.com/doi/10.1111/j.1551-2916.2011.04987.x/abstract)

[9] Nair M B, Suresh Babu S, Varma H K and John A 2008 A triphasic ceramic-coated porous hydroxyapatite for tissue engineering application *Acta Biomater.* **4** 173–81

[10] Maniatopoulos C, Rodriguez A, Deporter D A and Melcher A H 1986 An improved method for preparing histological sections of metallic implants *Int. J. Oral. Maxillofac. Implants* **1** 31–7

[11] Anderson D D *et al* 2011 Post-traumatic osteoarthritis: improved understanding and opportunities for early intervention *J. Orthop. Res.* **29** 802–9

[12] Ryan G, Pandit A and Apatsidis D P 2006 Fabrication methods of porous metals for use in orthopaedic applications *Biomaterials* **27** 2651–70

[13] Tan W, Sendemir-Urkmez A, Fahrner L J, Jamison R, Leckband D and Boppart S A 2004 Structural and functional optical imaging of three-dimensional engineered tissue development *Tissue Eng.* **10** 1747–56

[14] Hunter A, Archer C W, Walker P S and Blunn G W 1995 Attachment and proliferation of osteoblasts and fibroblasts on biomaterials for orthopaedic use *Biomaterials* **16** 287–95

[15] Chen C S, Mrksich M, Huang S, Whitesides G M and Ingber D E 1997 Geometric control of cell life and death *Science* **276** 1425–8

[16] Altman A M, Gupta V, Ríos C N, Alt E U and Mathur A B 2010 Adhesion, migration and mechanics of human adipose-tissue-derived stem cells on silk fibroin-chitosan matrix *Acta Biomater.* **6** 1388–97

[17] De Man F H R, Tigchelaar W, Marti R K, Van Noorden C J F and Van der Vis H M 2005 Effects of mechanical compression of a fibrous tissue interface on bone with or without high-density polyethylene particles in a rabbit model of prosthetic loosening *J. Bone Joint Surg. Am.* **87** 1522–33

[18] Gelinsky M 2007 Biphasic, but monolithic scaffolds for the therapy of osteochondral defects *Int. J. Mater. Res.* **98** 747–53

[19] Gomoll A H *et al* 2010 The subchondral bone in articular cartilage repair: current problems in the surgical management *Knee Surg. Sports Traumatol. Arthrosc.* **18** 434–47

INTERNATIONAL CONFERENCE

ON

BIOMATERIALS AND IMPLANTS: PROSPECTS AND POSSIBILITIES IN THE NEW MILLENNIUM

BIO 2011

CERTIFICATE

It gives us a great pleasure to certify that Cytocompatibility - short term implantation studies on a biphasic ceramic scaffold for use in osteochondral defect amelioration of B.F. Francis, Sachin Shenoy, Suresh Babu S., H.K. Varma & Annie John has been awarded Best Poster prize for poster/~~essay~~ competition in the **International Conference on Biomaterials and Implants: Prospect and Possibilities in the New Millennium (BIO 2011)** organized by Bioceramics and Coating Division, Central Glass and Ceramic Research Institute, Kolkata during July 21-23, 2011.

Indranil Manna

(Prof. Indranil Manna)
(Prof. Indranil Manna)
Chairman, BIO 2011

Dbasu

(Dr. Debabrata Basu)
Convenor, BIO 2011

DoNDs-12

International Conference on Design of Biomaterials

XXIII Annual Meeting of SBAOI & VI Annual General Meeting of STERMI

December 9-11, 2012 | Indian Institute of Science, Bangalore

PRESENTATION CERTIFICATE

This is to certify that MR. B. F. FERNANDEZ

of SREE CHITRA TIRUNAL INSTITUTE FOR MEDICAL SCIENCES & TECHNOLOGY, THIRUVANANTHAPURAM

has presented a poster on LIGHTING THE PATH: CELL TRACKING IN COMPLEX 3D - CERAMIC SCAFFOLDS

and this contribution is co-authored by H.K. VERMA & ANNIE JOHN

B Basu

Prof. Bikramjit Basu
Conference Chair

SOCIETY FOR BIOMATERIALS AND ARTIFICIAL ORGANS (INDIA)

(Member, International Union of Societies for Biomaterials Science and Engineering)
Registration No. 110/86, Thiruvananthapuram, India

CERTIFICATE

This is to certify that

B. F. FERNANDEZ
SCTIMST, TRIVANDRUM

has won the

Best Poster Presentation Award (First)

during XXIII National Conference of the Society,
December 9-11, 2012 at Indian Institute of Science,
Bangalore

BANGALORE, INDIA
DECEMBER 9, 2012

PRESIDENT

SECRETARY

Government of Kerala

KSCSTE

KERALA SCIENCE CONGRESS 25

trivandrum india technopark harmony at work

सत्यमेव जयते
Department of Science & Technology

25th KERALA SCIENCE CONGRESS

29th January - 1st February 2013, Thiruvananthapuram

BEST PAPER AWARD

This is to certify that the research paper titled Cell ceramic mediated tissue engineered approaches for Osteochondral reconstruction in Orthopaedics *by* Francis P. Fernandez, Annie Jhon, Varma H.K *has won the* ***Best Paper Award*** *in* Health Science *in the 25th Kerala Science Congress held during the 29th January to 1st February 2013 at Technopark, Thiruvananthapuram.*

Thiruvananthapuram
01 - 02 - 2013

Prof. V.N. Rajasekharan Pillai
President, 25th Kerala Science Congress
Executive Vice President, KSCSTE and
Principal Secretary, S&T Department, Govt. of Kerala